UNIVERSITY OF NOTTINGHAM

DEPARTMENT OF CIVIL ENGINEERING

VERY LONG BASELINE INTERFEROMETRY AND GEODETIC APPLICATIONS

by

David Neil McLintock, B.Sc., A.S.C.E.

Thesis submitted to the University of Nottingham
for the degree of Doctor of Philosophy

May 1980

TABLE OF CONTENTS

LIST OF FIGURES

LIST OF PLATES

VERY LONG BASELINE INTERFEROMETRY AND GEODETIC APPLICATIONS

ABSTRACT

Very Long Baseline Radio Interferometry is one of the most recently developed and potentially most useful geodetic measuring techniques. The high accuracy which it can achieve over great distances makes it ideally suited for studies of many interesting geodetic and geophysical phenomena. The major asset of the system is that, unlike the majority of other accurate techniques, all measurements are independent of the Earth's gravity field.

This thesis contains details of the basic theory of the VLBI technique and describes a model which has been developed to analyse data from the system. This is followed by a description of the application of the variation of co-ordinates method to the adjustment of VLBI observations and details the conditions and restrictions to be applied to the adjustment process. The basic procedure and equipment required to make the observations is described and details are given of the Nottingham University Long Baseline Interferometry Programs (NULBIP) which have been developed to perform the data analysis.

Data has been obtained and analysed from two independent sets of observations using two different VLBI observing systems. The Canadian system has been used for observations using the three antenna array comprising the Chilbolton Observatory, England, the Algonquin Radio Observatory, Canada, and the Owens Valley Radio Observatory, U.S.A. Observations have also been processed from the Haystack-Goldstone baseline in the U.S.A., observed using the NRAO Mk I VLBI system. The software which has been developed has been tested by comparison with independently derived results on these baselines.

The analysis of all the data has shown the VLBI method to be a highly accurate technique capable of measuring intercontinental distances with sub-metre accuracy. The results have indicated the many potential uses of VLBI in geodetic and geophysical research, the major ones of which have been described. The magnitude of systematic scale and orientation errors inherent in the Navy Navigation Satellite System (otherwise known as the TRANSIT system) have been measured by comparing these VLBI results with satellite-Doppler results derived from observations made near the radio telescopes.

ACKNOWLEDGEMENTS

The work leading to this thesis was carried out at the Department of Civil Engineering at the University of Nottingham, with the support of both the Head of Department, Professor R.C. Coates, and Professor P.S. Pell. During this period of research, the author was sponsored by the United Kingdom Science Research Council.

The author expresses his appreciation of the guidance and encouragement given by his supervisor, Professor V. Ashkenazi, throughout this study.

Sincere thanks are extended to all the geodesists and astronomers who have given valuable advice, either personally or through correspondence, notably Dr P. Barber, Dr J. Campbell, Dr D. Fort, Dr R. Langley, Dr P. Richards, Dr A.R. Robbins, and Dr M. Quigley.

The fieldwork involved in obtaining the data described in this thesis has been extensive. The author acknowledges the work of all those involved at both the Observatories and the data processing centres, especially Mr J. McGiveney of the Chilbolton Observatory and the members of the LBI team at the Science Research Council's Appleton Laboratories. Furthermore, the author acknowledges the organisations and individuals involved in the satellite-Doppler observing campaigns, especially Major J. Eady and Mr R. Fenner of the Ordnance Survey of Great Britain. The author would also like to thank the Royal Greenwich Observatory, and especially Dr B. Yallop, for the provision of a program to compute the apparent places of stars.

The author is grateful to the other members of the Nottingham University Surveying Research Group, especially Mr S.A. Crane, Dr A.H. Dodson, Dr R.M. Sykes, and Dr R. Wood, for many useful discussions on both the theoretical and programming details of the data processing.

The author extends his appreciation to the Ordnance Survey for the use of the data from the Triangulation of Great Britain. He also wishes to thank Mr G.L. Haskins, Chief Surveyor, and his colleagues in the Topographical Department of Shell U.K. Exploration and Production for their help and consideration during the completion of this work.

The author would like to thank his parents for their support and encouragement and Sam and Megan for their unending patience and understanding. This thesis is dedicated to his wife, Jan, for her ceaseless encouragement and help during this period of research.

Finally, the author would like to thank Miss Jane Clerbaut for typing this thesis in her usual neat and efficient style.

CHAPTER 1:

INTRODUCTION

1. INTRODUCTION

Since the development of the first radio telescope by Jansky in the 1930's, the science of radio astronomy has greatly increased our knowledge of the universe. In radio interferometry it has also provided the geodesist and geophysicist with a powerful measuring instrument with which to study the Earth itself.

The technique was originally developed in the 1950's in order to study the structure of certain galaxies and stars emitting radio energy. It involves two, or more, separate radio antennae observing the same distant radio source, for example a quasar, and hence simulating one large radio antenna of a diameter equivalent to the distance between the two. The study of the interference patterns derived by comparing the signals received at the different antennae yields information concerning the structure of the observed radio source. In order to perform this task, an approximate knowledge of the distance and direction of the baselines connecting the antennae is required, and hence it has proved possible to 'reverse' the system and compute the baseline parameters from these observations.

In the early stages of the development of the technique, it was necessary that the antennae of the array were linked by cables. This is primarily because the received high frequency signal must be reduced to a lower frequency to enhance transmission, data handling, and comparison with the signals received at the other antennae. This frequency reduction involves 'beating' the received signal against a purely harmonic signal derived from a local oscillator. The instability of this local oscillator necessitated that the same signal be distributed to all the antennae of the interferometer array. Cable-link interferometry was followed by radio-link interferometry in which the same local

oscillator signal was distributed to all the antennae by means of a radio-link. The received signals were also tramsitted by this method which enabled baselines of around 150 km in length to be observed.

The major breakthrough resulting in longer observed baselines came in 1967 with the first successful use of a "tape recorder interferometer". This involves the use of separate local oscillators at the antennae and the recording of the received signal on magnetic tape. This became possible with the development of very stable atomic frequency standards which are used to drive the local oscillator at each station, and also high quality tape recording equipment. With the development of this method the stations of an interferometer array are completely independent and hence the only restriction on the length of an observed baseline is that both antennae are able to observe each source simultaneously. The application of this technique on long baselines is known as Very Long Baseline Radio Interferometry, or VLBI.

As already explained, the VLBI technique involves observing the signals arriving at the Earth from a radio source at two radio antennae. The radio source should ideally be an extragalactic 'point' source and is commonly a quasar, Seyfert galaxy, or Lacertid. Due to the extreme distance of these radio sources from the Earth, the signal can be regarded as arriving as a plane wavefront, each wavefront being received at the separate antennae at a different epoch. This difference is known as the delay time and is the primary observable of the technique. The received signal at each antenna is recorded on magnetic tape along with precise timing information derived from the station clock which is driven by the atomic frequency standard. The recorded tapes from each station are subsequently brought together at a processing centre and the observed delay time is established. This is achieved by a complex

cross-correlation process in which several minutes of data recorded on the two tapes are temporally offset relative to each other in a correlator until the recorded signals are seen to reinforce each other when combined. The recorded timing information enables a precise determination of the offset of the tapes and also enhances the quality control of the data recordings. A lack of synchronisation between the station clocks will clearly affect the measured delay time but will not affect the determination of the baseline parameters from the solution.

The description above is a simplified one as the delay time is continually changing due to the rotation of the Earth during the observations. This is easily compensated for in order to measure the delay time but it also leads to another observable, the fringe frequency or delay rate, which is a measure of the rate of change of delay with respect to time. It is of more limited use than the delay observable as it is insensitive to the polar component of the baseline. However, it is nevertheless a very useful measurement.

Using the delay observable, a number of observations of at least three sources enables a solution to be performed for the three components of the baseline (hence defining its distance and direction), the declinations and all but one of the right ascensions of the observed sources, and a model expressing the relative behaviour of the clocks at each station as a function of time. The baseline components are computed in terms of a classical geodetic system defined using the BIH zero longitude and Conventional International Origin and hence requiring knowledge of the pole position and UT1-UTC correction at the epoch of observation. The technique gives only information concerning the relative positions of the antennae and does not evaluate their absolute positions on the Earth.

The greatest asset of the method is that it is a geometrical technique which is completely independent of the Earth's gravity field, usually the limiting factor in any Earth or satellite based system. Furthermore, the scale of the system is defined by the velocity of propagation of microwaves in vacuo, a value very accurately known, and the orientation of the system is defined by the "fixed" positions of the observed radio sources. These positions are related to the Earth based co-ordinate system via the epochs of the observations and the pole positions.

The accuracy achieved is almost independent of the baseline length due to theinstrumental arrangement. Each antenna has receiving and recording equipment which will not be at all affected by any other station. Consequently, the recorded data from each station can be brought together in the correlator and the observed delays and fringe frequencies are determined with an accuracy dependent on the quality of the recordings, a factor which is independent of the antennae separation. The expression "almost independent of baseline length" is used for two reasons. Firstly, if the antennae are close together then the accuracy will improve due to the received signal at each antenna passing through the same area of the atmosphere and hence reducing the effect of any unmodelled atmospheric effect on the results, and secondly, for baselines approaching the diameter of the Earth, the number of available sources to observe will decrease which may, if limited observing time is available, degrade the solution.

The accuracies achieved by the technique depend largely on the particular VLBI system being used. The latest development, the NRAO Mark III system, is designed to determine the two equatorial components of the baseline to an accuracy of 5 cm, and the polar component to an

accuracy of 8 cm. The most common system in use, the NRAO Mark II system, exhibits a standard deviation of the baseline length of around 40-50 cm. The lengths of the baselines should remain constant whereas the components will change according to the errors in UT1 and the pole position.

A system which exhibits this level of accuracy clearly has many uses in geodesy and geophysics. It would be extremely useful in the establishing of a global geodetic reference system and for establishing connections between existing datums. As it suffers very little from systematic error effects, it can be used to calibrate lesser order surveying systems and can be applied to studying effects such as changes in UT1, polar motion, Earth tidal movements, local crustal motion, tectonic plate motions, precession, and nutation. Further developments in instrumentation, including the use of satellites to act as data links or radio sources, will further add to the range of effects which can be studied by this precise measuring technique.

The purpose of this research work has been firstly to assess the accuracies which can be achieved from the VLBI technique over baselines of several thousand kilometres in length using two different interferometer systems. Secondly, the objective has been to apply the results obtained to the calibration of the Navy Navigation Satellite System (also known as the TRANSIT system). In order to perform these tasks, a number of computer programs have been written which will process delay and/or fringe frequency (or delay rate) data observed by either two or three antennae using either of two different VLBI observing systems. These programs constitute the NULBIP (Nottingham University Long Baseline Interferometer Program) suite of programs. Having illustrated the accuracies which are achievable, the thesis then goes

on to discuss the possible applications of the technique in geodesy and geophysics.

The data used has been obtained from two sources. The majority consists of data observed by the three station array comprising the Chilbolton Observatory in Hampshire, England, the Algonquin Radio Observatory in Ontario, Canada, and the Owens Valley Radio Observatory in California, U.S.A. This data was observed in May 1977 and January 1978, using the Canadian VLBI system. The second data set consists of data from one observing period on the Haystack-Goldstone 4000 km baseline in the U.S.A. using the NRAO Mark I interferometer system. Satellite-Doppler observations have been made near all five of these telescopes at varying times and this data has been used in order to assess the systematic errors inherent in the Doppler system by comparing the Doppler results with those obtained from the VLBI observations.

The basic theory of the VLBI method is described in Chapter 2. This is followed, in Chapter 3, by a description of the adjustment method used together with its requirements and limitations. A description of the observing procedure and equipment is given in Chapter 4 while Chapter 5 describes the NULBIP suite of programs which have been written to process the data. The VLBI and Doppler observations which have been made are described in Chapter 6 and the results are presented and compared in Chapter 7. Chapter 8 discusses the application of VLBI to several topics in geodesy and geophysics. The thesis is concluded in Chapter 9.

CHAPTER 2:

THEORY OF VERY LONG BASELINE INTERFEROMETRY

2.1 PRINCIPLE OF VLBI OBSERVATIONS

2.1.1 The VLBI Technique

The primary purpose of geodetic Very Long Baseline Interferometry is to obtain, from observations of extragalactic radio sources, the length and direction of the baseline between two widely separated radio antennae.

Distant extragalactic sources, for example quasars and Seyfert galaxies, emit random radio signals over a very wide frequency band and are at such a distance from the Earth that these signals can be regarded as coming from a 'point' source and to be reaching the Earth as plane wavefronts. If such a signal were to be received by two different antennae on the Earth then, in the idealised case of a non-rotating Earth, error free receivers, and no atmospheric refraction, the signals arriving at each station would be identical but separated in time by a constant delay. Thus if it were possible to record the signal on an error free, infinite bandwidth recording system, together with exact timing information as to the epoch at which the signals were received, it would be possible simply to compare the recordings and measure the time delay between the signal arriving at each of the antennae.

This idealised example cannot, of course, be realised. The Earth will rotate during the propagation of the wavefront between the antennae, the received signals at the separate antennae will have been affected differently by the atmosphere, and the receiving, recording, playback, and timing systems will not be perfect. Consequently a complex model of the baseline-source geometry must be established in order to derive the desired parameters from the observations.

The VLBI observational technique, ignoring for the moment the

effects of Earth rotation and atmospheric refraction, is illustrated in Fig. 2.I. The signal from the source covers a wide frequency bandwidth but the receivers are only capable of accepting a small section of this. This received frequency (RF) is usually chosen to be in the Gigahertz region and is centred about the quoted observing frequency (i.e. a 10.68 GHz observing frequency implies observations of a frequency band centred about 10.68 GHz). It is reduced to an intermediate frequency (IF) in the video band by 'beating' it against a very stable frequency derived from a local oscillator which is phase-locked to an atomic frequency standard. The resultant signal is then recorded on high data rate magnetic tape along with precise timing information provided by a clock which is also controlled by the atomic standard. The tapes from each antenna are transported to a central processing centre where they are played back and the separate data streams are correlated for different constant temporal offsets of the two tapes. The observed delay time, τ, is determined from the known offset of the two tapes, determined from the timing information contained on them, which gives the maximum correlation coefficient.

Each observation may consist of as much as five minutes of recorded data from which a delay time at a specific epoch is deduced. This smoothing over a long period is necessary as the recorded signals include a large proportion of 'noise'. On the assumption that the noise is random, the correlation of the signals should not be too greatly affected if each observation is derived from the recordings over a long enough time interval, although the signal to noise ratio (SNR) will directly affect the quality of the observed data.

The rotation of the Earth is continually changing the delay time and therefore allowance must be made for this effect in the playback

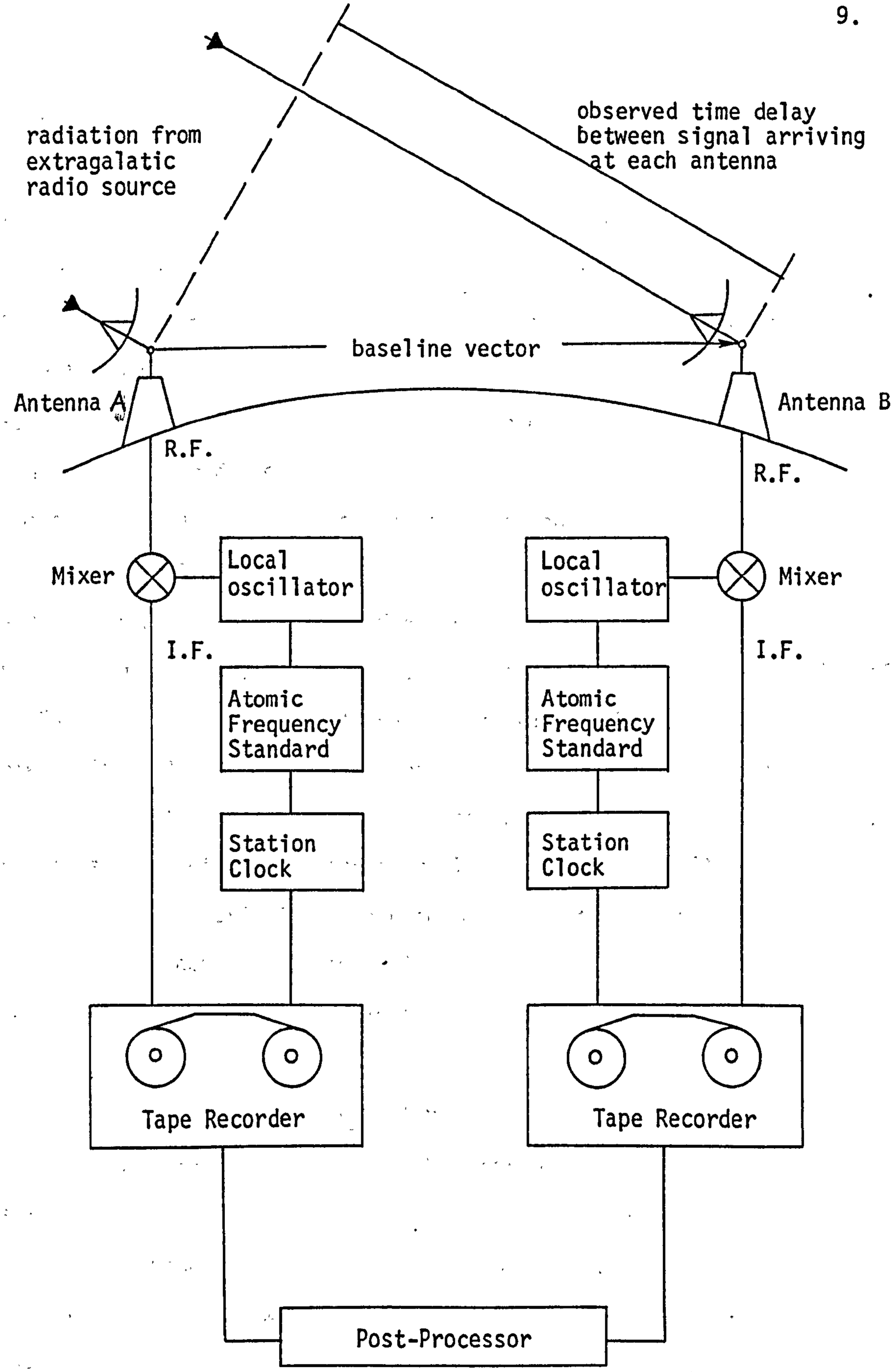

Fig. 2.I Basic VLBI system

and correlation procedures when several minutes of data are used for each observation. This effect also results in a further VLBI observable which is a measure of the rate of change of the delay time, namely the 'delay rate' or 'fringe frequency' observable (see §2.1.4). The absolute synchronisation of the clocks at each station is not critical since the observation of a number of different sources in different areas of the sky enables the offset of the clocks and their inconsistent behaviour to be modelled in the adjustment process (see §2.4.7). Similarly, the effect of errors in the assumed source positions is minimised by solving for all but one of the observed source co-ordinates (see §3.4.3). Other factors affecting the operation of the system are antenna geometry effects (§2.4.1), Earth tides (§2.4.3), the rotation of the Earth during the time between the arrival of the signal at each antenna (§2.4.4), atmospheric refraction (§2.4.5 and §2.4.6), polar motion (§2.2.2), the movement of the source positions with time (§2.3), and the effects of general and special relativity (§2.4.8).

A fuller description of a general VLBI system, together with references and comments on several particular systems including the two from which data has been used in this study, is contained in Chapter 4.

2.1.2 Co-ordinate Reference Systems

The parameters involved in VLBI data reduction are based on several different co-ordinate systems and it is therefore essential to define the relationships and transformations between them.

An antenna reference point will usually be connected to the local national triangulation and its position defined with relation to the geodetic datum (usually an ellipsoid of revolution) of that country. Consequently, it is necessary to define the relative positions,

orientations, and shapes of the different geodetic data upon which the separate antennae are defined. This allows all antennae, irrespective of their geographical location and local geodetic datum, to be defined in the same system, referred to here as the "Average Terrestrial" system (see §2.1.2.1).

Star positions are now conventionally documented in terms of their right ascension and declination at the epoch 1950.0. However, due to the effects of precession and nutation (see §2.3.3 and §2.3.4 respectively) the positions of the celestial equinoxes and celestial poles (Smart, 1977) change with time. Therefore, the star co-ordinates with respect to the equinoxes and poles at the epoch of observation differ from those of the 1950.0 catalogued positions. A corrected position, at epoch t, is known as either the true position of the star referred to the true equinox and equator of date or as its position relative to the true celestial system (see §2.1.2.2).

The polar axes (the polar axis is that axis from the origin in the direction of a defined north pole) of the Average Terrestrial system and the true celestial system are not parallel. The axis of rotation of the Earth is affected by precession and nutation but the mean axis 'wobbles' about the true or instantaneous axis due to other causes, this movement being termed 'polar motion' (see §2.2.2). The displacement of the instantaneous axis of rotation from the mean axis, defined as the Conventional International Origin (CIO) or mean pole of 1900-1905, is computed and documented at 5-day intervals by the Bureau International de l'Heure (BIH). Certain other agencies also compute this data (see §2.2.2) but the BIH results are most commonly used. Parameters defined in the Average Terrestrial system can therefore be transformed into an instantaneous terrestrial system (see §2.1.2.3), whose polar axis is

parallel to that of the true celestial system, by means of the polar motion data. The directions of the equatorial axes of the true celestial system are related to those of the instantaneous terrestrial system by the epoch and hence all the terrestrial and celestial parameters can be related (§2.1.2.3). However, the overall results of the analysis for the Earth-based parameters and the star positions will be in terms of the Average Terrestrial and 1950.0 celestial systems respectively.

2.1.2.1 Terrestrial Co-ordinate Systems

Conventional survey and computational techniques will usually result in the position of a point being specified in terms of its latitude, longitude, and height relative to the appropriate national geodetic datum. This geodetic datum is generally an ellipsoid of revolution whose size, shape, and position will usually be defined so that the reference surface (the surface of the ellipsoid) most closely approximates to the geoid in the area concerned. The geoid is "that equipotential surface of the Earth's attraction and rotation which, on average, coincides with mean sea level in the open ocean" (Bomford, 1975). Consequently, it is necessary that the computed co-ordinates of the reference point of each antenna on its respective local datum be transferred onto a common datum for the ensuing computations.

The definition of a reference ellipsoid requires the choice of eight independent parameters, either implicitly or explicitly. These are that (Bomford, 1975),

(i) the minor axis of the ellipsoid must be parallel to the Earth's mean axis of rotation, the line joining the Earth's geocentre to the Conventional International Origin (CIO) (defines 2 parameters),

(ii) the lengths of the major and minor axes, a_e and b_e, or the major axis and the flattening, a_e and f, of the ellipsoid must be defined (2 parameters),

(iii) the position of the centre of the ellipsoid must be fixed (3 parameters),

(iv) the zero of longitude must be defined, usually taken to be parallel to the Greenwich Mean Astronomic Meridian (GMAM) (1 parameter).

The CIO is the mean position of the pole of rotation between 1900 and 1905 as determined by the definition of the latitude of five observatories of the International Latitude Service (ILS) (see §2.2.2). The GMAM is a plane, parallel to the mean axis of rotation, defined by the weighted mean of the longitudes of 54 observatories as determined by the Bureau International de l'Heure (BIH). It is the meridian of a fictitious mean observatory.

The position of a point, P, on the Earth's surface is specified in terms of the geodetic latitude, longitude, and height above the ellipsoid surface (see Fig. 2.II and Fig. 2.III). The geodetic latitude, ϕ, is the angle between the line passing through P, normal to the reference surface (the geodetic normal), and the equatorial plane (the plane perpendicular to the mean rotation axis and passing through the ellipsoid centre). The geodetic longitude, λ, is the angle between the meridian (the great 'circle' defined by the intersection of the ellipsoidal surface and the plane containing the rotation axis and P) through the point, P, and the zero meridian, i.e. the true Greenwich meridian, measured in the plane of the equator. The latitude and longitude are measured positive northwards and eastwards respectively. The height above the ellipsoid is a combination of the height above the geoid, h,

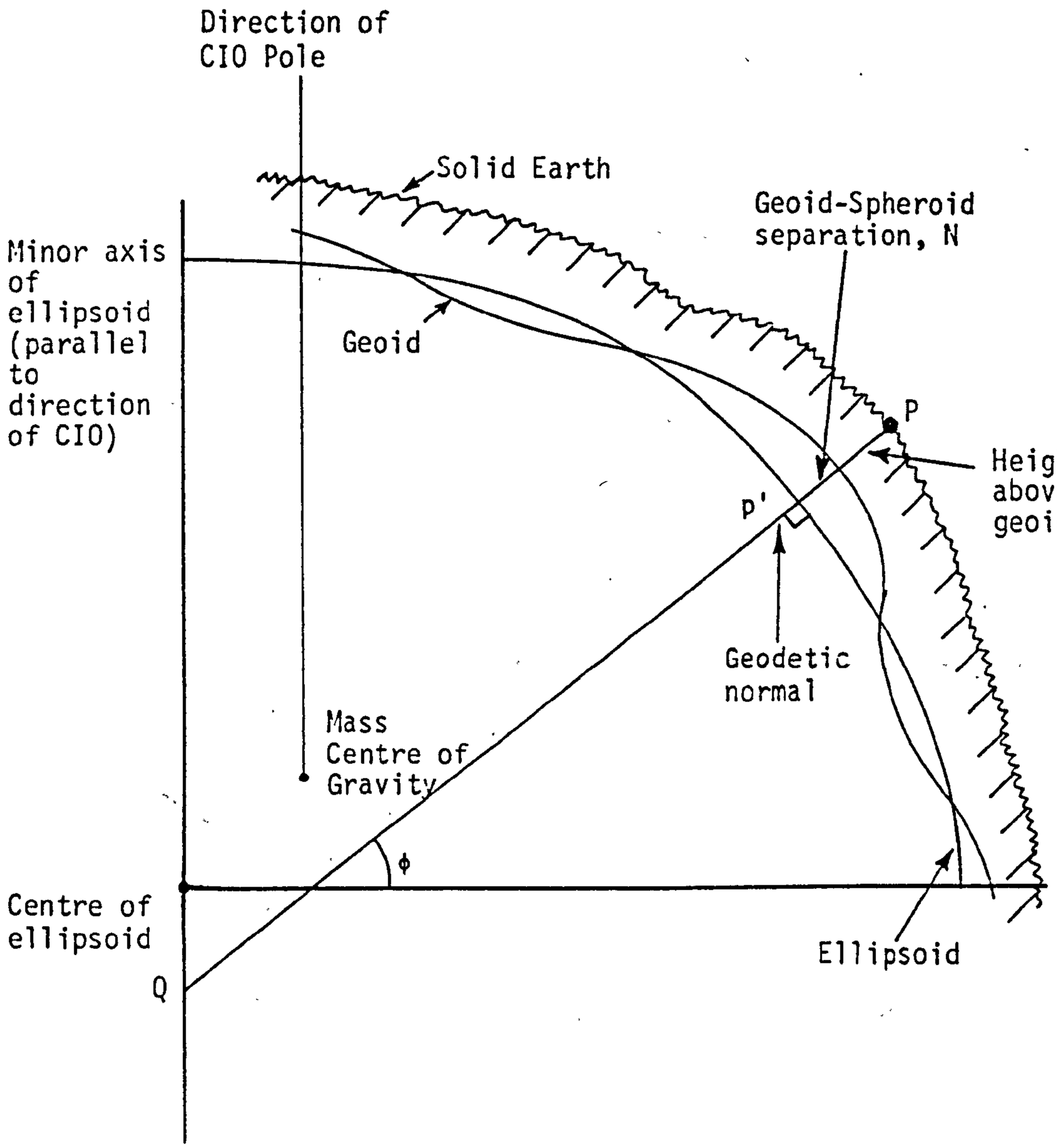

Fig. 2.II Ellipsoidal Reference System illustrated in a meridianal section

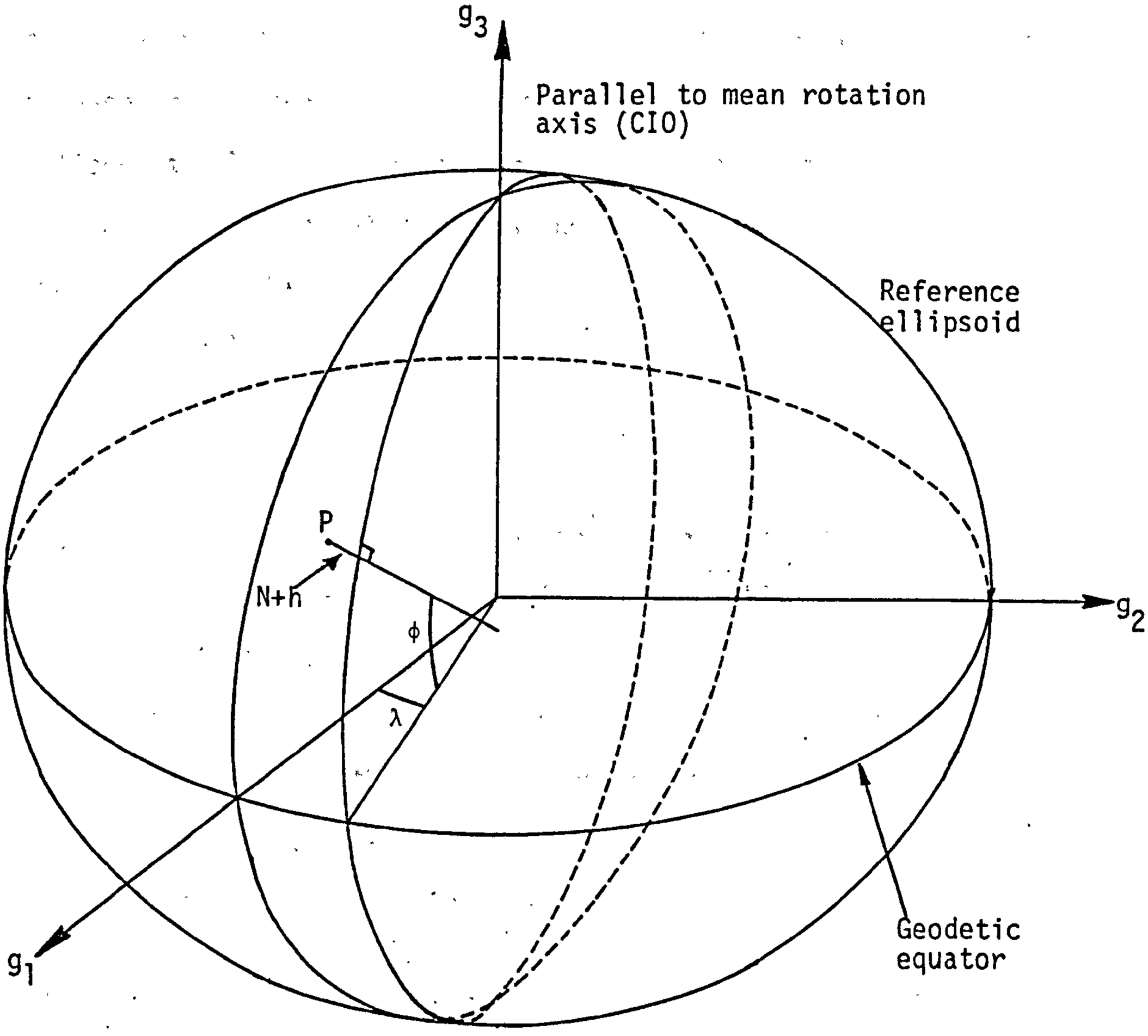

Fig. 2.III The ellipsoid reference system and the cartesian co-ordinate system g_i, i = 1 to 3

and the geoid-spheroid separation, N. The height above the geoid is measured along the plumb line (the line which is perpendicular to the Earth's equipotential surface at P) and not along the geodetic normal but the difference is insignificant for this application (Mueller, 1969). The geoid-spheroid separation can be measured by either astronomical observations, satellite altimetry, or interpolation from existing geoid maps. The accuracy with which it is known varies greatly depending on the country concerned but in the United Kingdom it is typically around the one metre level.

Introducing a cartesian co-ordinate system whose axes are defined as:

g_3 = the line coinciding with the rotation axis of the ellipsoid, and hence parallel to the CIO, positive northwards,

g_1 = the line defined by the intersection of the zero geodetic meridian and the geodetic equator, positive towards Greenwich,

and g_2 = the line forming a right-handed system with g_1 and g_3,

the co-ordinates of a point can be expressed in this system as:

$$\begin{aligned} X_1^g &= (\nu + h)\cos\phi\cos\lambda, \\ X_2^g &= (\nu + h)\cos\phi\sin\lambda, \\ X_3^g &= (\nu(1 - e^2) + h)\sin\lambda, \end{aligned} \tag{2.1}$$

where ν = the transverse radius of curvature, PQ (Fig. 2.II) = $a_e(1 - e^2\sin^2\phi)^{-\frac{1}{2}}$,

and e = the eccentricity of the ellipsoid = $\sqrt{\dfrac{a_e^2 - b_e^2}{a_e^2}}$.

This cartesian co-ordinate system is illustrated in Fig. 2.III. It is

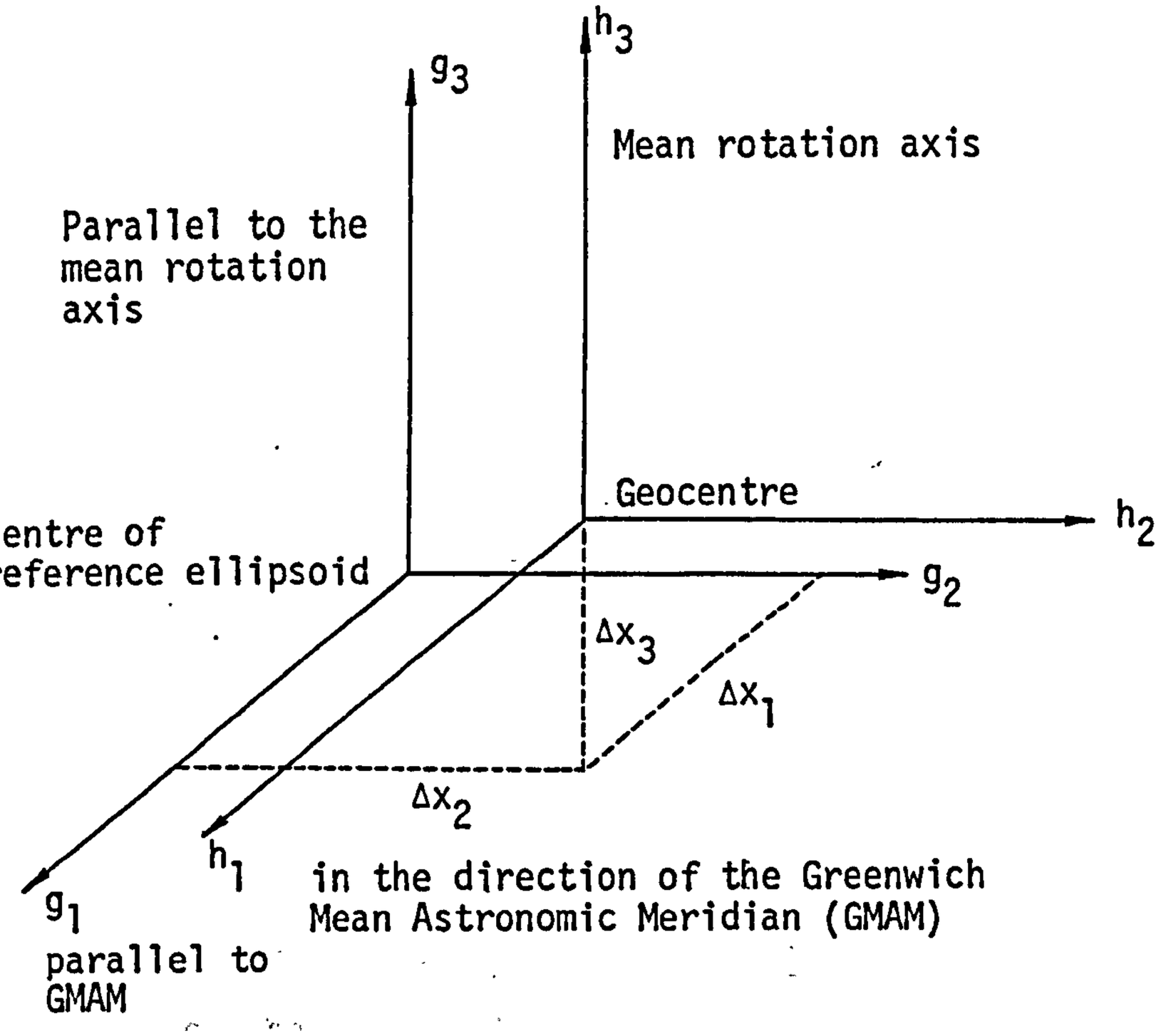

Fig. 2.IV Transformation of g_i, i = 1 to 3, cartesian co-ordinate system into the Average Terrestrial System h_i, i = 1 to 3

now necessary to define the "Average Terrestrial" system whose axes are:

h_3 = collinear with the line joining the geocentre to the CIO (i.e. the mean rotation axis), positive northwards,

h_1 = the line defined by the intersection of the GMAM with the reference equator (the plane perpendicular to the mean rotation axis and passing through the geocentre), positive towards Greenwich

and h_2 = the line forming a right-handed system with h_1 and h_3.

This set of axes will rotate with the Earth.

Clearly, the axes of the co-ordinate systems h_i, i = 1 to 3, and g_i, i = 1 to 3, are parallel and therefore the transformation from one to the other involves only a translation, as shown in Fig. 2.IV. Thus:

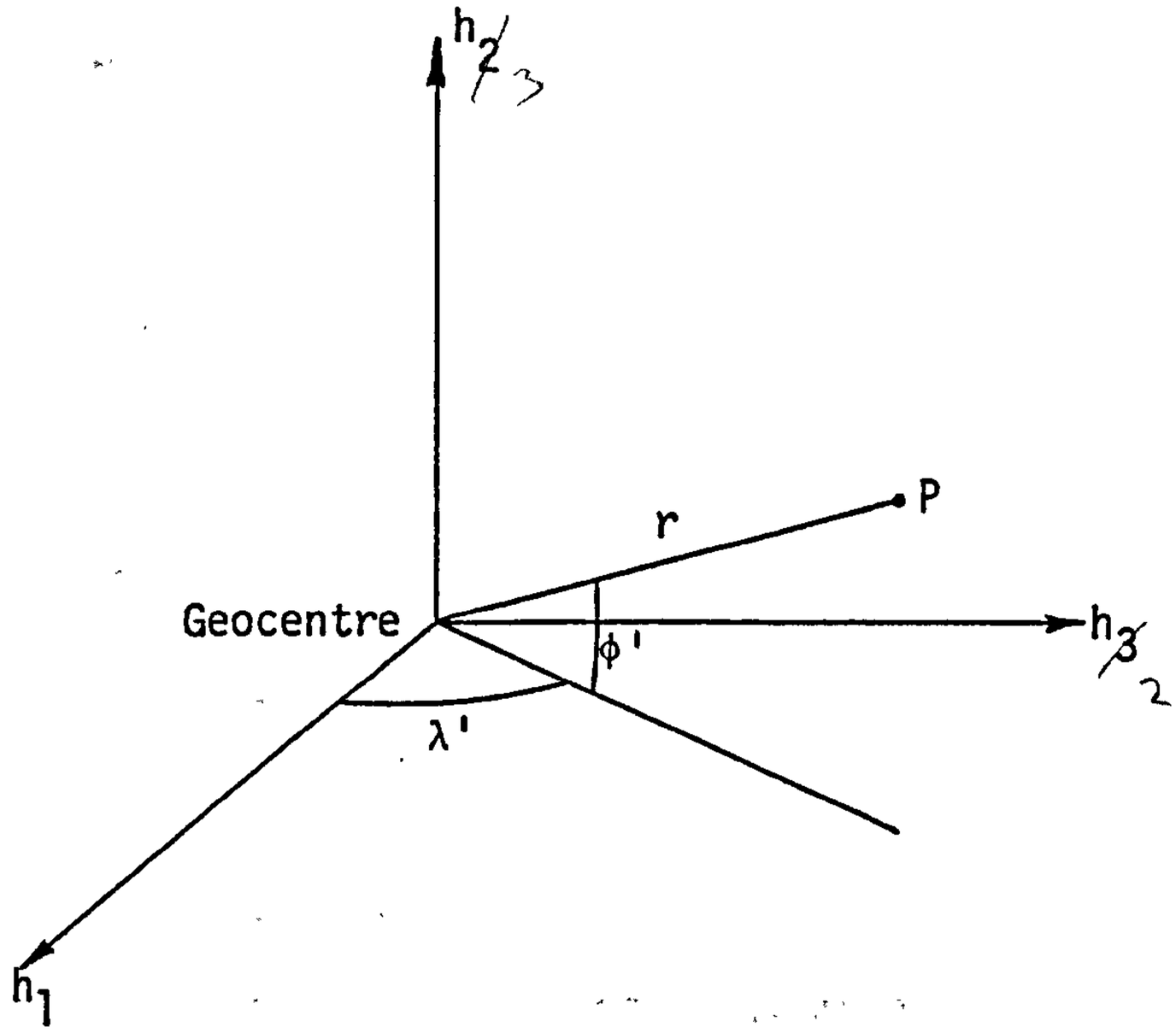

Fig. 2.V Geocentric ellipsoidal co-ordinates on the h_i, i = 1 to 3, system

$$\begin{aligned} X_1^h &= X_1^g + \Delta X_1, \\ X_2^h &= X_2^g + \Delta X_2, \\ X_3^h &= X_3^g + \Delta X_3. \end{aligned} \tag{2.2}$$

It may be that the origin of the local geodetic datum is also at the geocentre in which case ΔX_i, i = 1 to 3, will equal zero. In this case the local datum is known as an absolute reference system. For the most common case when ΔX_i, i = 1 to 3, are not all equal to zero, the local datum is known as a relative reference system. The transformation back from the baseline components obtained in the VLBI analysis, which will be relative to the Average Terrestrial system, to co-ordinates on the appropriate national geodetic data is dealt with in §8.2.1.

It is a common practice in astronomy to express the co-ordinates of a station in terms of its geocentric latitude, ϕ', geocentric longitude, λ', and geocentric radius, r, as shown in Fig. 2.V. The axes of this

system are those previously defined as h_i, i = 1 to 3, and therefore the co-ordinates of the station in this system can be derived from either:

$$\begin{aligned} X_1^h &= r \cos \phi' \cos \lambda', \\ X_2^h &= r \cos \phi' \sin \lambda', \\ X_3^h &= r \sin \phi', \end{aligned} \qquad (2.3)$$

or from (2.2) according to the data available.

2.1.2.2 Celestial Co-ordinate Systems

The fundamental astronomical reference systems are based on the celestial equator and the ecliptic (see Fig. 2.VI). The celestial equator is the circle on the celestial sphere, the sphere of infinite radius having the Sun at its centre and upon which all the stars are assumed to lie, defined by the intersection of the plane perpendicular to the Earth's axis of rotation and passing through the Sun, and the surface of the celestial sphere. The ecliptic plane is the mean plane of the Earth's orbit around the Sun, ignoring short term periodic perturbations. The angle between these two planes is termed the obliquity of the ecliptic, ε. The fundamental reference parameters for angular directions are the equatorial plane and the ascending node of the ecliptic on the equator (known as the 'vernal equinox', 'the equinox', or the 'first point of Aries', and denoted by γ). It is equivalent to the point at which the Sun, on its apparent orbit around the Earth, crosses the equator from north to south.

Star catalogues, referenced to a specific epoch, give the co-ordinates of each star in terms of its right ascension, α_o, and declination, δ_o (see Fig. 2.VI). The right ascension is the angle

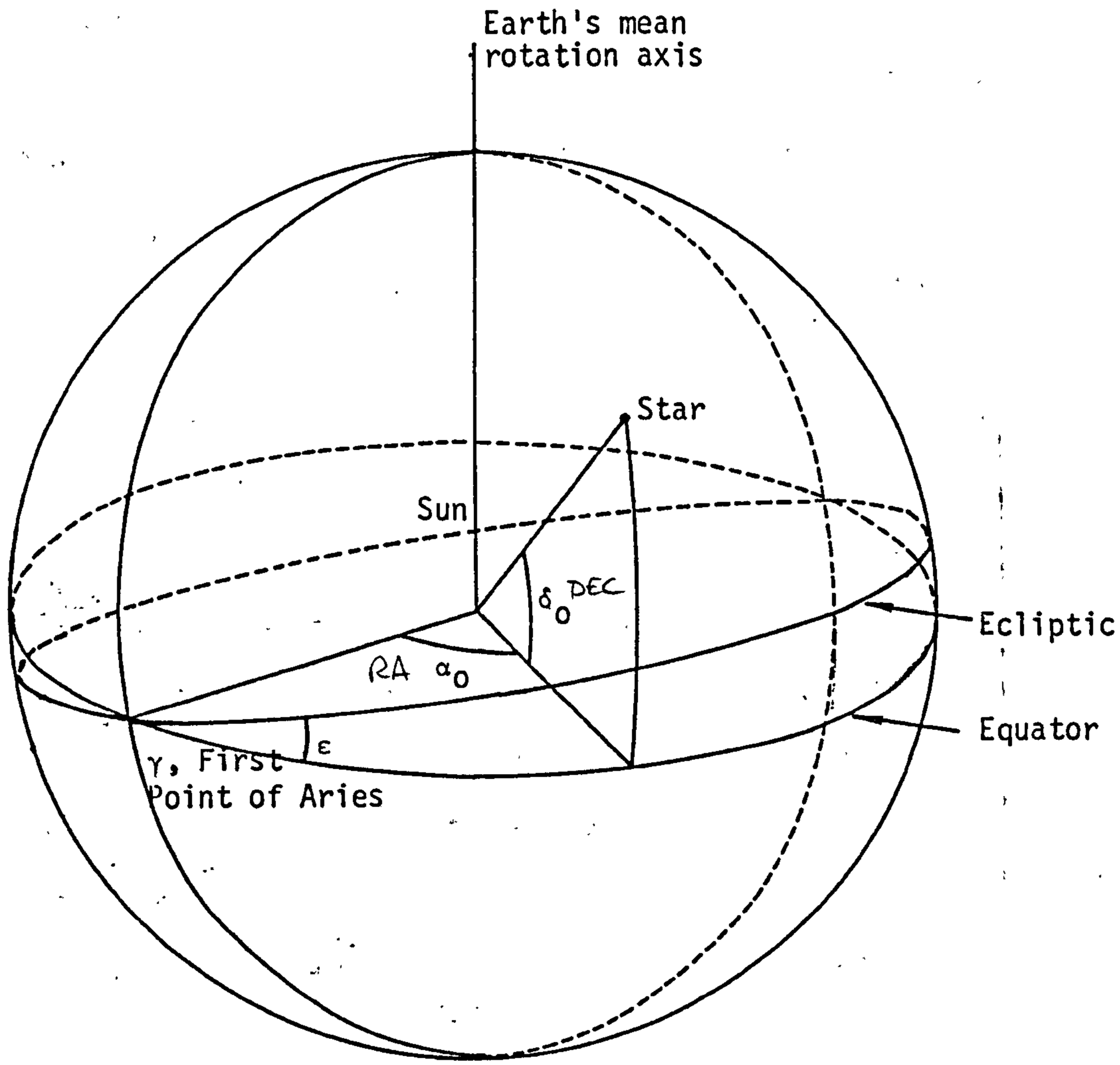

Fig. 2.VI The Celestial Sphere at epoch 1950.0

between the celestial meridians through the star and through the first point of Aries, as measured in the equatorial plane and positive eastwards. The declination is the angle subtended at the celestial centre (the Sun) by the plane of the equator and the direction to the star, measured positive northwards. At the present time, the Fourth Fundamental Catalogue, FK4 (Fricke and Kopff, 1963), is considered to be the catalogue of highest positional accuracy and therefore the one to which others are compared. It contains the positions of 1535 stars at the fundamental epoch 1950.0 (see Appendix A.2) and may contain errors of 0".07 (Bomford, 1975). The co-ordinates of radio sources used in VLBI observations are consequently also referred to the epoch 1950.0 and comparison of star positions derived from VLBI observations to FK4 catalogued positions have shown good agreement (Clark et al, 1976).

The fundamental celestial cartesian co-ordinate system can be defined in terms of the three axes,

f_1 = the line joining the Sun to the mean equinox of the epoch 1950.0,

f_3 = the line joining the Sun to the mean north celestial pole of 1950.0,

and f_2 = the line perpendicular to f_1 and f_3 and forming a right-handed triad.

Mean equinox and mean pole in this context imply the equinox and pole positions have been corrected for the effect of precession only, and not for the effect of nutation (see later). With respect to this system of axes, the unit vector in the direction of a star, $\hat{S}_f$, whose catalogued 1950.0 co-ordinates are α_o and δ_o, is therefore:

$$\hat{S}_f = \begin{bmatrix} \cos \delta_o \times \cos \alpha_o \\ \cos \delta_o \times \sin \alpha_o \\ \sin \delta_o \end{bmatrix} \qquad (2.4)$$

As the centre of the celestial system is the Sun, its displacement from the Earth's geocentre, the origin of the Average Terrestrial system (see §2.1.2.1), should be taken into account. However, this parallax effect is negligible for VLBI sources and hence the vector $\hat{S}_f$ is applicable for a celestial system with the geocentre as its origin as well as for a system with the Sun as its origin (see §2.3.6).

The equator and ecliptic, and hence the equinox, are continually in motion due to the gravitational attraction of the Sun, Moon, and other planets on the Earth. (These effects, known as precession and nutation, are dealt with in §2.3.3 and §2.3.4 respectively.) Consequently, for use in the computations, the unit vector in the direction of the source must firstly be defined in relation to the true equinox and equator of date (i.e. the equator and equinox at the epoch of observation derived from those of 1950.0) by applying corrections for both precession and nutation. The true celestial cartesian co-ordinate system at the epoch of observation therefore has axes defined as:

e_1 = the line joining the geocentre to the true equinox of date,

e_3 = the line perpendicular to the true equator at the desired epoch and passing through the geocentre, positive northwards,

and e_2 = the line perpendicular to both e_1 and e_3 and forming a right-handed system.

Hence, the unit vector representing the true position of a star at a specific epoch and referenced to the cartesian system e_i, i = 1 to 3, is

of the same form as (2.4) but with the true star co-ordinates at the specified epoch replacing the catalogued co-ordinates. This set of axes, unlike the axes of the terrestrial systems defined in §2.1.2.1, will not rotate with the Earth but will remain fixed in space except for the slow movement due to precession and nutation.

2.1.2.3 Instantaneous Co-ordinate System

For use in the computational procedure, an 'instantaneous' cartesian co-ordinate system must be defined which is easily related to the Average Terrestrial system, h_i, i = 1 to 3, and the true celestial system, e_i, i = 1 to 3. The 'instantaneous' co-ordinate system at any epoch has its origin at the geocentre and its axes:

m_3 = in the direction of the instantaneous pole of rotation of the Earth,

m_1 = in the direction on the instantaneous Greenwich zero meridian,

and m_2 = forming a right-handed orthogonal system with m_1 and m_3.

It rotates with the Earth relative to the celestial sphere. All observations are evaluated in this system by transforming all the terrestrial and celestial parameters into it.

The transformation between the true celestial system and the 'instantaneous' system involves only a rotation about the e_3 axis by an amount equal to the Greenwich Apparent Sidereal Time (GAST) (see §2.4.2) at the epoch of observation (see Fig. 2.VII). Thus $\hat{S}_m$, the unit vector in the true direction of the source with respect to the 'instantaneous' system m_i, i = 1 to 3, is given by:

$$\hat{S}_m = \vec{R}\,\hat{S}_e \qquad (2.5)$$

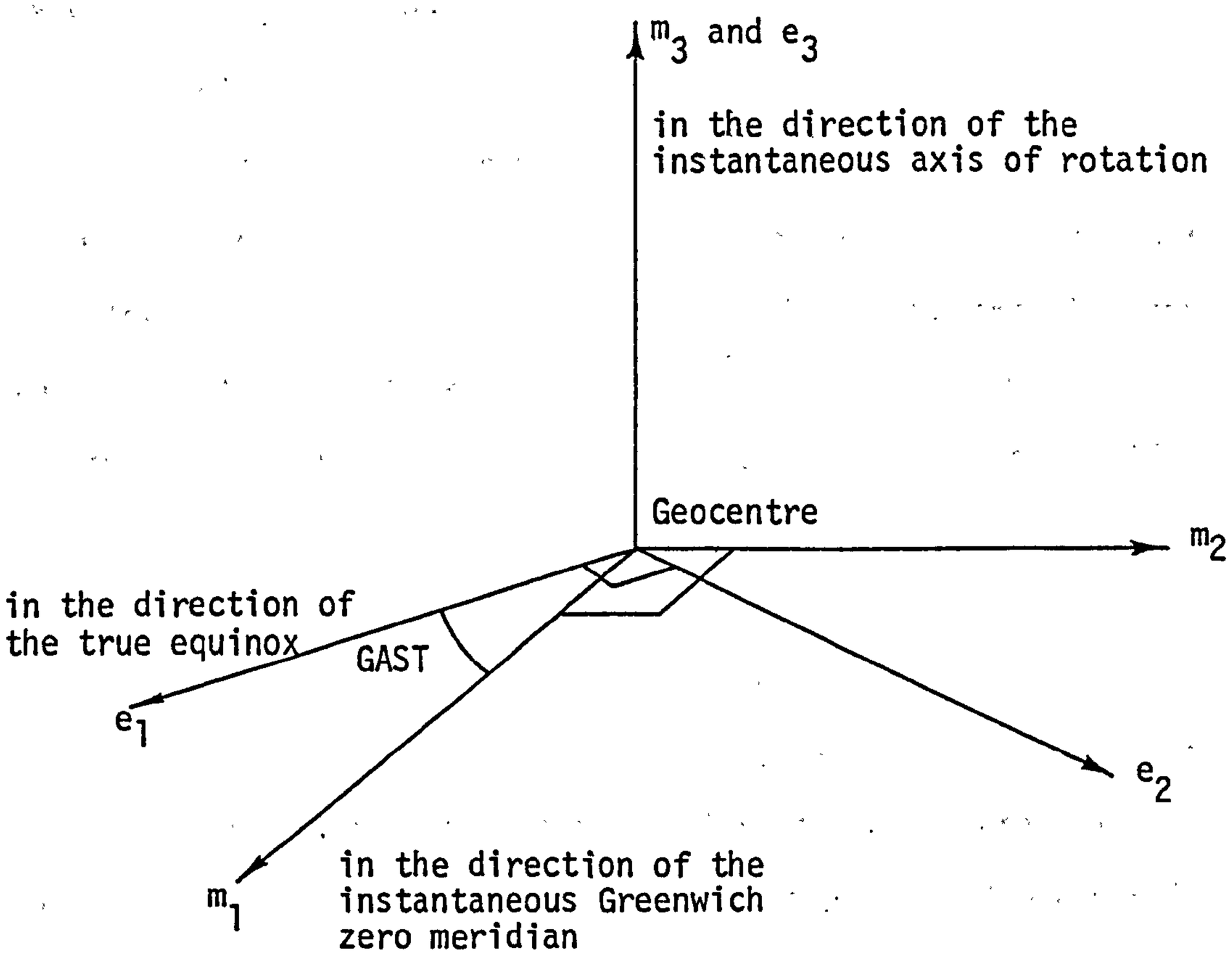

Fig. 2.VII Relationship between the cartesian co-ordinate systems e_i, i = 1 to 3, and m_i, i = 1 to 3

where $\hat{S}_e$ is the unit vector in the true direction of the source in the e_i, i = 1 to 3, system and:

$$\vec{R} = \begin{bmatrix} \cos GAST & \sin GAST & 0 \\ -\sin GAST & \cos GAST & 0 \\ 0 & 0 & 1 \end{bmatrix} \qquad (2.6)$$

This gives

$$\hat{S}_m = \begin{bmatrix} \cos \delta & \cos h \\ -\cos \delta & \sin h \\ & \sin \delta \end{bmatrix} \qquad (2.7)$$

where h = Greenwich Apparent hour angle of the source,

= GAST - α ,

and α and δ are the true right ascension and declination of the star. It must be noted that $\hat{S}_m$ is not the vector to be used in the data adjustment process. The true position of the star must be converted to an "apparent" position with respect to the e_i, i = 1 to 3, co-ordinate system by application of the corrections for aberration (see §2.3.2). The unit vector in the direction of the apparent source, $\hat{S}$, must then be formed and used in the adjustment.

The transformation from the Average Terrestrial system into the 'instantaneous' system is accomplished by two rotations whose magnitudes are equivalent to the displacement, along two orthogonal axes, of the direction of the instantaneous pole with respect to the CIO pole. If $\vec{b}_m$ is the interferometer baseline vector in the 'instantaneous' system and $\vec{b}$ the baseline vector in the Average Terrestrial system, then

$$\vec{b}_m = \vec{W}.\vec{b} \quad , \tag{2.8}$$

where $\vec{W}$ = the 'wobble' or polar motion matrix derived in §2.2.2.

2.1.3 Basic Delay Time Formula

Consider a set of axes (X,Y,Z) which are parallel to those of the 'instantaneous' cartesian co-ordinate system m_i, i = 1 to 3, but whose origin, for convenience, is at the telescope A (Fig. 2.VIII). The direction to the source, $\hat{S}$, is as given in (2.7) and is insignificantly affected by the origin being at telescope A rather than at the geocentre (see §2.3.6). If the Earth is presumed to remain stationary during the propagation of the wavefront from A to B then, considering only the baseline-source geometry, the geometric delay, τ_g, is given by:

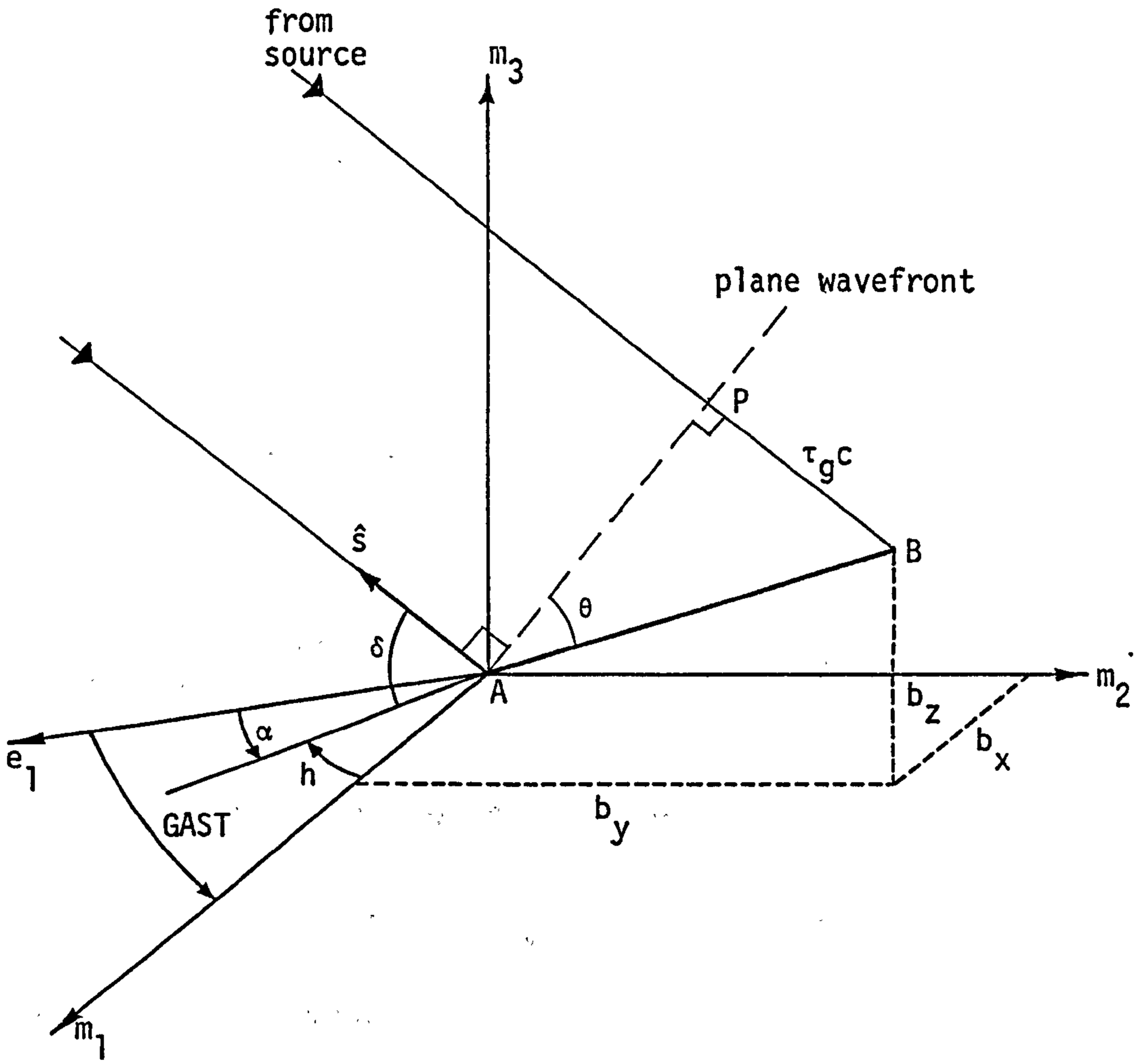

$\vec{b_m}$ or $\vec{AB}$: baseline vector

b_x, b_y, b_z : baseline components

α, δ : right ascension and declination of source

GAST : Grenwich Apparent Sidereal Time of the observation

h : apparent hour angle of source (GAST - α)

c : velocity of microwaves in vacuo

$\hat{s}$: unit vector in the direction of the source

τ_g : the geometric delay

PB or $\tau_g c$: delay distance

Fig. 2.VIII Basic delay geometry

$$\tau_g = \frac{|\vec{b}_m| \sin\theta}{c}, \tag{2.9}$$

and

$$\vec{b}_m.\hat{S} = |\vec{b}_m|\ |\hat{S}|.\cos(90^o + \theta). \tag{2.10}$$

Expanding (2.10) gives:

$$\begin{bmatrix} b_x \\ b_y \\ b_z \end{bmatrix} . \begin{bmatrix} \cos\delta\cos h \\ -\cos\delta\sin h \\ \sin\delta \end{bmatrix} = |\vec{b}_m|\cos(90^o + \theta),$$

$$\Rightarrow \quad -\sin\theta = \frac{(b_x\cos\delta\cos h - b_y\cos\delta\sin h + b_z\sin\delta)}{|\vec{b}_m|} \tag{2.11}$$

Therefore, combining (2.9) and (2.11) gives:

$$\tau_g = \frac{-1}{c}(b_x\cos\delta\cos h - b_y\cos\delta\sin h + b_z\sin\delta). \tag{2.12}$$

Consideration of the definition of the scalar product, $(\vec{a}.\vec{b})$ is the component of the vector $\vec{a}$ in the direction of the vector $\vec{b}$ (Lennox and Chadwick, 1972), (2.12) can be more concisely expressed as:

$$\tau_g = \frac{-\vec{b}_m.\hat{S}}{c} \tag{2.13}$$

Clearly, knowing the values of c and $\hat{S}$ in (2.13) and observing τ_g, the baseline vector b_m can be obtained.

The derivation of this formula implies positive delay for a signal arriving at antenna A before antenna B and therefore the sign of this formula may alter depending on the particular VLBI system. The use of the geocentre as the origin of the co-ordinate system employed in the data reduction procedure will not affect this expression for the geometric delay time as a translation of the origin will not alter the baseline components.

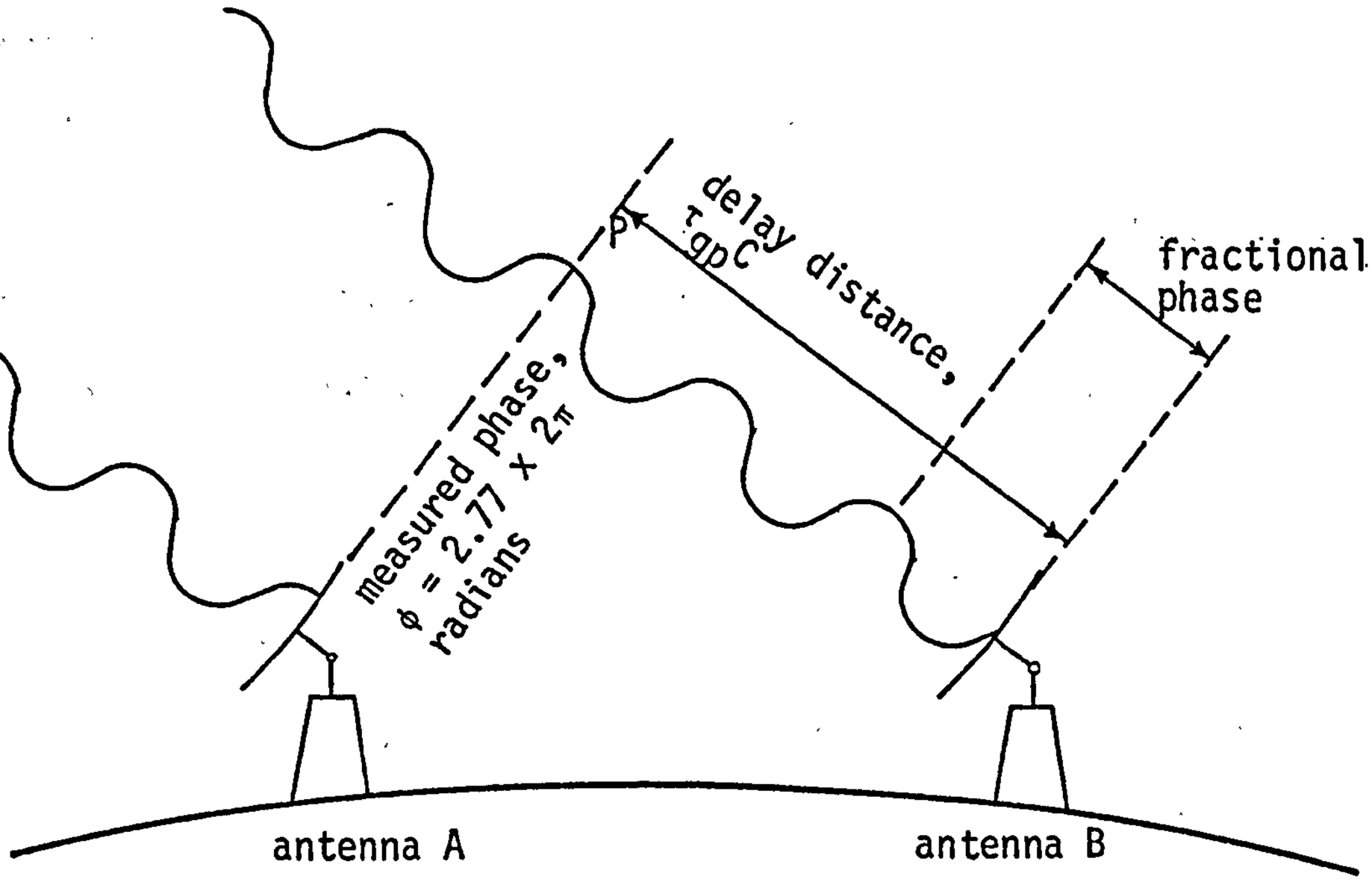

Fig. 2.IX Interferometer phase geometry

2.1.4 Phase, Group Delay, and Fringe Frequency

The delay time equation (2.13) gives the time travelled by a wavefront from a source between it reaching each of two antennae. Assuming this wave to be a pure sine wave, it has a specific wavelength and velocity. Hence the phase in the absence of the atmosphere (i.e. the number of radians travelled by the wave in time τ_g (see Fig. 2.IX, in which the antennae foci are omitted for clarity) is given by:

$$\phi = \frac{2\pi \tau_{gp} c}{\lambda}, \qquad (2.14)$$

where λ = wavelength,

ϕ = phase,

τ_{gp} = phase delay (i.e. the delay time associated with this pure sine wave).

The fractional phase, i.e. the point on the phase cycle at which the wave reaches an antenna, can be measured extremely accurately (2-3^{o}) but

problems exist within the overall system which result in integer-cycle (2π) ambiguities in the determination of the phase and phase delay due to the unknown number of whole wavelengths in the wave transit from P to B (see §4.1.2). These problems chiefly arise due to unknown phase effects caused by local oscillator instability and refraction in the atmosphere, and also due to the correlation process itself. It might be possible to measure phase by continual tracking from an initial epoch at which the phase were known, but any loss of data acquisition could introduce ambiguity. Consequently, phase and phase delay are not used as primary observables except on short baselines, where accurate a priori knowledge serves to eliminate the ambiguity, and in certain other circumstances (see §8.7.3) (Campbell, 1978).

In practice, observations are made over a finite frequency bandwidth and hence the delay measured is the 'group delay', i.e. the delay of a combination of waves of different frequencies and wavelengths. The dispersive nature of the Earth's atmosphere results in the velocity of a signal being dependent on its frequency. The phase velocity of an electromagnetic wave is the velocity of a single frequency pure sine wave such that:

$$V_p = \frac{c}{n},$$

where V_p = phase velocity,

and n = phase refractive index of the medium.

The combination of several waves of different wavelengths, and therefore different velocities, results in the combined wave travelling with a group velocity, V_G, given by (Bomford, 1975),

$$V_G = \frac{c}{n_G},$$

where n_G = group refractive index of the medium.

The group delay is one of the two primary observables in the data analysed in this thesis and hence the remainder of this chapter is specifically designed to be applied to group delay observations. However, in most cases, the derived corrections and formulae apply equally well to phase delay measurements.

Due to the rotation of the Earth, the delay distance, τ_C, is changing F wavelengths of the observing wavelength, λ, in one second. Therefore, the signal received at the antennae is a combination of the observed frequency from the source, ω, and a component due to the Earth's rotation, F. This frequency is known as the 'fringe frequency' or 'fringe rate' and is given by (Jones, 1969):

$$F = \frac{d(\tau_C)}{dt}\Big/_{\lambda} ,$$

$$= \omega . \frac{d\tau}{dt} , \qquad (2.15)$$

which from (2.14) becomes:

$$F = \frac{1}{2\pi}\frac{d\phi}{dt} . \qquad (2.16)$$

Although the absolute phase is very difficult to measure without ambiguity, the changing phase can be measured relatively simply and hence fringe frequency is the second type of primary observable. Fringe frequency is also dependent on many other factors affecting the phase of the interferometer (e.g. changing atmospheric refraction, precession, nutation, clock errors) which are dealt with in §2.5.

In part of the data used here, the 'delay rate', $d\tau/dt$ (the rate of change of delay with respect to time) is employed as an observable instead of the fringe frequency. Equation (2.15) shows the simple relationship connecting these two.

2.2 TERRESTRIAL PARAMETERS AND TRANSFORMATIONS

2.2.1 Baseline Definition

It is clearly necessary to be able to define an antenna reference point to which all baseline solutions can be referred. It is also essential that this reference point be an easily identifiable point on the antenna structure so that conventional survey measurements can be taken to it in order to connect VLBI observations to the local triangulation. Although radio telescopes are usually immense structures this is in fact not a difficult task.

An antenna is steered by means of rotations about two mutually orthogonal axes, one of which remains stationary with respect to the Earth while the other rotates about it. Theoretically, the fixed axis may be in any position but the three usual systems are (Robertson, 1975):

(i) the fixed axis is aligned with the local vertical, termed an altitude-azimuth mount,

(ii) the fixed axis is horizontal, termed an X-Y mount, and

(iii) the fixed axis is in the direction of the Earth's axis of rotation, termed an equatorial mount.

Therefore, for an altitude-azimuth mounted antenna for example, the antenna rotates in a horizontal plane about the fixed vertical (azimuth) axis while the horizontal (elevation) axis rotates around it and controls the angle of elevation of the antenna in the vertical plane.

The definition of the antenna reference point with respect to these axes is again dependent on the individual antenna structure. If the two axes intersect, then the antenna reference point is this point of intersection. If the two axes do not intersect, then the reference point is the intersection of the plane of rotation of the moveable axis with the line of the fixed axis. This is illustrated for an altitude-azimuth

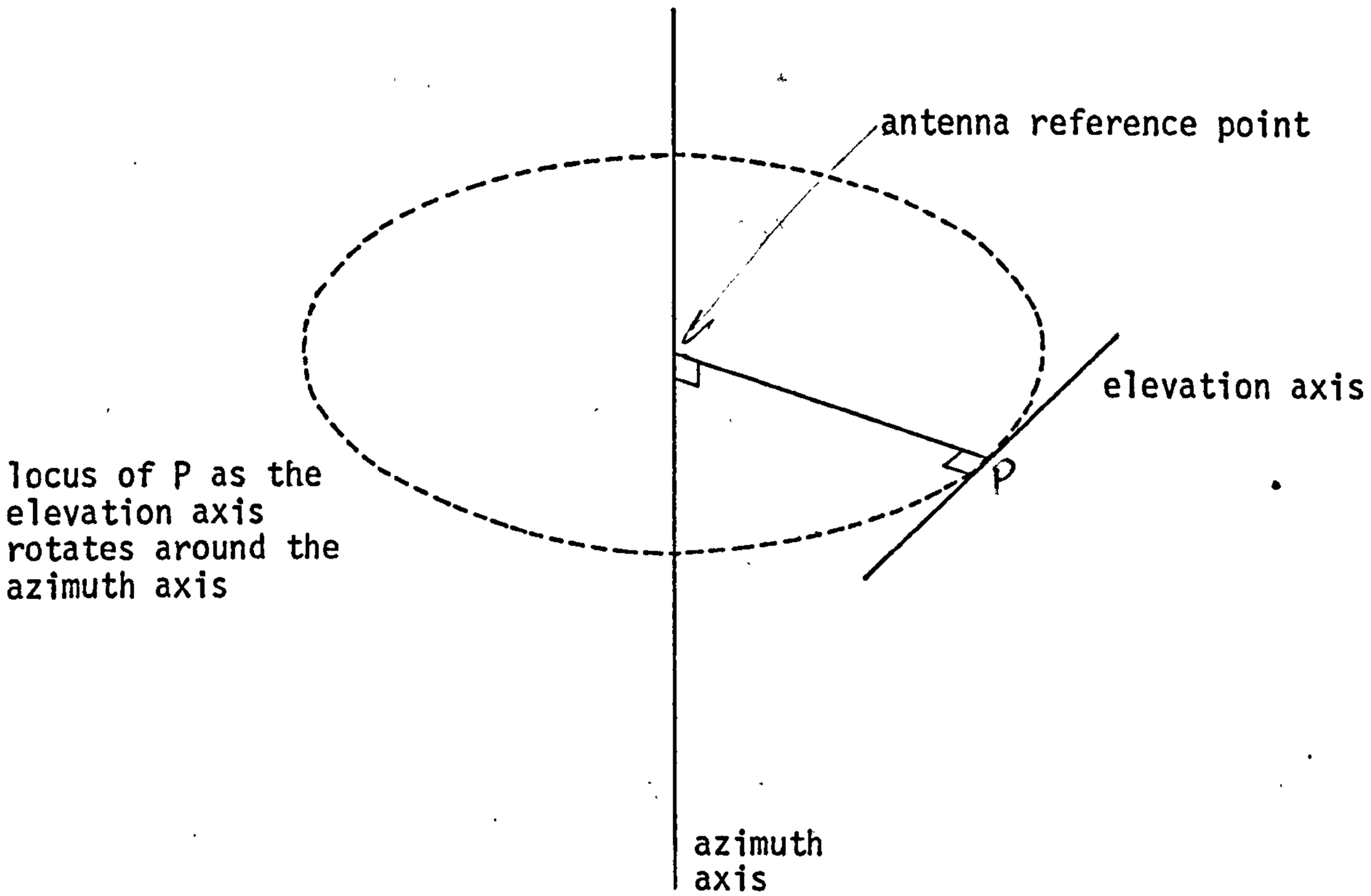

Fig. 2.X Definition of the antenna reference point for an altitude-azimuth mounted antenna with non-intersecting drive axes

mount in Fig. 2.X. The effect on the observations of axes which do not intersect is discussed in §2.4.1 for delay observations and in §2.5.3 for fringe frequency observations.

2.2.2 Polar Motion

The rotation axis of the Earth is affected by precession and nutation and hence, notwithstanding other effects, is defined parallel to the rotation axis of the celestial sphere. However, there is a motion of the Earth relative to its axis of rotation which results in the body of the Earth moving with respect to the rotation axis, this motion being termed 'polar motion'. In other words, if a rigidly mounted telescope on the Earth is pointed in the direction of the CIO,

it will, in principle, remain pointing in the direction of the CIO but its direction with respect to the instantaneous axis will be continuously changing (Bomford, 1975). The movement of the axis can be categorised as follows (Bomford, 1975):

(a) A periodic motion around a mean position with an amplitude between 0".06 and 0".1 and a period of one year. This is presumed to result from meteorological causes.

(b) A periodic motion around a mean position of amplitude between 0".08 and 0".18 and period 14 months. This is known as the Chandler period and is due to the uneven mass distribution within the Earth causing the directions of the principal axis of inertia and the rotation axis to differ slightly.

(c) The movement of the mean position of the pole by 0".2 along meridian 90^{o}W in the last 60 years.

In 1899, the International Latitude Service (ILS) was formed and consisted at that time of six observatories at approximately latitude $39^{o}8'$, namely Misuzawa, Carloforte, Tschardjui, Ukiah, Gaithersburg, and Cincinnati (Henriksen, 1977). This network had the prime purpose of observing the zenith distances of specified stars in order to determine the motion of the actual rotation axis of the Earth with respect to the body of the Earth. The ILS continued this work, with an occasionally changing observing network, until 1962 when the International Polar Motion Service (IPMS) was formed. The IPMS consists of about 50 observatories and includes the five observatories of the ILS that were still observing in 1962. Another organisation, the Bureau International de l'Heure, also computes polar motion data which, together with their computation of UT1 (see §2.4.2 and Appendix A.4), comprises a definition

of the orientation of the Earth in space. The computed data from the BIH is published about one month after observation in the monthly BIH Circular D reports. This data is summarised annually in the BIH Rapport Annuel. The BIH data consists of a combination of IPMS data and data obtained from a number of independent observatories, for example, in 1969 data from 76 observatories was used (Fliegel and Wimberley, 1974). The variability of the rotational behaviour of the Earth makes extrapolation of the Circular D data unreliable and, therefore, for use in space craft navigation the BIH Rapid Service was established (Fliegel and Wimberley, 1974). This service obtains data from about ten of the most reliable observatories and computes UT1 and polar motion data at 3.5 day intervals (as opposed to the Circular D 5-day intervals) and makes this data available soon after observation. The classical method of determining the polar motion involves using the Horrebow-Talcott observation and reduction method on pairs of stars which lie on the same meridian at opposite and equal distances from the zenith (Bomford, 1975 and Henriksen, 1977). The observations are generally made with Visual Zenith Telescopes (VZT's), Photographic Zenith Telescopes (PZT's), and occasionally with Floating Zenith Telescopes (FZT's).

Aside from the BIH and IPMS, the only continuous monitoring and publishing of polar motion data is carried out by the Doppler Polar Motion Service (DPMS) of the United States Department of Defense (DoD). In addition, data is observed and computed intermittently by several other organisations involved in lunar and satellite laser ranging, observations of celestial radio sources (of which VLBI is one such technique), and observations of artificial satellites. §8.3.2 contains a discussion of VLBI as applied to the computation of polar motion (Fanselow et al, 1978).

The position of the instantaneous pole with respect to the CIO is published in the BIH Circular D in terms of a displacement in the direction of an x-axis along the Greenwich meridian and a y-axis along longitude 90^{o}W. These values of the pole position, x_p and y_p, are given in seconds-of-arc and hence represent the direction of the instantaneous axis rather than the position of the instantaneous pole. The values are given to the nearest 0".001 although the precision of each co-ordinate is around 0".01 ($\sim$ 0.3 m) (Henriksen, 1977 and Yumi, 1972). A plot of the motion of the pole during 1977 with respect to these axes is given in Fig. 2.XI.

To reconstruct the baseline geometry existing at the epoch of observation, the a priori baseline components in the Average Terrestrial system, h_i, i = 1 to 3, must be rotated into the instantaneous terrestrial system, m_i, i = 1 to 3, such that:

$$\vec{b}_m = \vec{W}\,\vec{b}.$$

This will result in all the quantities of the baseline-source configuration being relative to either the 'm' or 'e' systems whose polar axes are coincident and whose x and y axes are separated by an angle equivalent to the GAST at the observation epoch (see §2.4.2). This rotation from the Average Terrestrial system to the instantaneous terrestrial system is achieved by a rotation of y_p about the h_1 axis followed by a rotation of x_p about the m_2 axis. In matrix notation this is (see Appendix B):

$$\vec{W} = R_1(y_p)R_2(x_p)\ ,$$

$$= \begin{bmatrix} \cos x_p & \sin x_p \sin y_p & -\sin x_p \cos y_p \\ 0 & \cos y_p & \sin y_p \\ \sin x_p & -\cos x_p \sin y_p & \cos x_p \cos y_p \end{bmatrix} \qquad (2.17)$$

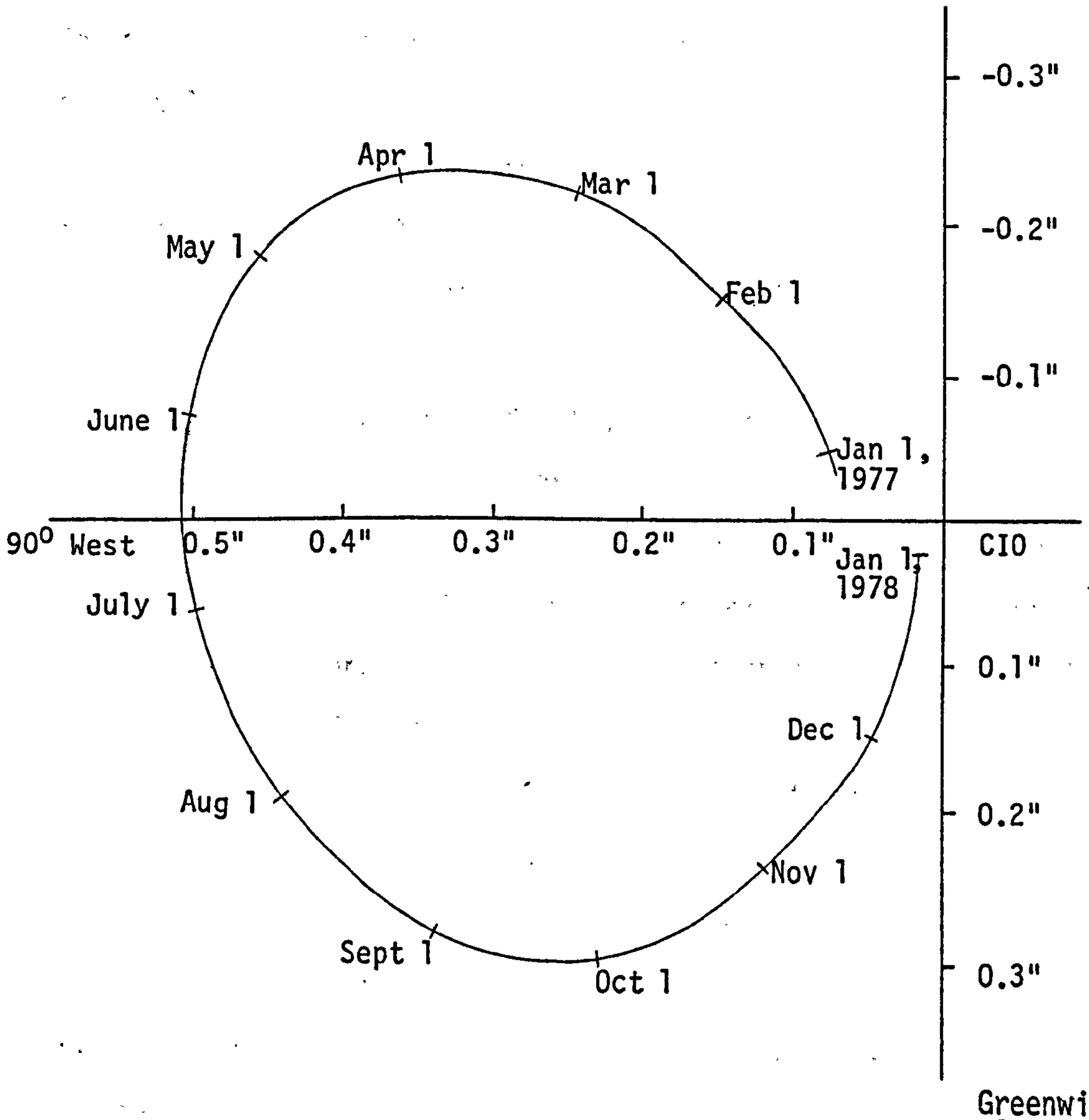

Fig. 2.XI Plot of the motion of the instantaneous pole with respect to the Conventional International Origin for 1977 (from the smoothed values given in the BIH Rapport Annuel, 1977)

2.3 SOURCE POSITIONS AND TRANSFORMATIONS

2.3.1 Introduction

The equatorial and ecliptic planes are continuously in motion in relation to each other due to the gravitational attraction of the Sun, Moon, and the other planets. This motion can be divided into the effects known as 'precession' and 'nutation' (see §2.3.3 and §2.3.4 respectively). Precession is the regular motion of the pole of the equator about the pole of the ecliptic resulting in a westerly motion of the equinox on the equator of about 50".4 per year. Nutation is a short periodic motion of the celestial pole about the precessed, or mean, pole. The mean place of a star is its position with respect to the mean equator and equinox of date, i.e. the equator and equinox of the fundamental epoch (1950.0) corrected for the effect of precession only. The true place of a star is its position with respect to the true equator and equinox of date which are derived from those of the fundamental epoch corrected for both precession and nutation. The apparent position of a star differs from this true position due to the effect of annual aberration (§2.3.2.1). The effects of proper motion of a star (§2.3.5) and parallax (§2.3.6) are negligible for sources used in VLBI. A correction for the effect of diurnal aberration is not required, as it is equivalent to the 'retarded baseline' correction (see §2.4.4), but it is nevertheless described in §2.3.2.2.

The rigorous reduction detailed in the following sections involves the application of corrections for annual aberration, precession, and nutation to the catalogued 1950.0 source co-ordinates in order to give the apparent place of the star at a subsequent epoch. The unit vector in the direction of the apparent source position at epoch t is (Mueller, 1969, and Scott and Hughes, 1964):

$$\hat{S} = \begin{bmatrix} -D \\ C \\ C \tan \varepsilon \end{bmatrix} + NP\, \hat{s}_f \qquad (2.18)$$

where P = the precession matrix,

N = the nutation matrix,

and C and D are the Besselian day numbers at epoch t, ε is the obliquity of the ecliptic at epoch t, and $\hat{s}_f$ is defined in (2.4). This implies that the catalogued co-ordinates are first corrected for precession, then nutation, and then the aberration correction is added.

2.3.2 Aberration

Due to the motion of the Earth and the finite velocity of light, c, an observed source appears to be in a direction slightly displaced from its actual geometric direction. Consider a ray of light emitted from a star at time t and arriving at a point on Earth, moving with a velocity vector $\vec{v}$, at a time $t+\Delta t$ (see Fig. 2.XII). The distance travelled by the light is $c.\Delta t$. The law of aberration states that the apparent direction of the star at epoch $t+\Delta t$, as viewed from antenna A, is in the direction A_oS. In other words, the apparent (observed) direction at time $t+\Delta t$ is the same as the geometric direction at time t if the point A were moving with a constant linear velocity $\vec{v}$ (E.S.A.E., 1977)*. Thus, due to aberration, there is an angular displacement $(\theta-\theta_1)$ between the geometric and observed directions.

Considering the triangle SA_oA in the diagram and applying the sine rule:

$$\frac{\sin A_o\hat{S}A}{\sin S\hat{A}_oA} = \frac{A_oA}{SA},$$

---

* E.S.A.E. is a standard abbreviation for "Explanatory Supplement to the Astronomical Ephemeris".

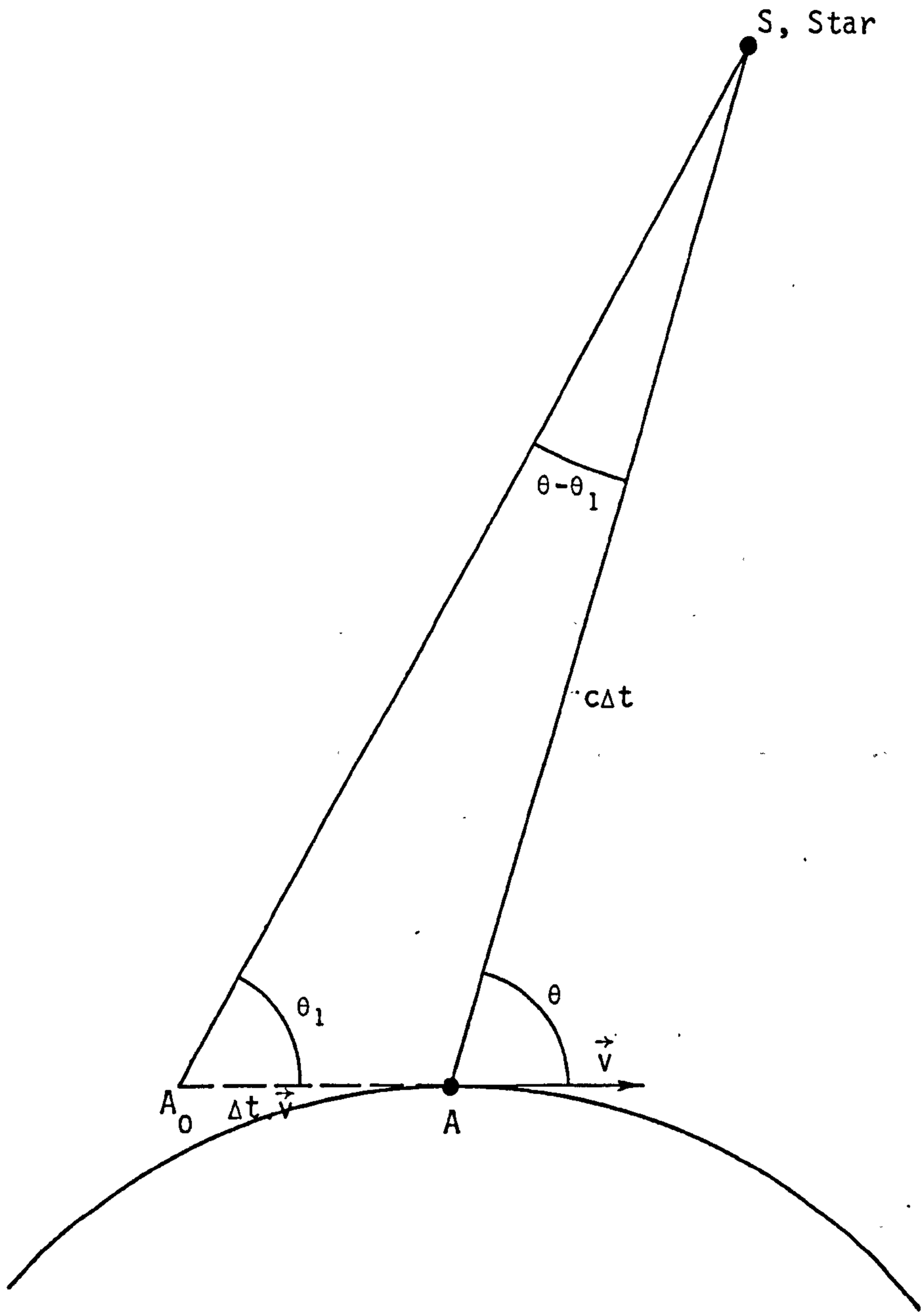

Fig. 2.XII The principle of aberration

$$\Rightarrow \quad \sin(\theta-\theta_1) = \frac{\Delta t|\vec{v}|}{c.\Delta t} \sin \theta_1.$$

$(\theta-\theta_1)$ is small, therefore $\sin(\theta-\theta_1) = (\theta-\theta_1)$ in radians, and hence:

$$(\theta-\theta_1)'' = \frac{V}{C} \sin \theta_1 \text{ cosec } 1'',$$

$$= \kappa \sin \theta_1. \qquad (2.19)$$

κ is defined as the constant of aberration and is currently accepted as 20".496 on the assumption that the Earth's orbit is circular.

The total phenomenon is termed 'stellar aberration' and it can be categorised into three separate effects. Firstly, annual aberration (§2.3.2.1), which is caused by the rotation of the Earth around the Sun; secondly, diurnal aberration (§2.3.2.2) caused by the rotation of the Earth about its own axis, and finally, secular aberration due to the motion of the centre of mass of the solar system in space. The effect of secular aberration is usually unknown and hence is assumed to be implicitly included in the catalogued star positions.

2.3.2.1 Annual Aberration

Annual aberration is the displacement of the observed position of a star from its geometric position due to the rotation of the Earth around the Sun. The apparent position of a source will therefore move on an elliptical path of semi-major axis 20".496, period one year, and with an eccentricity depending on the stars' position, about the geometric position. Fig. 2.XIII illustrates the resultant geometry (assuming the Earth's orbit is circular) where λ_s equals the true celestial longitude of the Sun (Mueller, 1969). Fig. 2.XIV shows the situation on the celestial sphere with the observer, A, at its centre and moving in the direction AF (Mueller, 1969). S is the geometric source position,

Fig. 2.XIII The geometry of annual aberration

S' the apparent source position, $(\theta-\theta_1)$ the angle of aberration, and ϵ the obliquity of the ecliptic as given in (2.31). By the definition of the law of aberration (§2.3.), A, S, S', and F are coplanar. From the spherical triangle SS'T in Fig. 2.XIV (see Appendix E):

$$\begin{aligned} \Delta\alpha &= \alpha' - \alpha = \kappa \sin\theta \cos\psi \sec\delta , \\ \Delta\delta &= \delta' - \delta = -\kappa \sin\theta \sin\psi , \end{aligned} \tag{2.20}$$

where α and δ = geometric right ascension and declination of the source, and α' and δ' = right ascension and declination of the source having corrected for annual aberration.

From the triangle SPF,

$$\begin{aligned} \sin\theta \cos\psi &= \cos\delta_F \sin(\alpha_F - \alpha) , \\ -\sin\theta \sin\psi &= \sin\delta_F \cos\delta - \cos\delta_F \sin\delta \cos(\alpha_F - \alpha), \end{aligned} \tag{2.21}$$

and from triangle FγL;

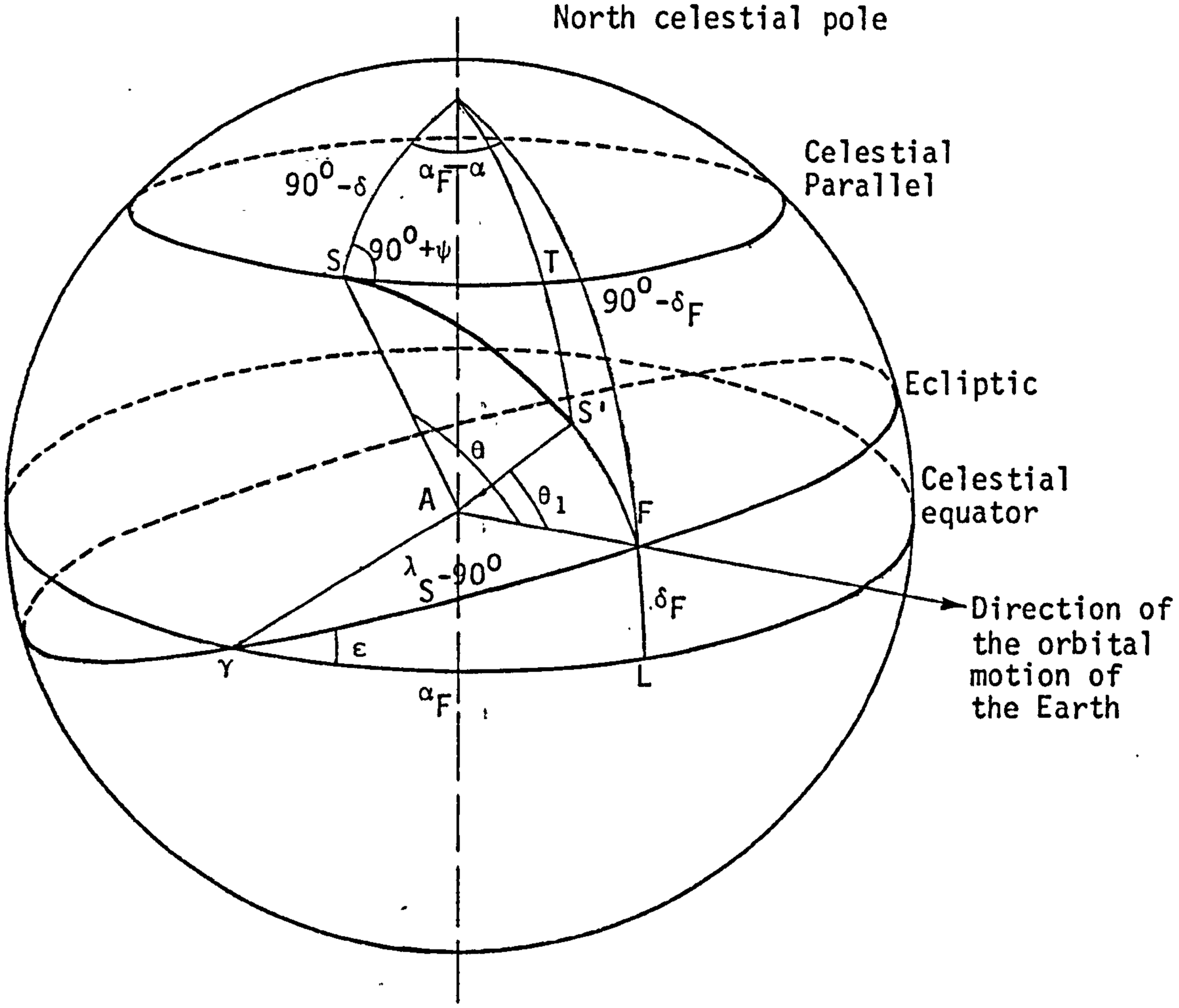

Fig. 2.XIV The effect of annual aberration on an observed star position assuming a circular orbit of the Earth around the Sun

$$\begin{aligned} \sin \lambda_s &= \cos \alpha_F \cos \delta_F , \\ -\cos \lambda_s \sin \varepsilon &= \sin \delta_F , \\ -\cos \lambda_s \cos \varepsilon &= \sin \delta_F \cos \delta_F . \end{aligned} \tag{2.22}$$

Combining equations (2.20), (2.21) and (2.22) yields the corrections to the source co-ordinates due to annual aberration as:

$$\begin{aligned} \Delta\alpha &= -\kappa \sec \delta(\cos \alpha \cos \lambda_s \cos \varepsilon + \sin \alpha \sin \lambda_s), \\ \Delta\delta &= -\kappa(\cos \lambda_s \cos \varepsilon(\tan \varepsilon \cos \delta - \sin \alpha \sin \delta) + \\ &\qquad \cos \alpha \sin \delta \sin \lambda_s). \end{aligned} \tag{2.23}$$

These expressions are simplified by the notation:

$$\begin{aligned} \Delta\alpha &= \alpha' - \alpha = Cc + Dd \\ \Delta\delta &= \delta' - \delta = Cc' + Dd' \end{aligned} \tag{2.24}$$

where $C = -\kappa \cos \varepsilon \cos \lambda_s$,

$D = -\kappa \sin \lambda_s$,

$c = \cos \alpha \sec \delta$,

$d = \sin \alpha \sec \delta$,

$c' = \tan \varepsilon \cos \delta - \sin \alpha \sin \delta$,

and $d' = \cos \alpha \sin \delta$.

C and D are termed the Besselian day numbers, and c, d, c' and d' are termed the star constants.

However, the Earth's orbit around the Sun is not circular but elliptical. This results in further terms of the annual aberration correction, known as the E-terms of elliptical aberration, which depend on the eccentricity, ε, and the longitude of perihelion, π, of the orbit and are of maximum amplitude 0".343. The perihelion is the position at which the Earth is at its closest to the Sun. These terms change very slowly and hence are conventionally included in the catalogued

star position and thus omitted from the annual aberration corrections. Consequently, the annual aberration correction strictly becomes (Mueller, 1969 and E.S.A.E., 1977):

$$\begin{aligned} \Delta\alpha &= Cc + Dd \\ \Delta\delta &= Cc' + Dd' \end{aligned} \qquad (2.25)$$

where c, c', d, d' are as given in (2.24),

$$C = -\kappa \cos\lambda_s \cos\varepsilon - \kappa e \cos\pi \cos\varepsilon,$$

$$D = -\kappa \sin\lambda_s - \kappa e \sin\pi,$$

and e = eccentricity of the orbit.

The elliptic aberration terms can be updated and added to the source co-ordinates to give the apparent co-ordinates.

The Besselian day numbers are quoted in the Astronomical Ephemeris for 0 hours ET for each day and can be interpolated for other epochs. These values are given with respect to the mean equator and equinox of the beginning of the nearest Besselian year. In order to convert these values, and hence the aberration vector in (2.18), to the true equator and equinox of date, the aberration vector formed from the documented data must be multiplied by the matrix B where:

$$B = R_3(-f)R_2(A)R_1(B)$$

and A and B are also Besselian day numbers and f is an "independent day number", all of these being tabulated in the Astronomical Ephemeris.

2.3.2.2 Diurnal Aberration

The diurnal aberration correction accounts for the difference between an observed star position and the geometric star position due to the rotation of the Earth about its own axis. It is not applied in this work in deference to the 'retarded baseline' correction (see §2.4.4).

The corrections to be applied to the source right ascension and declination are (Smart, 1977 and E.S.A.E., 1977):

$$\Delta\alpha = \alpha' - \alpha = 0^{s}.0213\ \rho \cos\phi' \sin h \sin\delta,$$
$$\Delta\delta = \delta' - \delta = 0''.320\ \rho \cos\phi' \cos h \sec\delta, \qquad (2.26)$$

where δ, α = uncorrected star co-ordinates,

δ', α' = corrected star co-ordinates,

ϕ' = geocentric latitude of the observer,

ρ = radius of the Earth at the observer divided by the equatorial radius,

and h = local hour angle of star.

The hour angle, h, is calculated from (Hotter, 1967),

h = Local Apparent Sidereal Time (LAST) - α

where LAST = UT + λ + 9.8565 x UT (hrs) + GAST + ΔE,

UT = Universal Time at the epoch of observation,

λ = observer's longitude,

GAST = Greenwich Apparent Sidereal Time,

and ΔE = the equation of the equinoxes, the right ascension of the mean equinox referred to the true equator and equinox.

2.3.3 Precession

General precession is the combination of luni-solar precession, the smooth long period motion of the pole of the equator around the pole of the ecliptic caused by the gravitational attraction of the Sun and Moon on the Earth's equatorial bulge, and planetary precession, the slow rotation of the ecliptic about a slowly moving diameter due to the gravitational effect of the planets on the Earth.

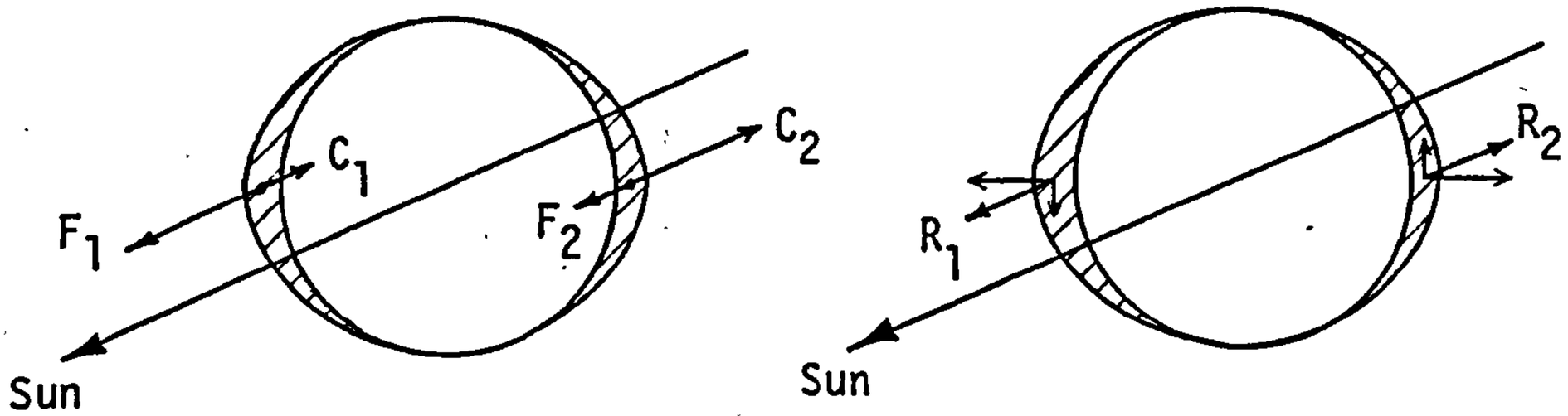

Fig. 2.XV The theory of luni-solar precession

Luni-solar precession rotates the mean celestial pole around the ecliptic pole with a period of about 25,800 years and amplitude of approximately 23.5^{o} (the obliquity of the ecliptic). This causes a westerly motion of the equinox, the origin of right ascension of the celestial system, of about 50."3 per annum. To illustrate this effect, the sun exerts an attractive force on the Earth's equatorial bulge as shown in Fig. 2.XV, where $F_1 > F_2$ (Mueller, 1969). The centrifugal forces, c_1 and c_2 ($c_1 < c_2$), generated on the equatorial bulge due to the rotation of the Earth around the Sun, combine with the forces F_1 and F_2 to give resultant forces, R_1 and R_2, as illustrated. The components of these resultant forces in the direction perpendicular to the equator exert a turning moment which attempts to rotate the equator towards the ecliptic. The combination of this turning moment and the rotational momentum of the Earth causes the characteristic precessional motion of the Earth's pole about the ecliptic pole.

The planetary precession is a much smaller effect resulting in the westerly motion of the equinox and a decrease in the obliquity of the ecliptic of 0".125 and 0".47 per annum respectively.

The precession as a whole is specified by the three angles ζ_0, z,

and θ. Referring to Fig. 2.XVI where t_o is the initial epoch (here 1950.0) and t is the subsequent epoch of observation, the three precession angles are defined as:

$90^o - \zeta_o$ = right ascension of the ascending mode of the equator of epoch t on the equator of t_o, referred to the equinox of t_o,

$90^o + z$ = right ascension of the ascending node of the equator of epoch t on the equator of t_o, referred to the equinox of t,

and θ = inclination of the equator of t_o to that of t_o.

From constants derived by Newcomb, the expressions for these three angles are (E.S.A.E. , 1977):

$$\begin{aligned} \zeta_o &= (2304".250 + 1".396\ T_o)T + 0".302T^2 + 0".018T^3, \\ z &= \zeta_o + 0".791T^2 + 0".001T^3, \\ \theta &= (2004".682 - 0".853T_o)T - 0".426T^2 - 0.042T^3, \end{aligned} \tag{2.27}$$

where the initial epoch is $1900.0 + T_o$ and the final epoch is $1900.0 + T_o + T$ and T_o and T are measured in tropical centuries (see Appendix A.6.1).

The rotation matrix to transform co-ordinates in the 1950.0 system to the mean celestial system of date is (Mueller, 1969):

$$P = R_3(-90^o - z)R_1(\theta)R_3(90^o - \zeta_o) \tag{2.28}$$

where $R_i(\alpha)$ represents an anticlockwise rotation of α about the i^{th} axis when viewed towards the origin from the positive end of that axis (see Appendix B). Therefore, the elements of the precession matrix in conventional notation are:

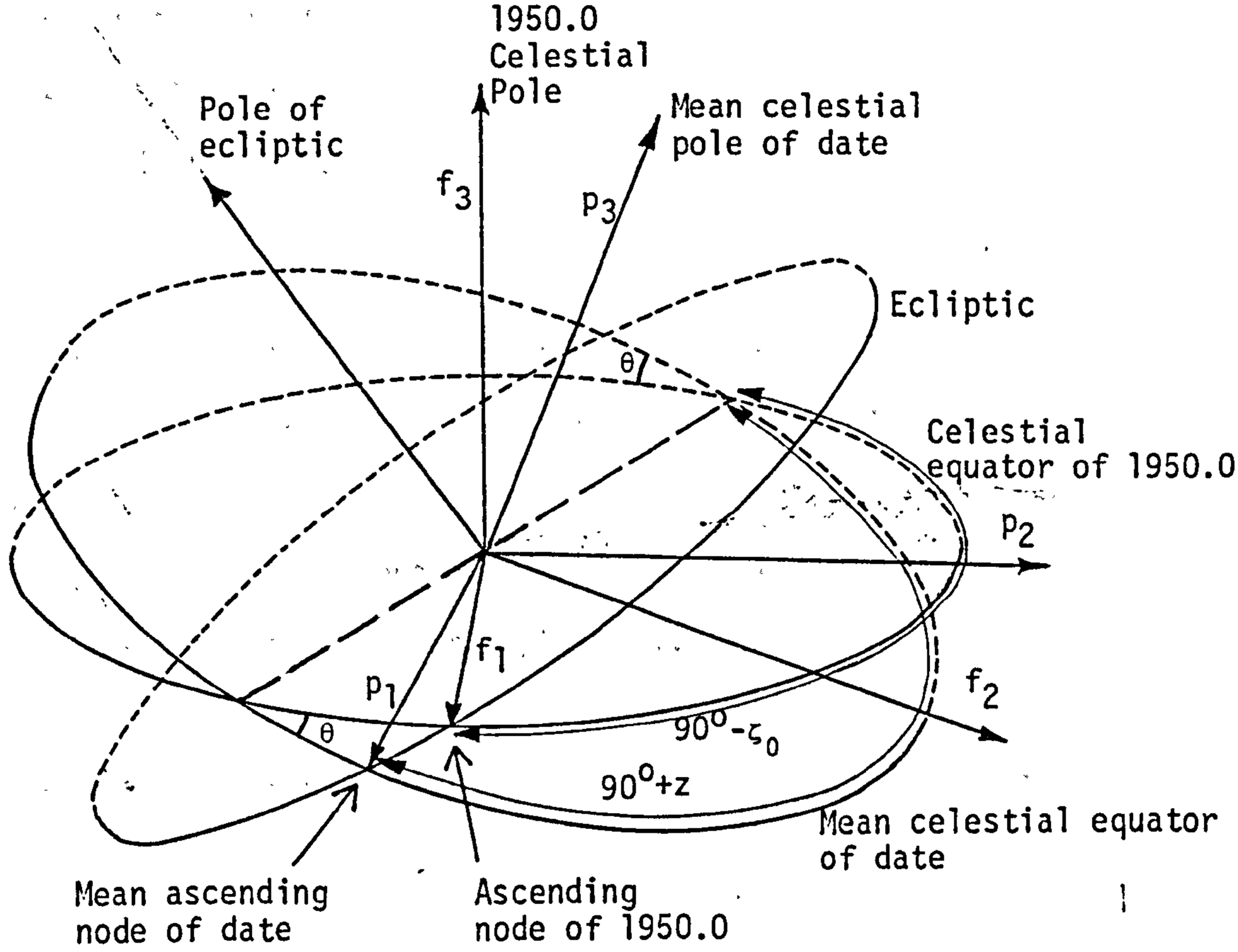

Fig. 2.XVI The definition of the precession angles ζ_0, z, and θ

$$
\begin{aligned}
p_{11} &= -\sin z \sin \zeta_o + \cos z \cos \theta \cos \zeta_o \,, \\
p_{12} &= -\sin z \cos \zeta_o - \cos z \cos \theta \sin \zeta_o \,, \\
p_{13} &= -\cos z \sin \theta, \\
p_{21} &= \cos z \sin \zeta_o + \sin z \cos \theta \cos \zeta_o \,, \\
p_{22} &= \cos z \cos \zeta_o - \sin z \cos \theta \sin \zeta_o \,, \\
p_{23} &= -\sin \theta \sin z \,, \\
p_{31} &= \cos \zeta_o \sin \theta, \\
p_{32} &= -\sin \theta \sin \zeta_o \,, \\
p_{33} &= \cos \theta.
\end{aligned} \tag{2.29}
$$

Newcomb's observationally determined value for the speed of general precession in longitude at the epoch 1950.0 of 5025".64 per tropical century is well known to be too low. However, it has been retained to provide computational continuity and internal consistency in the system of astronomical constants (Langley, 1979). The uncertainty in this value is between +1".3 and 0".0 (Melbourne et al, 1968), the upper value resulting in uncertainties in the precession angles of:

$$
\begin{aligned}
e(\zeta_o) &= 0".60T, \\
e(z) &= 0".60T, \\
\text{and} \quad e(\theta) &= 0".52T.
\end{aligned}
$$

2.3.4 Nutation

Astronomical nutation is the irregular elliptical motion of the true pole about the mean pole in a period of about 19 years and with an amplitude of approximately 9". The four dominant causes of the nutation are (Cannon, 1978):

(i) The precession of the plane of the lunar orbit with a period of 18.6 years (6789 days),

(ii) the eccentricity of the Earth's orbit, which has a period of 265 days,

(iii) the disappearance of the solar gravitational torque every 6 months (183 days) when the Sun crosses the equinoxes,

and (ix) the eccentricity of the lunar orbit, which has a period of 27.6 days.

The nutation is specified in terms of $\Delta\varepsilon$, the nutation in obliquity, and $\Delta\psi$, the nutation in longitude, as illustrated in Fig. 2.XVII where the axes e_i, i = 1 to 3, are those of the true celestial system as described in §2.1.2.2 and p_i, i = 1 to 3, are the axes of the mean celestial system of date. The theory upon which the present method for the calculation of the nutation is based can be found in Woolard (1953) and the numerical series for computing $\Delta\varepsilon$ and $\Delta\psi$ are tabulated in Appendix C (E.S.A.E., 1977).

From the diagram, the rigorous transformation necessary to transform a mean star position to its true position involves a rotation through the mean obliquity of the ecliptic, ε, about the mean equinoctial line (p_1 axis) followed by a negative rotation through the nutation in longitude, $-\Delta\psi$, about the mean ecliptic pole and, finally, a negative rotation through the true obliquity of the ecliptic, $-(\varepsilon+\Delta\varepsilon)$, about the true equinoctial line (e_1 axis). In matrix notation:

$$N = R_1(-\varepsilon-\Delta\varepsilon)R_3(-\Delta\psi)R_1(\varepsilon) \qquad (2.30)$$

where $\varepsilon = 23^{\circ}.452294 - 0^{\circ}.0130125T - 0^{\circ}.00000164T^2 + 0^{\circ}.000000503T^3$ (2.31)

with T measured in either tropical or Julian centuries since epoch 1900 January 0.5 ET (Julian Day 2415020.0) (see Appendix A.6.2).

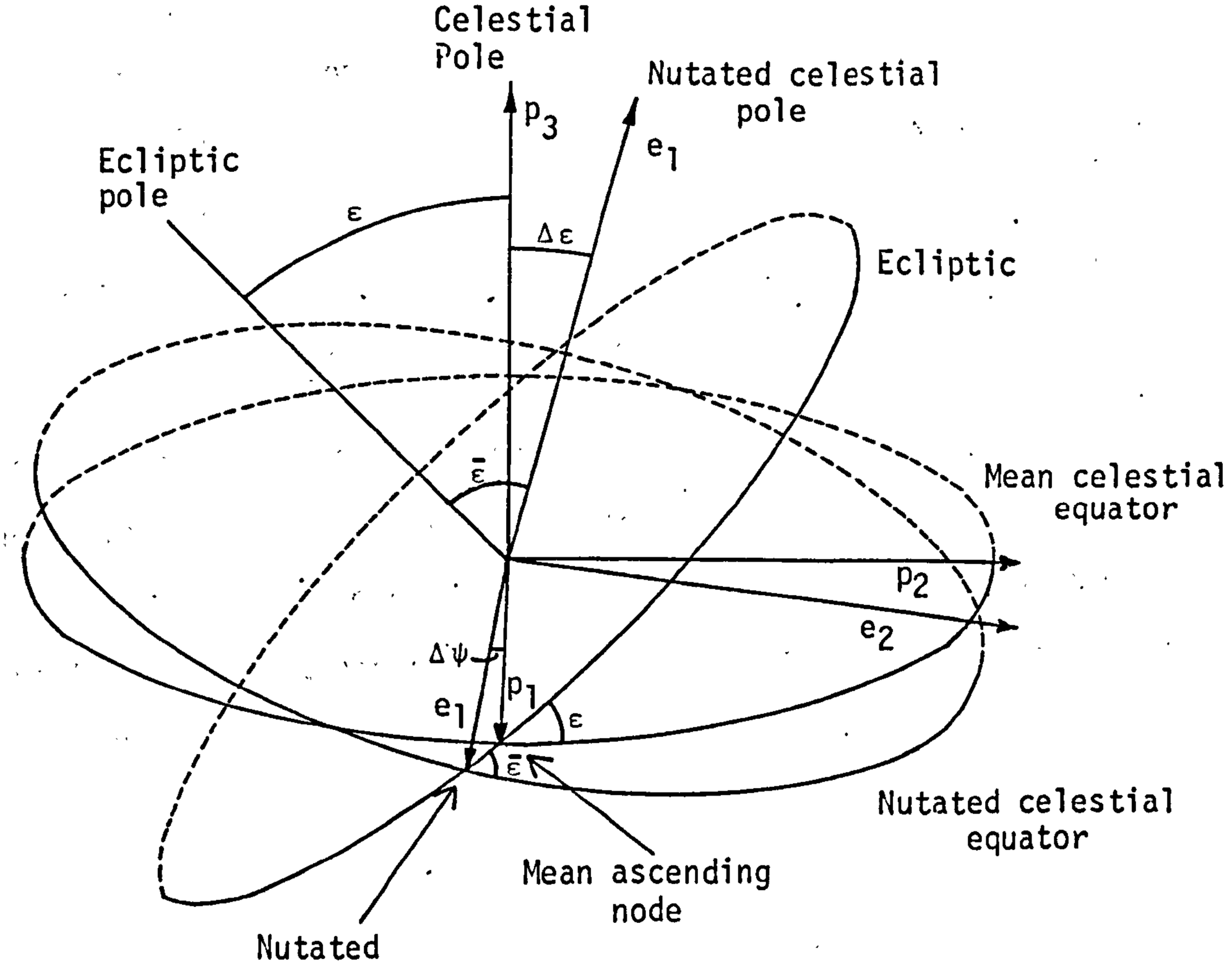

Fig. 2.XVII The definition of the nutation angles $\Delta\varepsilon$ and $\Delta\psi$

With $\bar{\varepsilon} = \varepsilon + \Delta\varepsilon$, expansion of (2.30) gives:

$$
\begin{aligned}
n_{11} &= \cos \Delta\psi, \\
n_{12} &= -\sin \Delta\psi \cos \varepsilon, \\
n_{13} &= -\sin \varepsilon \sin \Delta\psi, \\
n_{21} &= \sin \Delta\psi \cos \bar{\varepsilon}, \\
n_{22} &= \cos \bar{\varepsilon} \cos \varepsilon \cos \Delta\psi + \sin \bar{\varepsilon} \sin \varepsilon, \\
n_{23} &= \cos \bar{\varepsilon} \sin \varepsilon \cos \Delta\psi - \sin \bar{\varepsilon} \cos \varepsilon, \\
n_{31} &= \sin \bar{\varepsilon} \sin \Delta\psi, \\
n_{32} &= \sin \bar{\varepsilon} \cos \varepsilon \cos \Delta\psi - \cos \bar{\varepsilon} \sin \varepsilon, \\
n_{33} &= \sin \bar{\varepsilon} \sin \varepsilon \cos \Delta\psi + \cos \bar{\varepsilon} \cos \varepsilon.
\end{aligned}
\qquad (2.32)
$$

The components of $\vec{N}$ have a level of uncertainty around the 0".01 level due to the fluidity of the Earth's core, the elasticity of the Earth, the errors in the lunar theory used in the determination of the expansions for $\delta\varepsilon$ and $\delta\psi$, and the empirical nature of the determination of these expressions.

2.3.5 Proper Motion and Source Structure

The proper motion of a star is the angle, μ, subtended at the Sun and measured in arcseconds, through which the star moves in one year (Smart, 1977). Referring to Fig. 2.XVIII, the cartesian co-ordinates of a star, with respect to the f_i, i = 1 to 3, system described in §2.1.2.2, corrected for the effect of proper motion are (Hotter, 1967):

$$\hat{S}_p = \hat{S}_f + \vec{\dot{U}}T,$$

where $\hat{S}_f$ = unit vector in the direction of the catalogued star position as given in (2.4),

$\hat{S}_p = \hat{S}_f$ corrected for the effect of proper motion of the star,

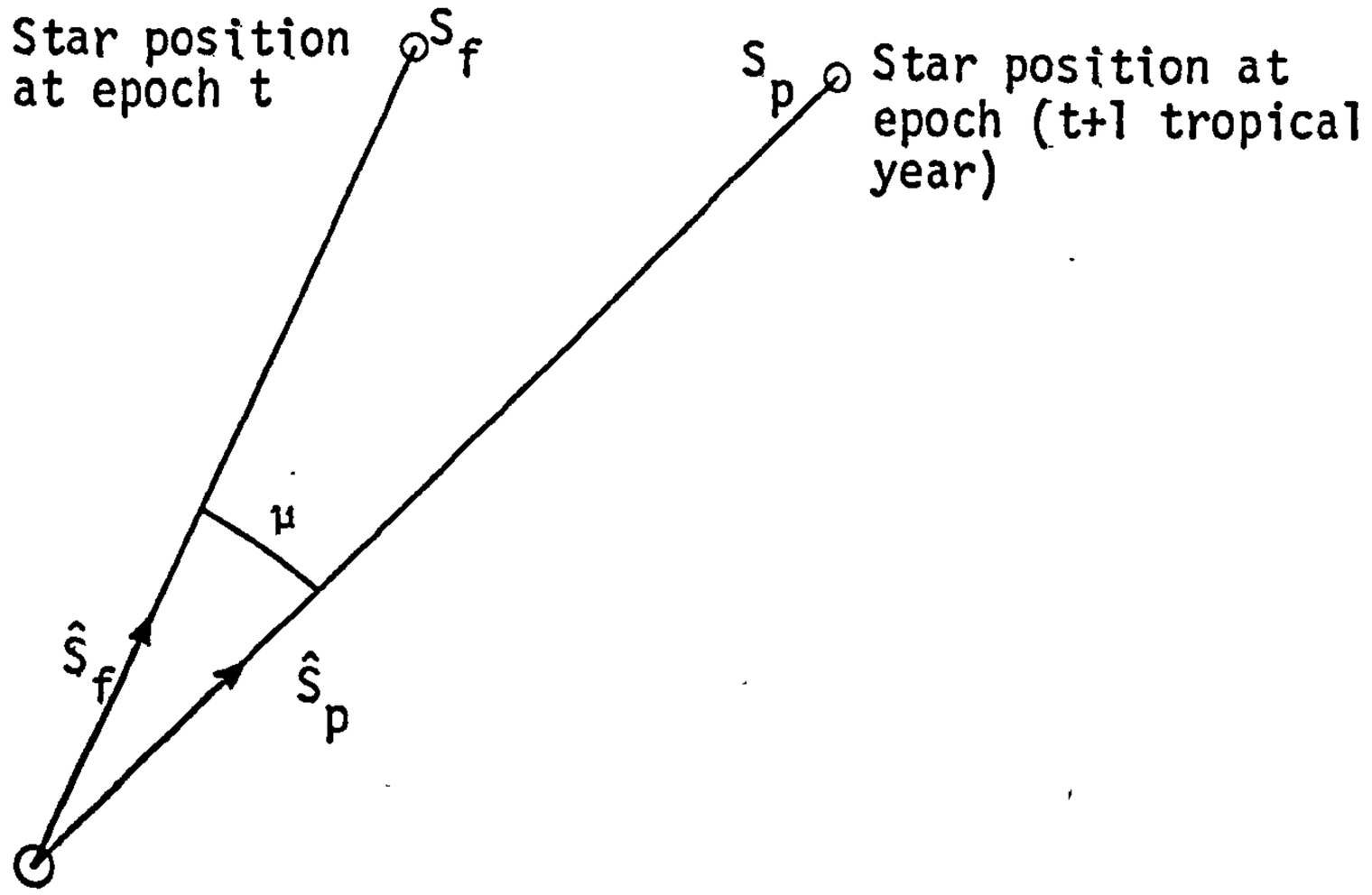

Fig. 2.XVIII The effect of proper motion on a star position

$$\vec{U} = \begin{bmatrix} \dot{\mu}_1 & \ddot{\mu}_1 \\ \dot{\mu}_2 & \ddot{\mu}_2 \\ \dot{\mu}_3 & \ddot{\mu}_3 \end{bmatrix}$$ ($\dot{\mu}_i$ and μ_i are the components of the velocity and acceleration of the star respectively),

and $$T = \begin{bmatrix} t \\ \frac{1}{2}t^2 \end{bmatrix}$$ (t is the elapsed time since the calaloguing epoch).

The values of $\dot{\mu}_i$, $\ddot{\mu}_i$, and t must be in compatible units.

For the extragalactic sources used in VLBI experiments this correction is expected to be less than 0".001 per century and is therefore not applied here. Clearly, the effect of proper motion of a source during observation is also ignored. Observations in the United States of close source pairs have yielded an upper limit of 0.0005 arcsec/year on their relative proper motion (Shapiro, 1976).

Although the theory presented here assumes that the observed quasars are 'point' sources, they have in fact an angular size of the order of milliarcseconds. The centre of brightness of a source may be in continual motion within the area of the source and hence it may appear

in a different place at different times and when viewed by different baselines. Changes in the brightness structure of the order of tenths of a milliarcsecond have been observed (Shapiro, 1978) and consequently an attempt is being made to calibrate the effect of source structure on the observations (Ryan et al, 1977)

2.3.6 Parallax

The unit vector in the true direction of the source at the epoch of observation has been defined in terms of a heliocentric system (see §2.1.2.2). The direction must therefore be referred to the geocentre by application of corrections for parallax. Considering the worst case of the Sun-Earth-source configuration illustrated in Fix. 2.XIX:

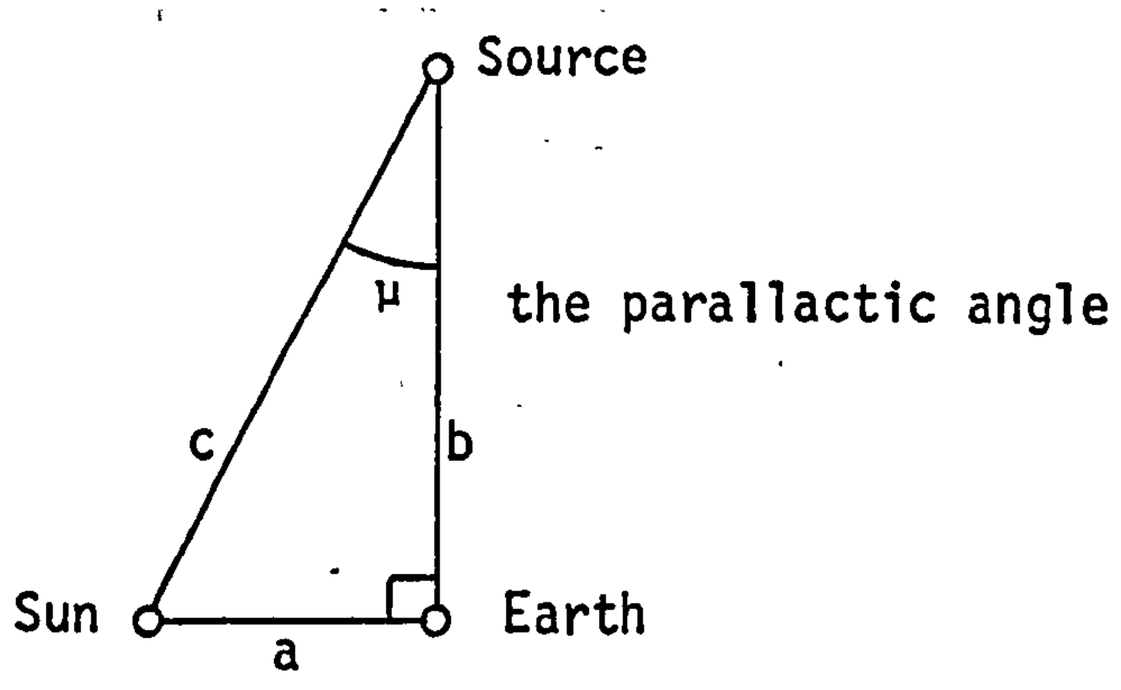

Fig. 2.XIX The parallax effect

$$\sin \mu = \frac{a}{c} \quad \text{or} \quad \mu \simeq \frac{a}{c}$$

where μ = the parallactic angle.

Therefore, a displacement in the direction of a star due to geocentric parallax (i.e. the displacement of the direction as viewed from the geocentre compared to the heliocentric direction) of 0".001 (5×10^{-9} radians) requires the ratio a:c to equal $1:2 \times 10^{7}$. Clearly, this effect is negligible as the distance of VLBI sources, such as quasars,

from the Earth is of the order of 7×10^9 light years (Robinson, 1972) compared with the distance of the Sun from the Earth of approximately 150×10^6 km (15.7×10^{-6} light years). Similarly, the topocentric parallax due to the displacement of the observer from the geocentre will not affect the direction of the source, but it may affect the phase measured by the interferometer.

In order that the parallax has an insignificant effect on the phase (see §2.1.4) measured by the interferometer of less than one wavelength, it is necessary that (see Fig. 2.XX) (Cannon, 1978):

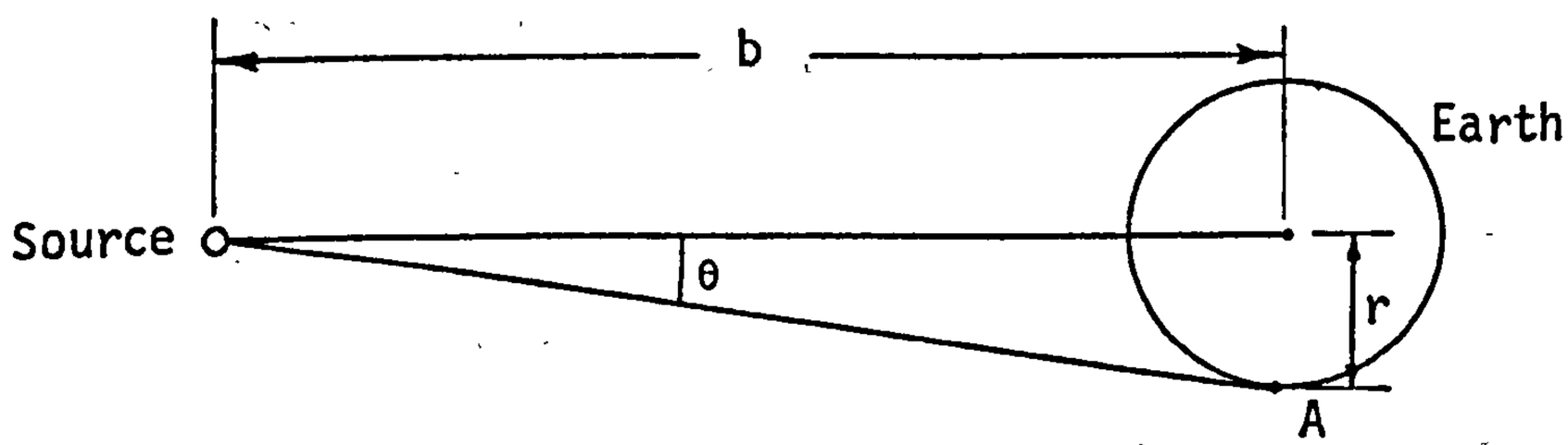

Fig. 2.XX The effect of parallax on interferometer phase

$$\frac{b(1 - \cos\theta)}{\lambda} < 1 ,$$

where $\theta \simeq \frac{r}{b}$.

This requires that:

$$b > \frac{r^2}{2\lambda} . \qquad (2.33)$$

Therefore taking $r = 6400$ km and $\lambda = 2.8$ cm, (2.33) requires that $b > 7 \times 10^{11}$ km or 0.1 light year. Clearly, this effect is insignificant

for extragalactic sources but not for sources within the solar system, especially for longer wavelength observations.

In conclusion, for VLBI observations using extragalactic sources, both topocentric and geocentric parallax may be ignored but for observations of sources within the solar system topocentric parallax will have a significant effect on the phase of the interferometer. All the data used in this thesis has been observed from extragalactic sources. For a full treatment of the corrections for parallax see (Mueller, 1969; Smart, 1977; and E.S.A.E., 1977).

2.4 REDUCTION OF VLBI OBSERVATIONS

2.4.1 Antenna Geometry

The signals arriving at an antenna will not be received and recorded at the antenna reference point. Consequently, the relationship between the observed delay time and that between a signal reaching each reference point must be evaluated (Cannon, 1978).

Assume a baseline is defined by the reference points of two antennae whose rotation axes intersect. If both antennae are observing the same source, then the baseline and the vectors in the direction of the source form a plane in which lie axes of symmetry of the paraboloid dishes of the antennae (Fig. 2.XXI). The geometric delay, τ_g, from (2.14) is the theoretical delay between the signal arriving at the two antenna reference points. Denoting the dimensions of the antennae in units of light travel time (i.e. instead of expressing a length in metres, it is given in terms of the time it would take light to travel that distance, e.g. 10 m = 10/c secs) the distance from the reference point to the paraboloid vertex is t_v and the distance from the vertex to the focus is t_f. The latter is equivalent to the distance between

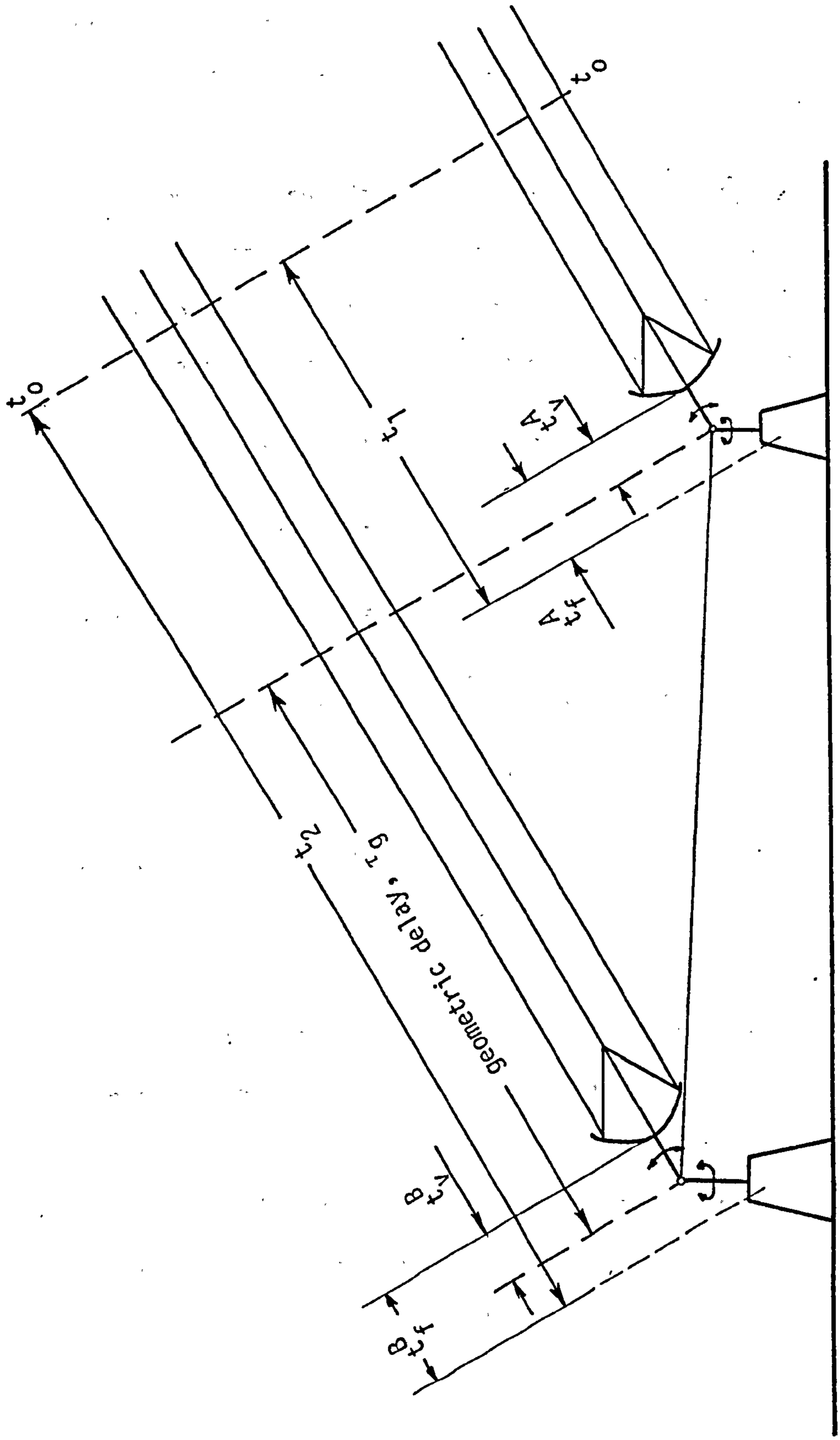

Fig. 2.XXI Effect of antennae geometry on the measured delay

the directrix of the paraboloid and its vertex. A further delay is caused by the finite time interval, t_i, between the signal arriving at the antenna feed horn, situated at the focus, and the recording of the data.

Therefore, considering a wavefront which arrives at the focus of antenna A at time $t + t_1$ and at the focus of antenna B at time $t + t_2$, the delay obtained at the subsequent correlation of the recorded data tapes is (again ignoring the atmosphere, Earth rotation, etc.):

$$\tau = (t_0 + t_2 + t_i^B) - (t_0 + t_1 + t_i^A)$$

$$= t_2 - t_1 + (t_i^B - t_1^A) \qquad (2.34)$$

Referring to the diagram:

$$\tau_g = (t_0 + t_2 - t_f^B + t_v^B) - (t_0 + t_1 - t_f^A + t_v^A)$$

$$= (t_2 - t_1) - (t_f^B - t_f^A) + (t_v^B - t_v^A) \; . \qquad (2.35)$$

Therefore, combining (2.34) and (2.35) gives:

$$\tau = \tau_g + (t_i^B - t_i^A) + (t_f^B - t_f^A) - (t_v^B - t_v^A) \; .$$

For an antenna in which the drive axes do not intersect, the distance between the focus and the reference point is continually changing according to the elevation of the antenna (Fig. 2.XXII). In this case, the distance t_v consists of two components, t_e which remains fixed and t_d which does not. Defining the vector $\vec{D}$ as connecting the reference point to the closest point on the line of the elevation axis:

$$t_d = \frac{\vec{D}.\vec{s}}{c} \; . \qquad (2.36)$$

Therefore, the observed delay, τ, is related to the geometric delay, τ_g,

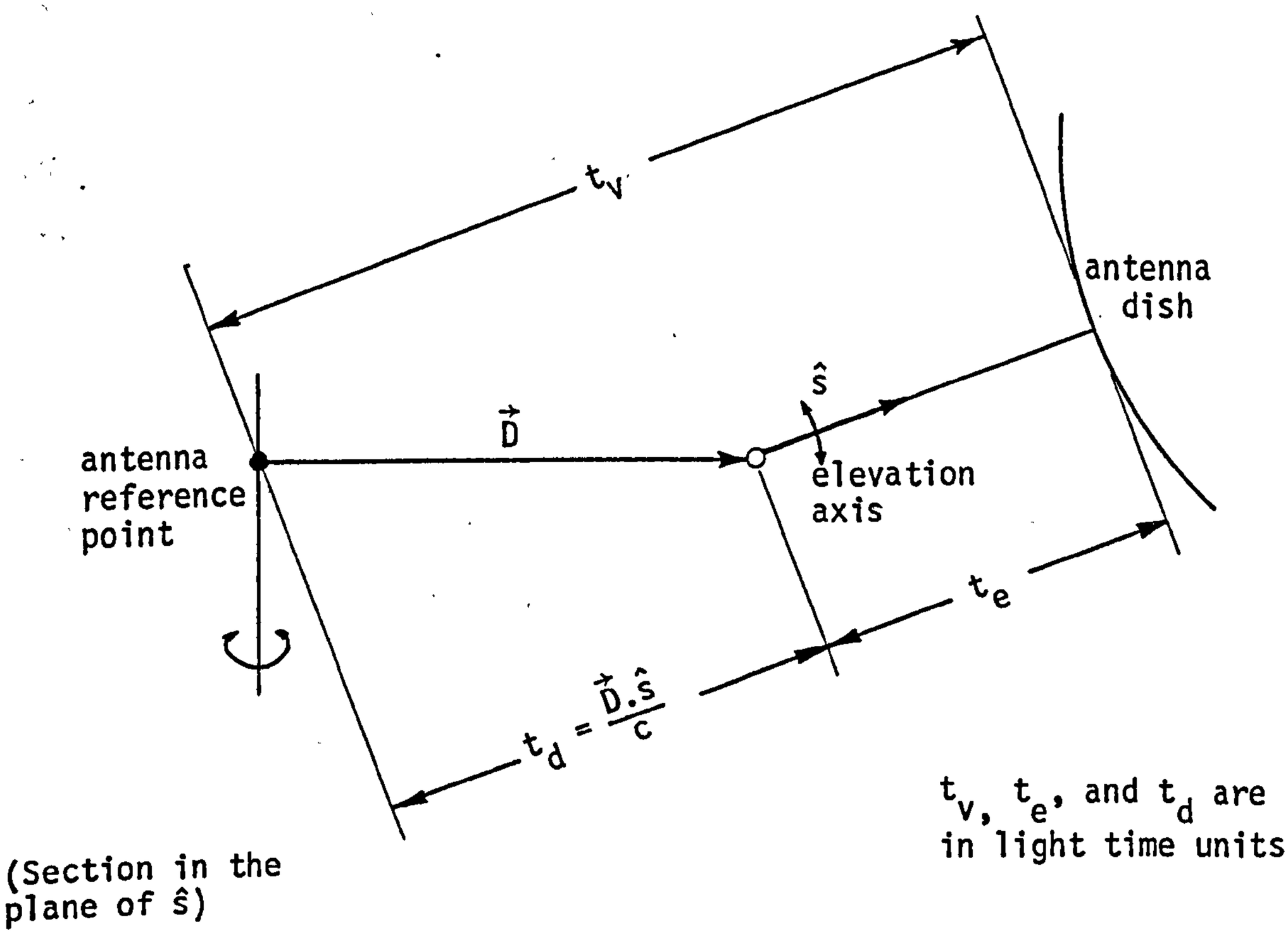

Fig. 2.XXII Effect of non-intersecting antenna drive axes on the 'antenna geometry' correction

by the relation:

$$\tau = \tau_g - \Delta\tau_d + \Delta\tau_{agi} \quad , \tag{2.37}$$

where $\Delta\tau_{agi}$ = the constant delay caused by the antenna geometry and instrumental effects,

and $\Delta\tau_d = t_D^B - t_D^A$ = the changing delay due to the offset of the antennae drive axes.

The whole or part of this term may disappear if both or either of the antennae have intersecting drive axes.

The term $(t_i^B - t_i^A)$ may change with time due to temperature, tension, and twist changes in the cables. This can be monitored but such calibrations have only recently been performed (Ryan et al, 1977) and no

allowance is made in this model. Hence $(t_i^B - t_i^A)$ is regarded as a constant for the interferometer. The terms $(t_f^B - t_f^A)$, and $(t_e^B - t_e^A)$, and $|\vec{D}|$ are also assumed to remain constant. Some very large telescope structures suffer appreciable deformation while observing (the reference point at the Effelsberg telescope in West Germany can move as much as 5 cm while tracking a source (Campbell, 1979)) and this must of course be modelled for high precision observations. Deformation of the dish surface itself due to wind and gravity loading and differential heating amounts to only a few millimetres as above this the telescopes would be unable to focus X-band signals (wavelengths of around 3 cm) (Ryan et al, 1977). Again, no data is available on antenna deformations and as the magnitude and direction of any such movement is unique to each antenna, no model has been formed.

In conclusion, the constant term $\Delta\tau_{agi}$ in (2.37) will not affect the estimation of the baseline parameters. As it is a constant term contributing to each observation, it is equivalent to an offset between the two station clocks and will hence affect the solution of the clock error model constant offset term, c_o (see §2.4.7).

2.4.2 Observation Epoch

As stated previously, a VLBI observation is obtained from several minutes of data which are then adjusted to give an observed value at a specific epoch. Imagining that the observation is of one particular discrete wavefront, the epoch of observation is given as the UTC time of the arrival of the wavefront at antenna A as kept by the clock at station A. Antenna A is hence known as the 'reference' station and antenna B is known as the 'remote' station. The choice of which antenna is the reference and which the remote station depends entirely on the

VLBI system being used but the above convention will be adhered to in the following sections. The expansion from this analogy of only one observed wavefront to the real case of a continuously received signal does not alter the situation.

The adjustment of the UTC observation epoch to an epoch expressed in terms of Greenwich Apparent Sidereal Time (GAST) is achieved in the following way. A summary of the various time systems used in this reduction and their respective properties is given in Appendix A.

(i) The UTC epoch is converted to a UT1 epoch by means of the UTC-UT1 values as published in the monthly BIH Circular D and yearly BIH Rapport Annuel. These values are tabulated at 5-day intervals to the nearest $0^s.0001$.

(ii) The time interval between 0 hr UT of the day in question and the derived UT1 epoch is converted to an interval in GMST by applying the standard conversion factor between universal and sidereal times of (E.S.A.E., 1977):

$$\text{ST interval} = \text{UT interval} \times (1.002737909265 + (0.589\times10^{-10})T_u) \quad (2.38)$$

where T_u = the number of Julian centuries of 36525 days of universal time elapsed since the epoch of Greenwich mean noon (12 hr UT) on 1900 January 0.

This mean sidereal time interval can be assumed to be equivalent to an apparent sidereal time interval over periods of less than one day without significant loss of accuracy.

(iii) The addition of the (assumed) GAST interval to the GAST at 0 hr UT for that day gives the GAST at the epoch of observation. The GAST at 0 hr UT is given for each day in the Astronomical Ephemeris

(A.E.) and hence there is no need for the computed intervals of GAST to be greater than one day.

The GAST is the angle between the true equinox of date and the Greenwich zero meridian as measured in the plane of the equator of the true celestial system defined in §2.1.2.2 or the 'instantaneous' system defined in §2.1.2.3, and as illustrated in Fig. 2.VII.

2.4.3 Earth Tides

The Earth is an elastic body and is deformed by the gravitational attractions of the Sun and Moon. Consequently, the overall baseline length and the baseline components are time dependent. The maximum tidal effect at one station is 78.13 cm (Melchior, 1978) and the tidal effect on the length of a VLBI baseline has a usual maximum value of around 20 cm.

There are three main spherical harmonic functions describing the tides, namely the sectorial function, which defines tides with a semi-diurnal period, the tesseral function, defining tides with a diurnal period, and the zonal function, whose tides are exhibit a fourteen day period for the Moon and a six-month period for the Sun. A description of the cause and effects of the different tidal functions, together with an overall description of tidal effects, theories, and instrumentation, is given in (Melchior, 1978). The components of the tidal forces along the three mutually perpendicular axes illustrated in Fig. 2.XXIII are:

$$OZ \; : \; \frac{\partial W}{\partial r}$$

$$OX \; : \; \frac{\partial W}{r \partial \phi}$$

$$OY \; : \; \frac{W}{r \cos \phi \; \partial \lambda}$$

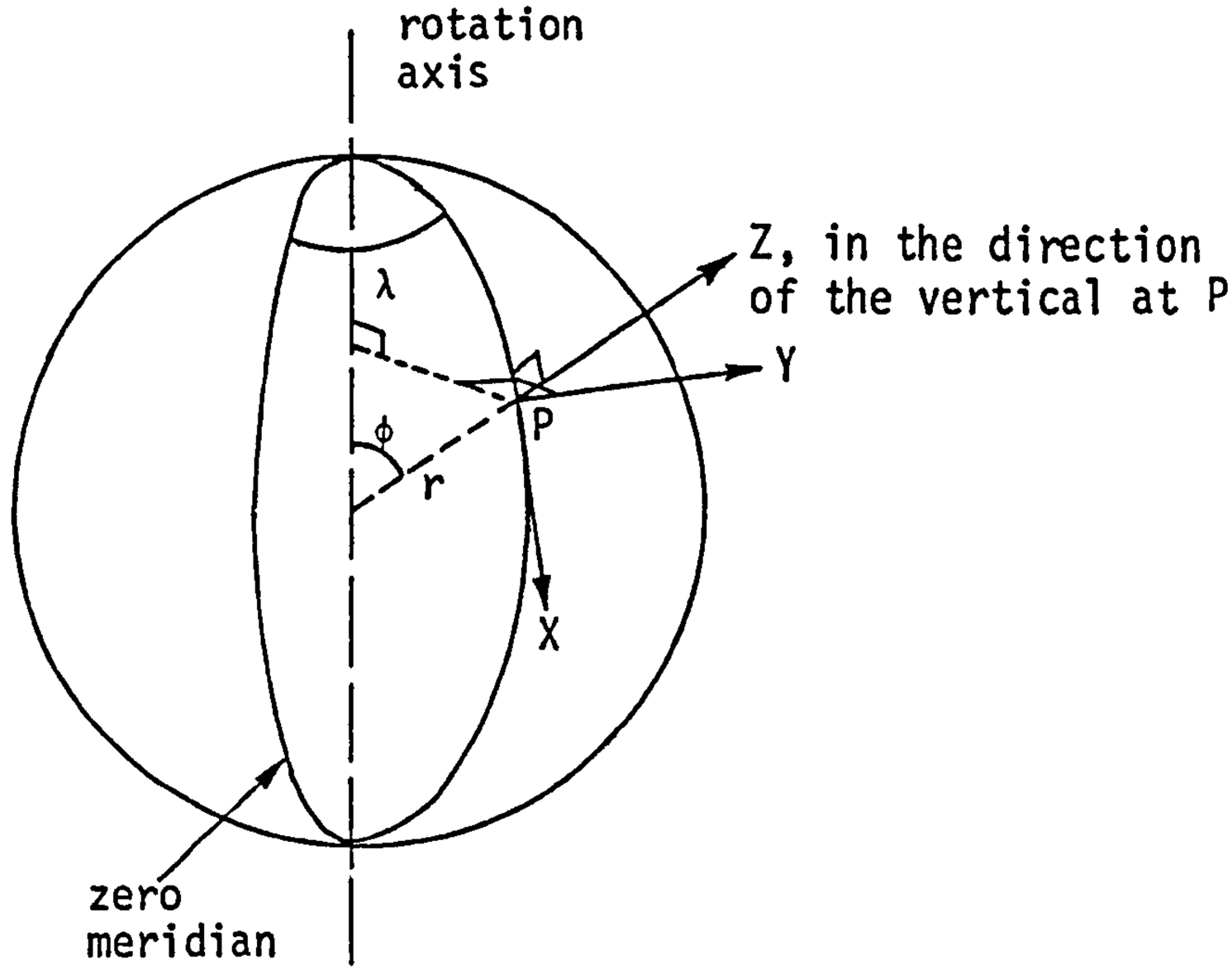

Fig. 2.XXIII Earth tide force components

where W is the gravitational potential and r, ϕ, and λ are the radius, latitude and longitude respectively of the station. In practice, these forces would be measured by the use of a gravimeter for the vertical (OZ) force and by horizontal pendulums for the horizontal (OX and OY) forces. The deformations in the X and Y directions are small (Robertson, 1975) and hence are not considered in the model applied here. The resulting tidal deformation, Δr, induced in the OZ direction at a station is given by:

$$\Delta r = \frac{hW}{g}$$

where g = gravity,

and h = a 'Love Number'.

The 'Love Number', introduced in 1909 by Love, relates the tidal force

to the resultant tidal deformation and is considered as h = 0.584 for this application. Inhomogeneities in the Earth's response to the tidal potential cause the Love's Numbers to be a function of station location and hence values of h may differ from 0.584 by up to 0.08 (Melchior, 1966).

The equation for the tidal deformation at a station is given by (Robertson, 1975 and Melchior, 1966):

$$\Delta r = hu \,, \tag{2.39}$$

where $u = A\{\cos^2\phi(a_1\cos(2LHA + \psi_1) + a_2\cos(2LHA - \mu + \omega + \psi_2)$
$+ a_3\cos(2LST + \psi_3) + a_4\cos(2(GST+\lambda) + \psi_4)) +$
$\sin 2\phi(a_5\cos(GST+\lambda+\psi_5) + a_6\cos(LHA - \mu + \psi_6) +$
$a_7\cos(LST - \sigma + \psi_7)) - (1.5\sin^2\phi - 0.5)(a_8 + a_9\cos(\mu-\omega)$
$+ a_{10}\cos 2\mu + a_{11}\sin 2\sigma)\}$,

μ = mean longitude of the Moon,
= (4.719967 + 8399.709T) radians,

σ = mean longitude of the Sun,
= (4.881628 + 628.3319T) radians,

ω = longitude of the lunar perigee,
= (5.835152 + 71.01803T) radians,

T = time in centuries since 1900.0 (see Appendix A),

GST = Greenwich Sidereal Time (see §2.4.2 and Appendix A),

LHA = lunar hour angle = GST - μ + λ,

LST = solar hour angle = GST - σ + λ,

$A = 26.7 \text{ cm} = \frac{D}{g}$,

D = Doodson's Constant = $2.627723 \text{ m}^2\text{s}^{-2}$,

and $a_1 = 0.908$ $\psi_1 = 0$

$a_2 = 0.174$ $\psi_2 = 0$

$a_3 = 0.423$ $\psi_3 = 0$

$a_4 = 0.115$ $\psi_4 = 0$

$a_5 = 0.531$ $\psi_5 = -90^o$

$a_6 = 0.377$ $\psi_6 = +90^o$

$a_7 = 0.176$ $\psi_7 = +90^o$

$a_8 = 0.739$

$a_9 = 0.083$

$a_{10} = 0.156$

$a_{11} = 0.073.$

For application to the determination of the a priori VLBI baseline, the components of this tidal movement in the Average Terrestrial system h_i, i = 1 to 3, are given by:

$$\Delta x_1^h = \Delta r \cos \phi' \cos \lambda'$$
$$\Delta x_2^h = \Delta r \cos \phi' \sin \lambda'$$
$$\Delta x_3^h = \Delta r \sin \phi'$$

where ϕ' and λ' are as defined in §2.1.2.1. Hence the baseline components in the direction of the i^{th} axis is given by:

$$b_i = (x_{i_B}^h - x_{i_A}^h) + (\Delta x_{i_B}^h - \Delta x_{i_A}^h) \qquad (2.40)$$

where $x_{i_B}^h$ and $x_{i_A}^h$ are defined in (2.2), i = 1 to 3, and subscripts A and B represent antennae A and B respectively.

2.4.4 Retarded Baseline

The equation for the geometric delay, τ_g, derived from §2.1.3, assumes a stationary Earth during the wave transit. Clearly, the rotation of the Earth about its axis will add another component to the delay time. Assuming the convention that the epoch, t, of an observation

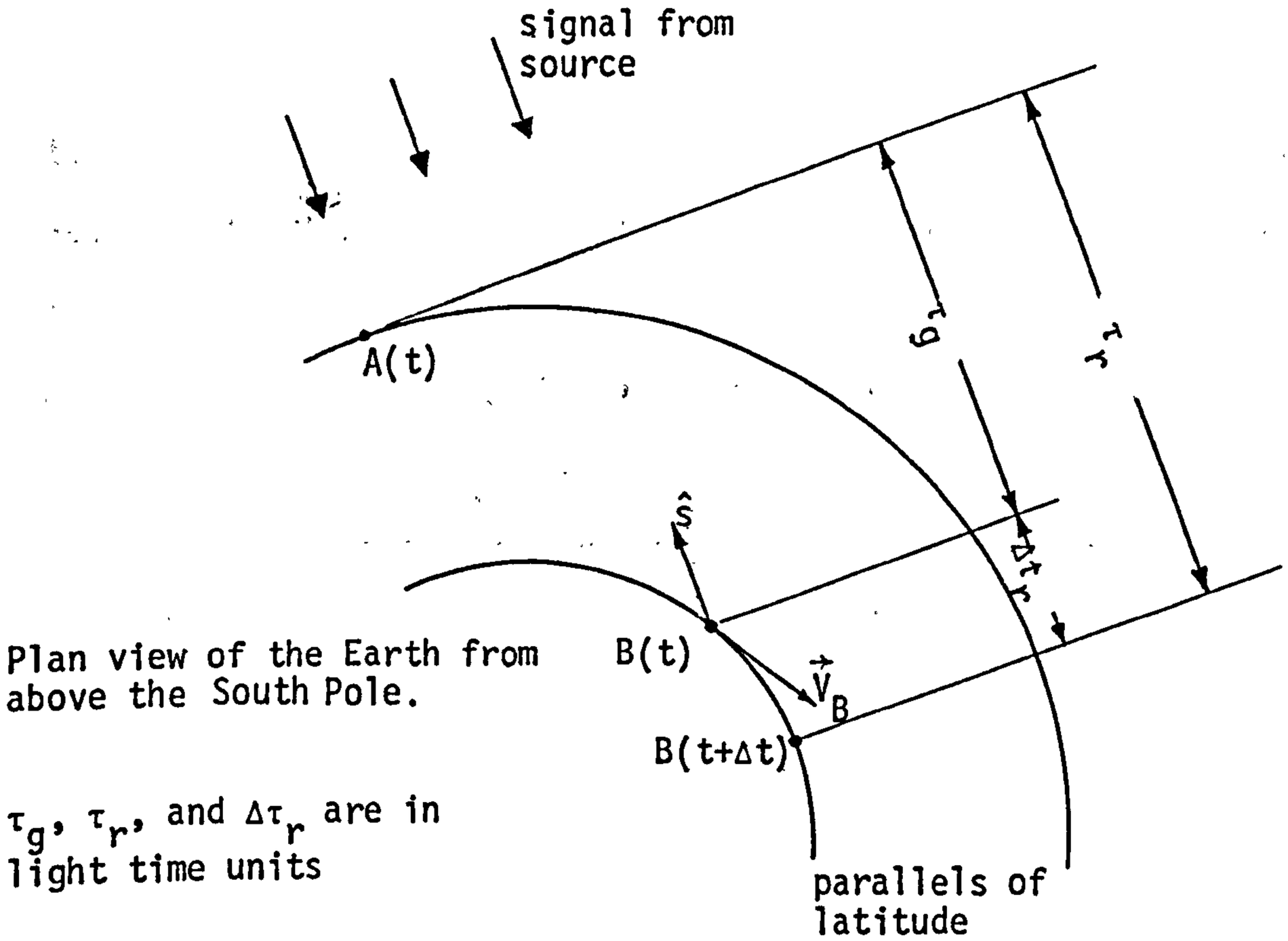

Plan view of the Earth from above the South Pole.

τ_g, τ_r, and $\Delta\tau_r$ are in light time units

Fig. 2.XXIV The retarded baseline correction

is the time of the signal arrival at antenna A and that positive delay implies arrival at antenna A first, then for positive delay the wavefront will reach antenna B at time t+Δt (see Fig. 2.XXIV). Denoting the position of antenna A at time t by A(t), the correction to be applied to the geometric delay will be the component of the vector B(t)B(t+Δt) in the direction to the source. Therefore,

$$\Delta\tau_r = \frac{-V_B \Delta\, t.\hat{s}}{c}, \qquad (2.41)$$

where $\vec{V}_B$ = the velocity vector of antenna B at epoch t due to Earth rotation.

The maximum geometric delay for terrestrial antenna sites is about 21 ms at which a movement of antenna B of about 10 m would occur, thus giving a contribution to the delay time of about 30 nanoseconds. It is appropriate to make the approximation that $\Delta t = \tau_g$ for use in (2.41)

since the additional delay time due to rotation of the Earth during the time interval $\Delta\tau_r$ amounts to only a few microns. The departure of the actual antenna position $B(t+\Delta t)$ from that assumed in (2.41), which computes the movement in the direction of the velocity vector of the antenna at epoch t, results in a negligible contribution to the delay time.

In conclusion, the formula for the delay time including the effect of Earth rotation during the wave transit is:

$$\tau_r = \frac{-\vec{b}.\hat{s}}{c}\left(1 - \frac{\vec{V}_B.\hat{s}}{c}\right) , \qquad (2.42)$$

where all the quantities are relative to the 'instantaneous' co-ordinate system m_i, i = 1 to 3, which is rotating with the Earth. Hence,

$$V_B = \Omega \begin{bmatrix} -r \cos\phi' \sin\lambda' \\ r \cos\phi' \cos\lambda' \\ 0 \end{bmatrix} , \qquad (2.43)$$

where Ω is the rate of rotation of the Earth as computed in (2.52) and r, ϕ', and λ' are the geocentric radius, latitude, and longitude as described in §2.1.2.1. Strictly speaking, ϕ' and λ' should be rotated into the 'instantaneous' system before being input to (2.43) but the polar motion values are insufficiently large to make this factor contribute significantly to the computed delay time. The assumption that $V_B(3)$ equals zero implies that the rotation axis of the Earth is stationary. Although this is clearly not the case, the resultant error is again negligible.

2.4.5 Tropospheric Correction

The troposphere (including the stratosphere) extends up to about

40 km above the Earth's surface and causes the retardation of a signal passing through it due to a decrease in the propagation velocity and a bending of the ray path. The amount of the effect of this refraction on range measurements varies from about 2 metres in the zenith direction to approximately 100 metres at the horizon (Chao, 1974). This refraction is dependent on the atmospheric constituents, the dispersion of the signal, and the non-homogeneity of the atmosphere, but is almost independent of the frequency of the signal.

Several models have been developed to compute the effect of the atmosphere on microwaves. These usually model vertical profiles for each of the meteorological components of the atmosphere based on surface measurements of temperature, pressure, and water vapour content. Measurements of the water vapour content along the line of sight to the source can also be made by water vapour radiometers which measure the microwave brightness around the 23 GHz water vapour emission line (Ryan et al, 1977) .. For convenience, the correction is divided into a part due to the dry component of the atmosphere and a part due to the wet component of the atmosphere. The dry component accounts for 85-90% of the refraction effect and can be reliably modelled to ±1% for elevation angles above 1^{o} (Robertson, 1975). The wet component is less well understood but as its contribution to the total correction is only 10-15% and the model is reliable to ±10%. then the resultant error is not unduly significant. In an ideal horizontally homogeneous (stratified) atmosphere, ray path bending will occur only in the great circle plane and hence will not affect the azimuth angle of observation. Above 10^{o}, the effect of ray path bending on the elevation of a source is negligible (Crane, 1976) and hence observations with either antenna observing below this value are rejected.

Two models have been used in this study. The are:

(i) the simplified Hopfield model which is based on the more complex atmospheric model of Hopfield (Hopfield, 1969 and 1972) and computes the atmospheric delay along the ray path using surface meteorological data,

and (ii) Chao's model, which computes the atmospheric delay along a ray path at any elevation angle from the atmospheric delay in the zenith direction (Chao, 1974).

Both these models are ideally suited for the use of average meteorological data for an observing period but can also be used for regularly observed data. The two models, along with conversion factors for different meteorological measuring units, are described fully in Appendix D.

For application to VLBI observations, the non-homogeneity of the atmosphere and the different elevation angles at which two antennae will track a source cause the tropospheric contribution to the single ray path at each station to be different. For the case of positive delay illustrated in Fig. 2.XXV, the plane wavefront GG' outside the Earth's atmosphere is differentially refracted such that when the signal arrives at A, the wavefront lies along AP. The delay due to the atmosphere along the ray path to antenna A, $\Delta\tau^{A}_{atm}$, is therefore A'P. The signal will continue along the path PB undergoing a delay due to the atmosphere of $\Delta\tau^{B}_{atm}$. On the assumption that the point P lies outside the troposphere then the geometric delay, τ_g, is related to the observed (in this case observed meaning corrected for tropospheric refraction only) delay, τ, by:

$$\tau = \tau_g - \Delta\tau_{trop} , \qquad (2.44)$$

where $\Delta\tau_{trop} = \Delta\tau^{A}_{atm} - \Delta\tau^{B}_{atm}$.

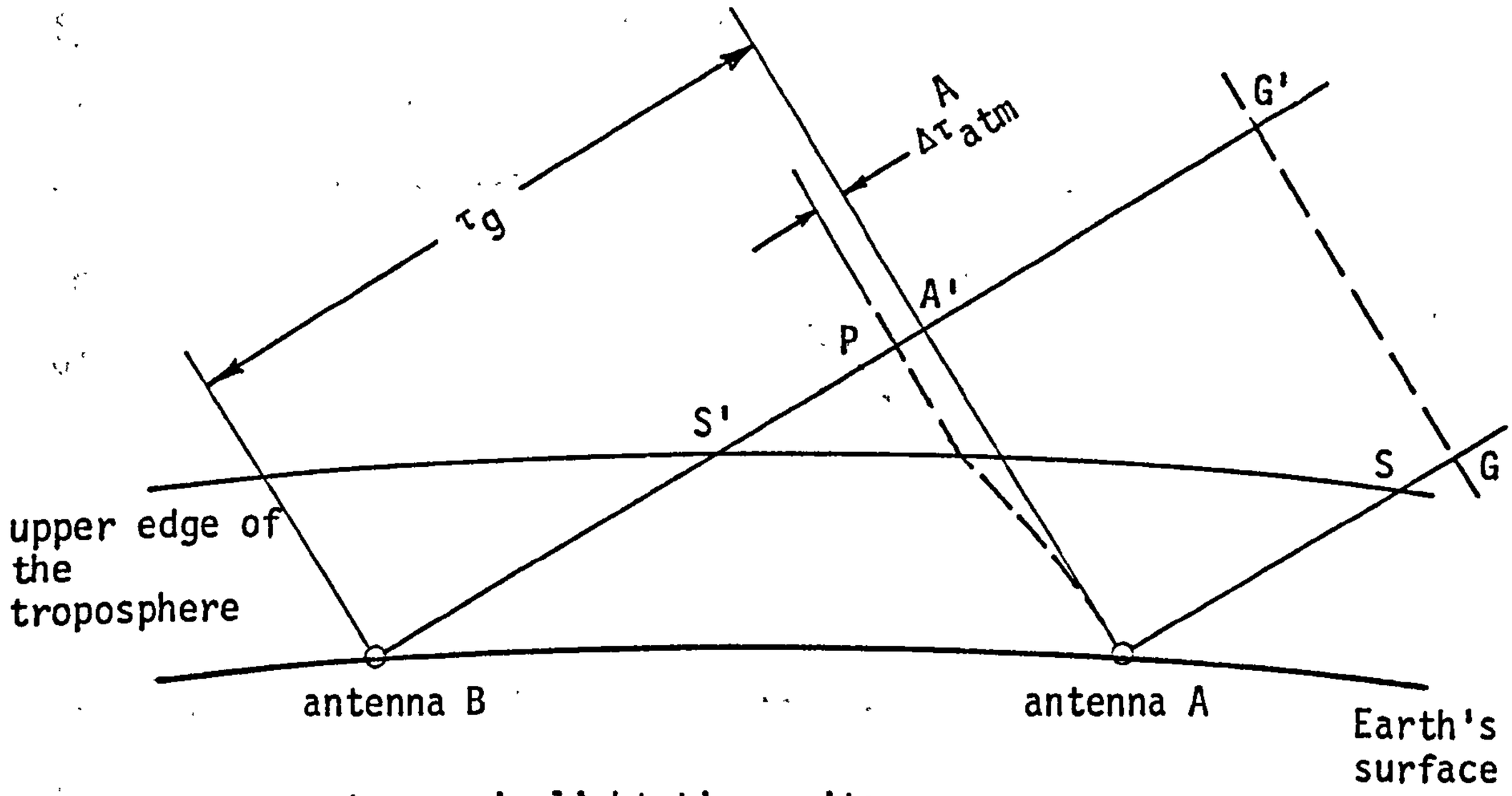

All measurements are in light time units

Fig. 2.XXV Tropospheric correction geometry

If the above assumption was not valid, then the tropospheric model would have to compute separate refraction effects for different levels of the troposphere leading to a less reliable correction term. Due to the rejection of low elevation observations this condition occurs rarely for long baselines and if P in the diagram is only just within the troposphere the error introduced will only be small as the tropospheric refraction effect decreases with height above the Earth.

It is possible to solve for a parameter representing the tropospheric contribution to the delay during part or the whole of an observing period. This is dealt with in Chapter 3.

2.4.6 Ionospheric Correction

The ionosphere is that part of the upper atmosphere between approximately 40 and 100 km where the existence of large quantities of

free electrons and ions, produced by ultraviolet radiation from the Sun, affects the propagation of radio waves. The ionospheric refractive index depends on the observing frequency, the Earth's magnetic field, the collision frequency, and the electron density of the ionosphere (Mathur et al, 1970). The refractive index for an observing frequency f is:

$$n = 1 + \frac{c_1}{f^2} + \frac{c_2}{f^3} + \frac{c_3}{f^4} + ... \qquad (2.45)$$

where the c terms are functions of time and position but independent of frequency (Wells, 1974). The third-order terms are mainly due to the Earth's magnetic field and hence for frequencies above 450 MHz are much smaller than the f^2 term (Bomford, 1975). Consequently, the refractive index can be approximated to (Bomford, 1975):

$$n = 1 - \frac{Ne^2}{2\pi m f^2}$$

where N = electron density (m^{-3}),

e = electron charge (1.6021×10^{-19} C),

m = electron mass (9.1091×10^{-31} kg),

and f = observing frequency (Hz).

The values used for e and m are from (Langley, 1979) and lead to the expression:

$$n = 1 - \frac{40.28N}{f^2} \ .$$

The phase delay of the ionosphere along the path length, s, is therefore:

$$\Delta\phi_{ion} = \frac{1}{c}\int(n-1)ds \ ,$$

$$= \frac{-40.28}{f^2 c}\int N ds.$$

This implies the phase is decreased by the plasma and the phase velocity exceeds that of light in vacuo. However, the group delay is increased by the same amount and therefore:

$$\Delta\tau_{ion} = \frac{40.28}{f^2 c} \int N ds.$$

This formula can also be expressed in terms of the angle, i, between the ray and the local vertical, and the zenith path length, h, by (Hagfors, 1976):

$$\Delta\tau_{ion} = \frac{40.28}{f^2 c} \int \frac{n}{\cos i} dh. \qquad (2.46)$$

This formula illustrates the elevation dependence of the ionospheric contribution to the observations. For all but the most exceptional of electron density profiles, ray bending may be ignored although, as evident from (2.46), the worst case is for low elevation observations which, as mentioned with regard to the tropospheric correction (§2.4.5), are rejected in the adjustment.

The integrated electron density may typically vary between 5×10^{17} m^{-2} by day to 5×10^{16} m^{-2} by night (Hagfors, 1976) although this may be even higher following solar storms. The density will also be positionally variable. The contribution of the ionosphere to a signal propagation time at a typical observing frequency of 10 GHz is around 1 nanosecond, increasing with lower elevation. Therefore, the contribution to a group delay observation (§2.1.3) has an expected maximum of 1 nanosecond but generally will be of the order of 0.3 nanoseconds (Langley, 1979). As is the case in the tropospheric correction to a group delay observation, (2.44):

$$\tau = \tau_g - \Delta\tau_{ion}, \qquad (2.47)$$

where $\Delta\tau_{ion} = \Delta\tau^A_{ion} - \Delta\tau^B_{ion}$.

The modelling of the ionosphere for use in VLBI experiments has shown insignificant changes in the post-fit residuals or baseline results (Robertson, 1975). Consequently, no attempt has been made to model the ionospheric contribution to the observations in this study. This results in the tropospheric correction parameters (when they are included as unknowns in the adjustment) absorbing part of the ionospheric correction. This should be remembered if these parameters are of special interest.

The removal of the first-order correction can be achieved by taking observations at two widely separated frequencies, as is being currently done by the American NRAO Mk III interferometer system (see Chapter 4) at X-band (8.4 GHz) and S-band (2.3 GHz). It should also be possible to form an ionospheric correction derived from satellite-Doppler measurements (also a dual frequency correction) in the vicinity of a VLBI observation direction. Other methods of measuring the electron density, for example radar sounding from the Earth and 'topside sounding' from satellites, are described in (Hagfors, 1976).

2.4.7 Clock Behaviour Model

The instrumental delay of an interferometer consists of three parts. Firstly, the delay between receiving of the signals and recording of the signals at each antenna (§2.4.1), secondly, the contribution due to non-intersection of the antennae drive axes (§2.4.1), and finally, an apparent delay caused by the continually changing relative offset between the clocks at the different antennae. As mentioned previously, no attempt has been made to model the first of these and therefore they will contribute towards the results of the clock behaviour model, as

will any inaccuracy in the modelling of the second factor.

The atomic frequency standard employed at each antenna phase-locks the station local oscillator chain and drives the station clock (see Chapter 4). Each clock is brought as close as possible to the UTC time scale by comparison with a 'master' clock or by synchronisation with Loran C timing signals (see Appendix A.7). However, there will inevitably be an initial offset and a relative drift of the time as kept by the clocks throughout the observations.

The relative clock offset can be modelled by the use of a polynomial in time such that $\Delta\tau_c$, the relative clock offset at time t, is given by:

$$\Delta\tau_c = c_0 + c_1 t + c_2 t^2 + \ldots \quad . \tag{2.48}$$

The major problem is to decide what order of polynomial to use. If too great an order of polynomial is employed, as well as reaching the point of 'diminishing returns' the model may force a fit onto an effect independent of clock behaviour and hence lead to erroneous, though apparently satisfactory, results.

It is current practice to use hydrogen maser frequency standards (§4.3.1) which it is claimed give a stability limit of 1 part in 10^{14}. At this stability, the effects of second and higher order error terms are less than one nanosecond per day and therefore a polynomial of order one would be satisfactory. However, this stability is frequently not achieved and higher order polynomials must be used. The decision to use a higher order polynomial is an empirical one which can be assessed by different criteria. Comparison of clock times with Loran C transmissions may give an impression of the clock behaviour (Langley, 1979). Otherwise, the study of the residuals of an adjustment using a

first-order polynomial may show definite higher-order effects which require removal (assuming these are clock errors and not due to some other cause). Furthermore, a clock may need more than one model applied to it if there are discontinuities in its behaviour or power failures during use. Fig. 2.XXVI is a plot of the residuals obtained from VLBI observations made between Haystack Observatory and Goldstone Observatory in the USA in August 1972 (see §6.2) with only a zero-order clock polynomial applied. The linear trend, normally modelled by using a first-order polynomial, is clearly visible. The definite lines formed by groups of points represent observations of the same source. A description of the method employed to produce this plot is given in §8.5. The computation of the model for the relative behaviour of independent atomic clocks from VLBI observations enables these clocks to be synchronised to a high degree of accuracy (Counselman et al, 1977).

A method of eliminating clock effects by observing two different sources simultaneously is described in (Robertson, 1975) and (Shapiro, 1978).

2.4.8 Relativity

Relativistic principles show that separate clocks will exhibit a different rate according to their individual velocities in space (Sears and Brehme, 1968). A full understanding of the relativistic conversion between the observed atomic time (time as observed by an atomic clock on the moving Earth) and co-ordinate time (time as measured in a solar barycentric co-ordinate system) would enable all observations to be reduced to the latter system and be adjusted, as described by Robertson (1975). However, for the adjustment procedure described and used in this work, all measurements are made and adjusted in an Earth-fixed system and hence the effect of relativity on the synchronisation of the separate

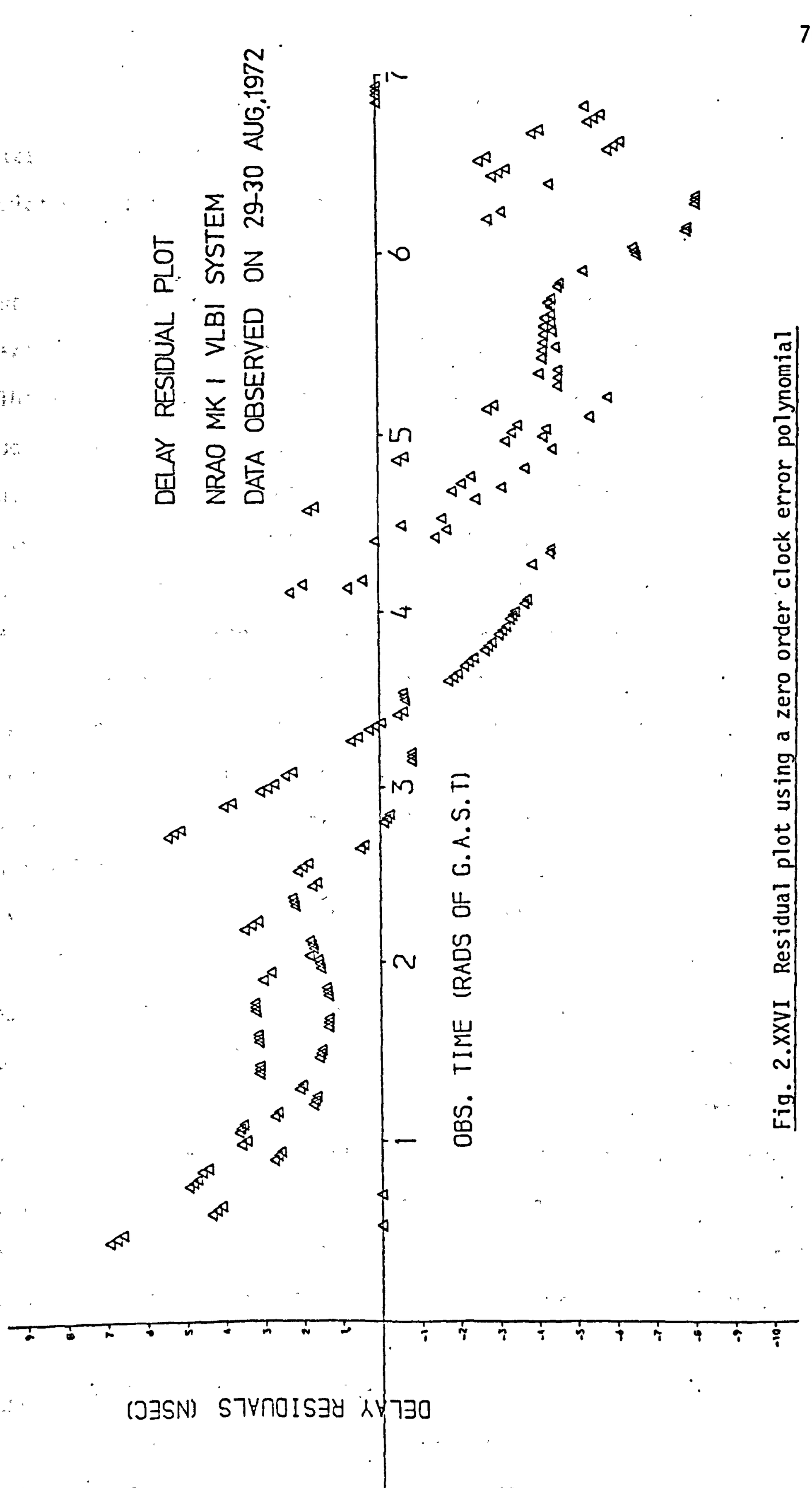

Fig. 2.XXVI Residual plot using a zero order clock error polynomial

station atomic clocks is of importance, rather than the overall relativistic effect on the clocks.

The relativistic effect on Earth-bound clocks can be divided into two distinct components, namely that which is the same for all Earth-bound clocks and that which is different for each individual clock (Thomas, 1975). The first of these components contains both the effect due to the speed of the centre of mass of the Earth and the 'clock invariant part' of the potential, located at the Earth's mass centre (i.e. that part of the gravitation potential due to the mass of all the other solar system bodies excepting the Earth). The residual terms, after removal of these two effects, are principally periodic in nature.

The second component, which causes a difference in the rate of the clocks, can also be split into two parts. Firstly, there is a contribution based on the clock geopotential and velocity relative to the centre of mass of the Earth. The velocity, v, of a clock relative to the Earth's mass centre causes relativistic effects of order $\frac{1}{2} v^2/c^2 \approx 10^{-12}$ seconds. However, the differential effect is of importance in VLBI and this is negligible. In fact, two clocks with the same geopotential height should run at the same rate whereas clocks at different geopotential heights have different rates, of the order of 1.1×10^{-13} s/km of differential altitude. This part of the clock rate difference will be constant for two specific clocks and hence will be absorbed into the relative clock drift term, c_1 of the clock error polynomial in the VLBI adjustment (see §2.4.7). The second part of the clock rate difference is periodic but much less significant than the previous component.

2.4.9 Full delay time equation

The delay time equation, ignoring relativistic effects and ionospheric refraction, with antenna A as the 'reference' station, and

treating the delay as positive when the signal reaches antenna A first, is:

$$\tau = -\frac{\mathbf{b}.\hat{\mathbf{s}}}{c}\left(1 - \frac{\mathbf{V}_B.\hat{\mathbf{s}}}{c}\right) - \Delta\tau_{trop} + c_0 + c_1 t \qquad (2.49)$$

where $\mathbf{b}$ = the baseline from antenna A to antenna B expressed in the instantaneous co-ordinate system m_i, i = 1 to 3 (§2.1.2.3), and corrected for antenna geometry effects (§2.4.1) and Earth tides (§2.4.3),

$\hat{\mathbf{s}}$ = the unit vector in the direction of the source in relation to the instantaneous co-ordinate system m_i, i = 1 to 3, having corrected for precession (§2.3.3), nutation (§2.3.4), aberration (§2.3.2), and the observation epoch (§2.4.2),

c = the velocity of propagation of microwaves in vacuo,

$\left(1 - \frac{\mathbf{V}_B.\hat{\mathbf{s}}}{c}\right)$ = the 'retarded baseline' correction (§2.4.4) where $\mathbf{V}_B$ is the velocity vector of antenna B, the 'remote' station,

$\Delta\tau_{trop}$ = the contribution to the delay time of the tropospheric refraction of the signal received at each antenna (§2.4.5),

and $c_0 + c_1 t$ = the clock error polynomial describing the relative behaviour of the clock at each station as a first order polynomial where t is the time since initialisation (further terms may also be added if necessary) (§2.4.7).

2.5 REDUCTION OF VLBI FRINGE FREQUENCY OBSERVATIONS

2.5.1 Basic Fringe Frequency Equation

The reduction methods described here apply equally well to both the delay rate and fringe frequency observables. However, allowance must be made for the fact that the delay rate is the fringe frequency divided by the observing frequency (see (2.15)) and hence all the formulae

derived here for the fringe frequency observable need to be divided by the observing frequency before being applied to delay rate data reduction.

There are certain features of the data reduction procedure which are identical for both the delay and the fringe frequency adjustment models. The baseline over which the observations are made (§2.2.1), together with the Average Terrestrial co-ordinate system h_i, i = 1 to 3, on which it is defined, are the same as for the delay observable. The application of the Earth tide correction (§2.4.3) and the polar motion transformation (§2.2.2) in order to define the baseline in the instantaneous terrestrial system m_i, i = 1 to 3 (§2.1.2.3), for each observation is defined and computed in the same manner for the fringe frequency observable as for the delay observable. Also, the definition of the co-ordinates of the observed sources, the co-ordinate systems on which these are based (§2.1.2.2), and the transformations relating to them (§2.3), are all the same. The continually changing values of precession and nutation do affect the observation of fringe frequency and are dealt with in §2.6.2. The rate of change of annual aberration is not significant and is hence not considered. Similarly, the time dependent changes in the baseline geometry due to Earth tides, polar motion and the (UT1-UTC) offset, are not considered due to their magnitude being insignificant. Furthermore, as no data is available and because it is only a very small effect at high frequencies, the correction to be applied to the fringe frequency in order to account for refraction in the ionosphere is not considered.

Throughout the VLBI data reduction process there are several time scales in use. Though the choice is somewhat arbitrary (Robertson, 1975) the delay rate is defined as the derivative of the delay with respect to the time as kept by the 'reference' clock (see §2.4.2). Therefore, the

fringe frequency is also defined as being proportional to the time as kept by the reference clock.

The basic fringe frequency equation is derived by differentiating the combination of (2.13), (2.5), and (2.18) to give:

$$F = -\frac{b_m \cdot w}{c} (RNP\dot{\hat{s}} + RN\dot{P}\hat{s} + \dot{R}(A + NP\hat{s})) \qquad (2.50)$$

where b_m = the 'instantaneous' baseline vector defined in (2.8),

$\hat{s}$ = the unit vector in the direction of the source with respect to the mean equator and equinox of 1950.0,

w = the observing frequency,

R = the GAST rotation matrix defined in (2.6),

N = the nutation matrix defined in (3.23),

P = the precession matrix defined in (2.29),

$\dot{P}$,$\dot{N}$ and $\dot{R}$ = the time derivatives of the precession, nutation and GAST rotation matrices respectively,

A = the aberration vector defined in (2.18),

and c = the velocity of propagation of microwaves in vacuo.

The derivative of the GAST rotation matrix is given by:

$$\dot{R} = \Omega \begin{bmatrix} -\sin(GAST) & \cos(GAST) & 0 \\ -\cos(GAST) & -\sin(GAST) & 0 \\ 0 & 0 & 0 \end{bmatrix} \qquad (2.51)$$

where $\Omega = 2\pi \times 1.00273790926 5/86400.0$ rads/sec (2.52)

= rate of change of sidereal time,

and 1.002737909265 = the conversion factor from Universal Time to Sidereal Time.

2.5.2 Precession and Nutation

The rate of change of precession and nutation with respect to time contribute several millihertz to the observed fringe frequency. It is therefore essential to model this contribution as shown in (2.50).

The matrix describing the rate of change of precession with respect to time is defined by differentiating (2.58) to give:

$$\begin{aligned}\dot{P} = {} & \dot{R}_3(-90^o-z)R_1(\theta)R_3(90^o-\zeta_0) + \\ & R_3(-90^o-z)\dot{R}_1(\theta)R_3(90^o-\zeta_0) + \\ & R_3(-90^o-z)R_1(\theta)\dot{R}_3(90^o-\zeta_0)\end{aligned} \tag{2.53}$$

where z, θ, and ζ_0 are the precession angles defined in (2.27) and R_i and $\dot{R}_i$ are defined in Appendix B. From (2.27):

$$\dot{\zeta}_0 = \left((2304".250 + 1".396T_0) + 0".604T + 0".054T^2\right)\frac{dT}{dt} \text{ arcsec/sec}$$

$$z = (\dot{\zeta}_0 + 1".582T)\frac{dT}{dt} \text{ arcsec/sec}, \tag{2.54}$$

$$\theta = \left((2004".682 - 0".853T_0) - 0".852T - 0".126T^2\right)\frac{dT}{dt} \text{ arcsec/sec},$$

where T_0 and T are measured in tropical centuries and related by the fundamental epoch of the star catalogue of $t_0 = 1900.0 + T_0$ and the final epoch of observation of $t = 1900.0 + T_0 + T$,

and $$\frac{dT}{dt} = \frac{1}{36525 \times 86400}.$$

This value for dT/dt may be used for any of the time scales, e.g. tropical, Julian and Besselian, without loss of accuracy in this context.

The matrix describing the rate of change of nutation with respect to time is obtained by differentiating (2.30) to give:

$$\dot{N} = \dot{R}_1(-\varepsilon-\Delta\varepsilon)R_3(-\Delta\psi).R_1(\varepsilon) + R_1(-\varepsilon-\Delta\varepsilon).\dot{R}_3(-\Delta\psi).R_1(\varepsilon) + R_1(-\varepsilon-\Delta\varepsilon).R_3(-\Delta\psi).\dot{R}_1(\varepsilon) \quad (2.55)$$

where $\Delta\psi$ and $\Delta\varepsilon$ are the nutation in longitude and obliquity respectively (see Appendix C and §2.3.4), ε is the obliquity of the ecliptic defined in (2.31), and R_i and $\dot{R}_i$, i = 1 to 3, are the rotation matrices defined in Appendix B. The full formulae in the expansion of (2.55) are given in Appendix C.2.

2.5.3 Antenna Geometry

The effect of antenna geometry on delay observations and their subsequent adjustment is described in §2.4.1. This section explains the application of the corrections for the antenna geometry to observations of fringe frequency and therefore it may be necessary to refer to the detailed descriptions of the separate effects given in §2.4.1.

For an antenna whose rotation axes intersect, the difference, t_v, between the time a signal arrives at the antenna focus and the time it would arrive at the antenna reference point can be assumed constant and therefore does not contribute to the fringe frequency observable. This is not the case if an antenna deforms as it moves but this is such a small effect, and also a very difficult one to monitor, that it can safely be ignored. The instrumental delay, t_i, caused by the finite time between receiving and recording of the signals is also assumed constant. This may not be the case due to changes in temperature, tension, and twist of the cables and overall instrumental imperfection. These very small changes are ignored in this work due to no data being available. It is, however, noteworthy that a constant drift in the instrumental delay would be absorbed in the 'c_1 term' (see §2.4.7) of the clock error polynomial.

The only effect of antenna geometry necessitating the application of a correction to fringe frequency observations is that caused by the offset of the drive axes which exists in some antennae. From (2.37), the correction to the fringe frequency caused by this effect is given by:

$$\Delta F_D = w(\dot{t}_D(A) - \dot{t}_D(B)) \qquad (2.56)$$

where ΔF_D = the overall correction to the computed fringe frequency caused by antennae with non-intersecting drive axes,

$\dot{t}_D$ = the contribution to the delay rate due to the continually changing distance between the antenna focus and the antenna reference point of an antenna,

and subscripts (A) and (B) denote antennae A and B respectively.

Equation (2.56) assumes positive delay for a signal reaching antenna A first and $\dot{t}_D$ will equal zero for antennae with intersecting rotation axes. Differentiating (2.36) gives:

$$\dot{t}_D = \frac{\mathbf{D}.\dot{\hat{\mathbf{s}}}}{c} + \frac{\dot{\mathbf{D}}.\hat{\mathbf{s}}}{c}, \qquad (2.57)$$

where all the vectors are relative to the instantaneous co-ordinate system m_i, i = 1 to 3, $\hat{s}$ is defined by (2.5) and (2.18), and D is the vector connecting the antenna reference point to the closest point on the line of the altitude axis (for an altitude-azimuth antenna).

2.5.4 Retarded Baseline

Having received a signal at one antenna, the Earth will rotate while the signal is propagating to the other antenna. This effect, known as the 'retarded baseline', is described for the delay observable in §2.4.4 and the correction given in (2.41) and (2.42).

The 'retarded baseline' effect also necessitates that a correction is made to the computed fringe frequency. The form of the correction is obtained by differentiating (2.41) with respect to time. Ignoring terms of less than 10^{-14} sec/sec, the correction is

$$\Delta F_r = - \frac{\dot{w} V_B \tau_g \dot{\hat{s}}}{c} \qquad (2.58)$$

where $\dot{\hat{s}} = \dot{R}\hat{s}$ and $\dot{R}$ is defined in (2.51),

V_B = the velocity of antenna B, the remote station,

and τ_g = the geometric delay from (2.13).

The effect of changing precession and nutation on the retarded baseline correction is insignificant.

2.5.5 Tropospheric Correction

The effect of the Earth's atmosphere on radio waves passing through it has already been described in §2.4.5. The form of the observed meteorological data and the two tropospheric models employed in this work, namely Chao's Model and Hopfield's Simplified Model, are described in Appendix D. Making the same assumptions for the fringe frequency as for the delay observable concerning both the nature of the atmosphere and the validity of the model used and described in §2.4.5, the tropospheric correction to a fringe frequency observation (assuming positive delay for a signal arriving at antenna A first) is:

$$\Delta F_{trop} = w(\dot{\Delta\tau}_{atm}(A) - \dot{\Delta\tau}_{atm}(B)) \qquad (2.59)$$

where ΔF_{trop} = the correction to the computed fringe frequency to account for the effect of tropospheric refraction,

and $\dot{\Delta\tau}_{atm}(A)$ and $\dot{\Delta\tau}_{atm}(B)$ = the rate of change of the delay, due to the atmosphere, of the signals arriving at antennae A and B respectively.

Except in cases of extremely unstable meteorological conditions, the tropospheric contribution to the fringe frequency and the delay rate consists mainly of a component due to the rate of change of elevation of the line of sight to the source with time. The rate of change of meteorological data with time also contributes to the tropospheric correction but to a much smaller extent. The total omission of the tropospheric correction in a fringe frequency adjustment will cause the resultant baseline length to contain large errors (around 60-80 m over 4000 km). The use of only average meteorological data will reduce this source of error to within a few metres of the "true" answer because of the dominant nature of the rate of change of elevation term in the correction model. This same situation occurs in satellite-Doppler position fixing systems using range-rate observations (see §6.3). This large error caused by the omission of the tropospheric correction in a delay rate adjustment does not occur in a delay adjustment although it will obviously degrade the results.

2.5.6 Clock Behaviour Model

The relative clock drift between station clocks at either end of a baseline is modelled by a polynomial in time, as described in §2.4.7. The resultant effect of this drift on fringe frequency observations is simply given by differentiating (2.48) with respect to time to give:

$$\Delta F_c = W\dot{\Delta\tau}_c = W(c_1 + 2c_2 t + 3c_3 t^2 + ...) , \qquad (2.60)$$

where $\dot{\Delta\tau}_c$ = the rate of change of relative clock drift,

c_1, c_2, c_3 = the coefficients of the polynomial,

and t = the time since the initialisation of the polynomial.

Clearly, a constant offset of the clocks will not affect the fringe

frequency observations apart from making the correlation process difficult for large offset values (see §4.3.2).

CHAPTER 3:

ADJUSTMENT OF VLBI OBSERVATIONS

3.1 INTRODUCTION

The observations constituting any surveying network will always be subject to observational errors and hence an adjustment method is required which will yield the most probable set of absolute or relative network station co-ordinates in a specific reference system. The adjustment procedure should also provide data concerning the accuracy of the adjusted parameters and must be capable of combining different types of observations in order to obtain the maximum information from the combined solution.

This chapter explains, without recourse to complex mathematical proofs (see Appendix F) the basic method of variation-of-co-ordinates (§3.2.1), the solution of the derived observation equations by the method of weighted least-squares (§3.2.2), and the computation of the covariance matrix of the solution vector (§3.2.3). The observation equations for both the VLBI group delay and fringe frequency observations are listed in §3.3. The observational requirements and restrictions necessary to adjust this delay and fringe frequency (or delay rate) data are outlined in §3.4 while the formulae for the assessment of the accuracy of the adjusted parameters are derived in §3.5. Finally, the data filtering techniques used to assess the reliability of individual observations and sets of observations are described in §3.6.

3.2 ADJUSTMENT AND ANALYSIS OF A GENERAL NETWORK

3.2.1 Variation of Co-ordinates

The method of variation of co-ordinates is commonly used to adjust conventional survey networks (Dodson, 1977 and Ashkenazi, 1968a) and is also suitable for the adjustment of VLBI delay and fringe

frequency data. The method assumes initial approximate values for all the unknown quantities and expresses the effect that changes in these values will have on the observed quantities in the form of observation equations. For example, if an observable P is a function of three unknown parameters r, s, and t such that:

$$P = f(r, s, t),$$

then the error in P, δP, caused by the inaccurate initial estimates of r, s, and t can be expressed as:

$$\delta P = g(\delta r, \delta s, \delta t),$$

where δr, δs, and δt are the differences between the true and the estimated parameter values. If these corrections are small, then the function g is accurately approximated by a linear function whose coefficients can be computed from the initial approximate parameter values such that:

$$\delta P = \frac{\partial P}{\partial r} \delta r + \frac{\partial P}{\partial s} \delta s + \frac{\partial P}{\partial t} \delta t. \qquad (3.1)$$

If the necessary corrections to the initial estimated values are large, then the practice is to perform a solution and then use the updated values as new estimates in a further adjustment. This procedure can be repeated until a stable solution is achieved.

If a *perfect* observation of the parameter P is made, then δP is related to the observation by the equation:

$$\delta P = P_o - P_c , \qquad (3.2)$$

where P_o = the observed value,

and P_c = the value computed from the initial approximate data

= f(r,s,t).

Hence, for many observations of P, a set of equations of the form:

$$Ax = b \ , \tag{3.3}$$

is derived where the i^{th} equation is of the form:

$$\left(\frac{\partial P}{\partial r}\right)_i \delta r + \left(\frac{\partial P}{\partial s}\right)_i \delta s + \left(\frac{\partial P}{\partial t}\right)_i \delta t = P_{o_i} - P_{c_i} \ , \tag{3.4}$$

and A = the matrix of coefficients $\left(\frac{\partial P}{\partial r}\right)_i$, $\left(\frac{\partial P}{\partial s}\right)_i$, ... etc.,

x = the vector of unknowns, $[\delta r, \delta s, \delta t]^T$,

and b = the vector of 'observed minus computed' values of P.

3.2.2 Weighted Least Squares

If a set of observations was made which contained no errors, then the observation equations in (3.4) could be solved for a unique vector of unknowns, x, providing that there were at least 3 independent equations in δP. However, this idealised case can never be realised because of observational errors, the difference between the observed value and the best estimate value being termed the observation residual, v. The least squares adjustment process is therefore designed to determine the statistically most probable solution vector by minimising the sum of the squares of the observation residuals satisfying the vector equation:

$$Ax = b + v \tag{3.5}$$

where v = the vector of residuals or observational errors,

and x = the most probable solution vector.

For independent observations, each individual observation is assigned a weight, W_i, which is a measure of the relative importance of

that observation and is defined as the reciprocal of its estimated a priori variance (i.e. the smaller the error the greater the weight of that observation). In the weighted least squares process, in order to compute the most probable vector of unknowns, the sum of the squares of the weighted residuals is minimised (see Appendix F.1) such that, for independent observations:

$$v^T W v = W_1 v_1^2 + W_2 v_2^2 + W_3 v_3^2 + \ldots \text{ etc.} = \text{a minimum}, \qquad (3.6)$$

where v = the vector of least squares residuals,

W = the weight matrix of the observations,

and W_i and v_i = the weight and residual respectively of the i^{th} observation.

For independent observations like those assumed above, the weight matrix is a diagonal matrix whereas for correlated observations it is a full matrix. In both cases, it is the inverse of the estimated covariance matrix of the observations, σ_{bb} (see Appendix F.2). VLBI observations are considered independent and hence possess a diagonal weight matrix.

The solution of (3.6) for the vector x is achieved by solving the equation:

$$(A^T W A)x = A^T W b \ , \qquad (3.7)$$

(see Appendix F.1 for the derivation of this formula).

These equations are known as the 'normal equations'. It is important in forming the normal equations that the dimensions of the weights of the different types of observations are such that each weighted observation equation is dimensionless and therefore makes its true contribution to the normal equations and hence to the overall solution (see §3.3). The normal equations are solved by first decomposing the

coefficient matrix A^TWA using Choleski's method (see Appendix F.4) and then by forward and back substitution (see Appendix F.5) to obtain the solution vector x. As a general rule, the left-hand-side of the observation equations should be computed to one more significant figure than the desired corrections, and the right-hand-sides must be computed to the same accuracy as these corrections (Cross, 1970).

3.2.3 Covariance Matrix

The covariance matrix of the vector:

$$x = [x_1, x_2, x_3, \ldots, x_n]^T ,$$

is defined as:

$$\sigma_{xx} = \begin{bmatrix} \sigma^2_{x1} & \sigma_{x1x2} & \cdots & \sigma_{x1xn} \\ \sigma_{x2x2} & \sigma^2_{x2} & & \vdots \\ \vdots & & \ddots & \\ \sigma_{xnx1} & \cdots & & \sigma^2_{xn} \end{bmatrix} \qquad (3.8)$$

where σ^2_{xi} is the variance of the vector element x_i and σ_{xixj} is the covariance of the pair of elements x_i and x_j. The covariance matrix of the unknown parameter vector x derived from the solution of (3.7) is given by (See Appendix F.6):

$$\sigma_{xx} = \sigma_0^2 \, (A^TWA)^{-1} \qquad (3.9)$$

where $(A^TWA)^{-1}$ = the inverse of the coefficient matrix of the normal equations,

and σ_0^2 = an unbiased estimate of the square of the standard error of an observation of unit weight, also termed the unit variance, and is given by (see Appendix F.3):

$$\sigma_0^2 = \frac{v^T W v}{n-k} ,$$

where n = the number of observations contributing to the solution,

k = the number of unknowns of the solution,

and hence n-k = the number of redundancies.

If the a priori weights of the observations have been estimated correctly, then the value of σ_0^2 derived from the adjustment should equal unity. If $\sigma_0^2 = k$ then the initial weights have been incorrectly estimated by a factor of k. The relationship between the estimated and adjusted covariance matrices of the observations, σ_{bb}, is therefore:

$$\sigma_{bb}(\text{unbiased}) = \sigma_0^2 . \sigma_{bb}(\text{estimated}), \qquad (3.10)$$

where $W = \sigma_{bb}^{-1}$.

The extraction of data from the covariance matrix of the unknowns, σ_{xx}, concerning the accuracy of various parameters of the solution is considered in §3.5.

3.3 VLBI ADJUSTMENT PROCEDURE

3.3.1 Delay Observation Equations

The basic geometric delay formula, as developed in §2.1.3 and including a second order clock error polynomial, is given by:

$$\tau = -\frac{1}{c}\{b_x \cos\delta_s \cos h_s - b_y \cos\delta_s \sin h_s + b_z \sin\delta_s\}$$

$$+ c_0 + c_1 t + c_2 t^2 , \qquad (3.11)$$

where b_x, b_y, b_z = the baseline components,

δ_s and α_s = the source declination and right ascension,

h_s = GAST - α_s,

GAST = Greenwich Apparent Sidereal Time at the epoch of observation,

c = velocity of propagation of microwaves in vacuo,

and $(c_0+c_1t+c_2t^2)$ = the clock error polynomial as described in §2.4.7.

The calculation of the delay requires a knowledge of several parameters whose values are not precisely known and which will consequently cause systematic errors in the solution if no allowance is made for them. It is therefore desirable to estimate initial values for these parameters and to solve for the difference between their estimated and most probable values in the adjustment process (see §3.2.1). The adoption of estimated or defined values for all the parameters on the right-hand-side of (3.11) leads to the formation of an observation equation for each observed delay time of the form:

$$\frac{\partial\tau}{\partial\delta_s}\delta\delta_s + \frac{\partial\tau}{\partial\alpha_s}\delta\alpha_s + \frac{\partial\tau}{\partial b_x}\delta b_x + \frac{\partial\tau}{\partial b_y}\delta b_y + \ldots. =$$

$$\tau_{observed} - \tau_{computed} + v \qquad (3.12)$$

as defined in (3.5). The partial derivatives of the delay with respect to the unknown parameters are computed from (3.11), $\tau_{observed}$ is the observed delay, $\tau_{computed}$ is the delay calculated from (2.49) and is hence the most accurate estimate of the delay from the available data, v is the residual error in the observation, and $(\delta\delta_s, \delta\alpha_s, \delta b_x, \ldots)$ are the unknown differences between the estimated and most probable parameter values.

Generally, the unknown parameters in a VLBI adjustment are the corrections to the initial estimated values of either the baseline components or the antennae co-ordinates themselves, the clock error polynomial coefficients, and the source co-ordinates. There are two methods of computing the baseline components, either solving for them directly or solving for the co-ordinates of each antenna. From the

co-ordinates of antennae A and B of (x_A,y_A,z_A) and (x_B,y_B,z_B) respectively, and the relationships $b_x = x_B-x_A$, $b_y = y_B-y_A$, and $b_z = z_B-z_A$, the observation coefficients for an adjustment using the antenna co-ordinates as unknowns are:

$$\frac{\partial\tau}{\partial x_B} = -\frac{1}{c}\cos\delta_s\cos h_s,$$

$$\frac{\partial\tau}{\partial y_B} = \frac{1}{c}\cos\delta_s\sin h_s,$$

$$\frac{\partial\tau}{\partial z_B} = -\frac{1}{c}\sin\delta_s, \qquad (3.13)$$

$$\frac{\partial\tau}{\partial x_A} = -\frac{\partial\tau}{\partial x_B},$$

$$\frac{\partial\tau}{\partial y_A} = -\frac{\partial\tau}{\partial y_B},$$

and $$\frac{\partial\tau}{\partial z_A} = -\frac{\partial\tau}{\partial z_B},$$

and for an adjustment using the baseline components as unknowns these coefficients are given by the relationships:

$$\frac{\partial\tau}{\partial b_x} = \frac{\partial\tau}{\partial x_B},$$

$$\frac{\partial\tau}{\partial b_y} = \frac{\partial\tau}{\partial y_B}, \qquad (3.14)$$

and $$\frac{\partial\tau}{\partial b_z} = \frac{\partial\tau}{\partial z_B}.$$

When the former method is used, the clock errors are also regarded in terms of the errors in the individual clocks such that:

$$c_0 + c_1t + c_2t^2 = (c_0 + c_1t + c_2t^2)_B - (c_0 + c_1t + c_2t^2)_A \qquad (3.15)$$

which will yield similar equations and relationships as exist between

(3.13) and (3.14). The observation equation coefficients for an adjustment in terms of the relative clock errors on a baseline rather than in terms of the errors in the individual clocks are:

$$\frac{\partial \tau}{\partial c_0} = 1 ,$$

$$\frac{\partial \tau}{\partial c_1} = t , \qquad (3.16)$$

and $$\frac{\partial \tau}{\partial c_2} = 2t.t^2.$$

The observation equation coefficients for the source co-ordinates are:

$$\frac{\partial \tau}{\partial \delta_s} = \frac{1}{c}\{b_x \sin \delta_s \cos h_s - b_y \sin \delta_s \sin h_s - b_z \cos \delta_s\},$$

(3.17)

and $$\frac{\partial \tau}{\partial \alpha_s} = -\frac{1}{c}\{b_x \cos \delta_s \sin h_s + b_y \cos \delta_s \cos h_s\} .$$

Further sources of systematic error may be modelled or it may be desirable for studies to be made of certain other parameters, for example Love's Number in the Earth tide correction. The only one of direct interest in this study is that for the tropospheric correction model of Chao (§2.4.5 and Appendix D.4) where an estimate of the correction to the atmospheric delay in the zenith direction at each antenna is made. For this case, referring to (D.19) and (D.20):

$$\frac{\partial \tau}{\partial \Delta\tau_{atm_A}} = \frac{0.9}{\sin E_A + (0.00143/(\tan E_A + 0.0445))} + \frac{0.1}{\sin E_A + (0.00035/(\tan E_A + 0.017))} \qquad (3.18)$$

where E_A is the elevation of the source as viewed from antenna A and 0.9 and 0.1 are the proportionate contributions of the dry and wet tropospheric components respectively. The $\partial\tau/\partial\Delta\tau_{atm_B}$ term is similar

to $\partial\Delta\tau_{atm_A}$ but has the E_A terms replaced by E_B and has the opposite sign on the overall equation.

It is essential that the units of the observation equations be consistent such that for each delay observation unknown d, the product $\frac{\partial\tau}{\partial d}\,\delta d$ is in the same units as the observed delay. Similarly, the weighting of an observation by multiplying it by the reciprocal of the standard error, or $W^{\frac{1}{2}}$ using the definition of an observation weight given in §3.2.2, should render all the $W^{\frac{1}{2}}\frac{\partial\tau}{\partial d}\,\delta d$ products, and the right-hand-side vector b (see (3.3)), dimensionless. Conventionally, natural units (metres and seconds of time) are always used for the parameters in the adjustment. For example, this involves expressing the observed delays and their standard errors in seconds of time, the baseline in metres, and the velocity of propogation of microwaves in vacuo in metres per second. This results in the unknowns being computed in their own natural units.

3.3.2 Fringe Frequency Observation Equations

The basic fringe frequency formula, as developed in §2.5 and including a second order clock error polynomial, is:

$$F = \left(-\frac{\Omega W}{c}\{b_x \cos\delta_s \sin h_s + b_y \cos\delta_s \cos h_s\}\right. \text{ SIGN INCONSISTENT WITH DELAY FORMULA}$$

$$\left. + wc_1 + 2c_2 tw\right. \qquad (3.19)$$

where w = the observing frequency,

and Ω = the rate of rotation of the Earth from (2.52).

All the unknown parameters for the fringe frequency adjustment are also unknowns in the delay adjustment from (3.11), the only differences being that fringe frequency observations are insensitive to the z-component of the baseline and unaffected by the c_0 term of the clock error

polynomial. Consequently, these two parameters are not present in (3.19). The computation of the observation equations from estimated and defined parameter values is performed in the same manner for the fringe frequency observable as is shown in (3.12) for the delay observable. The same theory and comments concerning the use of either antennae co-ordinates or baseline components in the adjustment apply for fringe frequency as stated for the delay in §3.3.1 and hence the observation equation coefficients for the antennae co-ordinate unknowns are:

$$\frac{\partial F}{\partial x_B} = -\frac{\Omega w}{c} \cos \delta_s \sin h_s ,$$

$$\frac{\partial F}{\partial y_B} = -\frac{\Omega w}{c} \cos \delta_s \cos h_s ,$$

(3.20)

$$\frac{\partial F}{\partial x_A} = -\frac{\partial F}{\partial x_B} ,$$

$$\frac{\partial F}{\partial y_A} = -\frac{\partial F}{\partial y_B} ,$$

and for an adjustment with the corrections to the baseline components as the unknowns rather than the antennae co-ordinates, the coefficients are:

$$\frac{\partial F}{\partial b_x} = \frac{\partial F}{\partial x_B} ,$$

(3.21)

$$\frac{\partial F}{\partial b_y} = \frac{\partial F}{\partial y_B} .$$

Again, the clock error polynomial may be regarded in two different ways as described in §3.3.1 and (3.15). In terms of the clock errors over a baseline rather than the separate errors of the two antenna of the baseline, the coefficients are:

$$\frac{\partial F}{\partial c_1} = W$$

$$\frac{\partial F}{\partial c_2} = 2tW \qquad (3.22)$$

The observation equation coefficients for the source co-ordinates are:

$$\frac{\partial F}{\partial \delta_s} = \frac{\Omega W}{c}\{b_x \sin\delta_s \sin h_s + b_y \sin\delta_s \cos h_s\},$$

$$\frac{\partial F}{\partial \alpha_s} = \frac{\Omega W}{c}\{b_x \cos\delta_s \cos h_s - b_y \cos\delta_s \sin h_s\}, \qquad (3.23)$$

and those for the correction to the estimated atmospheric delay in the zenith direction according to Chao's model (§2.4.5 and Appendix D.4) are:

$$\frac{\partial F}{\partial \Delta\tau_{atm_A}} = -w\frac{dE_A}{dt}(0.9X + 0.1Y)$$

where $\frac{dE_A}{dt}$ is as defined in (D.18),

$$X = \frac{\dfrac{0.00143}{(\cos^2 E_A \times (0.0445 + \tan E_A)^2)} - \cos E_A}{\left[\dfrac{0.00143}{0.0445 + \tan E_A} + \sin E_A\right]^2} \qquad (3.24)$$

and Y is as X but with 0.00035 replacing 0.00143 and 0.017 replacing 0.0445. The equation for $\partial\Delta\tau_{atm_B}$ is similar apart from E_B replacing E_A and the sign of the whole equation changing.

The observation equations coefficients for delay rate observations are the corresponding fringe frequency coefficients divided by the observing frequency, w. Consequently, the observed quantities are expressed in natural units of seconds per second for the delay rate and hertz (Hz) for the fringe frequency.

3.3.3 Single Baseline Adjustment

The standard set of unknowns for a single baseline adjustment of either just delay or both delay and fringe frequency observations, consist of the clock error polynomial terms, the baseline components, and the co-ordinates of each of the observed sources. The use of the baseline components instead of the antenna co-ordinates as unknowns (see §3.3.1) is preferred in this single baseline adjustment as it makes no difference to the solution and is computationally simpler. In the example described here, no further unknowns are considered (see §3.3.1) but they would be treated in a similar fashion as the unknowns that are included. Furthermore, the right ascension of source 1 is held fixed although it could have been any one of the source right ascensions (one fixed right ascension is a minimum requirement as explained in §3.4.3).

Each observation contains information concerning the clock error, the baseline, and only one source and therefore the normal equations coefficient matrix for observations of either delay or both delay and fringe frequency is of the form shown in Fig. 3.I. The shaded areas in the figure represent non-zero elements of the matrix. The solution of the normal equations (see §3.2.2) gives the solution vector and the inversion of this coefficient matrix yields the covariance matrix for the unknowns from (3.9). The extension of this example to cater for observations of fringe frequency only is a simple task which will be clarified in §3.4 where the necessary constraints and requirements are described.

3.3.4 Triple Baseline Adjustment

The standard vector of unknowns for a three station, three baseline, VLBI array using observations of either delay or both delay

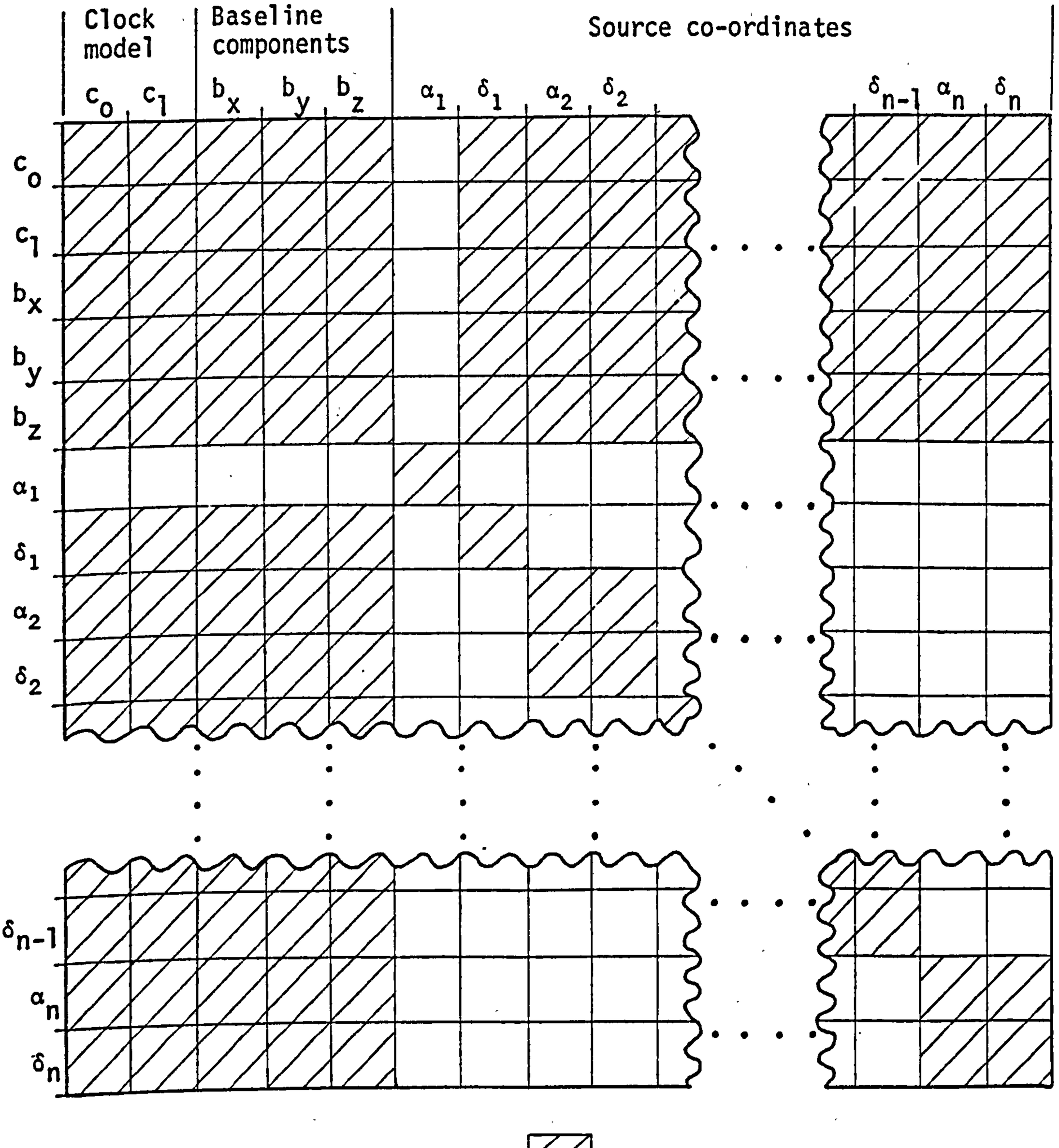

Fig. 3.I An example of a normal equations matrix for a single baseline adjustment showing the relation between the different rows and columns and their appropriate unknowns.

and fringe frequency consists of the corrections to the initial estimates of both the clock error polynomial coefficients and the co-ordinates for each antenna, and the co-ordinates of the observed sources. In this three baseline array the antenna co-ordinates are adjusted in preference to the baseline components so as to enforce a closure of the triangle formed by the three stations. A solution in terms of the baseline components would nevertheless be quite acceptable though it would give slightly different results. Further unknowns may also be added as described in §3.3.1 but none are considered in this particular example of an adjustment. When a solution is performed in this mode, the minimum requirement is that one clock, one station position, and one source right ascension must be held fixed (see §3.4 which also outlines another method other than fixing parameters).

Fig. 3.II illustrates the normal equations coefficient matrix for this example of a three antenna array observing a total of five sources and performing an adjustment of either just delay or both delay and fringe frequency observations in terms of the individual antennae co-ordinates and clock errors. The effect of the co-ordinates and clock of antenna A being held fixed (see §3.4.3) are shown, together with the effect of holding the right ascension of source 2 fixed. The result of antenna C not observing source 4 is illustrated. The non-zero elements of the matrix are represented by the shaded areas.

The solution of these equations and the subsequent error analysis proceed as described throughout this chapter and Appendix F.

3.4 ADJUSTMENT REQUIREMENTS

3.4.1 Minimum Delay Observational Requirement

The variation of geometric delay as defined in (2.49) with respect to time, maps out a cosine wave of wavelength 24 sidereal hours and of

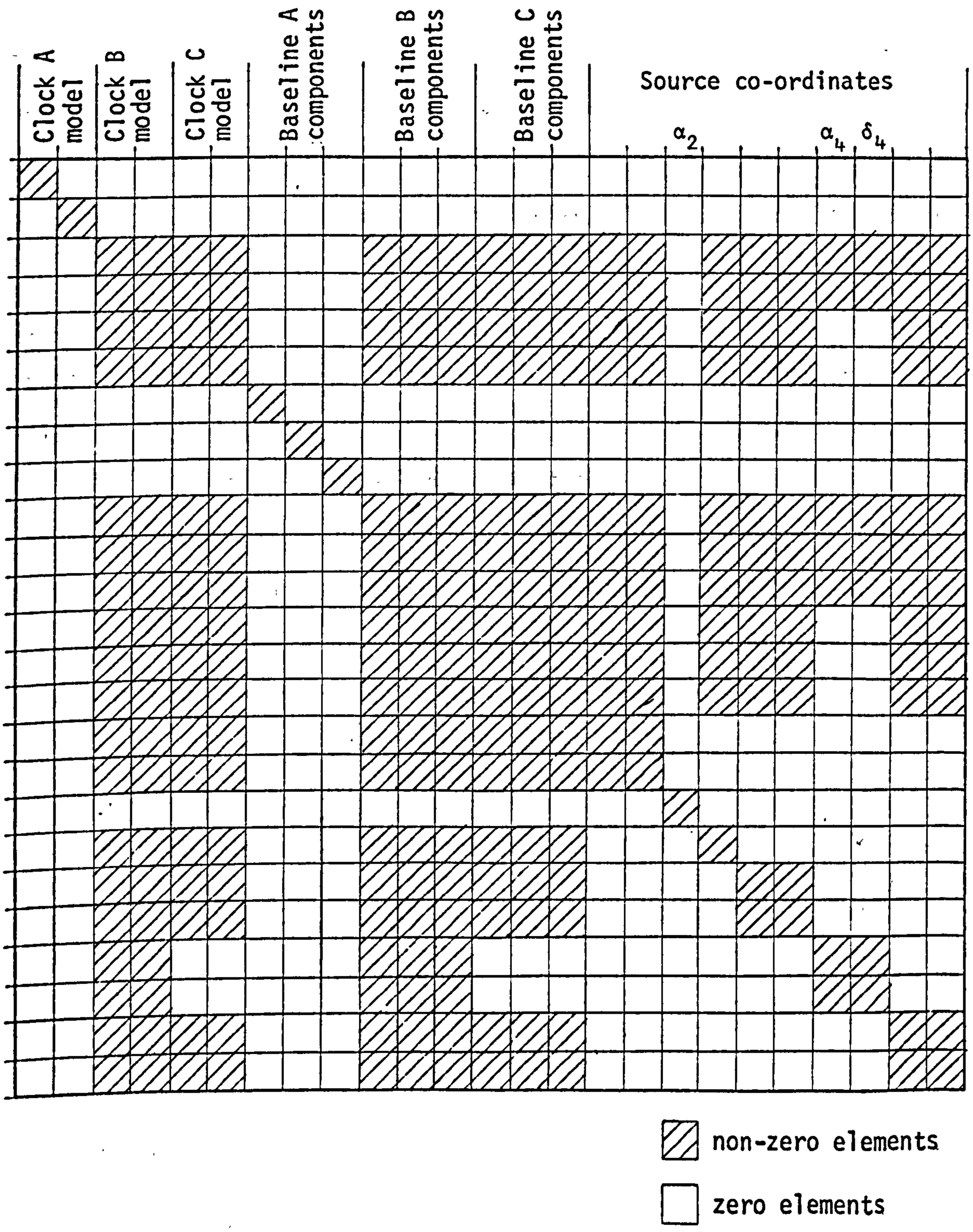

Fig. 3.II An example of a normal equations matrix for a 3 station-3 baseline adjustment in terms of the antenna co-ordinates and parameters as opposed to baseline co-ordinates and parameters

an amplitude which is a function of the equatorial component of the baseline, the declination of the source, and the velocity of propagation, c, of the signal from the source. The inclusion in the observed geometric delay of the errors due to the relative discrepancies between the station clocks results in this plot becoming a cosine wave superimposed on a curve representing this difference (see Fig. 3.III). If the time origin of the plot is the origin of the clock error polynomial, then the intercept of the curve on the delay axis will be the sum of the initial clock synchronisation error, c_o, and the geometric delay at the origin epoch, $\tau_g(o)$. The shape of the clock drift curve is a function of the first and higher order terms of the relative clock error polynomial although usually the second term would be the highest considered in an adjustment (see §2.4.7).

The combination of the basic geometric delay equation (2.13) and a first-order (linear) clock error polynomial (with well behaved hydrogen maser standards this first-order model should be satisfactory as discussed in §2.4.7) gives the equation for delay as (Barber, 1977):

$$\tau = S + Tt + U \cos(\Omega t + \beta), \qquad (3.25)$$

where $S = c_o + \frac{B}{C} \sin \delta_B \sin \delta_s$,

$T = c_1$,

$U = \frac{B}{C} \cos \delta_B \cos \delta_s$,

$\beta = h_s - h_B$ at $t = 0$,

$c_o + c_1 t$ = the clock error polynomial (t is the time since its origin, i.e. the time at which c_o is the relative clock offset),

B = the baseline length ($\sqrt{b_x^2 + b_y^2 + b_z^2}$),

Ω = rate of rotation of the Earth,

and δ and h are the declination and Greenwich hour angle respectively while subscripts S and B represent the source and baseline respectively.

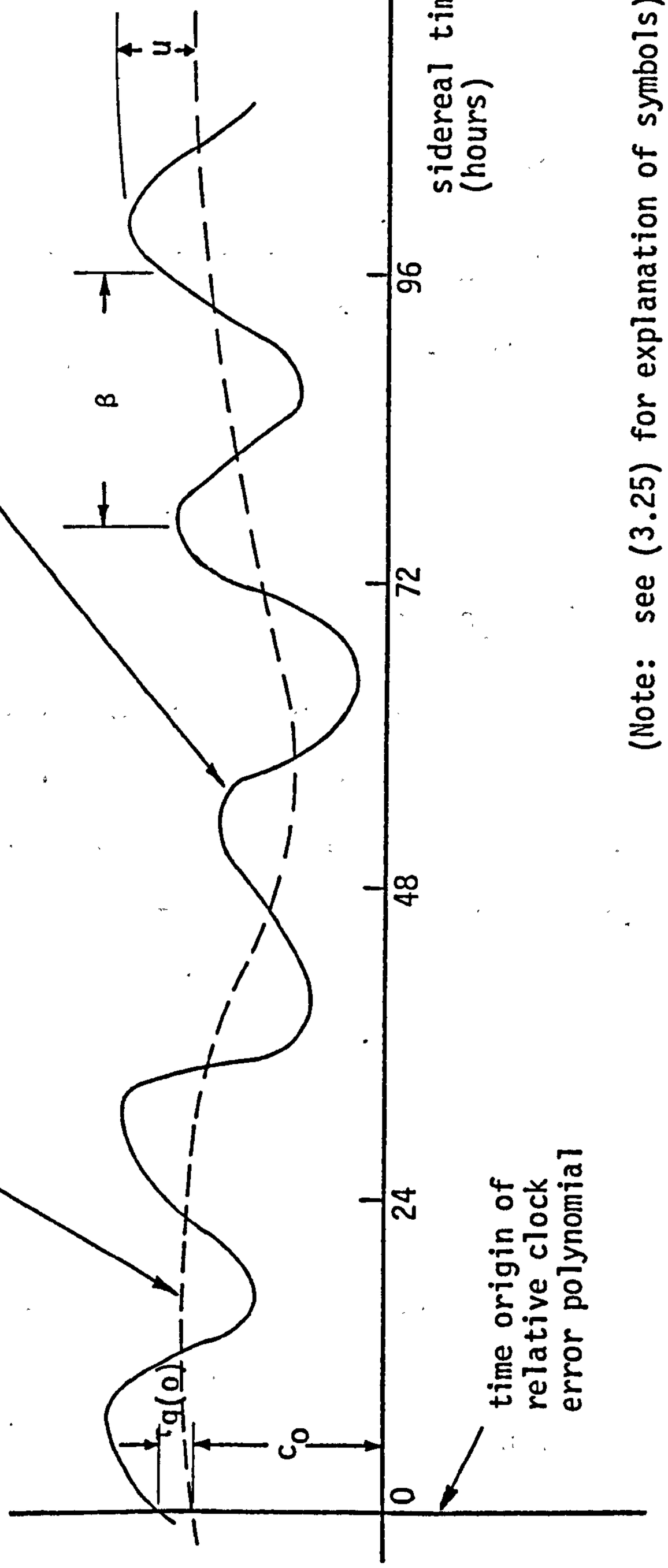

(Note: see (3.25) for explanation of symbols)

Fig. 3.III Curve of varying delay time with respect to time

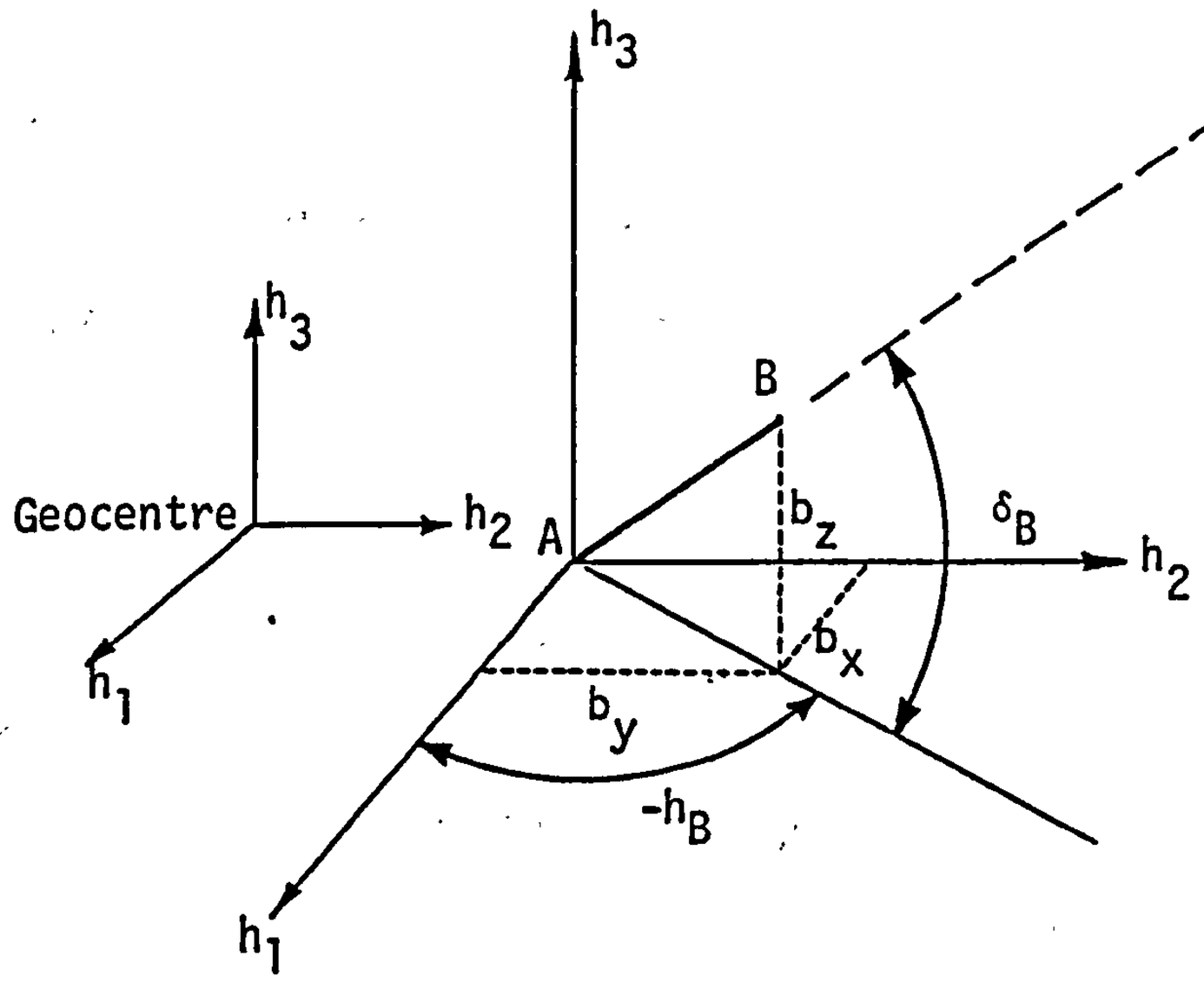

Fig. 3.IV Definition of hour angle and declination of the baseline

The declination and Greenwich hour angle of the baseline are obtained by extrapolating the baseline from antenna A through antenna B and on to the surface of the celestial sphere. Hence, the line is assumed to be radiating from the Earth's geocentre (i.e. parallax effects are negligible) and consequently (see Fig. 3.IV):

$$h_B = \tan^{-1} \frac{b_y}{b_x}$$ surely $-h_B$ from 3.IV ?

and $$\delta_B = \sin^{-1} \frac{b_z}{B} = \cos^{-1} \frac{\sqrt{b_x^2 + b_y^2}}{B} \qquad (3.26)$$

The baseline hour angle is often termed the longitude of the baseline. Here, although it is termed the hour angle, it is expressed in units of arc. Both these terms are defined relative to the Average Terrestrial system (see §2.1.2.1) upon which the baseline components are defined. Expansion of (3.25) shows the delay to be a function of a constant offset, a linear drift, a cosine term, and a sine term and consequently four or more delay observations on a single source yield four independent equations in S, T, U, and β. However, the required unknowns from a

VLBI analysis are the three baseline components, the two source co-ordinates, and the two clock error model coefficients, and therefore these cannot all be obtained from observations of one source only since the total number of independent equations is 4 and the total number of unknowns is 7. Observations of an additional source using the same station clocks results in the introduction of two new unknowns, the co-ordinates of the source, but also three more independent equations, the T term being common to all observed sources. The addition of a third observed source brings the total number of independent equations to 10 and the total number of unknowns to 11. However, it is necessary to define an origin of right ascension for the adjustment (see §3.4.3) and consequently one source right ascension is held fixed and the total number of unknowns is reduced to 10.

The minimum requirement for a full analysis of VLBI delay data observed over a single baseline is therefore that ten independent observations be made on three different sources. More observations of these three sources, plus observations of further sources, spanning a large fraction of the diurnal cycle give useful redundancies in the solution for the unknown parameters.

In order to extrapolate these minimum requirements to a larger interferometer array, consider an n station array in which each source is observed from all stations simultaneously. Furthermore, let this network be adjusted in terms of the parameters of each antenna (its co-ordinates and clock error relative to a station, or stations, whose a priori co-ordinates and clock are assumed fixed in the adjustment (see §3.4.3)) rather than the parameters for each baseline (see §3.3.1). In such an array, there are (n-1) independent baselines which each give 4 independent equations for the first observed source and 3 more for each subsequent observed source. Assuming a first-order clock error

polynomial is satisfactory to describe the clock behaviour at each station, there are 5(n-1) station unknowns (one station and one clock being held fixed in the adjustment) and (2s-1) source unknowns, where s is the number of sources and the origin of right ascension is defined by fixing the R.A. of one source. Therefore, in order to solve for all the parameters the following relationship between the number of independent equations and the number of unknowns must be satisfied:

$$4(n-1) + 3(s-1)(n-1) > 5(n-1) + 2s-1.$$

From this expression it can be shown that no matter how many antennae are participating in an experiment, at least two sources must be observed in order to give a solution for all the clock error parameters and the antenna and source co-ordinates.

3.4.2 Minimum Fringe Frequency Observational Requirements

The curve of varying geometric fringe frequency with respect to time is a sine wave of wavelength 24 sidereal hours and amplitude which is a function of the equatorial component of the baseline, the declination of the source, the rate of rotation of the Earth, the observing frequency, and the velocity of the propagation of the signal from the source. Inclusion of the clock error with the geometric fringe frequency results in this plot becoming a sine wave superimposed on a curve defined by the differential, with respect to time, of the clock error polynomial described in §2.4.7 (see Fig. 3.V). If the time origin of the plot is the origin of the clock error polynomial, then the intercept of this clock error curve is at c_1, the coefficient of the first-order term, and its shape is governed by the second and higher order terms. Assuming that it is sufficient to use a first-order polynomial to model the clock error in the adjustment, then:

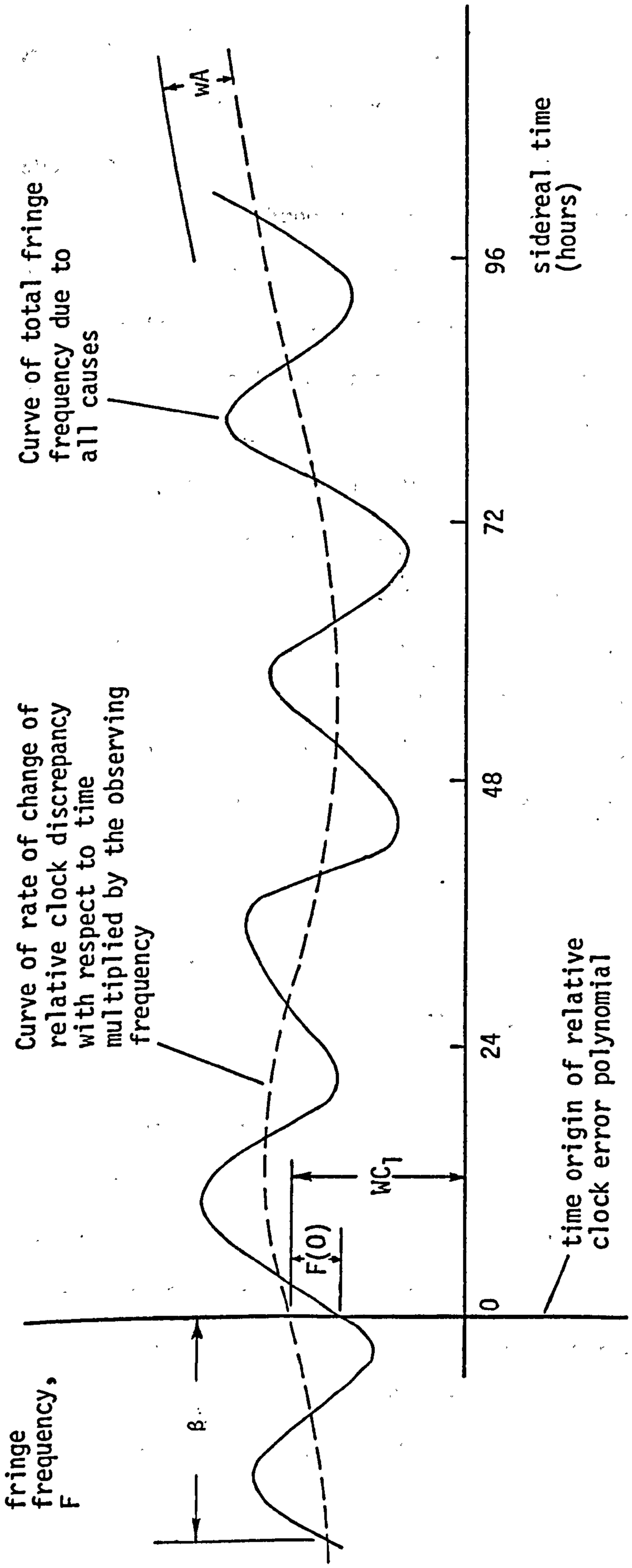

Fig. 3.V Curve of varying fringe frequency with respect to time

$$F = wc_1 + wA\sin(\Omega t + \beta) \quad , \tag{3.27}$$

where $A = -\frac{B\Omega w}{c} \cos \delta_B \cos \delta_s$,

w = the observing frequency,

and the other terms are as described for the delay in (3.25).

Therefore, three or more observations of a single source will yield three independent equations in c_1, A, and β, whereas the unknowns are 5 in total, namely the two equatorial components of the baseline, the two co-ordinates of the source, and the relative drift rate of the station clocks. Observations of each additional source will give two more unknowns but also only two more independent equations and hence the deficiency remains equal to two. The fixing of one right ascension to define an origin of right ascension reduces this to one, and therefore, in order to perform a solution, either one source declination is held fixed or an appropriately weighted "imaginary" observation of a source declination is included in the adjustment. This fixed source should preferably be a near-equatorial one (Shapiro, 1976).

3.4.3 Network Defect

The unknowns of the variation-of-co-ordinates method of adjustment §3.2.1) are corrections to estimated parameter values rather than corrections to the observations themselves. The application of the variation-of-co-ordinates technique to the adjustment, results in a rank defect (Ashkenazi and Grafarend, 1975) which causes the coefficient matrix of the normal equations to be singular. This results in the solution of the normal equations, and consequently the formation of the covariance matrix for the unknowns, being impossible. A matrix is said to possess a rank, p, if it contains at least one sub-determinant

of order p that does not equal zero, whereas all determinants of a higher order do equal zero (Ashkenazi, 1968). The order of the rank deficiency, otherwise known as the order of degeneracy, of the normal equations coefficient matrix is defined as the difference between the order of the matrix (i.e. the number of unknowns to be adjusted) and its rank.

The maximum degeneracy of a three-dimensional network is seven, three defects due to not positioning the network, three defects due to not orienting the network, and one defect due to not scaling the network. Consequently, constraints may have to be applied on certain parameters of the network adjustment model in order to remove any singularity from the normal equations coefficient matrix. Alternatively, a "free network" adjustment may be performed (Grafarend and Shaffrin, 1974; Ashkenazi, 1973; Mittermayer, 1972) although this is not used in this work and will not be discussed here.

There are two methods of introducing the restrictions necessary to remove this rank defect, namely either the inclusion in the adjustment of appropriately weighted "imaginary" observations of certain of the unknown parameters, or the fixing of some paramter values. The first of these two methods enables the parameters upon which the restrictions are being applied to be adjusted in the solution according to their own weights and the other observations in the network. However, it must be remembered that if such a restriction is applied to only one parameter controlling a defect (e.g. only one antenna position or only one source right ascension) then the a posteriori and a priori value and standard error of that parameter will be equal. The equations necessary to define a position are termed 'position equations' and similarly, those to define a direction are termed 'direction equations'.

4/1986 ✓

The second of these methods of removing defects involves fixing the values of certain parameters in order to apply the necessary restrictions to the adjustment. It is this method which is used throughout this study. This generally involves modifying either the observation equations (McLintock, 1976) or the normal equations (see §5.3.2) in such a way that the unknown associated with the fixed parameter is zero.

In a VLBI network, the positional defect may or may not exist depending on the form of the adjustment. If it is being performed in terms of the baseline components (see §3.3.1), then the position of the network in space is irrelevant. However, if the adjustment is being performed in terms of the absolute antenna co-ordinates, then one set of antenna co-ordinates must be either held fixed or located by 'position equations' in order to position the network in space. The scale of the VLBI system is implicitly defined by the value of the velocity of propagation of microwaves in vacuo used. Considering the possible orientation defects, the equatorial plane is implicitly defined as being perpendicular to the axis of rotation of the Earth and also parallel to the velocity vector of the Earth's rotation at any point (Shapiro, 1976) and hence two of the possible three defects are eliminated. It is necessary to define a direction on this plane in order to remove the third possible defect. This is achieved by fixing the right ascension of one source which locates the vernal equinox from which all the observation epochs are measured. It is said to provide the origin of right ascension. The use of a fixed source, rather than observations of the direction of one or more sources, is conventionally used so that, whatever the nature and accuracy of the observations, the baseline components obtained from different experiments can be related. A change in the orientation of the system will result

in a change in the baseline components but not in the baseline length. It would be equally valid to fix the hour angle of the baseline instead of one of the source right ascensions but this is not appropriate to this study which is primarily interested in the baseline components. Similarly, the declination of the baseline could be held fixed instead of a source declination.

In the same way that the co-ordinates of one station are held fixed in an interferometer array, the clock of one station is held fixed and hence the relative offset of the other clocks to this one are computed.

3.5 Statistical Error Analysis

The a posteriori covariance matrix of the vector of unknowns defined in (3.8) and (3.9) can be used to compute several criteria to assess the quality of the adjustment. It must be recognised, however, that this computed error analysis takes account of only the random errors remaining after all the corrections to the observations have been applied and is unable to assess any unmodelled systematic errors.

The leading diagonal of the covariance matrix has been defined (§3.2.3) as containing the variance, or square of the a posteriori standard error, of the corresponding unknown, and hence these quantities are readily accessible. The variances and covariances of an adjusted antenna location can be used to compute the variances and covariances of the adjusted position relative to any other set of orthogonal axes and hence the locus of the "absolute error ellipsoid" (Ashkenazi, 1972) can be determined. Similarly, the variance and covariance of each of the adjusted source co-ordinates (σ_δ, σ_α, $\sigma_{\delta\alpha}$, $\sigma_{\alpha\delta}$) can be used to compute their own "absolute error ellipses". The above are termed "absolute" error criteria as they refer to the accuracy of the station

or source positions with respect to their respective fixed origins. For the antenna position, the origin is one of the antennae (see §3.4.3) whilst for the source position the origin of right ascension is defined by fixing the right ascension of one source and the declination origin is defined either by the plane of rotation of the Earth in the case of delay observations or by the fixed declination in the case of fringe frequency observations.

It is often useful to know the relative accuracy of the positioning of two antennae or the direction of two sources, the covariance matrix contains all the necessary information to compute this data (Dodson, 1977). It is also possible, as for the "absolute" error criteria, to calculate this data with respect to any set of orthogonal axes and hence define the locus of the error data. This 'relative' error information is often of greater value than the 'absolute' error data; for example, in a conventional survey network two stations may possess a small relative error whilst both their individual absolute errors may be large due to being a great distance from the origin (Ashkenazi, 1972). This will also apply in a VLBI network with regard to the adjustment of the positions of both the stations and sources.

For any quantity which can be computed from the final adjusted co-ordinates it is possible to compute the corresponding a posteriori standard error from the covariance matrix. Referring back to the nomenclature of §3.2.1, if θ is a function of r, s, and t and is given by:

$$\theta = h(r, s, t),$$

then the value of θ computed from the final adjusted co-ordinates is of the form:

$$\theta = \theta_1 + \delta\theta ,$$

where θ_1 is the quantity computed from the initial approximate value and $\delta\theta$ is the change in θ_1 due to the adjustment. Any error in θ will be entirely due to the a posteriori error in $\delta\theta$ which is expressed in (3.1) as:

$$\delta\theta = \frac{\partial\theta}{\partial r}\delta r + \frac{\partial\theta}{\partial s}\delta s + \frac{\partial\theta}{\partial t}\delta t,$$

$$\text{or} \quad \delta\theta = g^T x' \tag{3.28}$$

where x' is the column vector of adjusted unknowns and g is the column vector of observation equation coefficients. From Appendix F.6:

$$\sigma_\theta^2 = \sigma_{\delta\theta}^2 = g^T \sigma_{xx}' g \tag{3.29}$$

where σ_{xx}' is the appropriate part of the covariance matrix in (3.8) associated with the unknown vector x' in (3.28) (i.e. it contains only the rows and columns of the total covariance matrix of the adjusted unknowns appropriate to the elements of the column vector x'). For any quantity which can be expressed in the form of (3.28), its standard error can be computed from the equivalent formula to (3.29).

There are three such parameters of interest here, namely the baseline length, declination, and hour angle (B, δ_B, and h_B respectively, see §3.4.1). A baseline length is given as a function of the baseline components as:

$$B = \sqrt{(b_x^2 + b_y^2 + b_z^2)} ,$$

and hence in (3.28):

$$g = \begin{bmatrix} b_x/B \\ b_y/B \\ b_z/B \end{bmatrix} \tag{3.30}$$

for a vector x' of:

$$x' = \begin{bmatrix} b_x \\ b_y \\ b_z \end{bmatrix}$$

This could equally well be performed for the antenna co-ordinates instead of the baseline components by substituting $b_x = x_B - x_A$, $b_y = y_B - y_A$, and $b_z = z_B - z_A$. Similarly, this can also be done for the baseline declination and hour angle described below using the same x' vector.

The declination of the baseline is defined in §3.4.1 and is given by:

$$\delta_B = \sin^{-1} \frac{b_z}{B}$$

Hence, for the baseline declination:

$$g = \begin{bmatrix} -b_x b_z / B^3 (\sqrt{1-(b_z/B)^2}) \\ -b_y b_z / B^3 (\sqrt{1-(b_z/B)^2}) \\ (\sqrt{1-(b_z/B)^2})/B \end{bmatrix} \qquad (3.31)$$

The baseline hour angle is also defined in §3.4.1 and is given by:

$$h_B = \sin^{-1} \left(\frac{b_y}{\sqrt{(b_x^2 + b_y^2)}} \right)$$

and hence for this parameter:

$$g = \begin{bmatrix} -b_x b_y / B_e^3 (\sqrt{1-(b_y/B_e)^2}) \\ (\sqrt{1-(b_y/B_e)^2})/B_e \\ 0 \end{bmatrix} \qquad (3.32)$$

where $B_e = \sqrt{b_x^2 + b_y^2}$ = the equatorial baseline component.

The standard error of each observation is obtained from the unit variance and the estimated a priori observation standard error as expressed in (3.10). This assumes therefore that the relative a priori weights are correctly estimated.

3.6 DATA FILTERING

3.6.1 Introduction

The errors inherent in the observed quantities derived from any observational procedure can be attributed to any combination of three causes, namely systematic errors, random errors, and blunders or gross errors. The effect of systematic errors on VLBI data, for example the differential atmospheric refraction and clock drift on a baseline, is minimised by mathematically modelling their contribution to the observations (see §2.4). The effect of random observational errors, otherwise termed noise, is minimised by the application of the weighted least squares technique to the adjustment of the observed data (see §3.2.2). Having applied the corrections and techniques mentioned above, gross errors and unmodelled systematic errors may remain and consequently corrupt the solution. These remaining errors must therefore be identified and eliminated using data filtering techniques. These systematic errors, however, cannot be entirely removed due to being absorbed in the adjustment and hence corrupting the assessment of the random errors.

There are both statistical and empirical tests for identifying bad data. The former method involves the application of standard statistical theories and tests to the observation residuals derived from the adjustment procedure in order to identify and reject individual observations, known as 'outliers' (see §3.6.2). This method assumes

that the residuals are normally distributed about a zero mean and that there are no unmodelled systematic errors. The assumption is checked by the application of a chi-squared normality test to the observation residuals (§3.6.3). Individual observations are also rejected by comparing computed criteria with empirically determined threshold values (§3.6.4).

3.6.2 Statistical Rejection of Outliers

The weighted residuals from a least-squares adjustment can be assumed to be normally distributed provided that an adequate model of the inherent systematic errors is applied. Residuals of observations containing gross errors will fall outside this distribution and therefore it can be used for detecting these large errors.

Considering n observations of a parameter, x, which have been drawn from a normally distributed population of mean value μ and variance σ^2, the estimated population mean and variance are given by:

$$\bar{x} = \frac{1}{n} \sum_{i=1}^{n} x_i \,, \tag{3.33}$$

and $$s^2 = \frac{1}{n-1} \sum_{i=1}^{n} (x_i - \bar{x})^2 \,, \tag{3.34}$$

respectively. It can be shown (Chatfield, 1970) that the probability, F(z), that an element, drawn randomly from a normally distributed population with zero mean and unit standard deviation, is less than or equal to z is given by:

$$F(z) = \frac{1}{\sqrt{2\pi}} \int_{-\infty}^{z} e^{-z^2/2} \, dz \tag{3.35}$$

This function is tabulated in standard statistical tables and can also be expressed for use with a computer as (Abramowitz and Stegun, 1965):

$$F(z) = 1 - \tfrac{1}{2}(1 + c_1 z + c_2 z^2 + c_3 z^3 + c_4 z^4)^{-4} , \qquad (3.36)$$

where $c_1 = 0.196854$,

$c_2 = 0.115194$,

$c_3 = 0.000344$,

and $c_4 = 0.019527$.

The error in this approximation is less than 2.5×10^{-4}. If the sample variance is σ and not 1, it can be shown that the probability that a chosen element will lie in the range $-z\sigma$ to $+z\sigma$ is given by:

$$F'(z) = 2F(z) - 1. \qquad (3.37)$$

In order to reject observations which are thought to possess gross errors, a criterion must be defined such that observation residuals not satisfying it are rejected. For example, if the criterion for rejection was chosen to be that an element had to lie with $\pm 2\sigma$ of the population mean, then from the statistical tables:

$$F(2) = 0.9772,$$

$$\Rightarrow F'(2) = 0.9544.$$

As the population mean and standard deviation (μ and σ) are not generally known, the sample mean and standard deviation ($\bar{x}$ and s) are used. Therefore, for z = 2 in (3.37), the probability that a sample has an element with a deviation from the mean less than 2s is 0.9544 and, conversely, the probability that an element lying outside these bounds is wrongly discarded is 0.0446.

The value of z adopted to achieve efficient functioning of the data filtering process can either be an empirically derived value or it may be computed as a function of each individual sample size. A criterion attributed to Chauvenet can be used which is based on the premise that

an observation in a sample of n observations should be rejected if it has a deviation from the mean greater than that corresponding to a probability of 1/2n (Neville and Kennedy, 1968). For example, a sample of 25 observations gives 1/2n = 0.02 and the corresponding value of z as 2.33. The following algorithm may be used to compute z (Abramowitz and Stegun, 1965):

$$z = t - \frac{a_0 + a_1 t}{1 + b_1 t + b_2 t^2},$$

where $t = \sqrt{\log_e(1/p^2)}$,

$p = 1/4n$,

$a_0 = 2.30753$,

$a_1 = 0.27061$,

$b_1 = 0.99229$,

and $b_2 = 0.04481$.

The error in the computed value of z using this algorithm is less than 3×10^{-3}.

The practical method of applying Chauvenet's Criterion to the residuals of an adjustment is to compute the mean and standard deviation of the weighted residuals of a first adjustment and assess each residual in relation to the Chauvenet criterion. Unsatisfactory observations are rejected and a second adjustment is performed which is regarded as the final adjustment, no further filtering taking place.

3.6.3 Chi-squared Test

The procedure for filtering individual observations described in §6.3.2 is dependent on the weighted residuals of the adjustment being normally distributed about a zero mean. In order to check the validity of this assumption for a data set, a chi-squared test is applied to the

residuals (Wells and Krakiwsky, 1971). Data sets not satisfying this test are deemed not to be normally distributed and hence are presumed to contain unmodelled systematic errors. Such data sets must therefore be rejected from the adjustment.

OR DATA MIGHT NOT BE NORMALLY DIST (WHICH IS POSS)!

3.6.4 Empirical Tests

Individual observations or whole data sets may be rejected if they do not satisfy certain empirical criteria which have been determined from previous experience. For example, an observation is rejected if its observed minus computed value in the right-hand-side vector of the observation equations is greater than a specified threshold value. This may happen if the initial estimates of the parameter values are not sufficiently accurate but, if this is the case, the number of rejected observations should indicate a problem of this nature. Also, if the solution for certain parameters derived from an adjustment appeared in error compared with values obtained from previous experiments or reference texts, the complete data set may have to be rejected providing that it can be verified that these reference values are reliable.

CHAPTER 4:

VLBI OBSERVING TECHNIQUE AND SYSTEMS

4.1 INTRODUCTION

4.1.1 History

The technique of Very Long Baseline Interferometry arose from the necessity to improve the angular resolution obtained from observations made at radio frequencies, in order to study the angular structure of compact radio sources such as quasars. The angular resolving power of a radio telescope (in radians) is approximately equal to the ratio of the observing wavelength to the diameter of the antenna system (i.e. the diameter of the antenna dish for single antenna observations). Therefore, for wavelengths in the centimetre and metre region which are used in radio astronomy, antenna systems of several kilometres diameter are necessary in order to approach the angular resolution that is achievable using conventional optical astronomy observations at wavelengths around 5×10^{-7} m.

The angular resolution of single radio telescopes has improved from about 30^{o} for the first radio telescope, built by Jansky in the 1930's, down to about 1 minute of arc for the present day large dishes. Clearly, the achievement of high angular resolution necessitates the use of widely separated antennae receiving the same signals from a radio source and hence simulating a single radio telescope of diameter equal to the distance between them. For example, a baseline of 5300 km observing at a frequency of 10.68 GHz (2.8 cm wavelength) yields an angular resolution of about 4×10^{-4} seconds of arc.

Since its inception in the 1950's, the radio interferometry technique has developed through many stages resulting in increased accuracy and longer observed baselines. In order to convert the high frequency signals received by each of the antennae to a much lower frequency suitable for transmission and comparison, the signal is 'beat'

against the purely harmonic signal derived from a local oscillator. For antenna separations of up to approximately 5 km, the local oscillator transmissions can be distributed to the antennae by cables while for greater distances, up to about 150 km, the antennae could be connected by a radio link. However, for even greater antenna separations, the use of a single local oscillator for the entire antenna array was, and still is, impractical due to unknown distortions in the radio links, the difficulty of compensating for the different signal arrival times from the observed source at each antenna, and the difficulty of maintaining a radio link over long distances. The angular resolution obtainable from radio link interferometry is of the order of 0.1 seconds of arc but this clearly depends on the baseline length and the observing frequency.

The development of very precise and stable atomic frequency standards has eliminated the need for a physical link between the antennae. The received high frequency signals can now be heterodyned to a frequency suitable for recording on a standard magnetic tape recorder system. The very stable atomic frequency standards are used to drive the local oscillator at each station so that the signal characteristics are preserved in the mixing process down to the recording frequency. The inclusion on the recorded tapes of precise timing information, generated by a station clock which is also driven by the atomic frequency standard, enables subsequent comparison of the data from each station. 'Tape recorder interferometry' was first successfully performed by a Canadian research group in 1967 (Broten et al, 1967), followed later that year by an American group (Bare et al, 1967).

Having now overcome the problem of independently operating each antenna of an interferometer, the limiting factor is that both antennae must be able to observe any one source simultaneously and also, in order to provide a full solution for all the parameters of the adjusted model,

be able to observe a sufficient number of different sources (see §3.4). Consequently, the application of the technique becomes difficult for antenna separations approaching the diameter of the Earth.

The improved angular resolution provided by this technique has been used primarily in the study of the structure of compact radio sources. However, this work requires an approximate knowledge of the baseline components between the antennae and hence it has proved feasible to 'reverse' the system and obtain precise baseline measurements from these observations. The first paper outlining the use of VLBI in geodesy was published in 1969 (Jones, 1969) and since then the number of geodetic VLBI experiments has steadily increased.

4.1.2 Basic Observing Technique

The three basic observables of the VLBI technique containing useful geodetic information, namely delay, phase, and fringe frequency, have already been described in §2.1.3 and §2.1.4. This section is an introduction to the actual observing technique and the practical reasons behind the method employed.

Considering a 'point' source emitting monochromatic radiation, two antennae observing this radiation at a single frequency, a recording and processing system which uses the received signal directly, no atmospheric effects, no Earth rotation causing Doppler shifting of the observed frequencies, and no instrumental noise effects, the received signal at each antenna will have a perfect sinusoidal waveform with a wavelength simply related to the observing frequency by the velocity of propagation of the signal in vacuo. The received signal at each antenna (see Fig. 4.I(a) and (b)) would therefore be identical, even though each specific wavefront (for example, G in Fig. 4.I) had been recorded at antenna B a constant time after or before that wavefront had been recorded at antenna A.

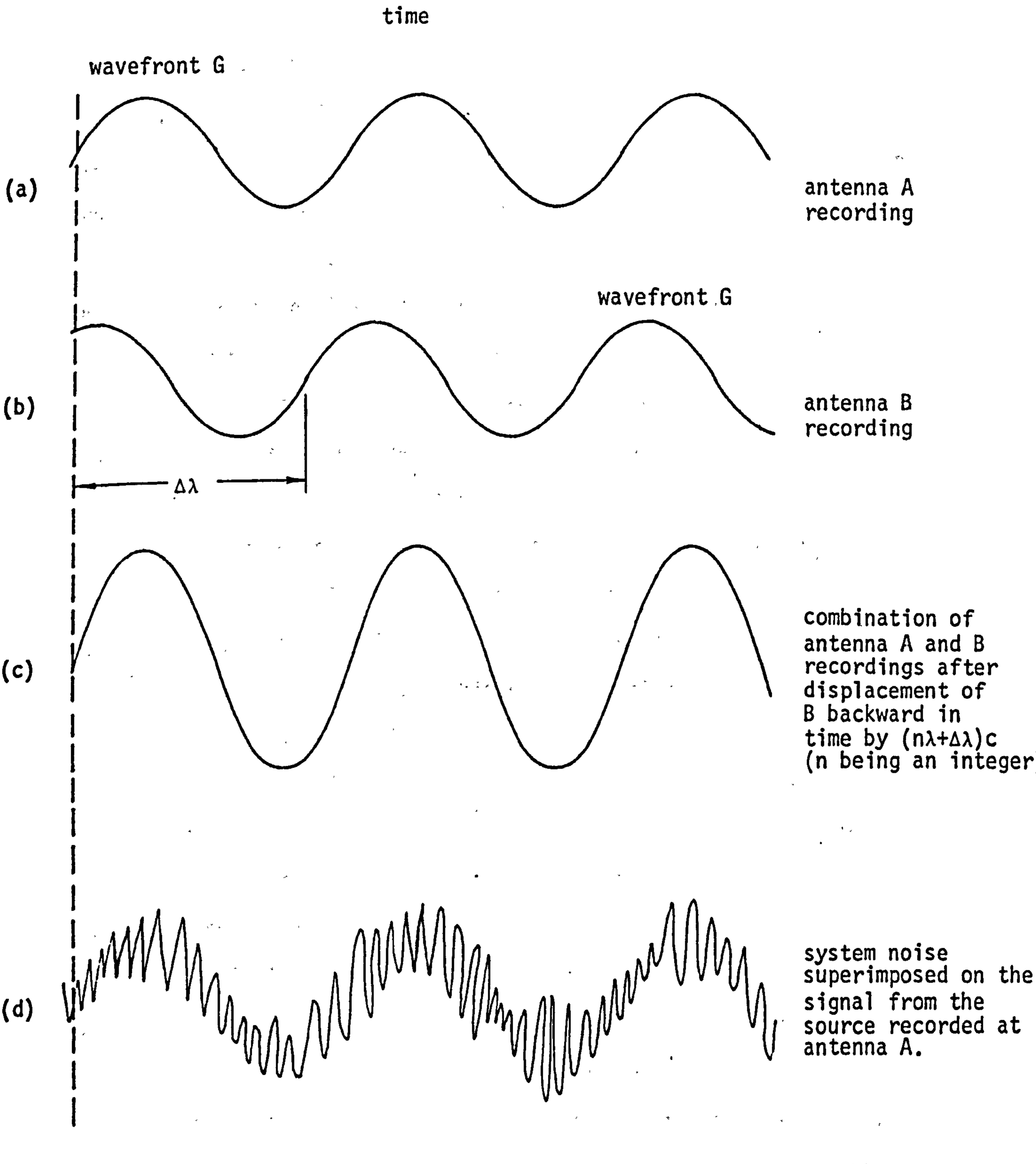

Fig. 4.I Recorded and combined signal waveforms

To assess the time delay between the signal arriving at each antenna, the recorded data tapes must be somehow combined. For these ideal monochromatic single frequency signals, a simple addition of the two waveforms can be used whereas for the real case a correlation process is required (see §4.3.2) (Rogers, 1976). This process of combining the recorded signals involves aligning the tapes using the recorded time marks and then offsetting one of them relative to the other until the combined (added) signals reinforce each other (see Fig. 4.I(c)). The amount of the offset required to achieve maximum correlation can be measured using the time marks and, referring to the diagram, this maximum correlation can be achieved by a displacement backward in time of $[(n\lambda + \Delta\lambda)c]$ of tape B, where n is any integer, λ is the wavelength of the sinusoid, c is the velocity of propagation of the radiation, and $\Delta\lambda$ is as defined in the figure. This situation clearly occurs many times and hence little useful information concerning the delay time can be extracted from this single frequency observation. The data is said to possess an 'integer cycle', 'phase', or '2π' ambiguity. The phase of the interferometer output at a specified epoch (in this context meaning the phase angle ϕ and not to be confused with the phase observable described in §2.1.4) can be measured extremely accurately ($2\text{-}3^{o}$) but the lack of knowledge concerning the integer number of wavelengths prior to the phase measurement results in a possible 2π-ambiguity which generally precludes its use as an observable in long baseline observations due to the unknown effects of the atmosphere and local oscillator and possible inaccurate a priori baseline knowledge.

In order to remedy this problem, imagine observing two of these monochromatic signals, whose separation is, say, d MHz, at each station. The combined signals from the two observing frequency channels at each

antenna are offset and combined to produce a signal exhibiting 'beats' or 'fringes' with a frequency of d MHz. The correlation of these combined signals from each station will consequently help to resolve the ambiguity inherent in single frequency observations although recourse to further observing frequencies may be required depending on the choice of the initial two frequencies and the accuracy of the a priori baseline knowledge. In practice, observations are generally made over a single finite frequency band whose size (bandwidth) is limited by the system characteristics. The wider the bandwidth the better the resolution of the delay time and, conversely very narrow bandwidth systems will give low resolution (see §4.4). Another method, employed in the NRAO* Mk I VLBI system among others, is 'bandwidth synthesis' (Rogers, 1970). This technique involves observing several narrow frequency bands distributed throughout a wide frequency band and therefore results in the recorded bandwidth being quite small but the effective (i.e. sampled) bandwidth being much larger than that attainable from single band observations. The effect of this on the observables is discussed in §4.4 and the bandwidth synthesis technique itself is described in §4.3.3.

The other major requirement for successful observations is the requirement of a high signal to noise ratio (SNR) of the recorded signal. Noise results primarily from atmospheric and receiver effects and has a random nature. Systematic effects, unless modelled correctly, will affect the accuracy of the computations performed with the data. Fig. 4.I(d) illustrates the case of noise superimposed on the received signal and indicates the need for a high signal to noise ratio so that the signal is not hidden.

---

* NRAO - National Radio Astronomy Observatory, Green Bank, West Virginia, U.S.A.

These effects, together with other requirements necessary for efficient functioning of a VLBI system, are dealt with in more detail in §4.4. A general description of a VLBI system is given in §4.3. This description is designed to illustrate a general VLBI system but in doing so uses examples of techniques used in specific systems with the intention of giving a broad understanding of the procedure involved. Where a description of a technique unique to a particular system is employed, reference is made to that system. Throughout this chapter, reference is made to the fringe frequency observable as opposed to the delay rate observable (see §2.1.4). The theory described applies equally well to both of these.

Several VLBI systems are in current use, data from two of which are used in this thesis. They are the NRAO Mk I* and the Canadian† VLBI systems, the former employing the 'bandwidth synthesis' technique. The most common system is the NRAO Mk II≠ whereas the latest and most accurate development is the NRAO Mk III@ system. Comparisons of certain features of the separate systems are made throughout the text although these four are by no means the only VLBI systems in use.

4.2 RADIATION SOURCES

This thesis deals only with observations of natural extragalactic radio sources and not with observations of artificial sources or satellites. Nor does it deal with radio sources emitting at discrete frequencies associated with the hydroxyl and water molecule spectral lines (Williams, 1976).

---

* See (Bare et al, 1967).

† See (Broten et al, 1967) and (Moran, 1976) for the system prior to June, 1975, and (Cannon, 1978) and (Langley, 1979) after June, 1975.

≠ See (Clark, 1973).

@ See (Ryan et al, 1977) and the "Mark III VLBI System Users Manual".

There are certain desirable characteristics for radio sources which make them suitable for use in VLBI observations. These are:

(i) a high signal strength in order to provide a good signal to noise ratio and to be of use for observations with inferior or smaller antenna systems,

(ii) emission over a broad band of frequencies (this is known as 'broad-band' emission and sources exhibiting this property are termed 'continuum sources'),

(iii) a small angular size so that the sources can be regarded as 'point' sources,

and (iv) a sufficient distance from the Earth-Sun system such that proper motion (§2.3.5) and parallax (§2.3.6) can be considered negligible.

How different sources affect the computation of the baseline will depend on the overall observing program (see §5.5). A description of the structure and properties of radio sources can be found in (Packolczyk, 1970 and Kraus, 1966).

Observations with an angular resolution around the milliarcsecond level have shown these radio sources to have a complicated structure and not to be 'point'sources. Mapping of the brightness distribution of a source can be performed (Pooley, 1976) and its position defined to be the centre of brightness. The difficulties encountered in early attempts at mapping are now being overcome and reliable maps with a resolution of approximately one tenth of a milliarcsecond are being obtained for some of the sources (Shapiro, 1978). The use of source positions to define a reference system is complicated by this definition of the centre of brightness of a source and the fact that the brightness distribution of each source is continually changing. This movement

has been observed to be as much as one tenth of a milliarcsecond over a period of a few months for some sources and hence this movement may need to be monitored continuously as a function of time and frequency if these sources are to be used in defining a reference system. This amount of movement is insignificant considering present attainable accuracy and is consequently not considered here.

The most common type of radio sources used for VLBI observations are quasars, for example 3C273, 3C279, 3C345, and 3C454.3. Other radio sources frequently used are Seyfert galaxies (e.g. 3C84 and 3C120), Lacertids (e.g. OJ287 and BL-LAC), nuclei of galaxies, and flare stars. The diameters of these various sources range from less than a milliarcsecond for 3C111 to almost an arcsecond for 3C236. The distance of extragalactic quasars can be as much as 7×10^9 light years (Robinson, 1972).

4.3 OBSERVING TECHNIQUE

4.3.1 Antennae Systems and Recording

There are four essential features of an antennae system suitable for VLBI observations which enable radio signals to be received and recorded at one antenna in such a manner as to allow subsequent correlation to take place with the recorded data from other antennae (Moran, 1976). These are:

(i) an atomic frequency standard to which the local oscillator is phase-locked and which drives the station clock (this is usually a hydrogen maser but a rubidium standard might (Knowles et al, 1978) or might not (Langley, 1979) prove satisfactory for geodetic work),

(ii) a video converter and formatter,

(iii) a facility by which the clocks at each station can be synchronised,

and (iv) a video tape recorder.

Fig. 4.II illustrates the basic elements of a general interferometer system. Antenna B will possess a similar system to that of antenna A although for clarity it is not shown here. Descriptions of various types of antennae are given by Welch (1976).

Although the observed sources emit radiation over a broad range of frequencies (see §4.2) only a narrow frequency band of bandwidth B is observed, known as the 'received frequency' or RF. Despite the observations being made over a finite frequency band, the 'observing frequency' used in the equations in Chapter 2 is defined as being at the centre of this frequency band. The voltages induced at the focus of each antenna by the received signals are amplified by a 'front-end' amplifier (the amplifier mounted at the antenna focus) of RF bandwidth B in order to select the specific part of the frequency spectrum to be observed. The RF signal is then mixed with a purely harmonic signal from the local oscillator to reduce it to a lower frequency known as the 'intermediate frequency' or 'IF'.

At this stage there is a marked difference between the different recording systems in that some record 'digital' data and some record 'analogue' data. For example, the NRAO Mk II interferometer system converts the IF signal to a video signal which is 'clipped' and 'one-bit digitised' at a sample rate of 4 MHz (one sample every 0.25 μs) before formatting and recording along with the necessary timing information. 'Clipping' is the process of discarding the high amplitude noise on the extremities of the received signal while 'one-bit digitisation' is the allocation of a 1 or a 0 to each sample according to the sign of the

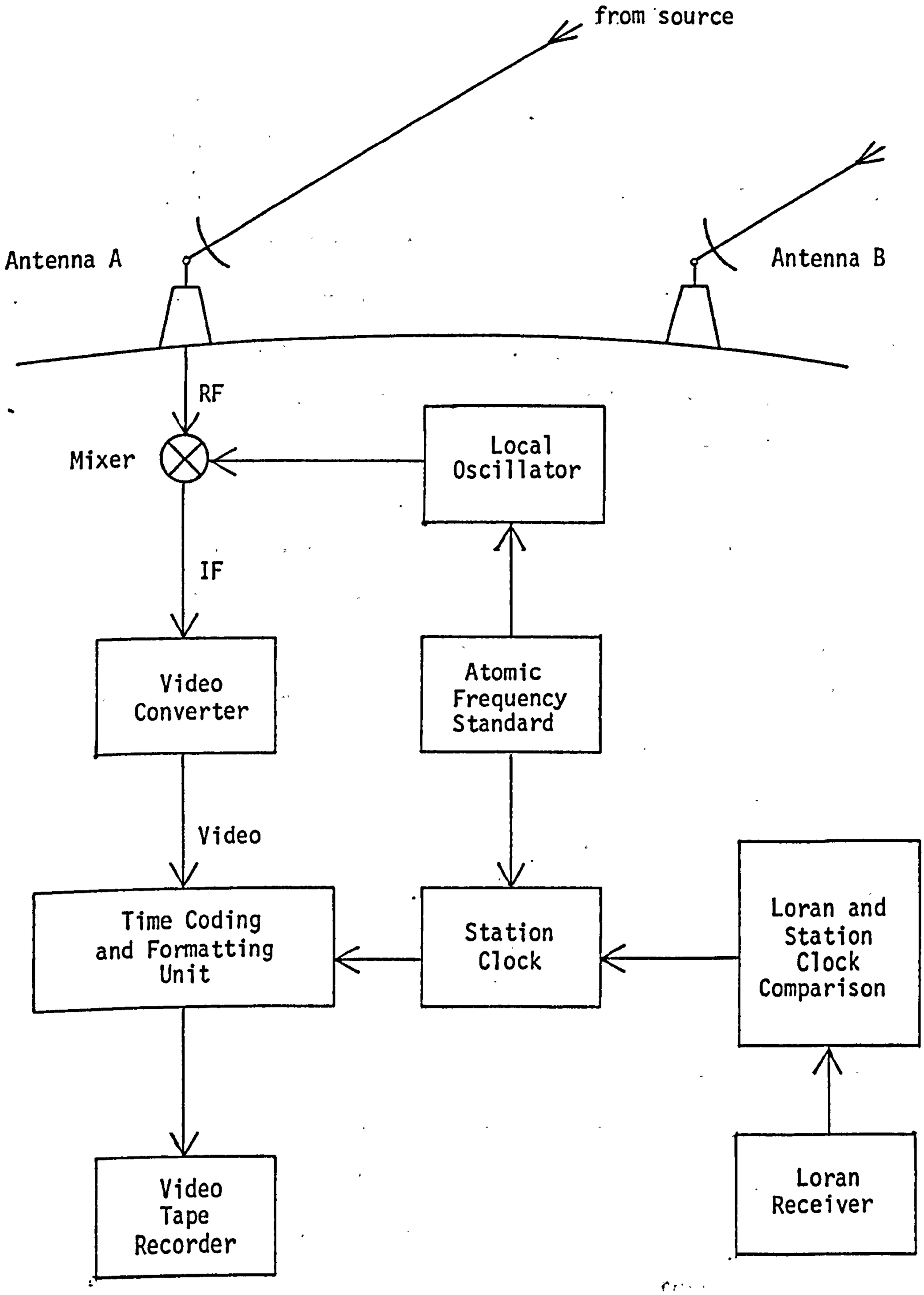

Fig. 4.II Basic elements of a VLBI receiving system

signal within the sample period (relative to the mean value). On the other hand, the Canadian VLBI system records analogue data without recourse to digitisation techniques, i.e. the video band signal produced from the IF signal by the video converter is recorded directly. The sensitivity of the Canadian system is greater due to its broader recorded bandwidth and the one-bit digitised representation of the signal in the NRAO Mk II system. The NRAO Mk I system also records digitised data but at a different rate and format to the Mk II system.

It is essential that each piece of data has a time allocated to it, either explicitly or implicitly, by the regular output onto the tape of timing information from the station clock. It is also necessary that the relative synchronisation of each station clock be known so as to ease the correlation process (see §4.3.2). Consequently, Loran-C* time signals are generally monitored during observation (see §4.4).

4.3.2 Playback and Correlation

The tapes recorded at the separate antennae of an interferometer array can be subsequently transported to a central processing centre for playback and correlation. There are five main functions of a playback system (Moran, 1976), namely:

(i) to reproduce the observed data from the tapes exactly as it was recorded using a tape recorder system, and to have a capacity to buffer† this data from the playback process,

(ii) to compensate for the delay between the arrival of a signal wavefront at each antenna and to correct for the

---

* see Appendix A.7 for a brief description of the Loran C system.

† a data buffer is a data store used as an interface between the magnetic tape and the data processor.

differential Doppler shift of the observed frequencies due to the relative velocities of the antennae,

(iii) to cross-correlate the data from each station,

(iv) to store the cross-correlation functions over the specified integration time for further processing,

and (v) to extract the observed quantities from the cross-correlation functions.

Before the actual correlation procedure can commence, the time-base (i.e. the timing information explicitly and implicitly contained on the tapes) on each of the tapes must be individually checked and, if necessary, corrected. This is performed in order to reproduce the correct relationship between the observed data and the timing information as existed at the epoch of observation. Corruption of the time-base may be due to mechanical jitter in the recording or playback tape recorders and also due to imperfect tapes. This process can be performed in several ways; for example, the NRAO Mk II system uses the clock information from the tapes to run a 'flywheel' which can insert or delete data bits when necessary. A recognisable check pattern is recorded on the tapes every 512 μs so that the clock counter can be reset if data bits are lost or gained between check patterns. Furthermore, recorded at the beginning of each tape is the epoch of the start of the tape and thereforethe result of this initial process is a pair of tapes, one from each antenna, upon which the timing information reproduces the epoch which each data sample represented at the recording stage. Having how been individually time-base corrected, the two tapes are temporally aligned in the processor by comparing the starting epochs of the tapes and the data is then stored for further processing.

Rather than the simple addition of received signal waveforms which

was used in the monochromatic single frequency observation example of §4.1.2, the recorded signals from real observations must be 'correlated'. This is due to the observed finite bandwidth and the use of the recorded intermediate or video band frequency rather than the observed radio frequency from which they are derived. This correlation process involves taking the cross-product of the waveforms recorded at the antennae over a specified integration interval such that the correlation function for an estimated delay τ is given by:

$$\rho(\tau) = \frac{1}{n} \sum_{t=0}^{s} x_1(t).x_2(t+\tau) \ ,$$

where $\rho(\tau)$ = the correlation coefficient,

n = the number of data samples in the integration period $t=0$ to $t=s$,

$x_1(t)$ = the recorded voltage induced at antenna 1 at time t,

and $x_2(t+\tau)$ = the recorded voltage at antenna 2 at time $t+\tau$.

This process amounts to multiplying the data stream from one tape with the (delayed) data stream from the other tape and integrating the product.

In order to compensate for the delay between the two recordings of a particular wavefront and to approximately align the recorded signal waveforms before correlation, one data stream is shifted relative to the other by an amount dependent on the sum of the expected delay, the estimated differential instrumental delay, and the estimated relative discrepancy between the station clocks. This offset data tape is said to form a 'delay channel'. Several delay channels are formed within the correlator at one time and are distributed about the expected delay computed from the estimated a priori information.

In the NRAO Mk II system, which employs one-bit digitisation as

previously described, the correlation function for continuum sources (see §4.2) is computed for an integration interval of 0.2 seconds in each of 31 separate delay channels, separated by 0.25 μs (i.e. the length of one data sample), and the resulting correlation functions are input to a computer for further processing. This process results in the compression of the observed data by a factor of 10^3. In the Canadian system, the analogue data is 12-bit digitised and sampled over an integration interval of one second in order to calculate the cross-correlation functions, before being output to a computer for further processing.

A typical plot of the output of the correlation process for the central nine delay channels of a VLBI correlator is shown in Fig. 4.III (Campbell, 1978). On the left of the diagram is the plot of the correlated signal from the two tapes having automatically corrected for the continually changing delay time which would otherwise destroy the apparent fringes. The plot on the right of the figure is of the correlation function derived from the separate delay channels of the correlator. The correlation function for a particular delay channel is obtained from the separate functions computed over the short integration period (e.g. 0.2 second for the NRAO Mk II and 1 second for the Canadian system) combined over a longer observation period of, say, 1 to 5 minutes. For this particular example the observed delay is in the region of 3.00 μs.

This cross-correlation function is the fringe amplitude, the amplitude of the interference fringes shown in Fig. 4.III, expressed as a function of delay time. This function is of the form "|sin x/x|", as illustrated in Fig. 4.IV, where this figure and the right-hand-side of Fig. 4.III represent the same curve. Values of the averaged correlation coefficient at points on this curve enable its maximum to be

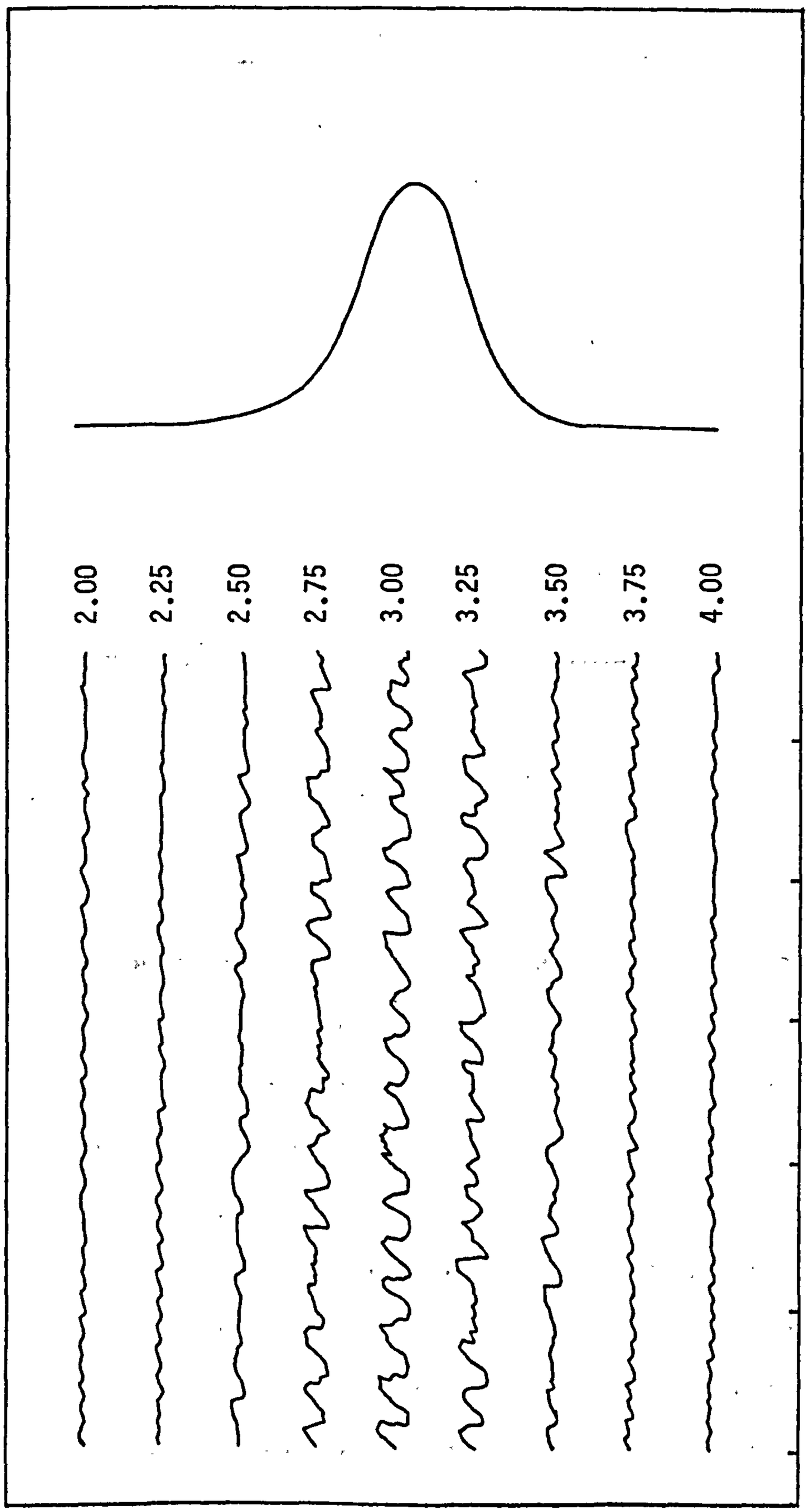

Fig. 4.III Display of nine channels of a VLBI correlator showing the interference fringes and the cross-correlation function

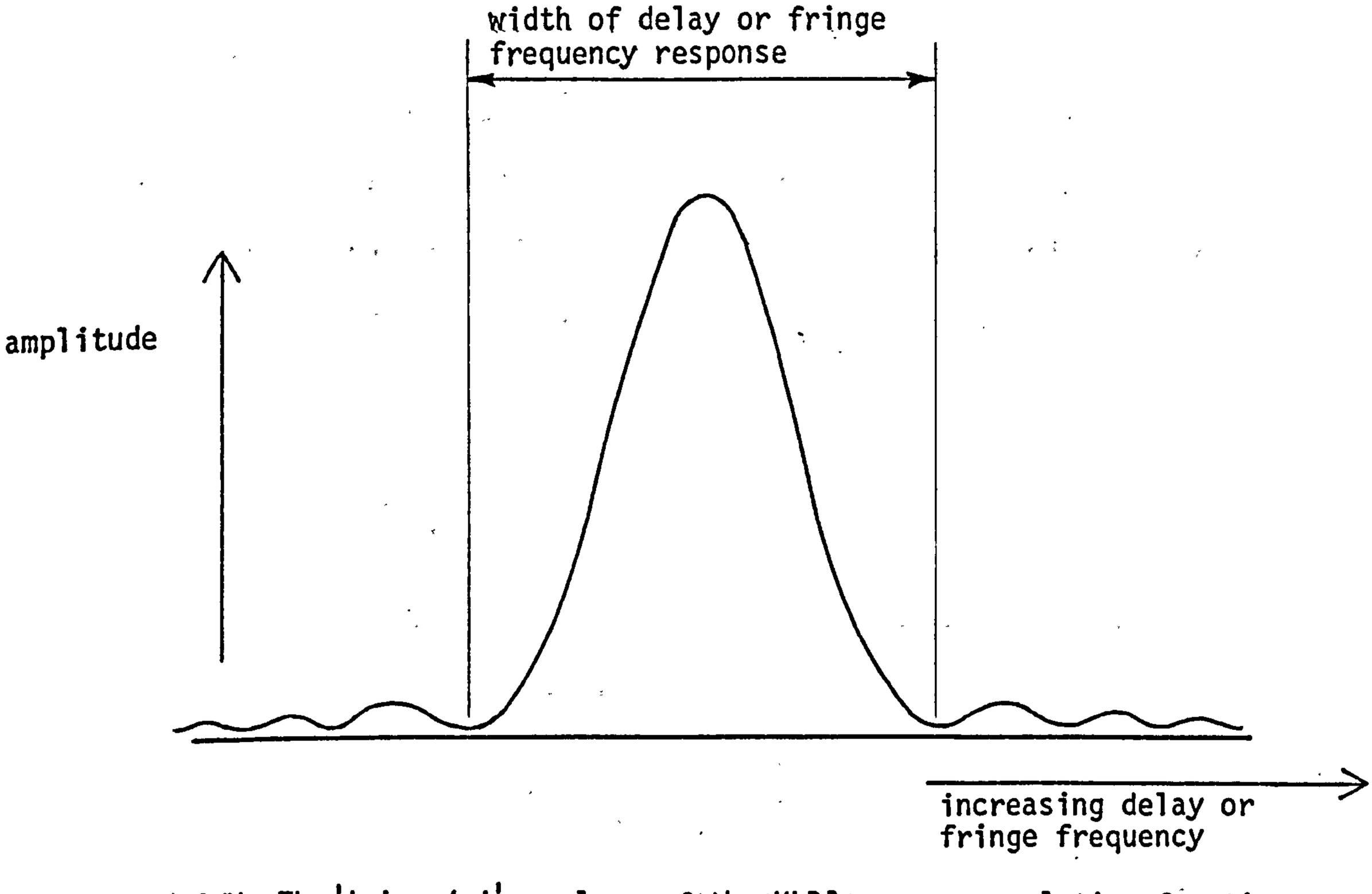

Fig. 4.IV The 'Isin x/xI' envelope of the VLBI cross-correlation function as a function of either the delay or the fringe frequency

computed and hence the observed delay established. The averaging time for an observation depends on circumstances and the observing system, but is typically between 1 and 5 minutes. The value for the Canadian system is usually around one minute while the value used in the NRAO Mk I system is typically 3 minutes, the duration of a recorded data tape.

The frequency of the interference fringes shown in Fig. 4.III is a measure of the rate of change of phase of the interferometer, referred to as the fringe frequency. Assuming the interference pattern is, over a restricted time interval, a truncated sine wave, its Fourier Transform (the fringe frequency spectrum) will also be of the form |sin x/x| as illustrated in Fig. 4.IV. A similar process as is applied to the delay computations will yield the observed fringe frequency.

As well as the delay and fringe frequency observables, the signal to noise ratio (SNR) of each observation is determined (see (4.8)). This is often used as a measure of the standard error of each observation and is hence used to calculate the weight of each observation in the adjustment procedure. In the Canadian system, the standard errors for fringe frequency and delay are derived from (Langley, 1979):

$$\sigma_F = \frac{15}{SNR} \text{ mHz} \tag{4.2}$$

and

$$\sigma_\tau = \frac{250}{SNR} \text{ ns} \tag{4.3}$$

The validity and application of this method is referred to in §7.1.

The data obtained from the Canadian VLBI system expresses the observed delay and fringe frequency in terms of three components. These are termed the 'expected', 'residual' and 'offset' delays and fringe frequencies. The 'expected' values are computed by a model of the interferometer and are the anticipated values of the observations. They are introduced into one of the data streams during the correlation process. The 'residual' components are determined using the peaks of the resultant correlation coefficient function plots (e.g. Fiv. 4.IV) and are the difference between the actual observation and the combination of the 'expected' and 'offset' values. The 'offset' delay and fringe frequency are values assigned during the correlation process for operational convenience. For instance, a frequency offset is introduced to avoid having a zero fringe frequency since this would make it difficult to distinguish variations in fringe amplitude from variations in the d.c. levels of the correlator.

4.3.3 Bandwidth Synthesis

'Bandwidth synthesis' is a technique by which it is possible to

observe a large 'effective' bandwidth, hence narrowing the delay response and improving the accuracy of the delay measurement (see §4.4), whilst only recording a much smaller bandwidth. In order to achieve this, several narrow frequency channels, distributed throughout a broad frequency band, are sampled either sequentially or simultaneously (Rogers, 1970 and Thomas et al, 1976).

From the relationship (2.15), differentiating with respect to the observing frequency w gives:

$$\frac{d\phi}{dw} = 2\pi\tau \ . \qquad (4.4)$$

Clearly, the slope of the curve of phase against observing frequency is a measure of the delay time since each separate observing frequency will exhibit a different phase, but the same delay time, at any instant.

The error in the estimation of the delay using this technique is (Shapiro and Knight, 1970):

$$2\pi\delta\tau \simeq \frac{\delta\phi}{w_{max} - w_{min}} \qquad (4.5)$$

where $w_{max} - w_{min}$ = the effective width of the frequency band,

$\delta\tau$ = the error in the estimation of the delay,

and $\delta\phi$ = a function of the error in the estimation of the phase for each of the separate narrow frequency bands ($\sim SNR^{-1}$).

Referring to (4.5), the removal of all 2π ambiguities (see §4.1.2) can reduce the error in the estimation of the delay to around 0.1 ns ($\simeq$ 3 cm) at typical VLBI observing frequencies . However, systematic effects due to the Earth's atmosphere are the dominant limiting factor rather than the VLBI system itself.

As the delay is the gradient of the graph of phase against frequency

(see (4.4)), in order to give good delay measurements, the relative phases rather than the absolute phases of the narrow bands must be consistent. The frequencies of these narrow bands must be chosen so as to eliminate any uncertainty due to integer-cycle (2π) ambiguities, the major problem in measurements of absolute phase. This type of work also necessitates accurate calibration of the observing equipment such that frequency dependent instrumental phase relationships are known and can be eliminated.

One method of determining the optimum distribution of the recorded frequency bands (Shapiro and Knight, 1970) is to initially take two bands, centred on frequencies w_1 and w_2 ($w_1 < w_2$), such that the expected differences in their phases derived from the cross-correlation process is much less than one cycle (2π radians). This condition ensures that the relative phase of these two bands is known. The next frequency band, centred on w_3 ($w_3 > w_2$), must be positioned such that the phase derived from the combination of w_1 and w_2 can be extrapolated to w_3 without introducing ambiguities. This is achieved by satisfying the equation:

$$w_3 - w_2 \leqslant \frac{w_2 - w_1}{\delta\phi} \qquad (4.6)$$

where $\delta\phi \simeq SNR^{-1}$ and the SNR is calculated as in (4.8). Further bands can be determined in a similar manner such that, for m bands:

$$w_m - w_{m-1} \simeq \frac{w_{m-1} - w_{m-2}}{\delta\phi} \simeq \ldots\ldots \simeq \frac{w_2 - w_1}{\delta\phi^{m-1}} \qquad (4.7)$$

4.4 SYSTEM REQUIREMENTS

The accuracy attainable from an interferometer is dependent on the design, quality and efficient functioning of all the separate hardware and software elements in the antennae systems and the recording, playback,

and correlation stages. This section deals with certain factors which directly affect the attainable accuracy of the interferometer system.

The width of the delay response illustrated in Fig. 4.IV is inversely proportional to the effective bandwidth. Therefore, in order to ensure obtaining interference fringes, the time separation of the delay channels (delay tap separation in the Canadian analogue system terminology) must be such that the |sin x/x| envelope cannot fall between two channels and hence remain unnoticed. The channel separation is usually made equal to half the width of the delay or frequency response in order to minimise the required amount of sampling. Clearly, the observed delay must also fall within the overall span of the delay channels. This is achieved by computing the expected geometric delay and estimating the instrumental and clock delay from the relationship between the local clocks and the Loran C time signals received during observation. Using this method, or by employing a 'travelling clock'* which visits all the participating stations and to which the local station clocks are adjusted, synchronisation to the order of ±1 μs or better can be attained.

As stated in §4.1.1, VLBI depends on atomic frequency standards to drive the local oscillator and local clock at each station. It is necessary that the phase stability provided by the atomic frequency standard is sufficient to maintain the characteristics of the received frequency band when mixed down to the video band. The better this objective can be achieved then the higher the SNR and the longer the integration periods can be. The phase stability will also be affected by atmospheric effects and the local oscillator itself introducing phase

---

* The United States Naval Observatory (UNSO) routinely visits observatories in order to synchronise the station clocks with the USNO's travelling Cesium-beam clock to within 1 μs.

noise into the signal. The stability of hydrogen-maser and rubidium standards is illustrated in Fig. 4.V (Vessot, 1976). In the long term, the relative drift of the station clocks is modelled in the data analysis as a polynomial in time (§2.4.7).

The tape recorder system (i.e. the magnetic tape itself and the recording and playback recorders) must be of sufficient quality and time-base stability that the sampled video band signal is reproduced in the correlator as it was originally recorded at the antenna. This necessitates a minimum of data contamination such that the time-base compensators are able to function satisfactorily and little data is lost. The limitation on the data storage capacity of the magnetic tape is governed by the tape recorder characteristics. The bandwidth and the data recording rate depend also on the timing accuracy achievable for each data sample.

The output of the correlation procedure is a set of observations, at different epochs, of delay and fringe frequency. The accuracy of a delay measurement is dependent on the observed bandwidth and the signal-to-noise ratio of the observation whereas the accuracy of a fringe frequency measurement is dependent mainly on the SNR. The width of the delay response is inversely proportional to the effective bandwidth and hence the larger the effective bandwidth then the narrower the delay response and the more accurate the delay measurement. The signal-to-noise ratio of an interferometer is given by (Shapiro and Knight, 1970):

$$SNR \simeq P \left(\frac{A_A \eta_A \; A_B \eta_B \; Bt}{T_A T_B} \right)^{\frac{1}{2}} \qquad (4.8)$$

where P = source strength (in flux units),

A_A and A_B = antennae surface areas,

η_A and η_B = antennae efficiencies

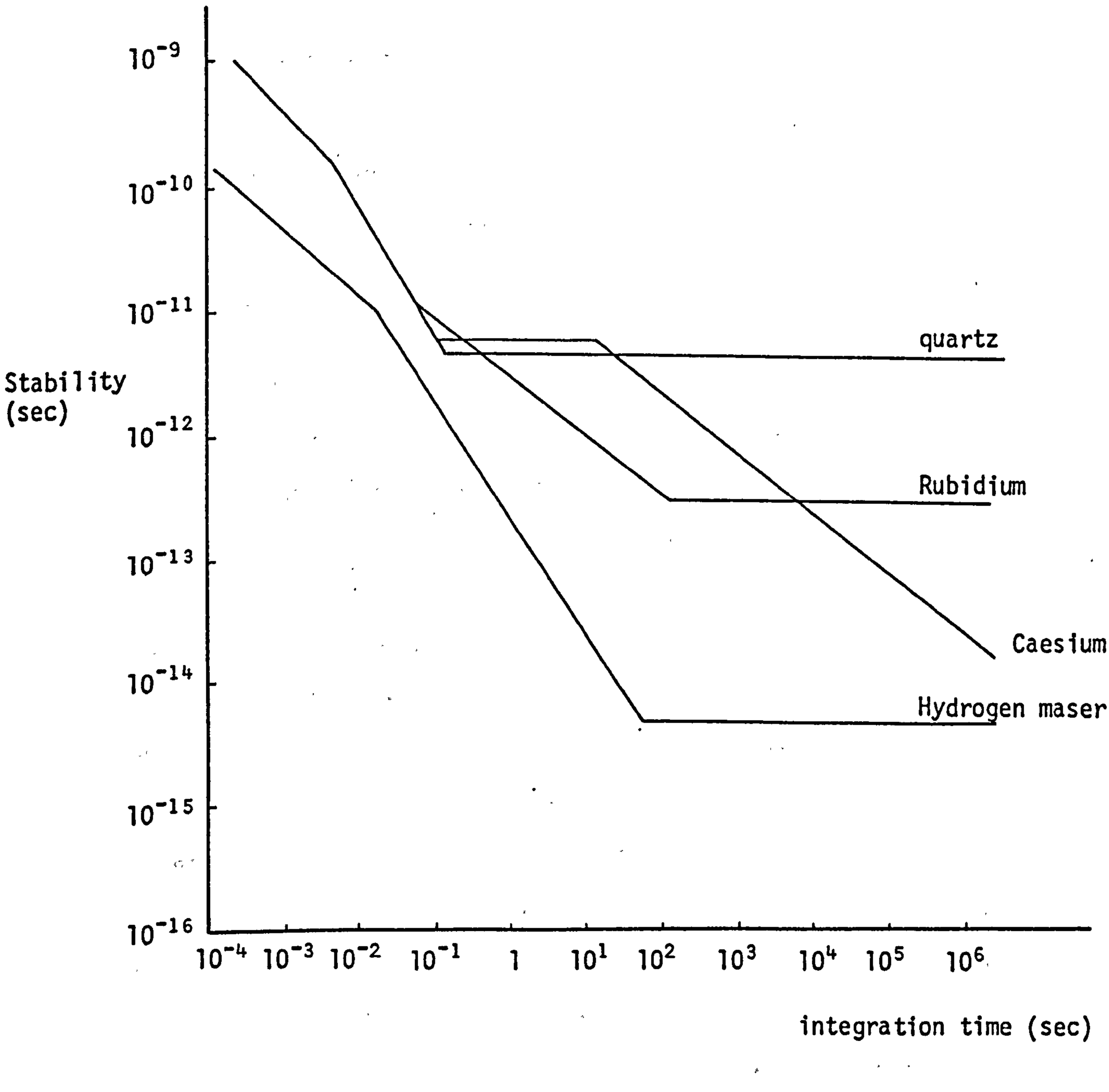

Fig. 4.V Plot of stability against integration time for various frequency standards

T_A and T_B = system noise temperatures

B = recorded bandwidth

and t = integration time of observation.

The subscripts A and B indicate antenna A and antenna B respectively. The antenna area is simply the surface area of the paraboloid dish and the system noise temperature is an operating characteristic of the antenna (Meeks, 1976). From (4.8) it is apparent that:

$$SNR \propto B^{\frac{1}{2}},$$

and hence the wider the recorded bandwidth the greater the SNR and the better the delay measurement. Similarly, this also results in a better fringe frequency measurement. A balance must therefore be achieved between using 'bandwidth synthesis' techniques having a broad effective (sampled) frequency band but narrow recorded bands, and wider single frequency band measurements.

This distinction between recorded and effective bandwidths must be emphasised. The SNR depends on the actual recorded bandwidth whereas the accuracy of an observation also depends on either the delay or fringe frequency response and hence on the effective bandwidth. The NRAO Mk I equipment using the 'bandwidth synthesis' technique (§4.3.3) has a broad effective bandwidth (often 23 or 46 MHz) but a narrow recorded bandwidth (360 kHz per channel). The Canadian system has a broad recorded bandwidth (4 MHz) but a relatively small effective bandwidth (also 4 MHz). Consequently, all other things being equal, the MK I system with 'bandwidth synthesis' will give better delay observations than the Canadian system but inferior fringe frequency observations due to the greater recorded bandwidth, and hence SNR, of the latter.

CHAPTER 5:

VLBI SOFTWARE

5.1 INTRODUCTION

The software which has been developed to process VLBI data is called the NULBIP (Nottingham University Long Baseline Interferometry Program) suite of programs. The programs are capable of adjusting data observed with the NRAO Mk I VLBI system over a single baseline and data observed with the Canadian VLBI system over one or three baselines (2 or 3 participating stations). In addition, simulation experiments can be performed with up to 4 observing stations (see §5.5). All the programs are capable of performing the adjustment with either delay data or fringe frequency (or delay rate) data or both together. The changes necessary to the program in order to handle data from other VLBI systems are almost all in the data input stage and hence the programs are very flexible. The programs comprising the NULBIP suite are summarised in Table 5.I.

The programs have been developed to run on the University's ICL 1906A computer and hence are written in extended Fortran IV, run under the GEORGE 3 operating system, and use the University's UNIQUE job control and filestore systems. The computer core store currently available on the ICL 1906A computer is about 150K words. The efficiency of the present VLBI adjustment programs could be improved, reducing the storage and run time required, but, as they require only half of the computer storage capacity and as they are not designed for use in a commercial environment, no attention has been paid to this improvement.

As an indication of the computing requirements, the single baseline adjustment program (CCOM1) has a run time of 451 seconds and core requirement of 74K for the Algonquin-Chilbolton May 1977 data, the triple baseline Canadian adjustment program (TRIG4) has a run time of 488 seconds and uses 79K of core for the May 1977 Algonquin-Chilbolton-Owens

Program Name	Adjustment Mode	VLBI System	No. of stations	No. of baselines	Observations
CCOM1	Observed Data	Canadian	2	1	Delay, and/or fringe frequency
TRIG4	Observed Data	Canadian	3	3	Delay, and/or fringe frequency
COM7	Observed Data	NRAO Mk I	2	1	Delay, and/or delay rate
EUROSIMI	Simulated Data	any	4	6	Delay, and/or delay rate

Table 5.I The NULBIP suite of programs

Valley interferometer array, and the single baseline NRAO Mk I data adjustment program (COM7) has a run time of 229 seconds and requires 67K of core store for the Haystack-Goldstone August 1972 experiment. These experiments are described and the results presented in Chapters 6 and 7.

In the remainder of this chapter the data obtained from the NRAO Mk I VLBI system is termed the 'Mk I data' and that obtained from the Canadian VLBI system is termed the 'Canadian data'.

5.2 VLBI DATA

5.2.1 Mk I Data

The Mk I data was supplied in condensed form on punched cards and consists of one observation of delay and one of delay rate per line of data. Each line contains:

(i) the coded identification name of the observed baseline (see §5.4.1),

(ii) the UTC epoch of observation (year, day, hours, minutes) which always falls on an exact minute,

(iii) the coded identification number of the observed source (see §5.4.1),

(iv) the observed group delay and the standard error of the delay observation (in μs and ns respectively),

(v) the observed delay rate and the standard error of the delay rate observation (both in ps/s).

The format of this data is illustrated in Appendix G.1. The observations are the 'natural' delay and delay rate as derived from the observing procedure described in Chapter 4, and include all the effects described in Chapter 2.

5.2.2 Canadian Data

The Canadian data is supplied by the National Research Council of Canada Herzberg Institute of Astrophysics on standard magnetic tape. Each baseline observing period has two separate files associated with it which, when combined, give all the necessary data for each observation. The data files resulting from the initial data preparation stage described here are formed by a combination of two methods, namely the use of programs run on the main computer and by manual editing using the University's UNILINE on-line system. The stages in the formation of the 'condensed' data files suitable for input to NULBIP, and the particular computing method used to derive each stage, are broadly described in this section and the details of the method are given in Appendix G.2.

The data on the first file, 'data file 1', consists of:

(i) the UTC epoch one second before the observation epoch (year, day, hours, minutes), the observation epoch always being one second after an exact minute,

(ii) the name of the observed source,

(iii) the coded identification of the observed baseline (see §5.4.1),

(iv) the 'residual' delay and the standard error of the delay observation (both in μs),

(v) the 'residual' fringe frequency and the standard error of this frequency observation (both in Hz),

(vi) the 'expected' delay (μs),

and (vii) the 'expected' fringe frequency (Hz).

The data on the second file, 'data file 2', consists of:

(i) the number of the observation within a particular continuous observing period on one source,

(ii) the UTC epoch one second before the observation epoch (year, day, hours, minutes),

(iii) the Greenwich Apparent Sidereal Time (GAST) of the observation (in hours to only 3 decimal places),

(iv) the observed source name,

(v) the coded identification of the observed baseline,

(vi) the sample rate of the data processing (see §4.3.2),

(vii) the observing frequency (MHz),

(viii) the approximate UT1-UTC correction (see §2.4.2) for the epoch of observation (secs),

(ix) the delay tap separation (see §4.4) of the correlator (μs),

(x) the 'offset' delay,

and (xi) the 'offset' fringe frequency.

The 'natural' or 'observed' delay or fringe frequency is a combination of the 'expected', 'residual', and 'offset' delays or fringe frequencies (see §4.3.2) such that:

$$\text{OBSERVED} = \text{EXPECTED} - \text{RESIDUAL} - \text{OFFSET}. \qquad (5.1)$$

Having established a common observation by comparing the UTC observation epochs on both files, the only data required from 'data file 2' above that contained in 'data file 1' are items (vii), (x) and (xi). Although some of the other parameters that 'data file 2' contains are needed for the adjustment, they are generated within NULBIP to a much higher degree of accuracy.

As many as 3500 observations may be made during a four-day observing session. This large number of observations results from the antennae continuously tracking the same source for an approximate

period of one hour, from which the correlation process (see §4.3.2) derives one observation per minute. It is not a complicated computing task to perform an adjustment using all the available data, but it is a relatively expensive one in computing terms and tests carried out using all the data have shown that very little is gained in accuracy by using more than 300 observations. Consequently, the large amount of data supplied in the two data files is subjected to a preprocessing phase which outputs the desired amount of 'condensed' data (this is unlike the case for the Mk I data (see §5.2.1) which is already in a highly condensed state and which therefore requires no preprocessing). The entire data preparation scheme designed to form single baseline data files suitable for input to NULBIP is shown in the flow chart, Fig. 5.I.

The first stage of the preprocessing phase involves the on-line editing of the two data files to make them suitable for use in the actual preprocessing program. Firstly, the necessary source data for all the observed sources (name, code number, 1950.0 right ascension and declination) are appended to the beginning of 'data file 1' and a recognisable terminator (99 in the epoch minutes column) is appended to the end of the file. A source code number is also added to the beginning of each observation line. The resulting data file contains more characters per line than is permitted for data input during a program run and consequently the file has to be split into two separate files called 'delay data file 1', which includes all the delay data, and 'frequency data file 1', which contains all the fringe frequency data. 'Data file 2' also has certain parameters removed which are not required in the preprocessing program or in NULBIP in order to reduce the data file width.

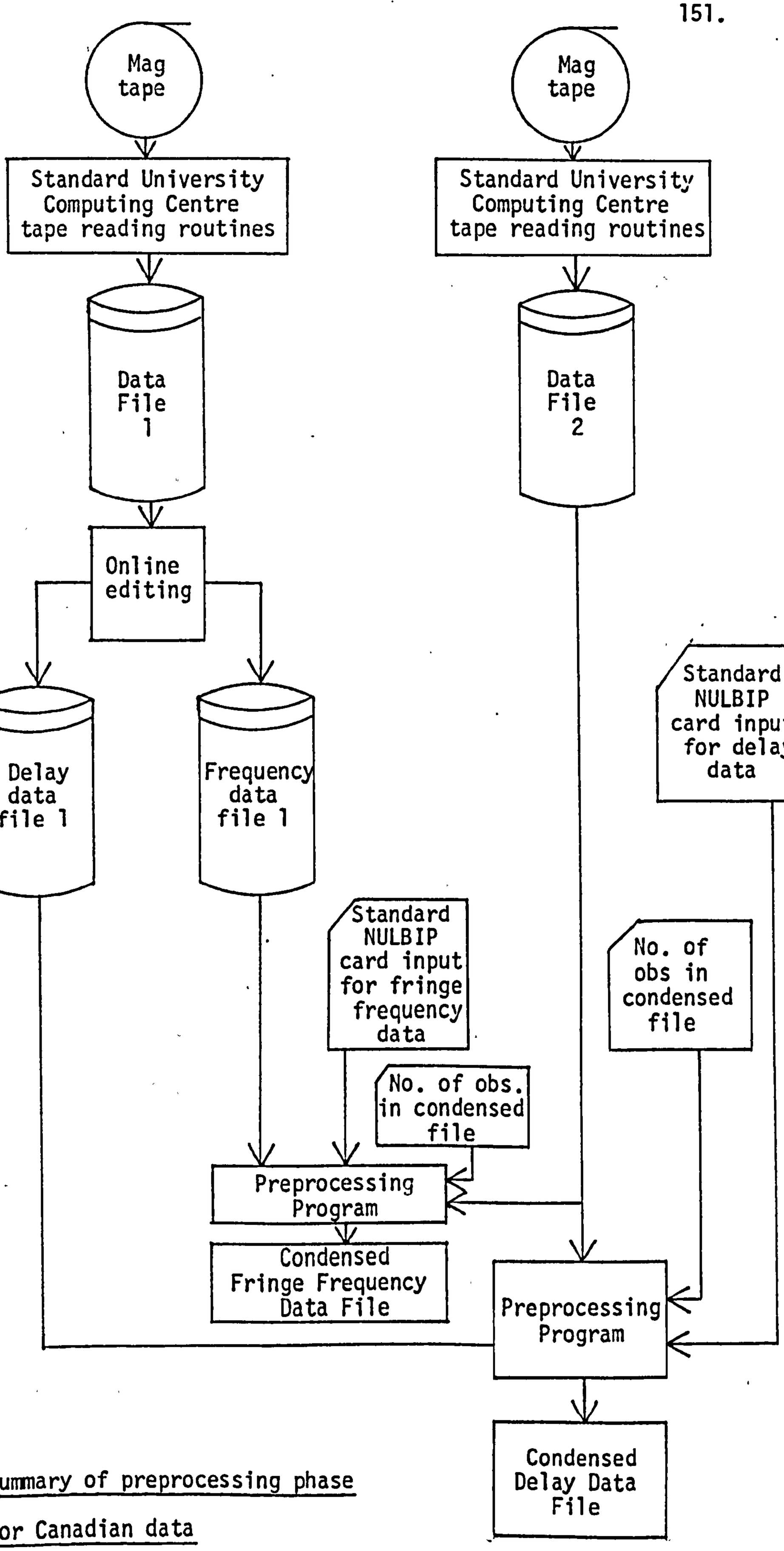

Fig. 5.I Summary of preprocessing phase for Canadian data

The data is input to the preprocessing program summarised in Fig. 5.I and detailed in the flow chart, Fig. 5.II. The input consists of:

(i) either the 'delay data file 1' or the 'frequency data file 1' (it can only deal with one of these at a time),

(ii) the data cards for NULBIP (see §5.3.1),

(iii) 'data file 2',

and (iv) a data card giving the desired number of observations, D, in the resultant condensed data file.

To form a condensed delay data file, the source data at the beginning of 'delay data file 1' is first read into the program and is both stored and output to the condensed data file. The first 300 observations of 'delay data file 1' are then individually input to the program. For each observation, the source and baseline names are checked (see §5.4.1) and the 'expected' observation and the standard error of the observation are inspected. If either of these is equal to zero or if the baseline or source name is not recognised, then the observation is rejected. The program computes the angle of elevation of the source from each antenna using the relevant computational routines described in Chapter 2 and §5.4.2. All observations which were made whilst either antenna was pointing at an elevation of less than 10^{o} to the horizon are rejected since the tropospheric refraction effects become large at these low elevations and any errors in the modelling of the atmosphere are exaggerated (see §2.4.5 and Appendix D). The observations surviving these initial filters are then output to a temporary disc store and the next 300 observations are input to the program and processed in the same fashion as the first 300. This procedure continues until all the

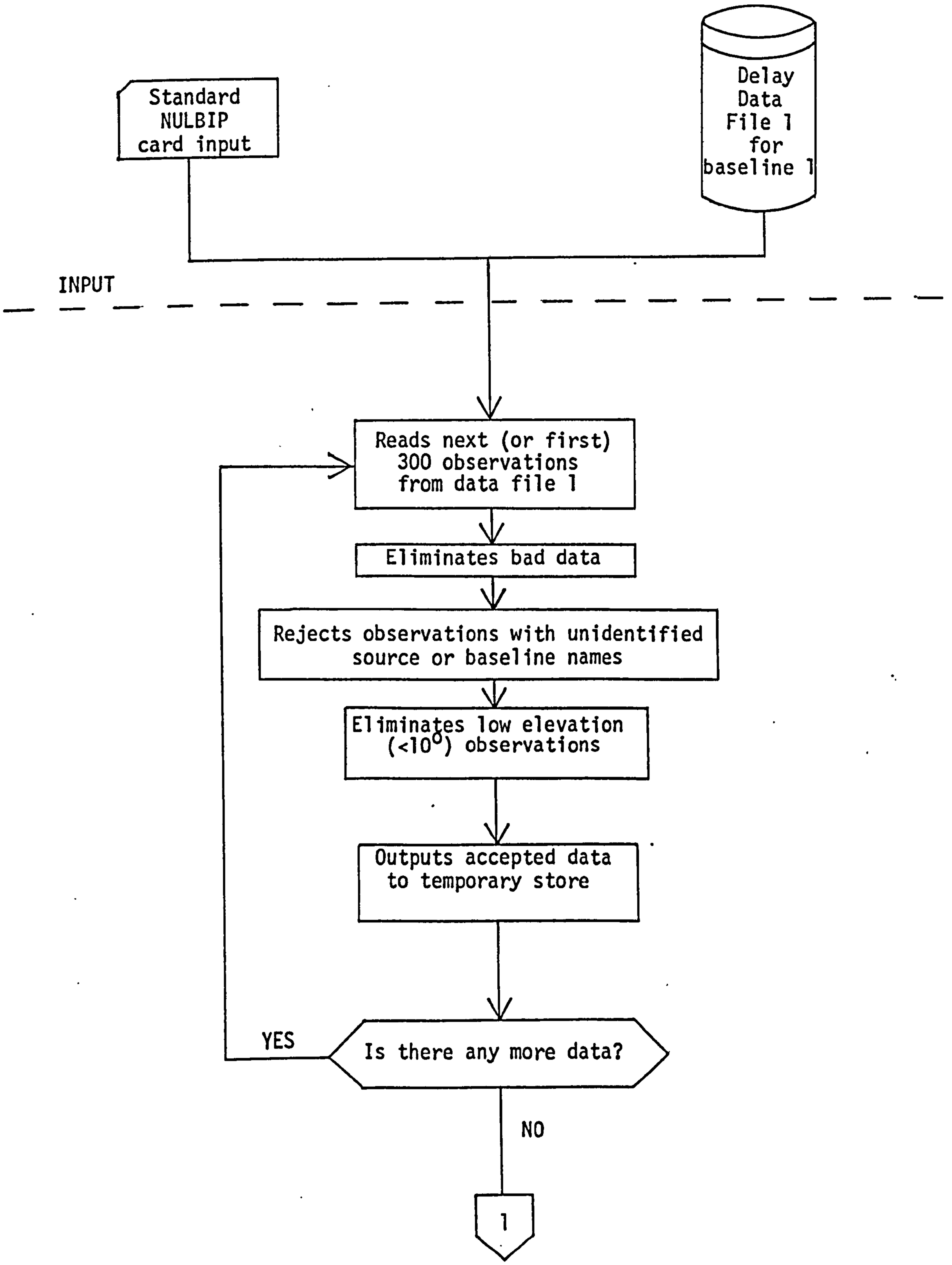
Standard NULBIP card input
Delay Data File 1 for baseline 1
INPUT
Reads next (or first) 300 observations from data file 1
Eliminates bad data
Rejects observations with unidentified source or baseline names
Eliminates low elevation (<10°) observations
Outputs accepted data to temporary store
YES
Is there any more data?
NO
1

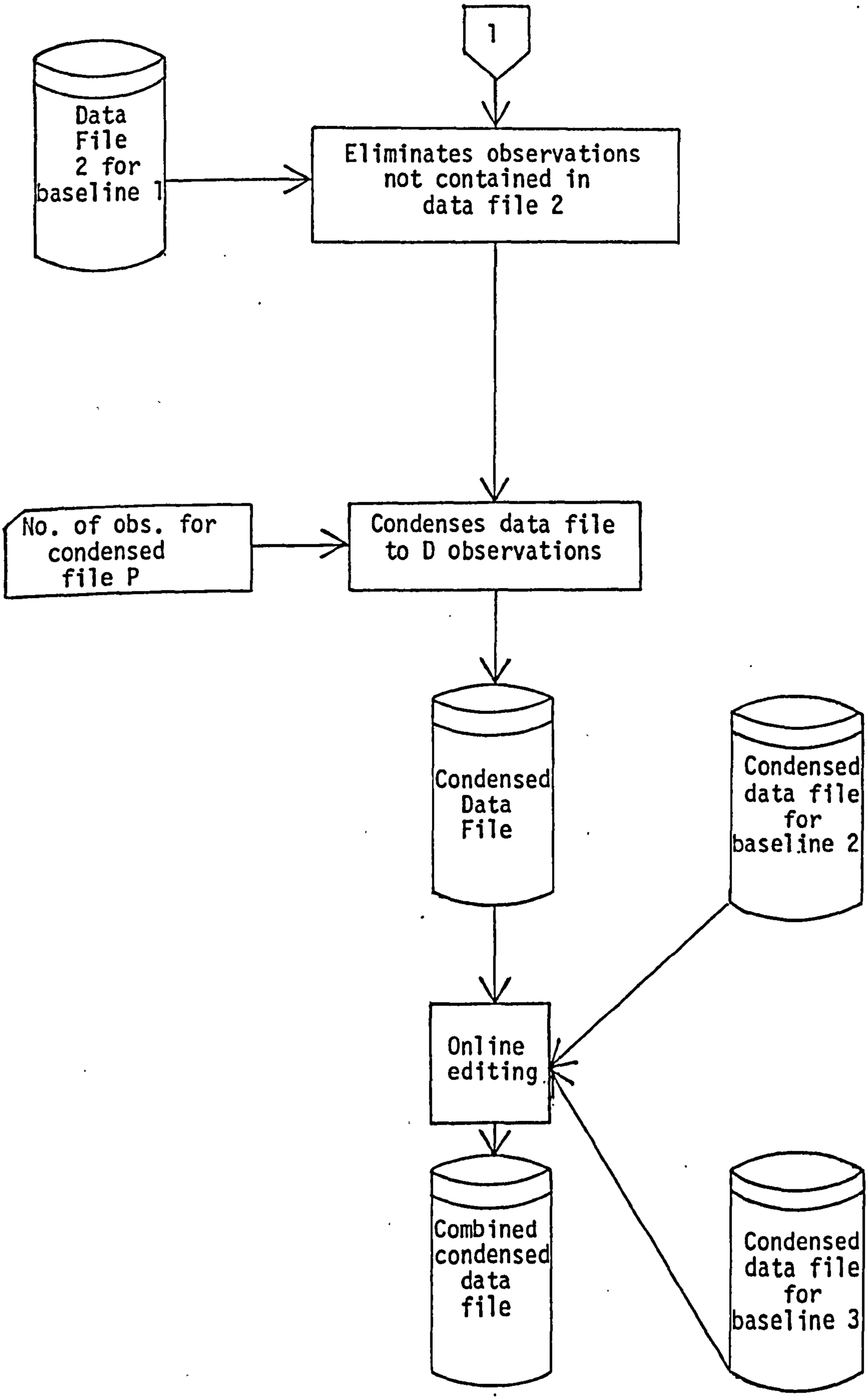

Fig. 5.II Details of preprocessing phase for the Canadian data

observations of 'delay data file 1' have been processed and those proving satisfactory have been output to the temporary disc file.

The observations are recalled from the disc store one at a time and a search is made for each equivalent observation in 'data file 2' by comparison of the observation epochs. If the corresponding observation does not exist in 'data file 2' then the observation is rejected but if it does exist, the two data records are combined and stored. The combined observation consists of:

(i) the code number of the observed source,

(ii) the UTC epoch one second before the observation epoch (year, day, hours, minutes),

(iii) the observed source name,

(iv) the coded identification of the observed baseline,

(v) the 'residual' delay and the standard error of the delay observation (both in μs),

(vi) the 'residual' fringe frequency and the standard error of the observation (both in Hz) (not used),

(vii) the 'offset' delay,

and viii) the 'expected' delay.

Every n^{th} observation of this data file is then output to a condensed data file for use in NULBIP, where n is a function of D, the number of observations required in the condensed file. Finally, the data terminator is appended to the end of the file.

A similar process is carried out separately for 'frequency data file 1' resulting in a condensed data file similar to that of the delay file but having the 'offset' and 'expected' fringe fequencies in items (vii) and (viii) respectively.

The output of the preprocessing phase as explained above is a set of separate data files, one for each different baseline and type of observation. This data is suitable for input directly into the single baseline adjustment program (CCOM1). To form a data file suitable for input to the three station-three baseline adjustment program, the three delay data files for each observing period are manually edited and combined using the UNILINE on-line system. Only one set of source data is required at the beginning of this combined file and similarly one terminator at the end. An identical process is carried out to form the combined fringe frequency data files as is used to form the combined delay data files.

Although the need for so much manual editing may appear inefficient, this is not in fact the case. The VLBI data provided to an independent agency, such as the University of Nottingham, is produced by specialist software which is designed by the organisation performing the post-processing according to their own requirements and therefore the data format may be subject to periodic changes. Consequently, it is not feasible to attempt to write a general preprocessing program and hence manual editing becomes an efficient alternative. The important factor is that the output of the preprocessing phase is always in a standard form such that it is suitable for direct input to NULBIP. Finally, although the maintenance of separate 'expected', 'residual', and 'offset' observations in the condensed data file may appear unnecessary, the values of these parameters themselves are often of interest and are therefore desirable in NULBIP.

The overall preprocessing phase does not identify and eliminate poor quality observations but only those which are deemed to be unsuitable. However, the percentage of poor quality observations is

very small and hence, although they will appear in the condensed data files, they will be rejected in NULBIP and will not significantly alter the number of observations contributing to the solution.

5.3 UNIVERSITY OF NOTTINGHAM VLBI PROGRAMS (NULBIP)

5.3.1 Data Input

There are two methods of reading data into NULBIP. They are from:

(i) disc files, which contain the observed sources and their co-ordinates and 'condensed' VLBI data (as described in §5.2.1 and §5.2.2),

and (ii) data cards, which contain all the required parameters of the adjustment.

The source data contains the name, source code number, and 1950.0 right ascension and declination of each source for which data is to be processed. In the case of the Canadian system, the VLBI observational data will have already been reduced to an easily manageable form by previous data processing (§5.2.2) and placed in file, and it can therefore be read directly into the main program. On the other hand, the Mk I data can be read directly into the program without recourse to data preprocessing. The appropriate program of the NULBIP suite to be used depends on the type of data (Mk I or Canadian) and the number of participating baselines (see §5.1).

The data input on punched cards is the same for all NULBIP programs and can be split into two types, namely observing period data and program option parameters. The data referring to the observing period consists of:

(i) the names of the participating antennae,

(ii) the co-ordinates of the participating antennae (geocentric radius, latitude, and longitude),

(iii) the dates of the observations,

(iv) the number of days on which observations were made,

(v) the number of sources observed,

(vi) the 'fixed' source in the adjustment (see §3.4.3),

(vii) the Greenwich Apparent Sidereal Time at 0 hr UT of each day on which observations were made (from the Astronomical Ephemeris),

(viii) a parameter indicating if a station clock has been reset during the observations,

(ix) the epoch at which the clock error polynomial is zeroed,

(x) the x and y components of polar motion, the UT1-UTC values, and the day numbers for which these values apply (at least six values of each, see §5.4.3),

and (xi) meteorological data (either real data with epochs of observation or mean values for the observing period) for each participating station.

The program option parameters are:

(i) the mode of output of the program, i.e. a parameter governing the quantity and type of program output (see §5.3.3),

and (ii) the type of data to be processed, i.e. delay only, fringe frequency (or delay rate) only, or both of these.

The overall data input and output system for the VLBI analysis in this thesis is illustrated in Fig. 5.III. The functions above the dashed

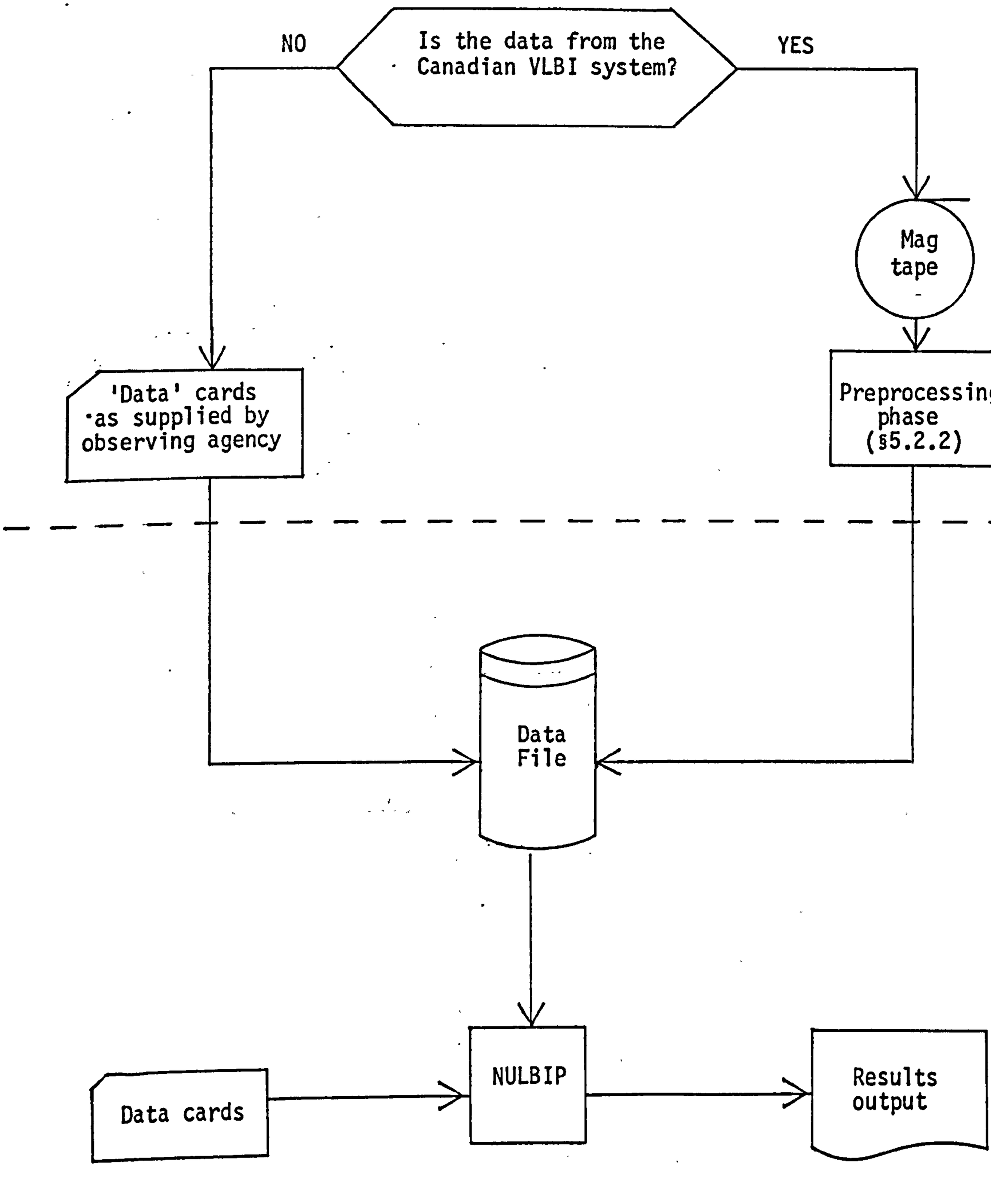

Fig. 5.III Data input and output scheme for NULBIP

line are those applicable to the specific data used here and may change for future data.

5.3.2 General Procedure

This section gives a general outline of the procedure adopted by NULBIP and illustrated in the flow chart, Fig. 5.IV. The input of data to NULBIP has already been described in §5.3.1. The special computational procedures required by NULBIP are mentioned and either will be dealt with in detail in §5.4 or have already been described in Chapter 2. In this section, reference is made to observations of fringe frequency although the Mk I data contains delay rate observations instead. The general computational process is the same for both and the differences are only in the expressions used in the particular computations, as defined in §2.1.4.

The observing period and program option data is firstly read into the program from the deck of data cards. This is followed by the input, from disc file, of each source name and its code number and 1950.0 source co-ordinates (see §2.3.1). The observed data is then read into the program, one observation at a time, from the same data file. The content of each observation record is described in either §5.2.1 for the Mk I data or §5.2.2 for the Canadian data.

Although the data may have been either preprocessed or checked beforehand, the validity of the source and baseline names is first confirmed (see §5.4.1). In the case of a three antennae array, the appropriate vector element in the baseline observation vector is coded according to the participating stations for use in the adjustment procedure. The source is also identified, coded, and stored for later use. The failure of the observation to satisfy either of these two criteria results in the rejection of the observation and causes the

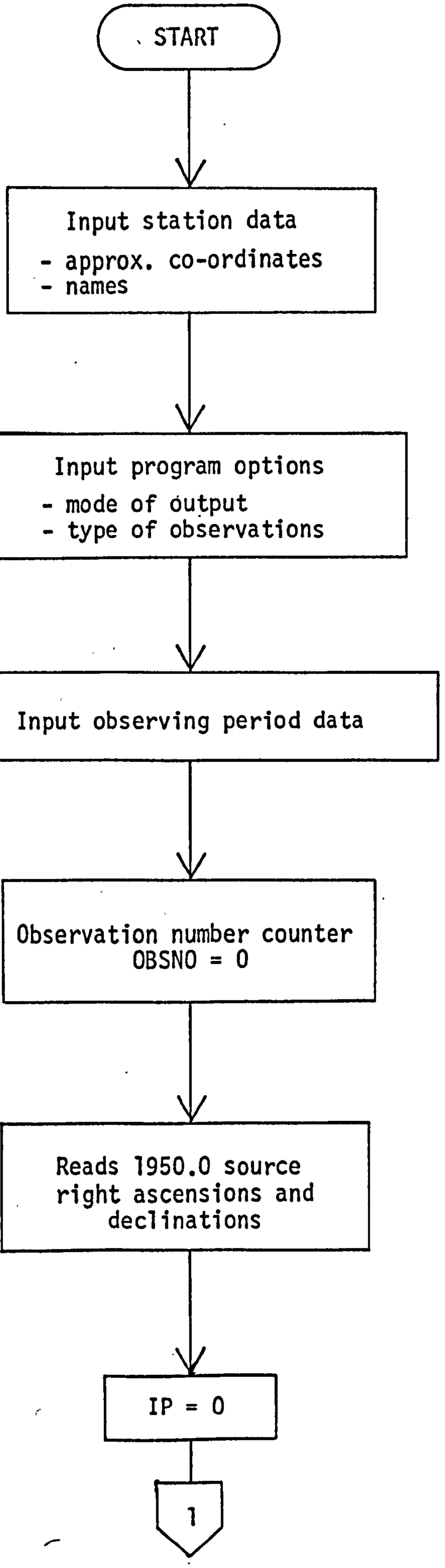

Fig. 5.IV General procedure of NULBIP

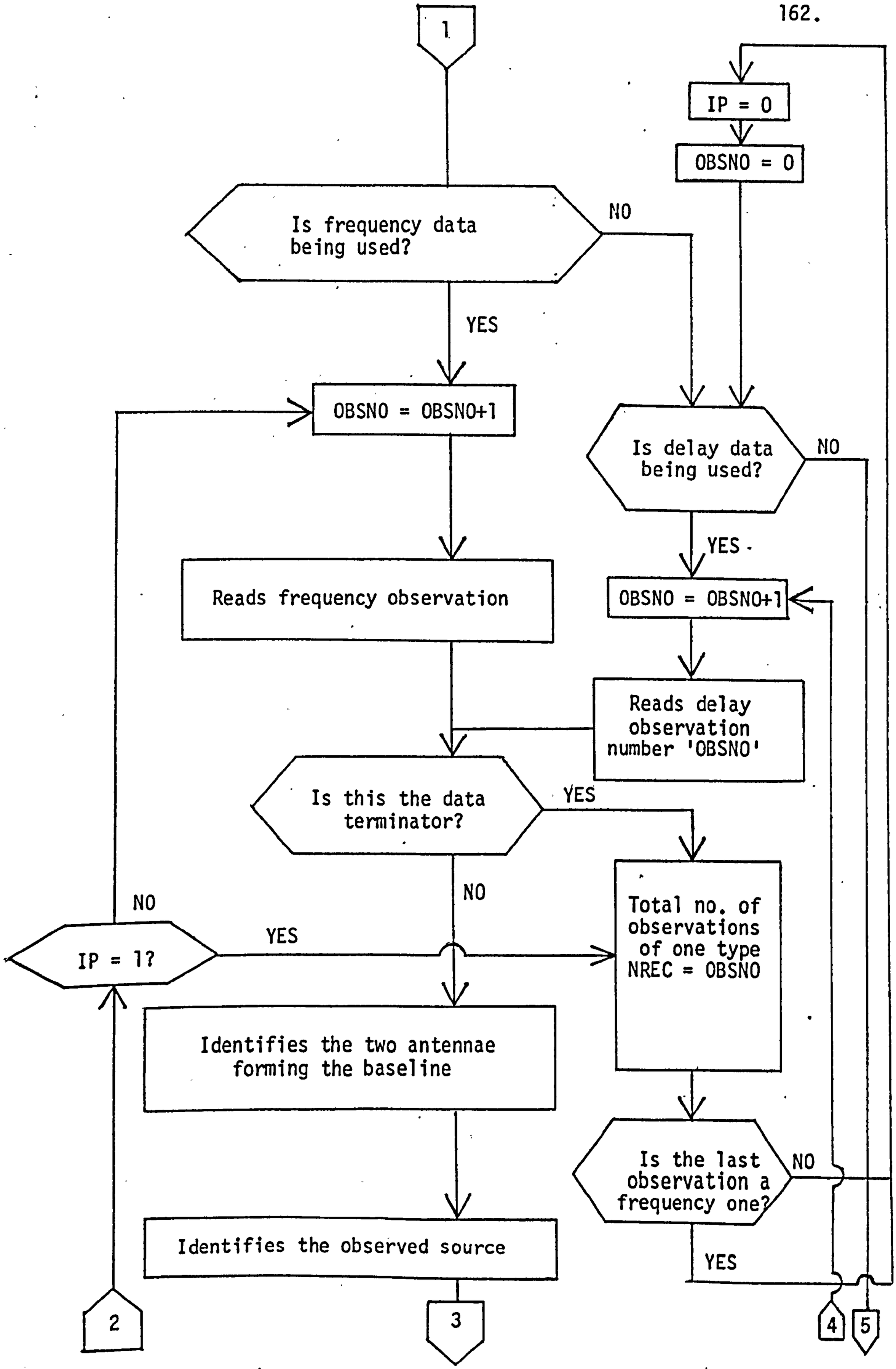
1
IP = 0
OBSNO = 0
Is frequency data being used?
NO
YES
OBSNO = OBSNO+1
Reads frequency observation
Is delay data being used?
NO
YES
OBSNO = OBSNO+1
Reads delay observation number 'OBSNO'
Is this the data terminator?
YES
NO
Total no. of observations of one type NREC = OBSNO
IP = 1?
NO
YES
Identifies the two antennae forming the baseline
Is the last observation a frequency one?
NO
YES
Identifies the observed source
2
3
4
5

2

3

4

5

Is either baseline or source name not recognised?

YES

NO

Corrects 1950.0 source co-ordinates to true celestrial co-ordinates of date

Is this a frequency observation?

NO

YES

Computes and stores all parameters relevant to observation epoch

- UTI-UTC
- x and y components of polar motion
- GAST
- time since zeroing of clock error polynomial(s)

Has the maximum number of observations of one type been passed?

YES

IP = 1

NO

6

7

8

9

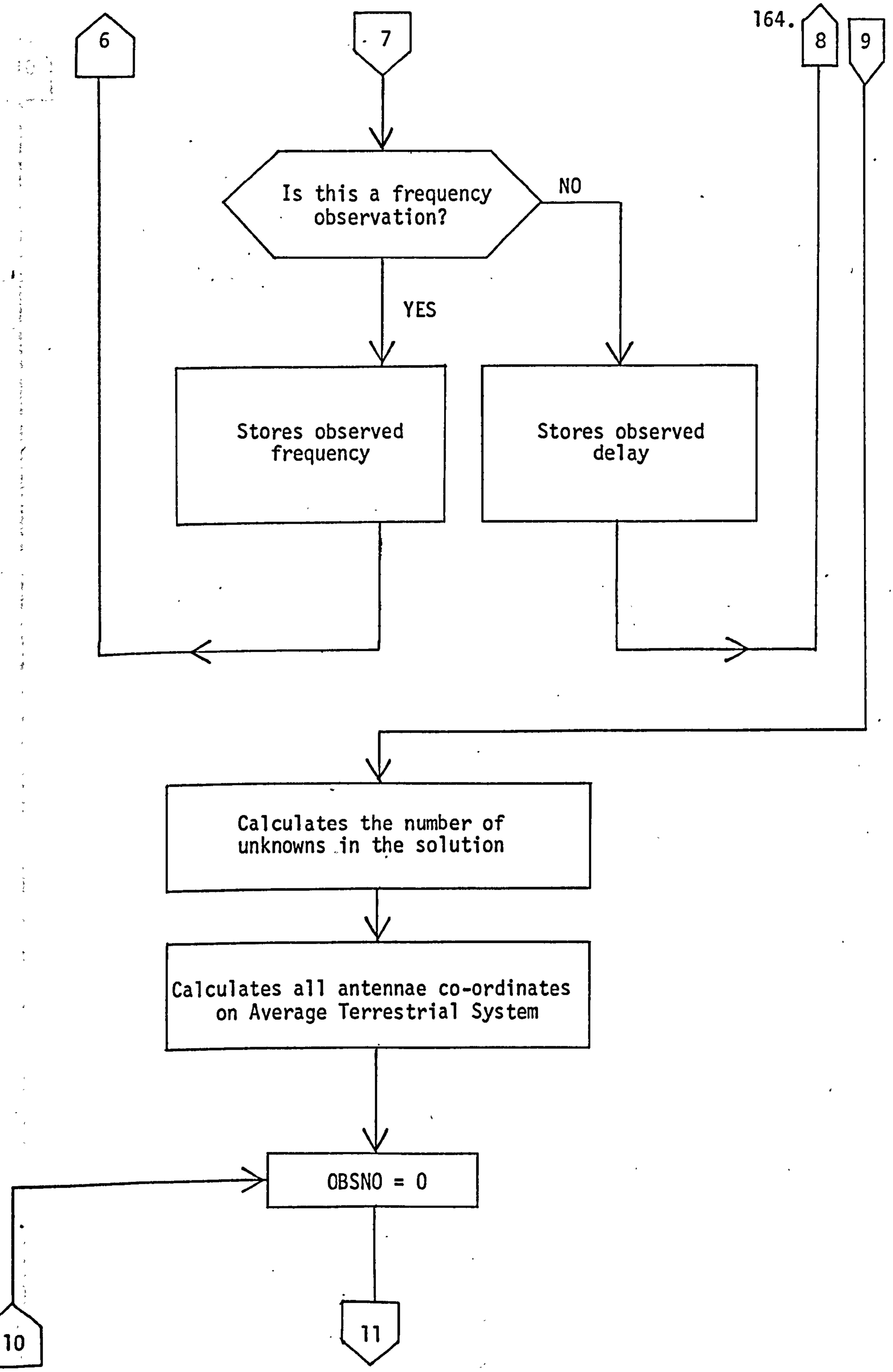
6
7
8
9
Is this a frequency observation?
NO
YES
Stores observed frequency
Stores observed delay
Calculates the number of unknowns in the solution
Calculates all antennae co-ordinates on Average Terrestrial System
OBSNO = 0
10
11

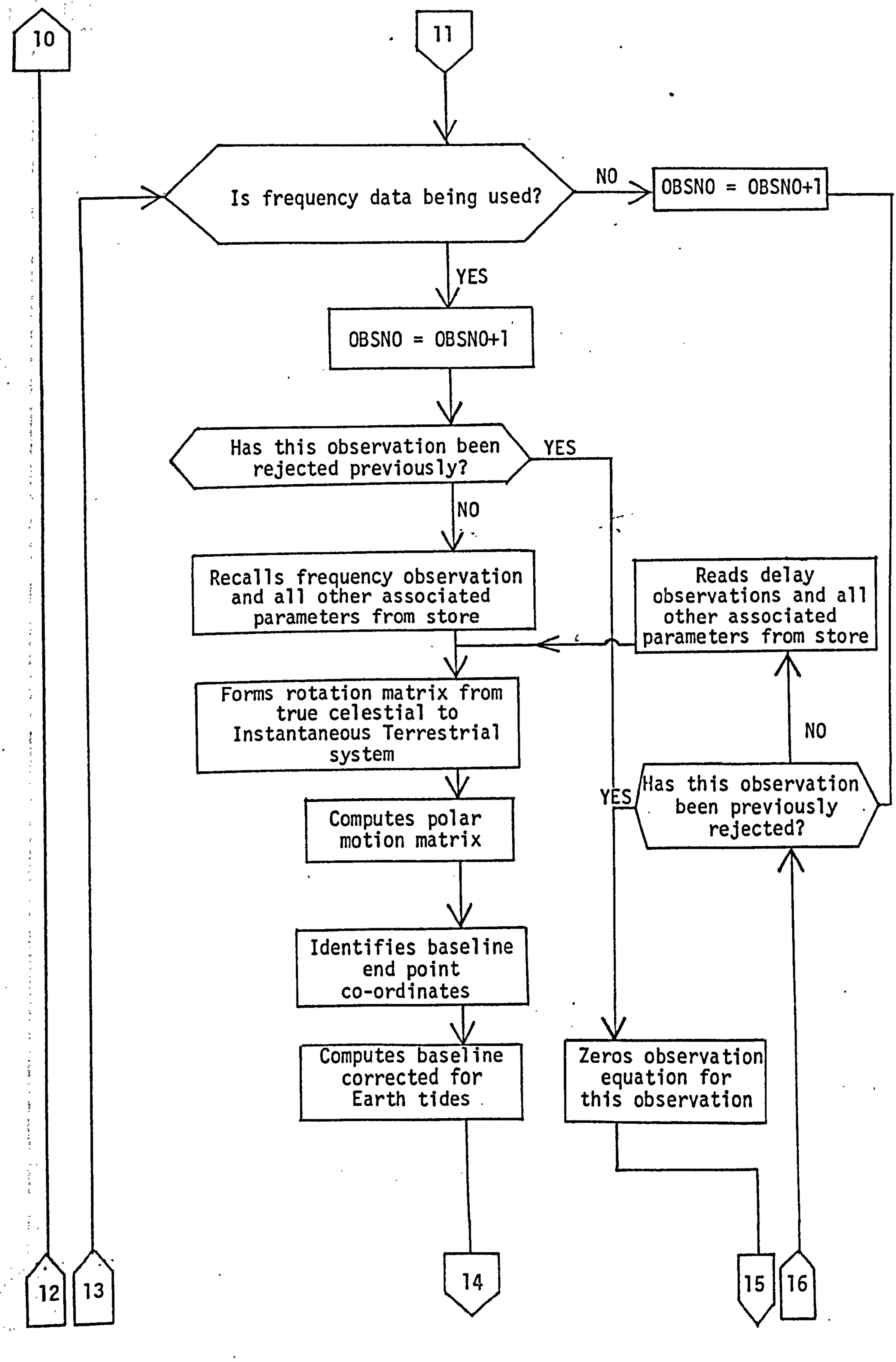
10
11
Is frequency data being used?
NO
OBSNO = OBSNO+1
YES
OBSNO = OBSNO+1
Has this observation been rejected previously?
YES
NO
Recalls frequency observation and all other associated parameters from store
Reads delay observations and all other associated parameters from store
Forms rotation matrix from true celestial to Instantaneous Terrestrial system
Has this observation been previously rejected?
YES
NO
Computes polar motion matrix
Identifies baseline end point co-ordinates
Computes baseline corrected for Earth tides
Zeros observation equation for this observation
12
13
14
15
16

12

13

14

15

16

Computes meteorological correction to observation

Computes 'retarded baseline' correction

Do the axes of each antenna intersect?

NO

NOT DONE

Compute antenna axis offset correction

YES

Is this a frequency observation?

NO

YES

Computes differential precession matrix

Computes differential nutation matrix

Computes frequency

Computes delay

Forms observation equation coefficients for left-hand-side and right-hand-side

Filter large RHS

NOT DONE ?

17

18

19

20

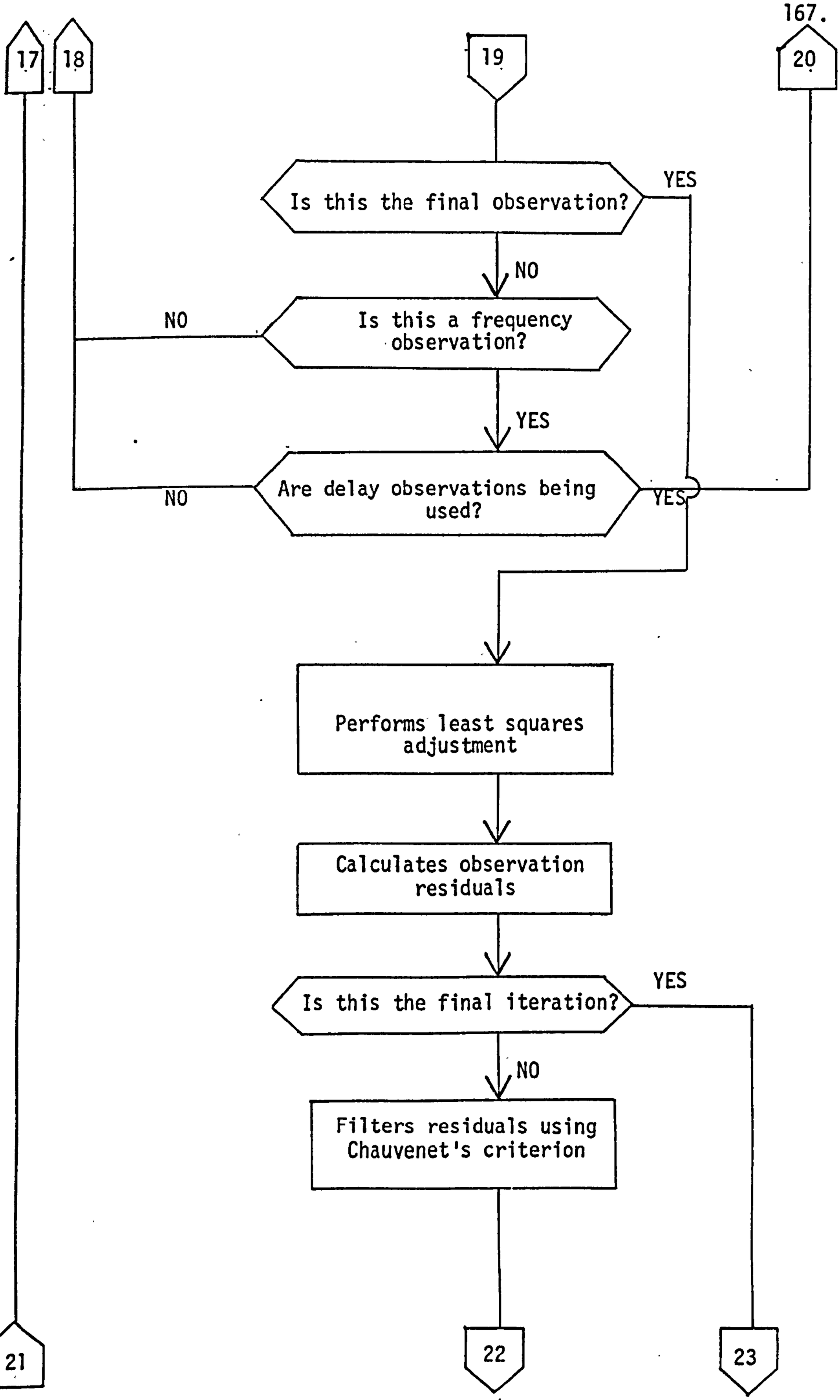
17
18
19
20
Is this the final observation?
YES
NO
Is this a frequency observation?
NO
YES
Are delay observations being used?
NO
YES
Performs least squares adjustment
Calculates observation residuals
Is this the final iteration?
YES
NO
Filters residuals using Chauvenet's criterion
21
22
23

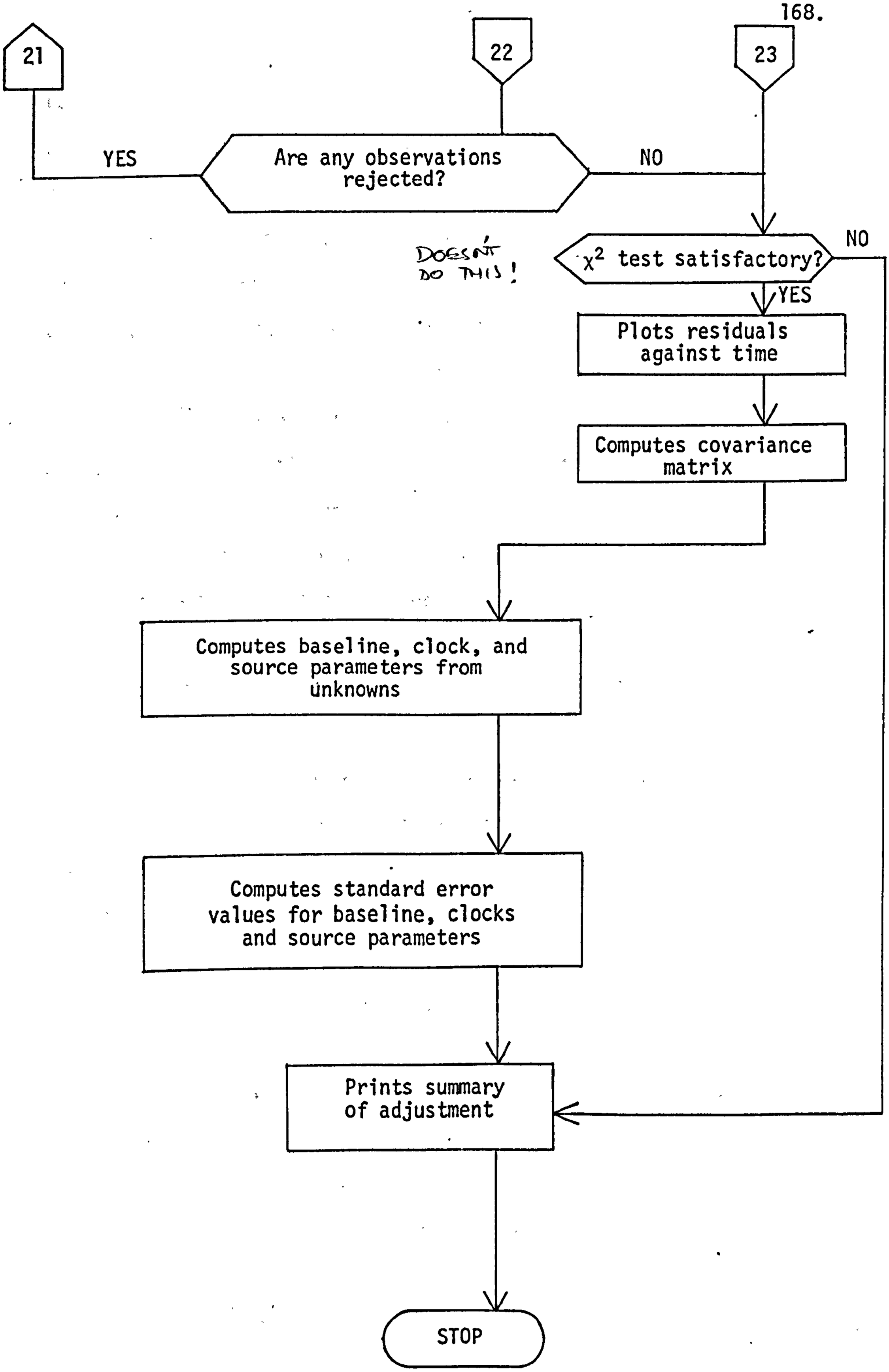
21
22
23
YES
Are any observations rejected?
NO
DOESN'T DO THIS!
χ^2 test satisfactory?
NO
YES
Plots residuals against time
Computes covariance matrix
Computes baseline, clock, and source parameters from unknowns
Computes standard error values for baseline, clocks and source parameters
Prints summary of adjustment
STOP

component of the edit vector (the vector listing the current status of each observation in the adjustment) to be amended from its original form in which all observations are assumed satisfactory.

Several parameters, associated with each observation and dependent on its epoch, are then computed and stored in the appropriate vectors, as explained below. The source co-ordinates must be updated to apparent positions relative to the true celestial system of date (see §2.1.2.2) by application of the corrections for annual aberration, precession, and nutation (see §2.3) using routines provided by the Royal Greenwich Observatory, Herstmonceux. The epoch for each observation is given in UTC and hence a corresponding time vector containing the GAST observation epochs must be established. This involves interpolation (see §5.4.3) of the input values of the UT1-UTC corrections for the epoch and hence the calculation of the UT1 observation epochs, from which the GAST epochs are obtained (see §2.4.2). The x and y components of polar motion are interpolated (see §5.4.3) from the input values for each observation epoch. For use in the clock error model (§2.4.7), the elapsed time since the origin of the polynomial is computed. Finally, each observation (and its standard error) is converted to the correct units and in the case of Canadian data, the 'expected', 'residual' and 'offset' values are combined to give the 'natural' observation.

A check is made after each observation has been processed in this way to ensure that the maximum number of observations has not been reached. Similarly, the recognition of the data file terminator will also complete the input of that observation type. In the case of Mk I data, all the data is read from the file, which contains both observation types, but only the data required for the proposed adjustment,

as specified by the program option parameters, are used. In contrast, for the Canadian data, only the type of data required for the adjustment is read into the program.

Finally, the data input is completed by the meteorological data for each station being read into the program. This may take the form of either meteorological observations taken at specified epochs, or mean meteorological data for the observing period, or a mean atmospheric delay in the zenith direction for the observing period. This completes the data input and the initial processing stage of the program.

The program then enters the adjustment phase. Firstly, the number of unknowns in the adjustment is computed. This is governed by the number of baselines, the number of sources, the order and number of clock polynomials, and the inclusion of any further parameters, e.g. meteorological unknowns, (see §3.3). The cartesian co-ordinates of each antenna in the Average Terrestrial system are then computed from the input co-ordinates (see §2.1.2.1) and the baseline components are computed. The observed values and their associated data are recalled from store one observation at a time. The rotation matrix transforming the true celestial into the 'instantaneous' co-ordinate system (see §2.1.2.3) and the polar motion matrix (see §2.2.2) transforming the Average Terrestrial into the 'instantaneous' system are established. From the coded baseline observation vector, the baseline endpoints are identified and their co-ordinates retrieved.

The parameters and corrections necessary for the calculation of the observation from a priori data are then computed. The co-ordinates of both antennae are corrected for Earth tidal movement (see §2.4.3) and hence the true a priori baseline at the epoch of observation, on

the Average Terrestrial system, is established. The dry and wet temperature and pressure if meteorological data is available, or the mean atmospheric delay in the zenith direction if this is available, together with the angle of elevation of each antenna at the epoch of observation are derived (see §5.4.2) and used in the calculation of the atmospheric correction to the observation (see §2.4.5, §2.5.5, and Appendix D). The velocity of the 'remote' antenna and hence the 'retarded baseline' correction (see §2.4.4 and §2.5.4) to the observation are also computed. If the antennae axes do not intersect, then a correction to the observation is computed (see §2.4.1 and §2.5.3).

In the case of a delay observation, the 'computed' delay is now derived as shown in §2.4.9. For fringe frequency observations, the differential precession and nutation matrices are established and the frequency computed using the expression derived in §2.5.1. The appropriate row of the observation equations matrix is formed and stored entirely in core, as is the right-hand-side 'observed minus computed' vector element (see §3.2.1). The next observation is recalled from store and the whole process repeated until all the observation equations have been formed. Any observations which are unsatisfactory according to the edit vector element have zeroes input to their observation equation. At this stage, the magnitude of the right-hand-side of each observation is checked and if it is found to be bigger than a specified value, then the observation is rejected (see §3.6.4).

IT ISN'T

After all the observations have been processed in this way and the observation equations formed, the normal equations (see §3.2.2) are computed and the values in certain rows and columns are eliminated, excepting leading diagonal elements, so that these parameters remain fixed in the adjustment (see §3.4.3). The normal equations are then 'scaled', solved, and 'descaled'. "Scaling' of the normal equations

involves manipulating of the matrix to give 1's on the leading diagonals so that the solution of the equations will not be affected by ill-conditioning of the matrices. 'Descaling' recovers the correct solution from the 'scaled' solution. The solution itself is performed by decomposing the normal equations matrix by Choleski's method (see Appendix F.3) and then forward and back substituting to give the desired unknowns (see Appendix F.4). Following this, the residual (see §3.2.2) of each observation is computed and then the value of σ_0 (see §3.2.3) for the adjustment. If this is the first solution, then the residuals are filtered using Chauvenet's criterion (see §3.6.2) and, if at least one residual is too large and hence is rejected, the whole solution process is performed again. After the second solution, or after the first if no residuals are found to be too large, the residuals are subjected to a chi-squared test to verify that they exhibit a normal distribution (see §3.6.3). A plot of observation epoch against the corresponding residual is produced which indicates the different sources (in coded form). The covariance matrix (§3.2.3) is calculated by inversion of the normal equations matrix in the manner described in Appendix F.5.

From the solution, the baseline, antennae, source, and clock model values are computed together with their standard errors from the covariance matrix (see §3.5.). Finally, the program outputs a summary of the adjustment as detailed in §5.3.3.

5.3.3 Program Output

The amount and type of output generated by NULBIP is governed by the value of the 'mode of output' option parameter in the input cards. This can take one of three values and the output for each one is:

Mode 2 - a results summary only containing:

(i) the values of the unknowns of the adjustment and their standard errors,

(ii) the adjusted baseline, antennae, source, and clock parameters,

(iii) the baseline declination, hour angle, and length (see §3.4.1) and their standard errors,

(iv) summary data of the adjustment itself, i.e. σ_0, the number of observations accepted and rejected (and why), the mean a priori standard error of each type of observation and each baseline, and the a priori co-ordinates of each antenna.

Mode 1 - a results summary, as described for mode 2 above, and all the input data as detailed in §5.3.1.

Mode 0 - a complete output of almost all phases of the program, i.e. the input data including the meteorological data, the observation equation right-hand-sides, normal equations, observation residuals, covariance matrix, and a results summary.

For program testing purposes it is an easy task to output any other desired parameter from the program.

5.4 COMPUTATIONAL PROCEDURES USED IN NULBIP

5.4.1 Baseline and Source Identification

The observing baseline in the Canadian data is represented by a code word comprising of four letters, the first two representing antenna A (the 'reference' antenna) and the second two representing

antenna B (the 'remote' antenna). For example 'ARCH' indicates that antenna A is Algonquin Radio Observatory (AR) and antenna B is Chilbolton Observatory (CH). The baseline code word for each observation is compared against the input participating station names and, in the case of the three baseline program, a vector is established containing a specific digit representing the observing baseline of each observation. For the input station names AR, OV (Owens Valley) and CH, the baseline identification vector contains:

1 for AROV,

2 for ARCH,

and 3 for OVCH.

The baselines OVAR, CHAR, and CHOV are not used in these data sets. If the baseline name is not recognised, then the observation is rejected.

The source code number associated with each observation for both Canadian and Mk I data should be contained in the vector of source code numbers in the source data block at the beginning of the data file. An observation of the source 3C273B by the Mk I system is illustrated in Fig. 5.V, along with the elements of the source data record for 3C273B

source code number

HG(33) 829721715 7865.766111 .153 -743155.184 .148

Observation of 3C273B by NRAO Mk I VLBI system

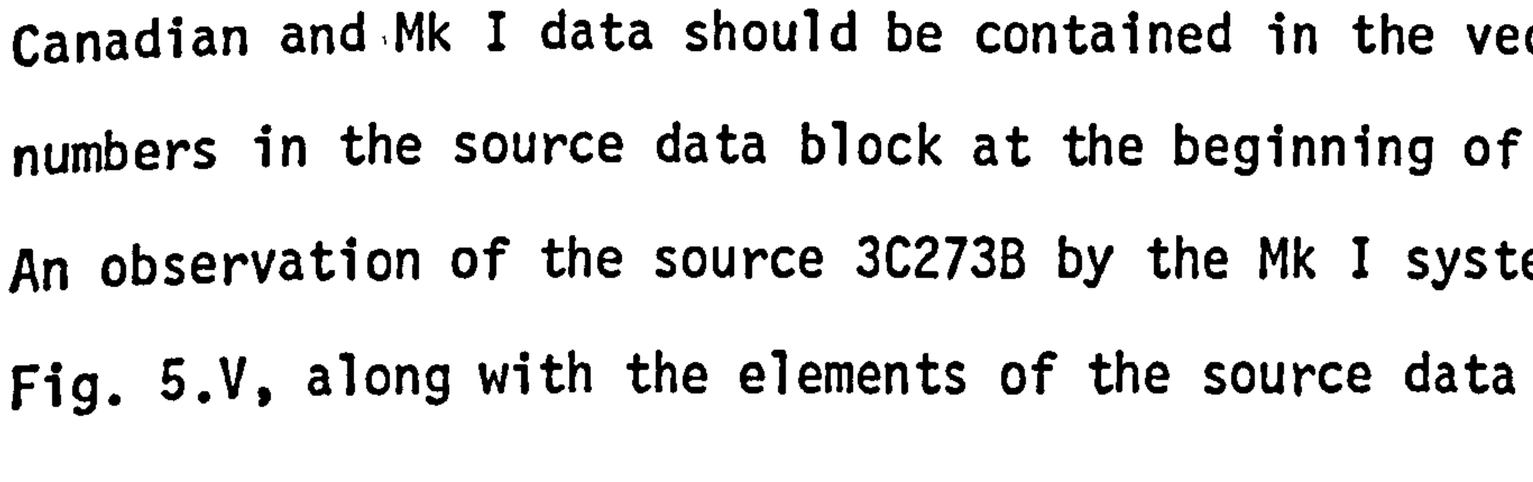

Source data record for 3C273B

Fig. 5.V Source Identification Method

(see Appendix G for a full explanation of the individual elements of each data record). The code for each observation is read and compared with each element of the vector of source code numbers, established from the input source data, until the correct element is located. A vector is established containing the number of the sequential position of the appropriate source in the source data list. In this example, 3C273B is the fourth source in the source data list and hence has the number 4 allocated to the appropriate element of the observed source vector. This technique enables simple allocation of storage space later in the program. If no corresponding source code number exists, then the observation is rejected.

5.4.2 Data Preparation for Tropospheric Model

There are two tropospheric correction models used in this study, both of which are described in §2.4.5 and Appendix D. The first, Chao's model, depends on a knowledge of the source direction and approximate antenna position, along with the excess delay in the zenith direction due to the atmosphere: It is therefore well suited for use with average meteorological data for a whole observing period although observed meteorological data may be used. The second, Hopfield's simplified model, also requires the source direction and approximate antenna position but also requires observation of dry and wet temperature, and pressure (or similar observations, e.g. relative humidity instead of wet temperature, which yield the same data (see Appendix D.2)). This model can easily be used for either average meteorological data or for observed data with observation epochs.

For the case of an average correction, the data can be used in the model directly as it is input to the program (having corrected the units

of measurement if necessary). In the case of observed data, the epoch of observation and the meteorological data are stored chronologically in separate vectors for each station. A linear interpolation is performed for each VLBI observation relating the VLBI observation epoch to the meteorological data observation epoch and hence to each type of observed meteorological data. This yields the value of each meteorological parameter for the desired epoch from:

$$X_{obs} = \frac{(t_{obs} - t_{i-1}) \times (X_i - X_{i-1})}{(t_i - t_{i-1})} + X_{i-1} , \qquad (5.2)$$

where X_{obs} = the calculated value of the meteorological parameter X at the epoch of the VLBI observation, t_{obs},

X_i and X_{i-1} = the observed meteorological parameter at the epochs defined by the i^{th} and $(i-1)^{th}$ elements of the particular meteorological parameter vector,

and t_{obs}, t_i and t_{i-1} = the epochs of the meteorological data parameters described above.

If the observation lies outside the time span of meteorological observations, then extrapolation of the observed meteorological data is required.

Besides the actual observed or average meteorological data, all tropospheric models require the elevation above the horizon of the line of sight of observation. The theory and formulae for this computation are described in Appendix D.3. The computation of the elevation of the line of sight is also required in the data filtering and preprocessing stages as well as in the tropospheric model itself. For fringe frequency and delay rate observations, the rate of change of elevation is required in the tropospheric model (see Appendix D.3). The rate of

change of the meteorological parameters themselves contribute very little to the overall correction and are hence ignored. The elevation is also used when considering the design of VLBI experiments (see §5.5).

5.4.3 Everett's Algorithm

The x and y components of polar motion and the UT1-UTC differences are tabulated at 5-day intervals in the BIH Circular D and Rapport Annuel. In order to compute the values at the epoch of observation, Everett's interpolation formulae is used. Everett's algorithm involves forming a central difference table, as shown below, where T_i are the tabulated epochs (at 5-day intervals) and X_i are the corresponding parameter values:

T_0	X_0							
		$\delta X_{0.5}$						
T_1	X_1		$\delta^2 X_1$					
		$\delta X_{1.5}$		$\delta^3 X_{1.5}$				
T_2	X_2		$\delta^2 X_2$		$\delta^4 X_2$			
		$\delta X_{2.5}$		$\delta^3 X_{2.5}$		$\delta^5 X_{2.5}$		
T_3	X_3		$\delta^2 X_3$		$\delta^4 X_3$			
		$\delta X_{3.5}$		$\delta^3 X_{3.5}$				
T_4	X_4		$\delta^2 X_4$					
		$\delta X_{4.5}$						
T_5	X_5							

The table is computed such that:

$$\delta X_{0.5} = \delta X_1 - \delta X_0,$$

and $$\delta^2 X_1 = \delta X_{1.5} - \delta X_{0.5}, \text{ etc.}$$

If the value of the paramter X(n) is required at an epoch n, which lies between T_2 and T_3, then Everett's formula gives:

$$X(n) = tX_2 + \begin{bmatrix} t+1 \\ 3 \end{bmatrix} \delta^2 X_2 + \begin{bmatrix} t+2 \\ 5 \end{bmatrix} \delta^4 X_2 + \begin{bmatrix} t+3 \\ 7 \end{bmatrix} \delta^6 X_2 + \ldots. \qquad (5.3)$$
$$sX_3 + \begin{bmatrix} s+1 \\ 3 \end{bmatrix} \delta^2 X_3 + \begin{bmatrix} s+2 \\ 5 \end{bmatrix} \delta^4 X_3 + \begin{bmatrix} s+3 \\ 7 \end{bmatrix} \delta^6 X_3 + \ldots.$$

where $s = \dfrac{n-T_2}{T_3-T_2}$,

$t = 1-s$,

$$\begin{bmatrix} r \\ k \end{bmatrix} = \frac{r(r-1)(r-2) \ldots. (r-k+1)}{k!}$$

For this application, the formula may be truncated at the fourth difference and hence there must be three input data points either side of every observation epoch.

5.5 OBSERVING PROGRAM DESIGN

The design of the observing schedule directly affects the accuracy of the parameter estimation procedure for a VLBI experiment. There are no definite rules concerning the optimum design for a given experimental objective (Robertson, 1975) and therefore it is largely an empirical procedure. However, there are several factors which require consideration, namely:

i) the antennae of the array (or at least some of them) need to simultaneously observe a source at a sufficiently high elevation and the source needs to be strong enough for the antenna systems to make useful observations (see Chapter 4),

ii) each particular source needs to be observed at different hour angles so that, firstly, the effect of any unmodelled time dependent

systematic errors in the adjustment are not transmitted directly into the baseline determination, and secondly, the observations should provide a well balanced baseline solution,

iii) observations on several sources should be included for the same reason as (ii) above and also so that sufficient sources are observed to give a solution for all the desired parameters (see §3.4),

iv) sources covering a wide declination range should be observed since this is the governing factor on the accuracy of the determination of the polar component of the baseline, and

v) the time required to move each antenna from one source to the next must be considered.

In order to allow for the considerations outlined above, and hence to obtain an efficient and successful observing program, recourse can be made to several techniques. To determine the availability of a source for observation, a program has been written to compute the elevation of a source (Appendix D.3) as viewed from up to five antennae throughout a 24-hour period. The graphical output, illustrated in Fig. 5.VI for source NRA0150, is a polar plot with the radiating arms representing time, in clockwise increments of one hour starting at 0 hour vertically upwards, and the circles representing elevation, increasing in increments of 10^{o} from 0^{o} in the centre to 90^{o} on the outer ring. In this case, the elevation plots are only given when all the antennae can view the source at an elevation greater than 10^{o}.

In order to obtain a well balanced solution, consideration of the 'uv-plane' coverage is useful. The uv-plane is defined as a plane parallel to the incident wavefront from a source, where u is in the direction of increasing right ascension and v is in the direction of

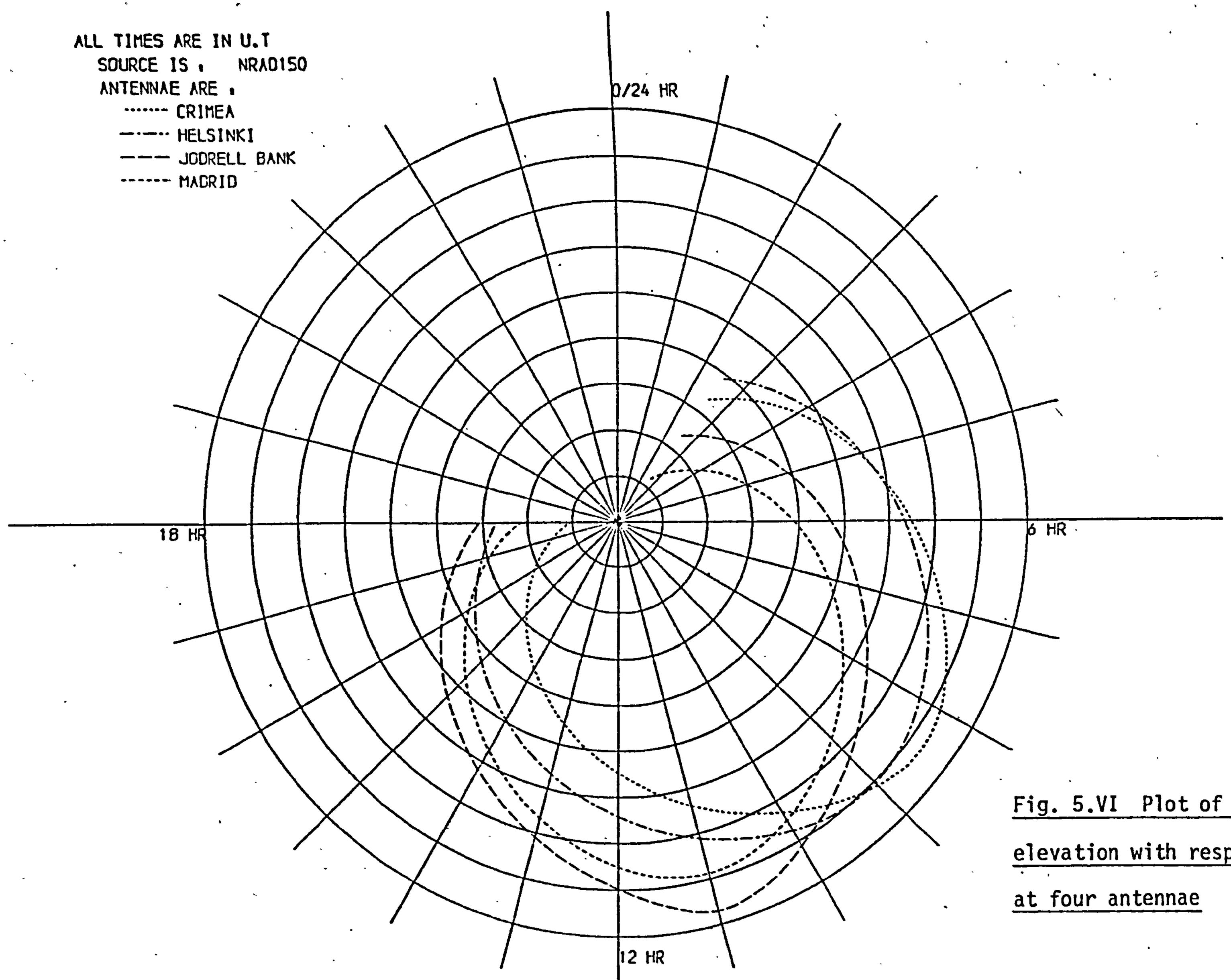

Fig. 5.VI Plot of source elevation with respect to time at four antennae

increasing declination (see Fig. 5.VII). The actual plane, therefore, remains fixed with respect to the source and its signal wavefront, but moves with respect to the antennae. One of the antennae of each individual baseline in an array is assumed to always lie at the origin of the uv-plane and the projection of the other antenna onto this plane defines the u and v components of this particular baseline at any epoch where:

$$u = \frac{w}{c} B \cos \delta_B \sin(H_S - H_B)$$
$$v = \frac{w}{c} B\left[\sin \delta_B \cos \delta_S - \cos \delta_B \sin \delta_S \cos(H_S - H_B)\right] \qquad (5.4)$$

and B = baseline length (comprising components b_x, b_y, b_z),

δ_S and H_S = declination and hour angle of the source,

δ_B and H_B = declination and hour angle of the baseline as given in (3.26),

w = observing frequency,

and c = velocity of propagation of microwaves in vacuo.

These formulae give u and v in radians as a measure of the baseline projection in terms of the observing wavelength. Therefore, considering one baseline only, its projection on the uv-plane describes an ellipse, centred at $(0, (w/c)B \sin \delta_B \cos \delta_S)$, with eccentricity of $\cos \delta_S$, and semi-major axis equal to the equatorial component of the baseline. This ellipse is a measure of the baseline projection and hence takes no account of whether both antennae can actually 'see' the source. In presentation of uv plots, this fact is catered for by computing the elevation of the line of sight to the source from each antenna and disregarding periods during which negative elevations occur at either antenna. Figs 5.VIII through 5.X show the assembly of the uv plot for a source of declination 50^o as observed from the four antennae at Jodrell Bank, Helsinki, Crimea,

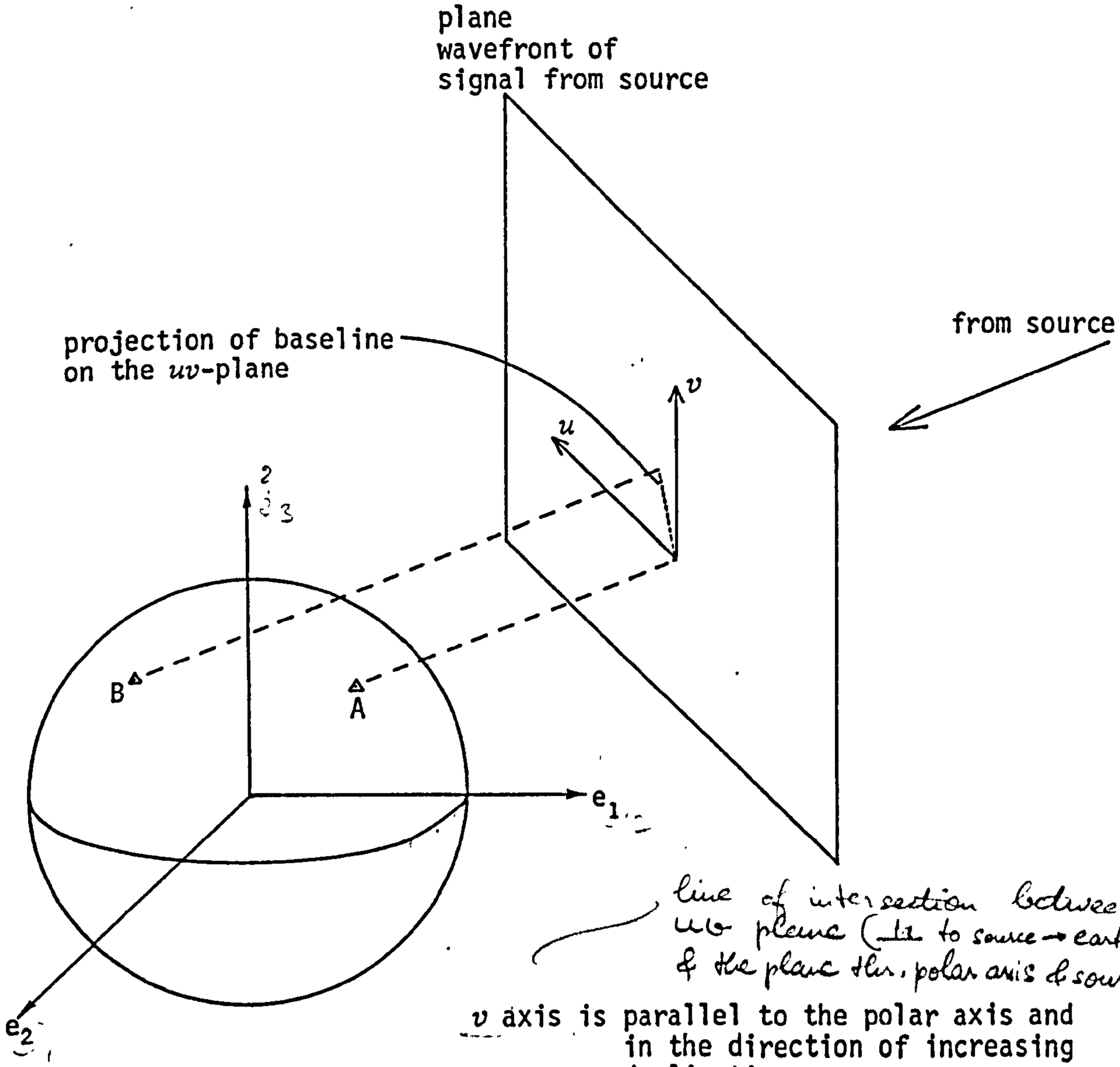

v axis is parallel to the polar axis and in the direction of increasing declination

u axis is parallel to the equator and in the direction of increasing right ascension

Fig. 5.VII Geometry of the *uv*-plane

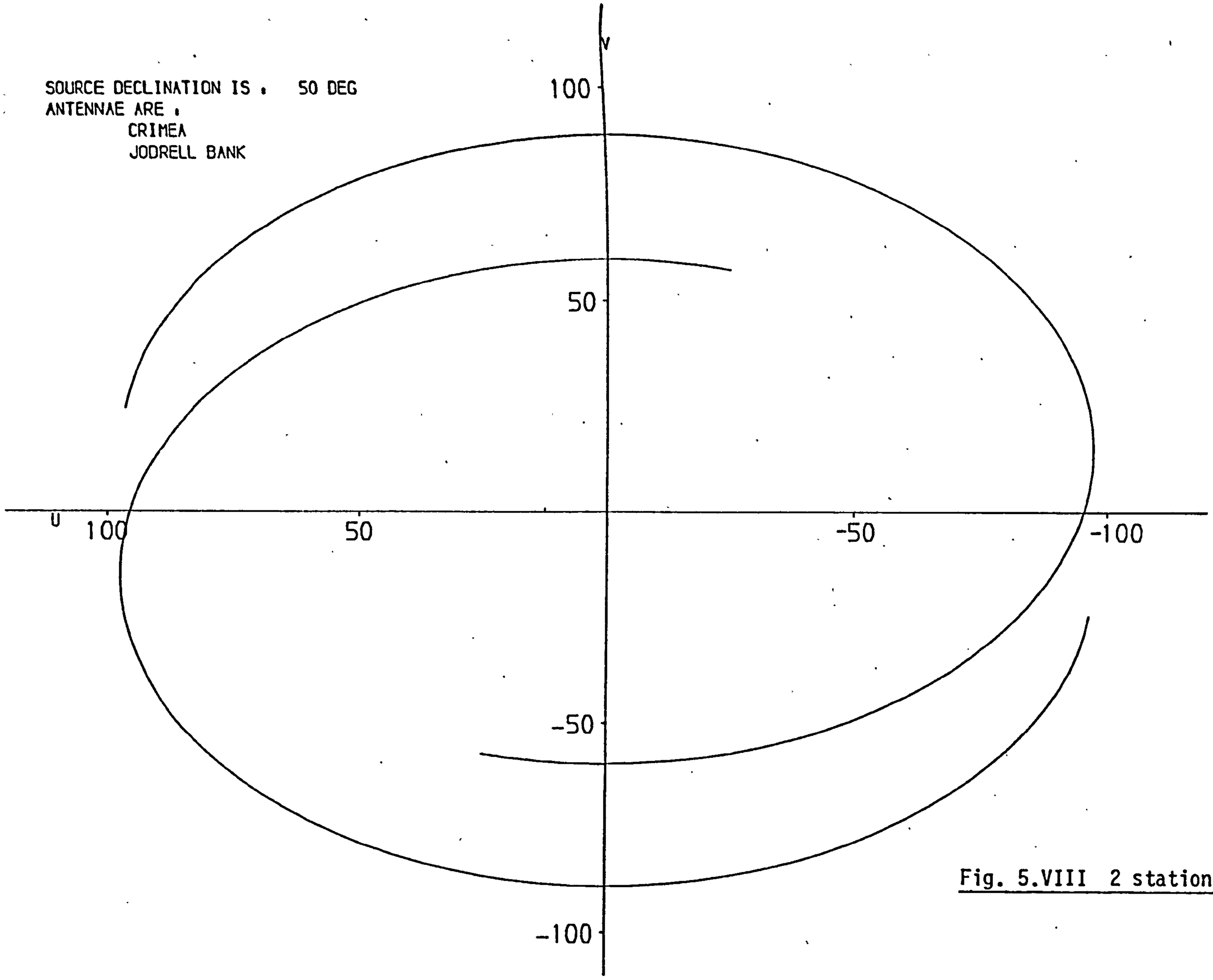

Fig. 5.VIII 2 station *uv* plot

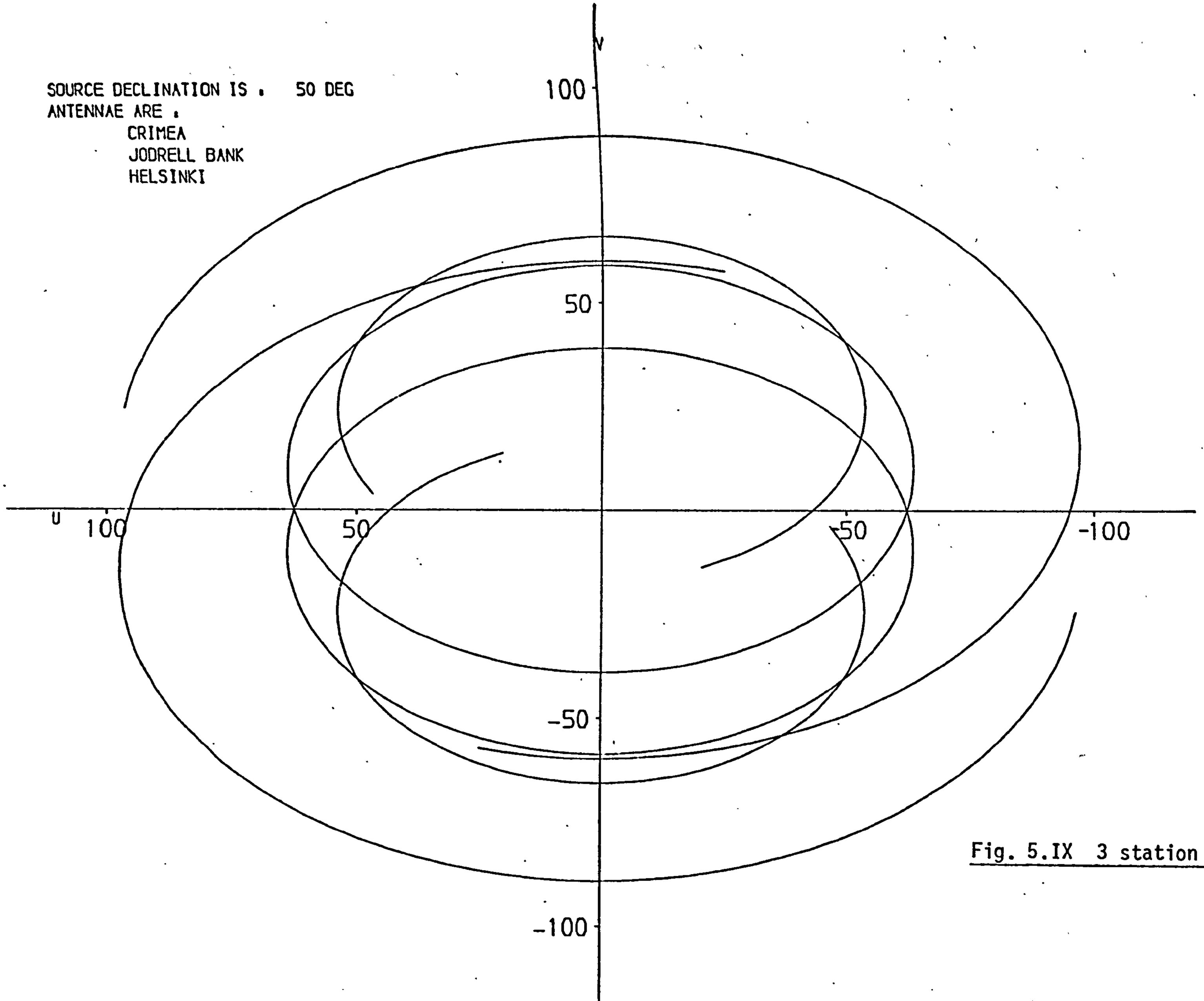

Fig. 5.IX 3 station *uv* plot

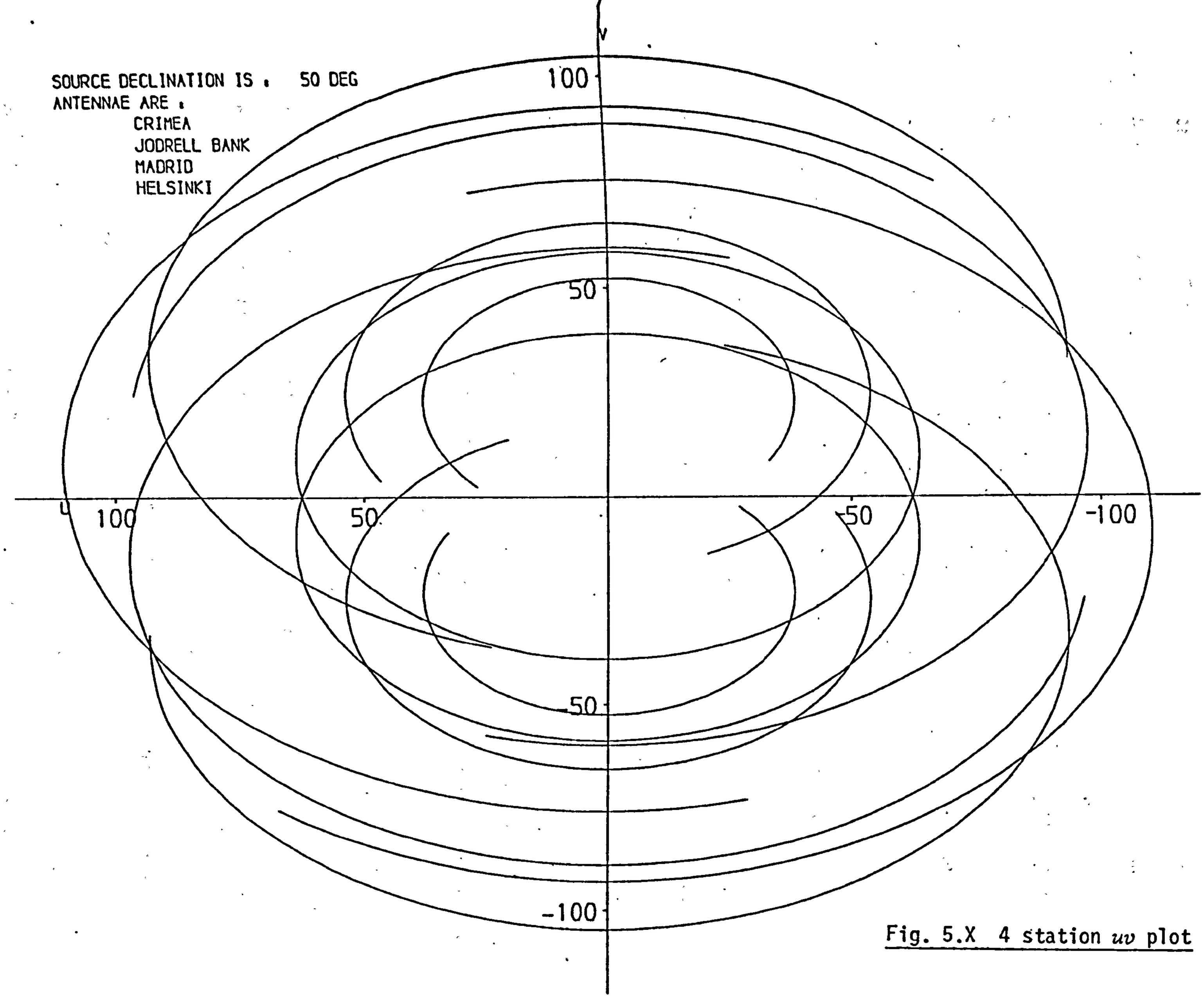

Fig. 5.X 4 station *uv* plot

and Madrid. Fig. 5.VIII is the plot for just Crimea and Jodrell Bank. Note that there are two curves, one for Crimea as the origin and one for Jodrell Bank as the origin. Fig. 5.IX illustrates the effect of adding Helsinki to form a three baseline array and, similarly, Fig. 5.X shows the full four station *uv* plot.

For each baseline, superimposing of all the *uv*-plane coverage plots for the different available sources gives a measure of the total possible coverage for the baseline. Hence, for a well balanced solution, observations should be made over the whole range of the combined *uv*-plane coverage.

Having designed the observing program, its effectiveness in determining all the baseline, source, and clock parameters can be assessed by performing an adjustment simulation. The program of the NULBIP suite which performs this task (EUROSIM1) is capable of handling 300 observations and four observing antennae (six baselines).

The basis of least-squares adjustment simulation is that the a posteriori standard errors of the unknown parameters (corrections to the initial approximate parameters) of a real adjustment are derived from the inverse of the normal equations coefficient matrix and the value of the unbiased estimate of the variance of an observation of unit weight (σ_o) obtained from the solution (see §3.2.3) (Ashkenazi, 1970). The normal equations coefficient matrix is independent of the observed data (assuming reliable estimates of the a priori parameters) and depends solely on information about an observation (e.g. epoch, observed source, expected observation standard error, observed baseline). Hence, for a newly designed observing program, the coefficient matrix can be formed and inverted. If the assumption is made that the a priori observation standard errors used in the formation of the normal equations matrix were

estimated correctly, then σ_o can be assumed to equal unity and the a posteriori standard errors can be extracted from the inverted normal equations coefficient matrix (see §3.5).

As a result of a simulation experiment, the potential accuracies of the proposed adjusted parameters can be assessed and, if necessary, observations may be subtracted, rearranged, or added, in order to improve the observing programme.

CHAPTER 6:

VLBI AND SATELLITE-DOPPLER OBSERVATIONS

6.1 VLBI OBSERVATIONS WITH THE ALGONQUIN-OWENS VALLEY-CHILBOLTON INTERFEROMETER ARRAY

A series of VLBI observations has been conducted over the last seven years between the National Research Council of Canada's Algonquin Radio Observatory (ARO), Lake Traverse, Ontario, and the United Kingdom Science Research Council Appleton Laboratory's Chilbolton Observatory, Chilbolton, Hampshire, using the Canadian VLBI system described in Chapter 4. Since June 1975, the Owens Valley Radio Observatory (OVRO), Big Pine, California, has also participated in these experiments, hence giving a three station, three baseline interferometer array. The data is derived from the recorded tapes using the playback and correlation facilities at the Herzberg Institute of Astrophysics in Ottawa. Although experiments have been performed at frequent intervals over this period, only the data from the experiments of 13th-16th May, 1977, and 17th-20th January, 1978, have been processed in this study, as it is, for various reasons, of a higher quality than the data from the other experiments (Langley, 1979).

The main object of the observations has been to study the structure and properties of the observed radio sources. Consequently, the extraction of geodetic information from the observed data has been of secondary importance when considering the design of the observing programmes. However, the data has nevertheless proved very useful for this application (Cannon et al, 1975, Cannon et al, 1979, and Langley, 1979). In the experiments, each source is tracked continuously, allowing for tape changes and other necessary stoppages, for as long a time as is feasible in order to obtain as large a coverage as possible of the *uv*-plane (the projection of the baseline on the plane of the oncoming wavefront, see §5.5). This often results in only two of the antennae being able to observe the source at any one time. The data

tapes record one hour of data each and are started as close to a UT hour as possible.

A view of the positions of the three antennae on the Earth's surface together with the three baselines is shown in Fig. 6.I. As can be seen from this diagram, the three antennae are all within 14^{o} of latitude and hence the polar baseline components are small with relation to the equatorial baseline components. The co-ordinates of the telescope reference points (see §2.2.1) as derived from terrestrial survey connections to the local datum are given in Table 6.I. This table contains the spheroidal co-ordinates (i.e. geodetic latitude and longitude, and height above spheroid level) of each antenna reference point on its own appropriate national geodetic datum, together with the semi-major axis and eccentricity of each ellipsoidal datum. From these values the cartesian co-ordinates relative to the national datum origin are computed in the manner described in (2.1). In the case of this North American and Ordnance Survey of Great Britain data, these co-ordinate systems can be simply translated into the Average Terrestrial system (§2.1.2.1) using the translation parameters given. The cartesian co-ordinates in this system are given in the table and may be used as initial approximate co-ordinates in the adjustment procedure. The position of an antenna reference point is determined using conventional land survey techniques by observations from nearby stations which have been connected to the particular national geodetic triangulation network. The precise method employed at the Chilbolton Observatory is described in §6.4.1 and the other telescope survey connections are outlined in §6.4.3.

A full description of the antenna and receiver systems is beyond the scope of this thesis. However, Table 6.II gives a brief summary of the necessary details and some of the equipment used. Each local

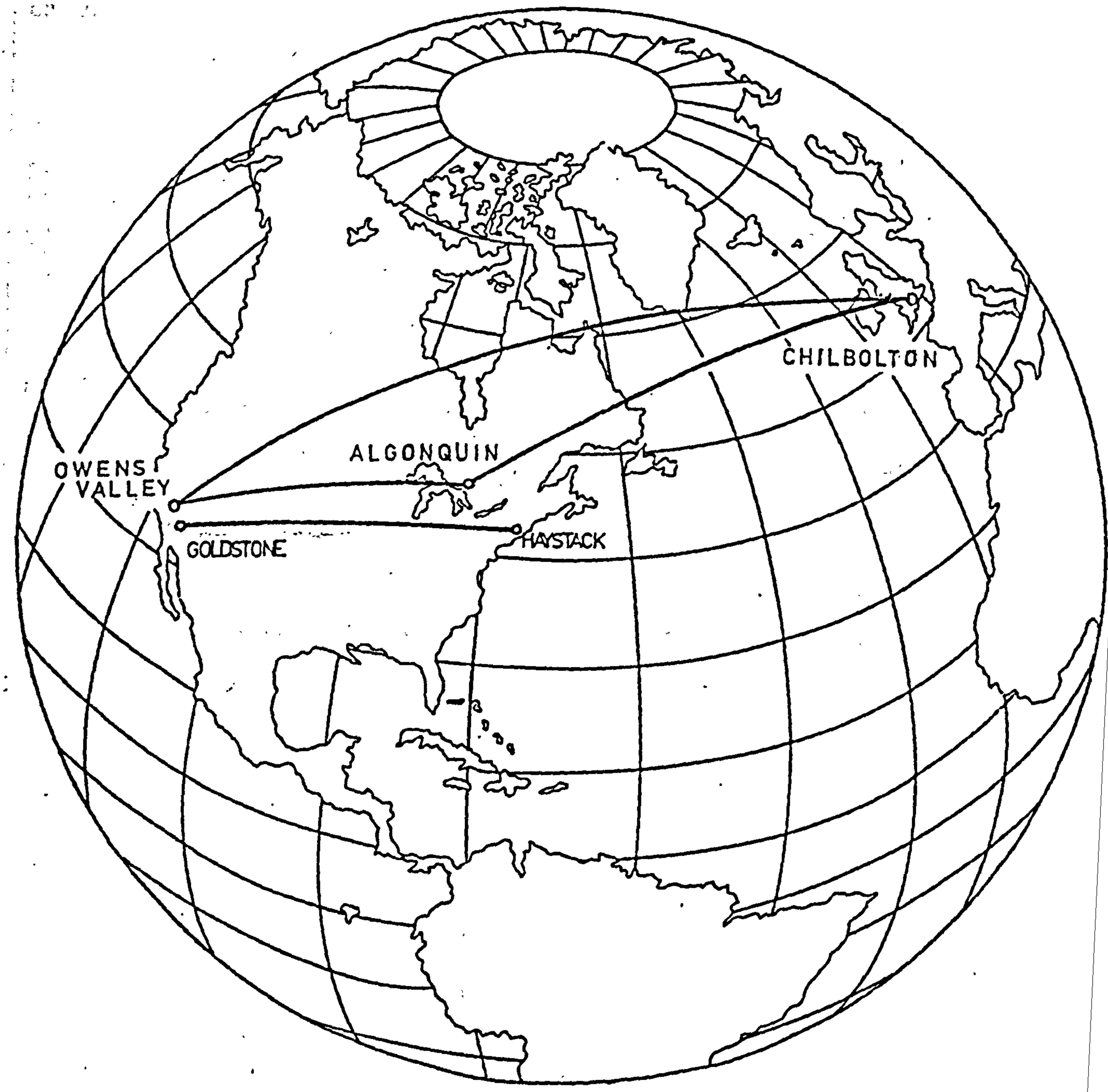

Fig. 6.1 Observed VLBI baselines

		Antenna		
		Algonquin	Chilbolton	Owens Valley
Spheroidal co-ordinates on the national datum*	ϕ	$45^{o}57'19.812"N$	$51^{o}08'40.059"N$	$37^{o}13'53.418"N$
	λ	$78^{o}04'22.945"W$	$1^{o}26'13.101"W$	$118^{o}16'54.367"W$
	N+h	260.42 m	100.37 m	1207.5 m
Cartesian co-ordinates relative to the national datum (from 2.1)	X	918043.65	4007940.69	-2409586.54
	Y	-4346292.73	-100539.84	-4478501.17
	Z	4561794.02	4943359.14	3838418.37
Cartesian co-ordinates≠ relative to the Average Terrestrial system	X	918012.90	4008295.69	-2409617.61
	Y	-4346142.00	-100651.84	-4478342.21
	Z	4561969.02	4943770.14	3838593.37

* For Algonquin and Owens Valley, the national datum is NAD27 based on Clarke's 1866 ellipsoid ($a = 6378206.4$ m, $e^2 = 0.006768658$). For Chilbolton the national datum is OSGB 70(SN) based on Airy's ellipsoid ($a = 6377563.396$ m, $e^2 = 0.00667054$).

≠ For Algonquin and Owens Valley, these co-ordinates are derived by applying the translation parameters $\Delta X = -20$ m, $\Delta Y = 153$ m, $\Delta Z = 175$ m (Ashkenazi, 1979) to the previous co-ordinates and rotating this system 0.51" eastward. For Chilbolton these co-ordinates are derived by applying the translation parameters $\Delta X = 355$ m, $\Delta Y = -112$ m, $\Delta Z = 411$ m (Ashkenazi et al, 1978a).

Table 6.I Co-ordinates for the Algonquin, Owens Valley, and Chilbolton radio telescopes

Antenna	Dish Dia. (m)	Type of mount	Intersect axes?	Atomic frequency standard	Observing frequency and bandwidth	
					May 1977	January 1978
Algonquin	46	Altitude/ azimuth	Yes	Hewlett-Packard H-10A hydrogen maser	10.68 GHz bandwidth ≃ 4 MHz	10.66 GHz bandwidth ≃ 4 MHz
Chilbolton	25	Altitude/ azimuth	No (offset = 0.306 m)			
Owens Valley	40	Altitude/ azimuth	Yes	NASA/GSFC* NP-3 hydrogen maser		

Table 6.II Brief summary of the antenna and receiver characteristics at the Algonquin, Chilbolton and Owens Valley antennae

Observing Session	Source of data	Observation Epoch		Polar Motion Components		UT1-UTC correction
		Date	Day Number	x (")	y (")	
13-16 May 1977	BIH Rapport Annuel	1 May	121	-0.181	0.454	0.3086
		6 May	126	-0.167	0.467	0.2927
		11 May	131	-0.152	0.478	0.2271
		16 May	136	-0.135	0.487	0.2619
		21 May	141	-0.117	0.494	0.2472
		26 May	146	-0.097	0.499	0.2332
17-20 January 1978	BIH Circular D	6 Jan	6	0.003	0.015	0.6334
		11 Jan	11	-0.016	0.018	0.6177
		16 Jan	16	-0.035	0.023	0.6021
		21 Jan	21	-0.053	0.030	0.5868
		26 Jan	26	-0.071	0.038	0.5716
		31 Jan	31	-0.090	0.049	0.5561

Table 6.III Earth orientation data for the experiments of May 1977 and January 1978

clock was synchronised using received Loran-C signals and/or a travelling clock (see §4.4).

The observed data was provided in the form described in §5.2.2 and Appendix G.2. Each observing period has further data associated with it, namely the x and y components of polar motion and the UT1-UTC differences at 5-day intervals to either side of the observing period, the nominal observing frequency, the observed sources, and the observed meteorological data. The epochs and the values of the Earth orientation parameters, as obtained from the BIH Circular D for January 1978 and the BIH Rapport Annuel for May 1977, are given in Table 6.III, the 'day number' representing the day of the calendar year. The nominal observing frequency is given in Table 6.II and the observed sources for each of the experiments together with the a priori source co-ordinates and the source of reference from which these values were obtained are given in Table 6.IV. The meteorological data for each antenna was either observed at the station itself or obtained locally. The form of the observed data and the location of the meteorological station relative to the particular antenna is given for the three stations in Table 6.V.

There were few problems affecting the quality of the data which cannot be allowed for using the data filtering techniques and mathematical model previously described. However, during the May 1977 observations the station clock at ARO was reset at 19.11 on 14th May due to poor stability before this time. Consequently, two clock error model polynomials must be formed for baselines incorporating this station during the May 1977 observations. Also, during the January 1978 experiments, observations made prior to 22.00 UT on 18th January were faulty due to a problem at the Chilbolton Observatory.

Source Name	Source co-ordinates		Observing Session		Source of Reference
	Right ascension (h-m-s)	Declination (d-m-s)	13-16 May 1977	17-20 January 1978	
3C273B	12-26-33.248	2-19-43.273	x	x	Clark et al, 1976
3C345	16-41-17.61	39-54-10.83	x	x	Clark et al, 1976
0J287	8-51-57.252	20-17-58.36	x	x	Clark et al, 1976
BL-LAC	22-00-39.362	42-02-08.69	x	x	
4C39.25	9-23-55.32	39-15-23.57	x		Clark et al, 1976
NRA015Ø	3-55-45.262	50-49-20.27	x	x	Clark et al, 1976
3C446	22-23-11.00	-5-12-17.00		x	Appleton Lab. (personal communication)
0235+16	2-35-52.50	16-24-14.00 OA		x	

Table 6.IV Observing frequency and the observed source co-ordinates for the observing sessions of May 1977 and January 1978 (these co-ordinates include the E-terms of elliptical aberration)

Antenna	Location of met. observations	Position relative to antenna	Observed data supplied
Algonquin	on-site	on-site	Relative humidity and temperature (^{o}C) at observation site and pressure (mb) corrected to antenna reference point.
Chilbolton	RAF met. station at Boscombe Down	12 mls (19 km) W of Chilbolton	
Owens Valley	Bishop Municipal Airport	10.4 mls (16.7 km) NNW of OVRO	

Table 6.V Summary of location of observation and form of observed meteorological data

6.2 VLBI OBSERVATIONS ON THE HAYSTACK-GOLDSTONE BASELINE

A series of VLBI experiments was carried out between April 1972 and January 1975, involving five widely spaced radio telescopes at Haystack (Massachusetts), Goldstone (California), Gilmore Creek (Alaska), Onsala (Sweden), and Green Bank (West Virginia) (Shapiro et al, 1974 and Robertson, 1975). The project was sponsored by three United States organisations, namely the National Science Foundation, the Advanced Research Projects Agency of the Department of Defense, and the United States Geological Survey. The NRAO Mk I interferometer system was used, including the bandwidth synthesis technique (§4.3.3), in order to derive observations of group delay and delay rate.

The data supplied for this study was that from the experiment of August 29th-30th, 1972, over the single baseline between the NRAO telescope at Haystack, Westford, Massachusetts, and the Jet Propulsion Laboratory (JPL) 'MARS' antenna at Goldstone, Mojave, California. The positions of the antennae and the baseline are shown in the diagram, Fig. 6.I. The antenna and receiver characteristics for each antenna, including the details of the bandwidth synthesis technique used, are tabulated in Table 6.VI. This particular experiment was designed with the intention of measuring the baseline length as well as for studying the source structure and consequently the observing program was organised in such a manner as to obtain an accurate baseline determination (unlike the Canadian experiments (§6.1) where the geodetic information is a spin-off from the main experiment objective of studying the source properties). This involved observing ten different sources with a good scattering of declinations in order to be able to compute the polar baseline component (the z component) with reasonable accuracy. No source above 40^{o} declination was observed because, at this time, none

	Observatory	
	Haystack	Goldstone
Dish diameter	120'	210'
Mount	Altitude-azimuth with intersecting axes	Altitude-azimuth with intersecting axes
Centre frequency of recorded signal	7.85 GHz	
Recorder bandwidth	360 kHz	
Synthesized bandwidth	23 MHz	

Table 6.VI Brief summary of the receiver and antenna characteristics for the Haystack and Goldstone Observatories, August 29-30th 1972

was known. The 192 observations were organised such that about three sources were observed in rapid succession, generally by taking three observations on one source and then moving on to the next. This process rotated such that each source was observed over a wide range of hour angles so as to give a balanced solution (see the specimen data in Appendix G.1).

The co-ordinates of the telescope reference points (see §2.2.1) are given in Table 6.VII. This table gives the spheroidal co-ordinates (geodetic latitude, ϕ, and longitude, λ, and the spheroidal height, N+h) of the reference point of each antenna on the appropriate national geodetic datum, in this case North American Datum 1927 (NAD 27), together with the semi-major axis and eccentricity defining the datum. From these values, the cartesian co-ordinates relative to a system defined by NAD 27 are computed and these co-ordinates are translated into the geocentric Average Terrestrial system (§2.1.2.1) using the translation parameters given. These cartesian co-ordinates in the Average Terrestrial system are used as the a priori approximate co-ordinates in the adjustment process, for which purpose any inaccuracy in the translation parameters is not critical. A description of the method employed and accuracies achieved in defining the antennae reference points is to be found in §6.5.1.

The observed data was input to the program in the form described in §4.3, §5.2 and Appendix G.1. The x and y components of polar motion and the UT1-UTC corrections at 5-day intervals for the period spanning the observations were obtained from the BIH Rapport Annuel, 1972, and are tabulated in Table 6.VIII where the 'day number' represents the day of the calendar year. The nominal observing frequency is given in Table 6.VI and the observed sources, their a priori co-ordinates, the references from which these co-ordinates were

		Antenna	
		Haystack	Goldstone
Spheroidal co-ordinates* on the national datum	ϕ	$42^{o}37'23.506"N$	$35^{o}25'33.340"N$
	λ	$71^{o}29'19.141"W$	$116^{o}53'19.150"W$
	N+h	145.34 m	1008.92 m
Cartesian co-ordinates relative to national datum (from 2.1)	X	1492417.47	-2353606.72
	Y	14457431.11	-4641490.31
	Z	4296691.78	3676870.17
Cartesian co-ordinates$^{\neq}$ relative to Average Terrestrial System	X	1492386.45	-2353618.20
	Y	-4457281.80	-4641484.49
	Z	4296866.78	3677045.17

* The national datum is NAD27 based on the Clarke 1866 ellipsoid ($a = 6378206.4$, $e^2 = 0.006768658$).

$\neq$ These co-ordinates are derived by applying the translation parameters $\Delta X = -20$ m, $\Delta Y = 153$ m, $\Delta Z = 175$ m (Ashkenazi, 1979), to the previous co-ordinates and rotating this co-ordinate system 0.51" eastward.

Table 6.VII Haystack and Goldstone radio telescope co-ordinates

Source of data	Observation epoch		Polar Motion Components		UT1-UTC correction(s)
	Date	Day Number	x(")	y(")	
BIH Rapport Annuel, 1972	Aug 15	228	0.102	0.433	0.2441
	Aug 20	233	0.113	0.429	0.2311
	Aug 25	238	0.123	0.424	0.2182
	Aug 30	243	0.131	0.418	0.2059
	Sept 4	248	0.139	0.410	0.1933
	Sept 9	253	0.145	0.400	0.1796

Table 6.VIII Earth orientation data for the August 29-30th, 1972, Haystack-Goldstone observations

Source	Source Co-ordinates		Source of Reference
	Right Ascension (h-m-s)	Declination (d-m-s)	
3C273B	12-26-33.248	2-19-43.27	Hazard et al,1971 + Clark et al,1976
3C120	4-30-31.605	5-14-59.48	Clark et al, 1976
0J287	8-51-57.252	20-17-58.36	
4C39	9-23-55.320	39-15.23.57	
0Q208	14-04-45.616	28-41-29.23	
3C345	16-41-17.610	39-54-10.83	
2134+00	21-34-05.209	00-28-25.00	
VRO	22-00-39.365	42-02-08.55	
3C454.3	22-51-29.522	15-52-54.29	
3C279	12-53-35.833	-05-31-07.99	

Table 6.IX Source co-ordinates of the observed sources of the August 29-30th, 1972, Haystack-Goldstone observations (including the E-term of elliptic aberration)

obtained, , are given in Table 6.IX. Observed meteorological data was not available for this experiment, nor was information concerning the state of the ionosphere. However, a mean value for the atmospheric delay in the zenith direction due to the atmosphere was provided and has been used in the data analysis with suitable modifications, described in §7.2, to account for both the dry and wet refractive components. There are no errors or problems within the supplied data which cannot be accounted for using the standard model described in Chapter 2.

6.3 THE NAVY NAVIGATION SATELLITE SYSTEM (NNSS)

6.3.1 General Outline

The United States Navy Navigation Satellite System (NNSS), or Transit system, enables the position of an Earth-bound receiver to be established to an accuracy of less than 5 m from only a few days of observations of artificial satellites. The system works on the principle that a constant frequency radio signal emitted from an orbiting satellite will be received on Earth as a continually changing frequency due to the Doppler frequency shift generated by the relative motion of the receiver and satellite. The Doppler shifted frequency can be measured and, knowing the position of the satellite on its orbit, the location of the receiver on the Earth can be computed. The basic theory of satellite-Doppler positioning is outlined in §6.3.2.

The initial concept was developed around 1957 by Guier and Weiffenbach in order to determine the positions of orbiting satellites by observing the Doppler shift of the satellite radio transmissions from several known locations. Dr F.T. McLure of the Applied Physics Laboratory at John Hopkins University, the developers of the present system, suggested that this method could be reversed and hence, knowing

the orbit of the satellite, the position of the Earth-based receiver could be computed. The first published description of such a system was by Guier and Weiffenbach in 1960. Between 1960 and 1967, the system was used on a limited military basis, primarily as a navigation and positioning aid for marine vessels, and then in 1967, the system was made available to non-military uses.

The present (1979) Transit system consists of five operational satellites in near circular polar orbits at nominal altitudes of 1100 km and with orbital periods of around 107 minutes. Each satellite emits two related frequencies, of approximately 400 MHz and 150 MHz, which are modulated in order to carry time signals and orbital parameters. From this orbital and time data, the satellite position at any epoch can be computed. This broadcast ephemeris (see §6.3.3.1) is determined from a combination of a geopotential model of the Earth together with data obtained by continual observations of the satellites by the four stations of OPNET (Operational Network) whose positions are assumed to be known. The individual predicted ephemerides computed at the NNSS Computing Centre are injected into each satellite memory every 12 hours, along with corrections to the rate and setting of the satellite clock.

Besides the broadcast ephemeris, the Topographic Center of the United States Defense Mapping Agency computes the 'precise ephemeris' (see §6.3.3.2) from data collected by the 21 stations of the worldwide Navy Tracking Network (TRANET). The Precise Ephemeris is post-computed and is hence more accurate than the predicted broadcast ephemeris. However, it is of more limited use as it is only computed for one or two satellites at any one time, is only available to certain users, and is provided only after a delay of several weeks.

There is a wide range of instruments and computing techniques available for satellite-Doppler positioning, the three main receiver

manufacturers being Magnavox, Canadian Marconi, and JMR. Several different data adjustment methods and corresponding computer software techniques are available extending from the standard single point positioning mode, accuracies of which are 2-5 m for the broadcast ephemeris and 1-2 m for the precise ephemeris, to the much more complex short arc adjustment techniques which establish, from observations from several stations, the relative receiver positions to sub-metre accuracy. This is obtained by allowing the orbital positions to move or 'relax' in the adjustment process. The progressive development of the receivers themselves, the adjustment techniques and software, and the methods of determining the satellite orbit from the geopotential model of the Earth and observed data, have enabled a continual improvement to be made in the accuracy and reliability of the system.

The user of the satellite-Doppler system is faced with the problem of relating absolute positions on either the broadcast or precise satellite reference system, neither of which is defined in the classical geodetic manner described in §2.1.2.1, to positions relative to conventionally defined geodetic data. Similarly, relative positions of satellite-Doppler stations are also subject to corrections, namely those of scale and orientation, in order to be referred to data based upon a conventional geodetic datum. The properties and definitions of the broadcast and precise reference systems are dealt with in §6.3.3.1 and §6.3.3.2 respectively, followed by the transformation from the Doppler system to a classical geodetic system in §6.3.3.3.

6.3.2 Basic Theory

This section gives an outline of the basic theory of satellite-Doppler positioning techniques without dealing with the different kinds

of satellite ephemerides (see §6.3.3) or with any adjustment method other than single point positioning. For a more complete discussion of the adjustment of raw satellite-Doppler data, see (Gough, 1978, Sykes, 1979, and Ashkenazi et al, 1977).

When a motorcycle, emitting a noise of constant pitch, passes a stationary observer, the pitch of the noise heard by the observer continually changes as the motorcycle approaches and passes him. This is a simple illustration of the received frequency being different from the emitted frequency due to the relative motion of the source and observer. This analogy of the motorcyclist and observer can clearly be extended to the case of a moving satellite and a stationary Earth-based receiver encountered in satellite-Doppler positioning. Without going into mathematical detail, a plot of frequency against time is shown in Fig. 6.II where

f_s = emitted satellite frequency,

f_r = received frequency,

c = velocity of propagation of microwaves in vacuo,

v = velocity of the satellite,

and $t(r_{min})$ = the time at which the source is closest to the receiver.

The satellite signal emitted at epoch t_1 arrives at the receiver at epoch $t_1 + \Delta t$, and is received at a frequency which differs from its emitted frequency according to the amount of the Doppler shift. Similarly, the satellite signal emitted at epoch t_2 arrives at the received at epoch $t_2 + \Delta t_2$. The received frequency, f_r is mixed with an internal receiver reference frequency, f_g, and a count of the number of cycles of the frequency $(f_g - f_r)$ received in a given time is made by the receiver. This Doppler count, N, illustrated in Fig. 6.II, is the basic observable of the satellite-Doppler system. The integrated

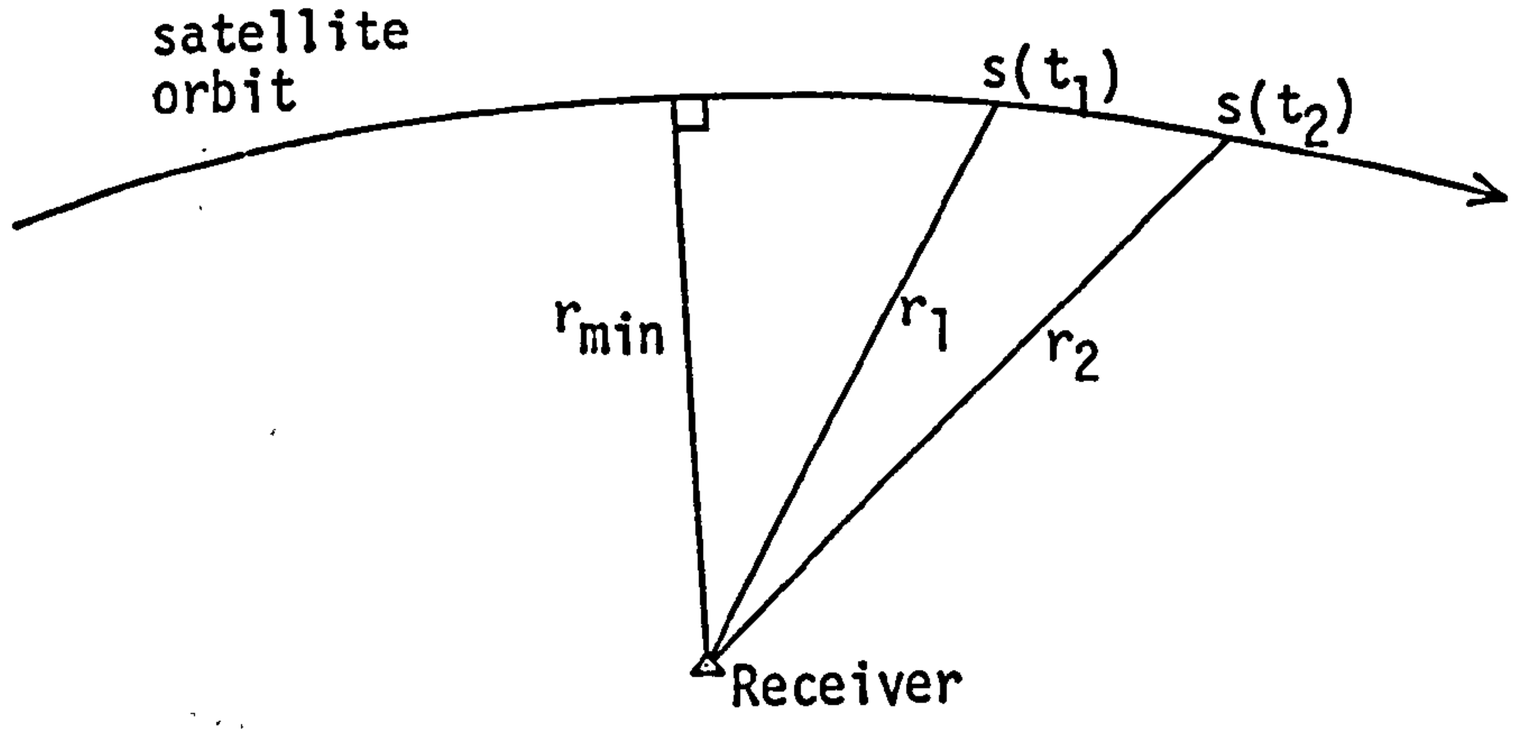

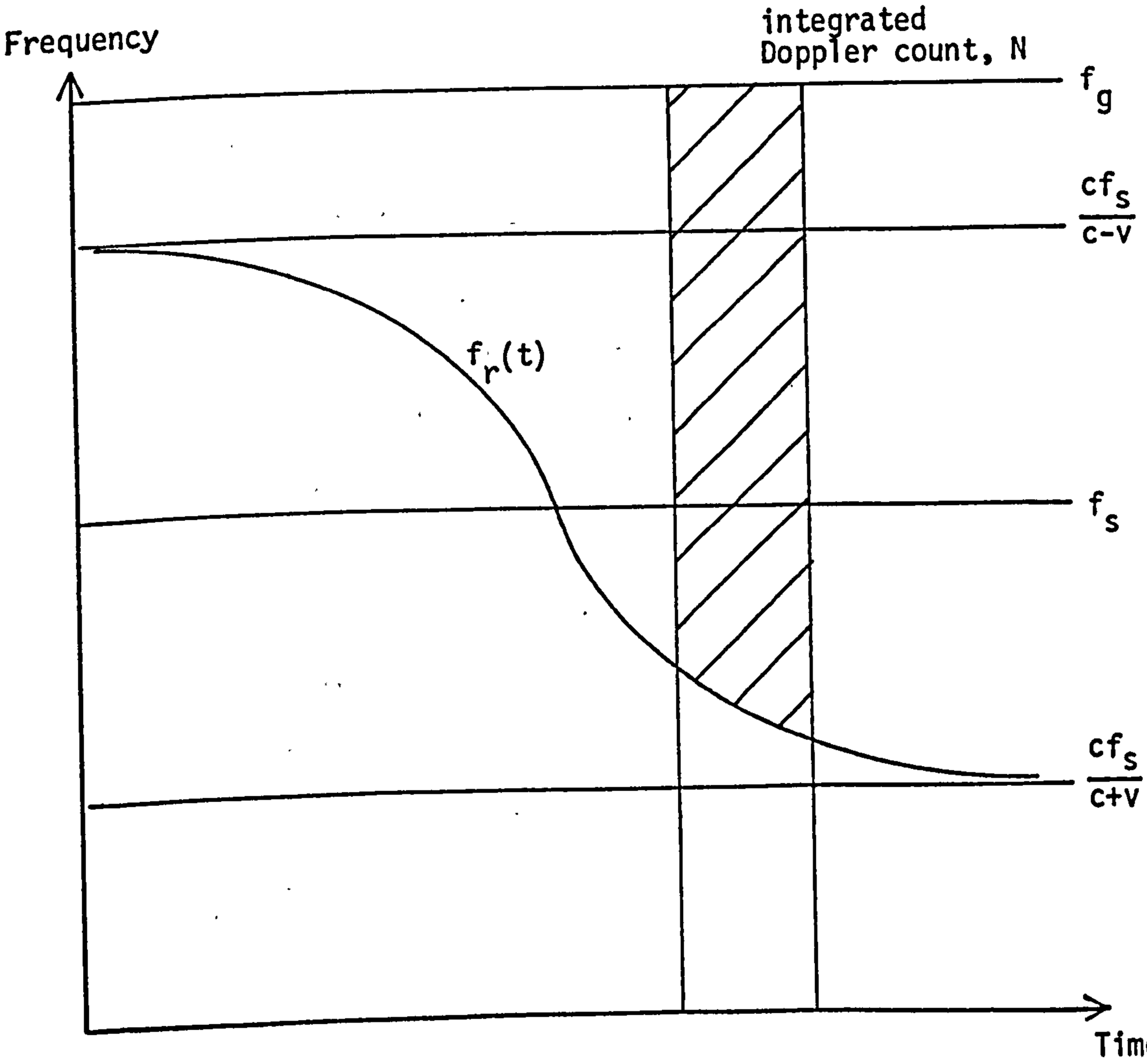

Fig. 6.II The Integrated Doppler Count

Doppler count recorded between epochs $t_1+\Delta t_1$ and $t_1+\Delta t_2$ is therefore given by:

$$N = \int_{t_1+\Delta t_1}^{t_2+\Delta t_2} (f_g - f_r)dt \ ,$$

which, neglecting relativity effects, becomes:

$$N = \int_{t_1+\Delta t_1}^{t_2+\Delta t_2} \left(f_g - f_s\left(1 - \frac{\dot{r}}{c}\right)\right)dt \ , \qquad (6.1)$$

where $\dot{r}$ = the rate of change of range to the satellite.

As $\Delta t_1 = r_1/c$ and $\Delta t_2 = r_2/c$, (6.1) becomes:

$$N = (f_g-f_s)(t_2-t_1) + f_g\left[\frac{r_2-r_1}{c}\right] \qquad (6.2)$$

This derivation is based on the satellite time framework, t being the time kept by the satellite. The modulated signal containing the broadcast ephemeris has a specific bit pattern which is recognised by the receiver and the Doppler counts are 'gated' accordingly. These counts are nominally 4.6 seconds (on the majority of receivers) with the satellite also emitting a time marker every two minutes. Alternatively, the receiver can observe the Doppler counts in the local time framework such that:

$$N = \int_{\tau_1}^{\tau_2} (f_g-f_r)d\tau \ ,$$

where τ is the time as kept at the receiver. This yields the equivalent equation to (6.2) as:

$$N = (f_g-f_s)(\tau_2-\tau_1) + f_s\left[\frac{r_2-r_1}{c}\right] \qquad (6.3)$$

From both (6.2) and (6.3), if f_g, f_s, c, and $(\tau_2-\tau_1)$ or (t_2-t_1), are known, then each observation of N yields an equation in which the only

unknown is the range difference (r_2-r_1). (A slightly different principle is used in the TRANET receivers (see §6.3.3.2), where a set number of Doppler counts is observed and the time interval required to obtain this number of counts is the measurable quantity.) This implied measurement of (r_2-r_1) is used to obtain a solution for the co-ordinates of the receiver (see later). However, the observed raw Doppler counts must first be reduced by the application of corrections for both ionospheric and tropospheric refraction.

A first order ionospheric refraction correction is performed by use of the dual frequency measurement capability of the Doppler system. The ionospheric refraction (see §2.4.6) is frequency dependent and therefore the Doppler counts of the nominally 400 MHz and 150 MHz frequency signals can be combined to give a correction which has an unmodelled effect of generally less than 1% of the total correction (Wells, 1974). This correction can be performed either by the receiver itself (e.g. the JMR-1 performs it automatically within the instrument) or may require application in the preprocessing software, as is the case for the CMA-722B receiver which outputs the raw Doppler count data from both 400 and 150 MHz channels. The effect of the troposphere (see §2.4.5) is to retard the signal and to cause a bending of the path through the atmosphere. Many models exist to correct for this effect on the observed Doppler counts, that of Hopfield described in Appendix D.3 being one of the most popular. Other less significant corrections, for example relativity and the modelling of satellite and receiver frequency drifts during the observations, may be applied. It is also common practice to accumulate the basic 4.6 second Doppler counts into longer period counts (for '30 second' Doppler counts, the 26 4.6 second counts observed in a 2 minute period are accumulated into only four

counts, consisting of 6, 7, 6, and 7 4.6 second periods). This accumulation process eases the data handling problems whilst still maintaining the same accuracy standards obtainable with the shorter interval counts (Ashkenazi, McLintock, and Sykes, 1978).

As previously mentioned, each individual observation is a measure of the range difference (r_2-r_1), as given in (6.2) and (6.3). Consequently, knowing the position of the satellite at the start and finish epochs of each Doppler count from the information contained in the broadcast ephemeris or by the use of the precise ephemeris, the position of the receiver can be computed by a 'variation of co-ordinates' adjustment as described in §3.2.1. In this single point positioning mode of adjustment, the frequency difference between the ground reference and satellite frequencies is also an unknown in the adjustment. More complex models may also solve for further unknowns, for example tropospheric bias parameters and the co-ordinates of the satellite itself.

The volume of data required to provide an adequate solution and the time needed to collect this data are dependent on the required accuracy and the position of the ground station. Each acceptable satellite pass will generally consist of 10-18 minutes of data and, as the satellites are in polar orbits, there are more observable satellite passes in high latitudes than there are in equatorial regions. Also, when using the precise ephemeris, only the one or two satellites for which the ephemeris is computed are of interest. The potential accuracies of the different observing and adjustment modes, together with the amount of data required for each, are discussed in (Sykes, 1979).

6.3.3 Ephemerides, Co-ordinate Reference Systems, and Transformations

6.3.3.1 Broadcast Ephemeris

The broadcast ephemeris is emitted from the satellite in terms of coded message words contained in the modulated satellite signal. It is given in terms of an approximate precessing orbital ellipse and corrections to that ellipse. The satellite positions defined by this information have a positional accuracy of 19, 15, and 9 metres in the along track, across track, and radial directions respectively (Arur, 1977).

The broadcast ephemeris for each satellite is predicted from observations made at four tracking stations in the USA (Maine, Minnesota, Hawaii, and California) comprising the Operational Network (OPNET). The predicted ephemeris, generally computed from the previous 36 hours of data, is injected into the satellite every 12 hours along with timing information to regulate and reset the satellite clock. The majority of the error in the broadcast ephemeris is simply due to the inaccuracy in predicting certain geophysical and astronomical effects. The major error sources are radiation pressure and drag on the orbiting satellite, inaccuracies in the geopotential model used, the prediction of UT1 and polar motion (see Appendix A.4 and §2.2.2), and instabilities in the satellite oscillator. The first effect causes the large along track error in the ephemeris mentioned previously and hence it is desirable to have a well balanced set of passes contributing to the solution (i.e. equal numbers of north going and south going passes and an equal east-west distribution).

The geopotential models and co-ordinate reference systems employed in the computation of the broadcast ephemeris have been in a constant state of imporvement since the system was developed (Sykes, 1979). It is beyond the scope of this work to go into the history of this

development but it is necessary to describe the present system.

In 1975, the WGS 72 model of the gravity field (Seppelin, 1974) was introduced for the computation of the broadcast ephemeris and has been maintained to the present day. The spherical harmonic expansion of this model contains a set of terms up to and including order 27. The co-ordinate reference system used is named NWL-10D and is defined by the adoption of a set of co-ordinates for the four OPNET tracking stations. The scale of the system is defined by the value of the Earth's gravitational constant, GM, of 398600.8 km^2/sec^3 (Seppelin, 1974). Two further points are also worthy of note. In the computation of the satellite co-ordinates from the ephemeris, it is necessary to use a value for the Earth's rate of rotation relative to the true equinox of $0.7292115855 \times 10^{-4}$ rads/sec. Furthermore, in order to maintain internal consistency with the ephemeris system, the velocity of the propagation of the signal should be taken as 299792500.0 m/sec.

6.3.3.2 Precise Ephemeris

The precise ephemeris for a satellite is computed from observations of the satellite orbit at 13 permanent stations, 4 mobile stations, and the 4 OPNET stations, which together comprise the worldwide TRANET (Navy Tracking Network). It is a post-computed ephemeris and hence is more accurate but of more limited use than the broadcast ephemeris. It is also only available to 'bona fide" users. The cartesian co-ordinates of the satellite on the precise ephemeris system, together with the satellite velocity components along the directions of these axes, are given to the user for each UTC minute for the periods of visibility of the satellite from the ground station. The positional

accuracy of the precise ephemeris is about 2 m in each co-ordinate (Arur, 1977).

Between January 1st, 1973 and June 15th, 1977, the NWL-9D co-ordinate reference system was used for the precise ephemeris whilst the NWL-10E model of the Earth's geopotential was used. Since June 15th, 1977, the precise ephemeris has been based on the NSWC 9Z-2 co-ordinate system and the NSWC 10E-1 geopotential model. This change did not noticeably affect users of the precise ephemeris. The scale of the ephemeris is defined by the value of the Earth's gravitational constant of 398601.0 km^3/sec^2, different from that used for the broadcast ephemeris, whereas the values used for the rate of rotation of the Earth and the velocity of light are the same as those used for the broadcast ephemeris.

6.3.3.3 Transformation between Doppler and a Classical Geodetic System

In order to make use of Doppler results, a consistent co-ordinate system must be established. Unfortunately, there are two separate Doppler systems based on which the position of a ground station will possess different co-ordinates. Discrepancies between positions determined on the two systems arise from the way in which each of the systems is defined. In particular, different ephemeris co-ordinate systems, geopotential models, and values for the Earth's gravitational constant, GM, are used. Furthermore, different Earth orientation values are used in the two systems. Firstly, the broadcast ephemeris timing is relative to UT1 whereas that for the precise ephemeris is relative to UTC (see Appendix A.4), and secondly, there is likely to be a difference between the predicted pole position and the post-computed pole position due to the great difficulty in predicting polar movement.

Due to these differences between the two ephemerides, it is

recommended (Sykes, 1979) that co-ordinates derived in the broadcast system should be transformed into the precise system before conversion to conventional geodetic co-ordinates. The required transformation is detailed in (Ashkenazi et al, 1978a).

Neither the broadcast or precise co-ordinate system is a classical geodetic system of the type described in §2.1.2.1 (i.e. based on the CIO pole and BIH zero longitude). Consequently, in order to convert co-ordinates defined in the precise ephemeris system into classical geodetic co-ordinates, certain transformations must be applied. Early comparisons of Doppler results, computed using the precise ephemeris system, with the BC-4 world satellite triangulation network (Anderle, 1974) and with the high accuracy traverses in the United States (Anderle, 1976) showed the Doppler system to be too large in scale by about 1 ppm ± 0.2 ppm relative to the other systems. It has been suggested (Hothem etal, 1978) that part of this apparent scale error was due to an incorrect Doppler position fix at a key station in the whole Doppler network. This station at the Goldstone DSN*/VLBI site in California, originally occupied in June 1972, was reoccupied in late 1976. It was found that the position derived from the earlier observations was too high by 4 m which would account for an apparent scale discrepancy of about +0.6 ppm in the system.

The NSWC 9Z-2 precise Doppler co-ordinate system can be expected to be too large by 0.38 ppm for two reasons (Anderle, 1976). Firstly, the scale of the system is defined by the gravitational constant, GM, of 398601 $km^3\ s^{-2}$ rather than the currently quoted best value of 398600.5 $km^3\ s^{-2}$ (IAU, 1977) and secondly, the satellite ephemeris is referenced to the position of the centre of gravity of the satellite

---

* DSN - Deep Space Network.

rather than to the electrical centre which is situated approximately 1 m nearer the Earth. Recent comparisons of Doppler derived positions with other space systems (Strange and Hothem, 1978) have indeed shown a scale discrepancy of +0.4 ± 0.1 ppm while (Langley et al, 1979) achieved similar results.

The precise Doppler co-ordinate system also requires a longitude rotation in order to make it agree with the mean Greenwich meridian as defined by the BIH. Comparisons of Doppler measurements with gravimetric deflections at stations in the United States indicated that the Doppler derived positions needed rotating 0.26" eastward in order to agree with the origin of longitude in the USA. Unfortunately, this was initially misunderstood as being the correction necessary to relate the Doppler positions to the BIH zero longitude (Strange and Hothem, 1978). The BIH zero longitude is in fact 0.51" east of the origin of longitude in the USA and hence it would be expected that longitudes derived in the precise Doppler system should be corrected by 0.77" eastward in order to relate them to the BIH zero longitude. Comparisons with other space systems have yielded values of, for example, 0.8" ± 0.05" (Strange and Hothem, 1978) and 0.89" ± 0.01" (Langley et al, 1979).

The application of these scale and longitude corrections should refer the Doppler derived positions to a classically defined geodetic reference system. It remains then to simply apply the relevant transformation parameters (Ashkenazi et al, 1978) in order to relate the geocentric Doppler system to any other defined datum.

6.4 ALGONQUIN-CHILBOLTON-OWENS VALLEY DOPPLER EXPERIMENTS

6.4.1 Chilbolton and Barton Stacey Site Survey

In April 1977, the Ordnance Survey of Great Britain (OSGB) carried out a series of observations at the Chilbolton Observatory. The purpose of this exercise was to connect both the reference point of the Chilbolton radio telescope (see §2.2.1), and a triangulation pillar, the Chilbolton North Pillar, to the OSGB 70(SN) triangulation network. Chilbolton North Pillar stands approximately 64 metres from the radio telescope and was to be used for the location of the satellite-Doppler antenna in the joint VLBI/Doppler experiments. At the same time, the aerial bolt hole at the TRANET Doppler station (§6.3.2) at nearby Barton Stacey was also connected to the network and to the Chilbolton antenna.

The Chilbolton Observatory site was connected to the triangulation by observations from and to second order triangulation stations in the area. This entailed establishing a station outside the Observatory compound and employing a 10 feet high tripod above the point. Having connected the site to the triangulation in this way, a local network was established between this station, two further pillars within the Observatory compound, and the axes of the radio telescope itself. The azimuth axis of the telescope was located by plumbing and a permanent mark was made in the basement, as illustrated in Fig. 6.III. For observations to this position, a tripod and reflector were centred over the mark and viewed through the main double doors in the telescope base. For observations of the altitude axis, an apparatus was made consisting of a steel bar which fitted rigidly into the end of the axis, and upon which was mounted a reflector. In order to ensure that the reflector was mounted precisely on the line of the axis, the reflector could be

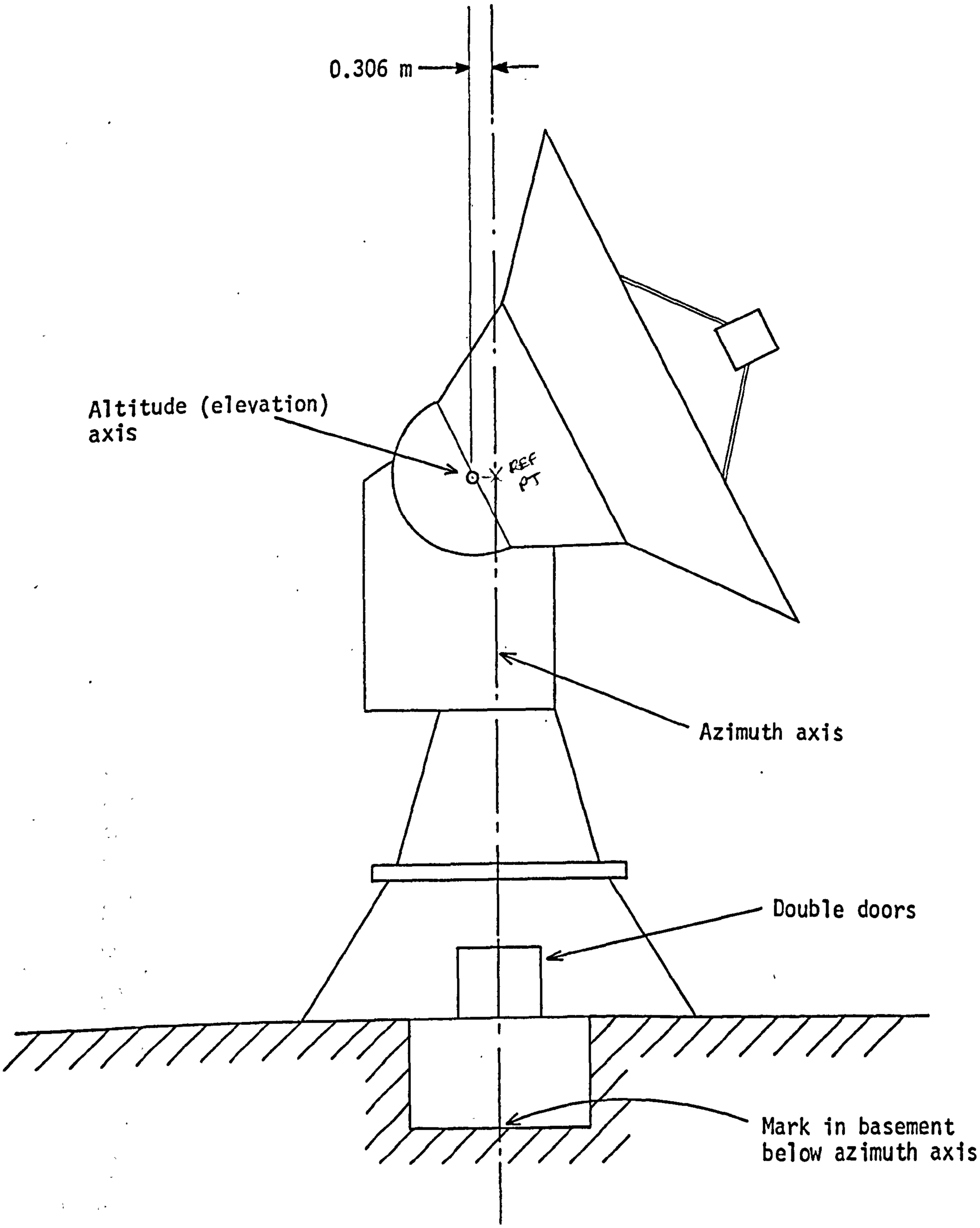

Fig. 6.III The Chilbolton Radio Telescope

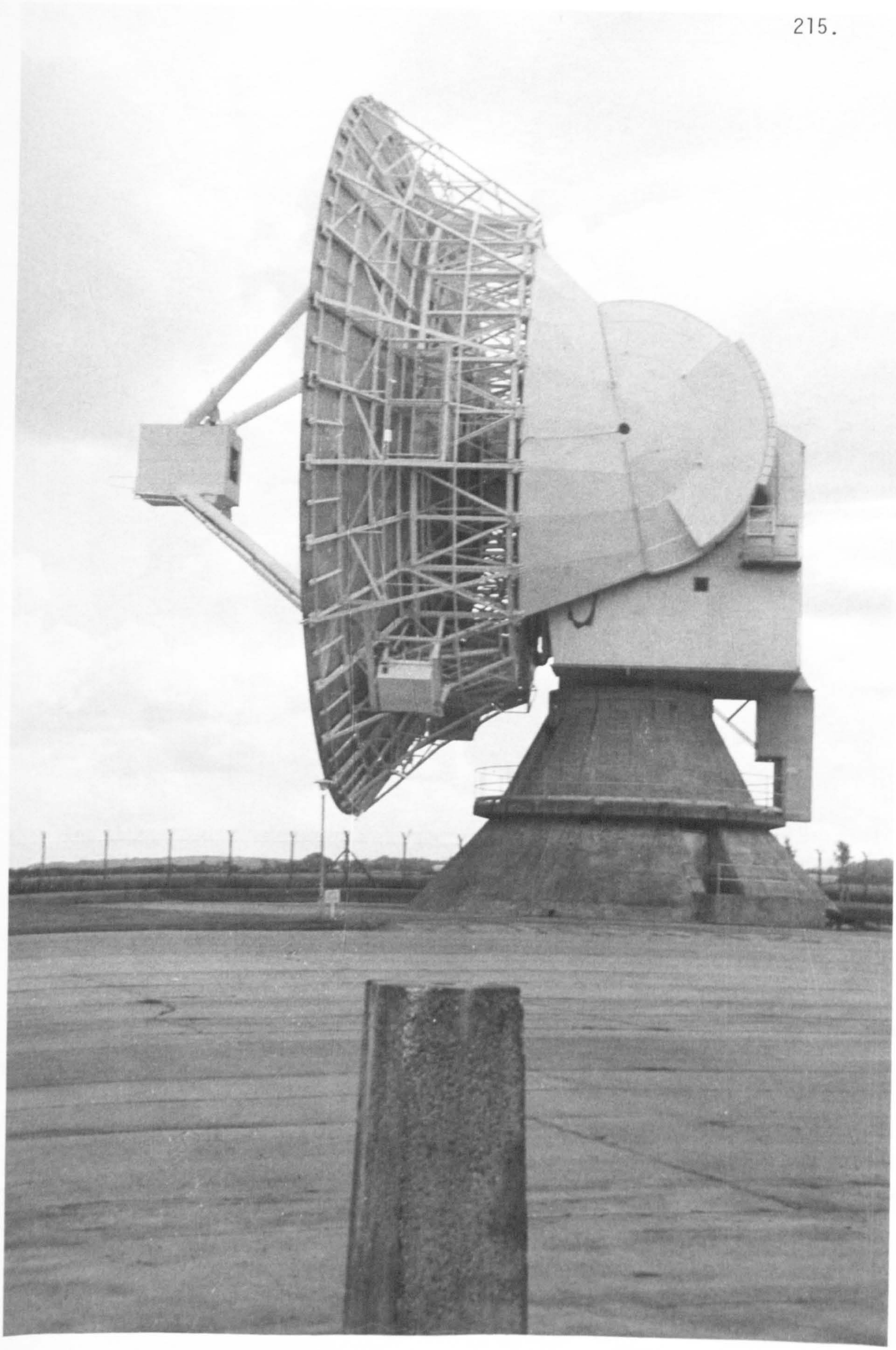

Plate 6.I Chilbolton North Pillar and Radio Telescope

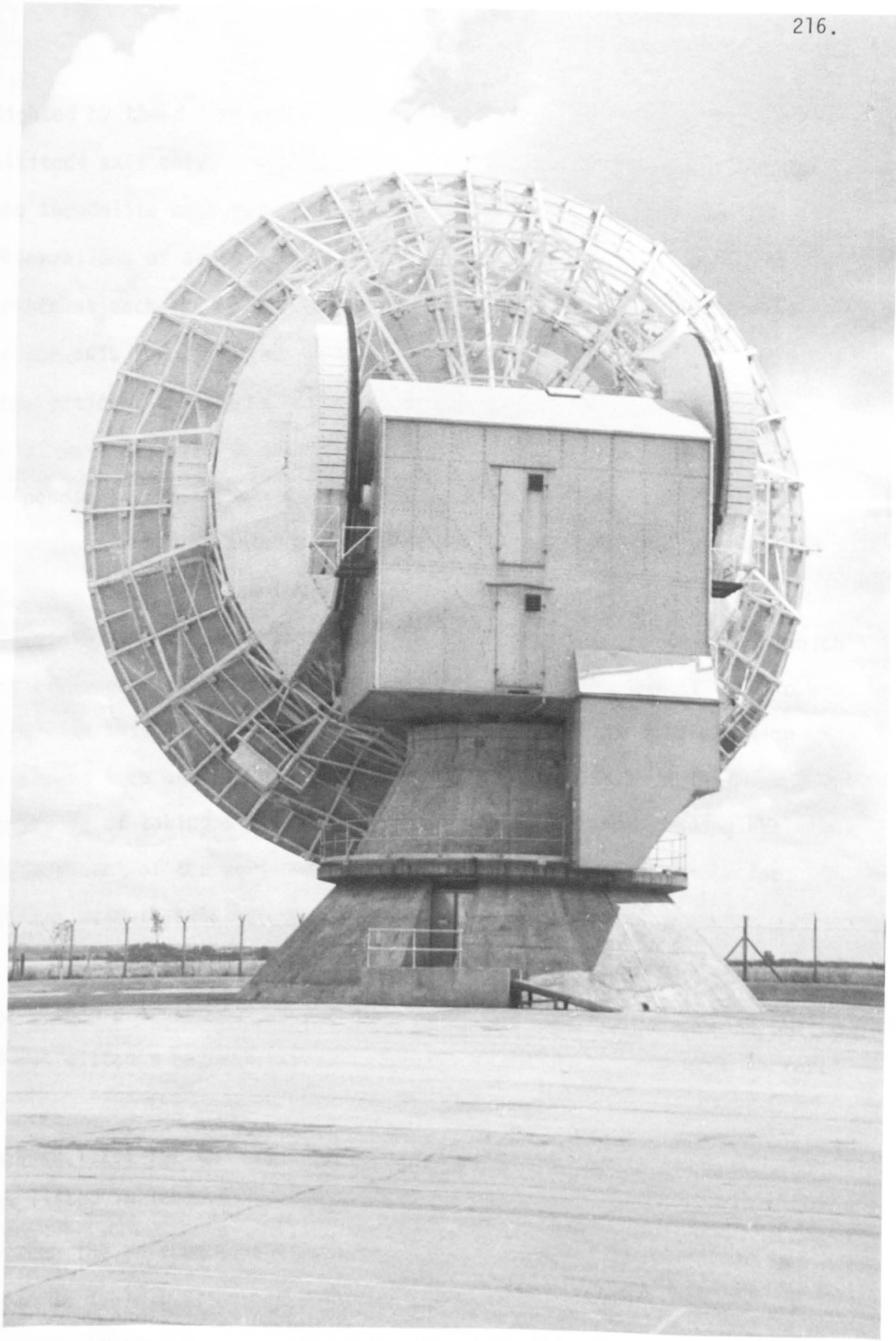

Plate 6.II Chilbolton Radio Telescope

sighted by theodolite while the telescope was rotated about the altitude axis only. Any movement of the reflector as viewed through the theodolite necessitated adjustment of the reflector on the bar. Observations of distance and both horizontal and vertical angles to points at each end of the axis established the positions of the ends of the axis for different azimuth directions of the antenna. These observations, combined with those to the targets below the azimuth axis, were adjusted to give the offset of the two axes in a plane perpendicular to the altitude axis (see §2.4.1), the OSGB (70)SN co-ordinates of the antenna reference point (the point of intersection of the azimuth axis and the plane perpendicular to the azimuth axis containing the altitude axis) and the angle from the horizontal in which the altitude axis rotates. The vertical angle measurements used to establish this latter value yielded an accuracy in its determination of around 1 cm and hence a further method was developed. This consisted of taking a theodolite into the telescope and reading the dislevelment of the vertical bubble against the vertical circle for various azimuth settings of the telescope (Eady, 1979).

These methods established that the plane of rotation of the axis was within 6 arcseconds of the horizontal and that the perpendicular offset distance between the two axes was 0.306 metres (Ordnance Survey, 1977). The OSGB 70(SN) spheroidal and cartesian co-ordinates (see §2.1.2.1 for the conversion formula) for the North Pillar are listed in Table 6.X. The offset vector between the reference point of the telescope and the North Pillar is given in Table 6.XI. The relative positions of these two points are shown in Plate 6.I.

At the same time that the Chilbolton telescope was connected into the national triangulation, the local observed network was extended

to incorporate the TRANET Doppler antenna location at Barton Stacey, approximately 6 km from Chilbolton. This simply involved establishing a station about 100 m from the TRANET antenna and then taking bearing and distance observations to the reference position. Fig. 6.IV is a diagram showing the TRANET aerial, its electrical centre, and the surveyed point. This network connection was performed in order to ensure accurate relative positions of the Chilbolton stations and the Barton Stacey Doppler site. The use of previously derived co-ordinates for Barton Stacey might not have provided good relative accuracy due to the separate observing sessions and the use of different connection stations to the Ordnance Survey triangulation. The geographical and grid co-ordinates of the Barton Stacey aerial are given in Table 6.X and the offset of this point from the Chilbolton radio telescope reference point is given in Table 6.XI.

6.4.2 Chilbolton Doppler Observations

Between the 9th and 15th May 1977, satellite-Doppler observations were made at the Chilbolton Observatory concurrently with VLBI observations being made there and at other locations. The Doppler station at the Chilbolton Observatory site was a triangulation station, known as the Chilbolton North Pillar, which had been surveyed during the observations described in the previous section. This station was not occupied during the January 1978 VLBI experiments. For the May 1977 experiments the Doppler receiver was operated jointly by the University of Nottingham and the Ordnance Survey of Great Britain. The receiver used was a Canadian Marconi CMA 722B, owned by the University of Nottingham, interfaced to an 8-track punched paper tape recorder, and powered by mains electricity. Meteorological data was continuously

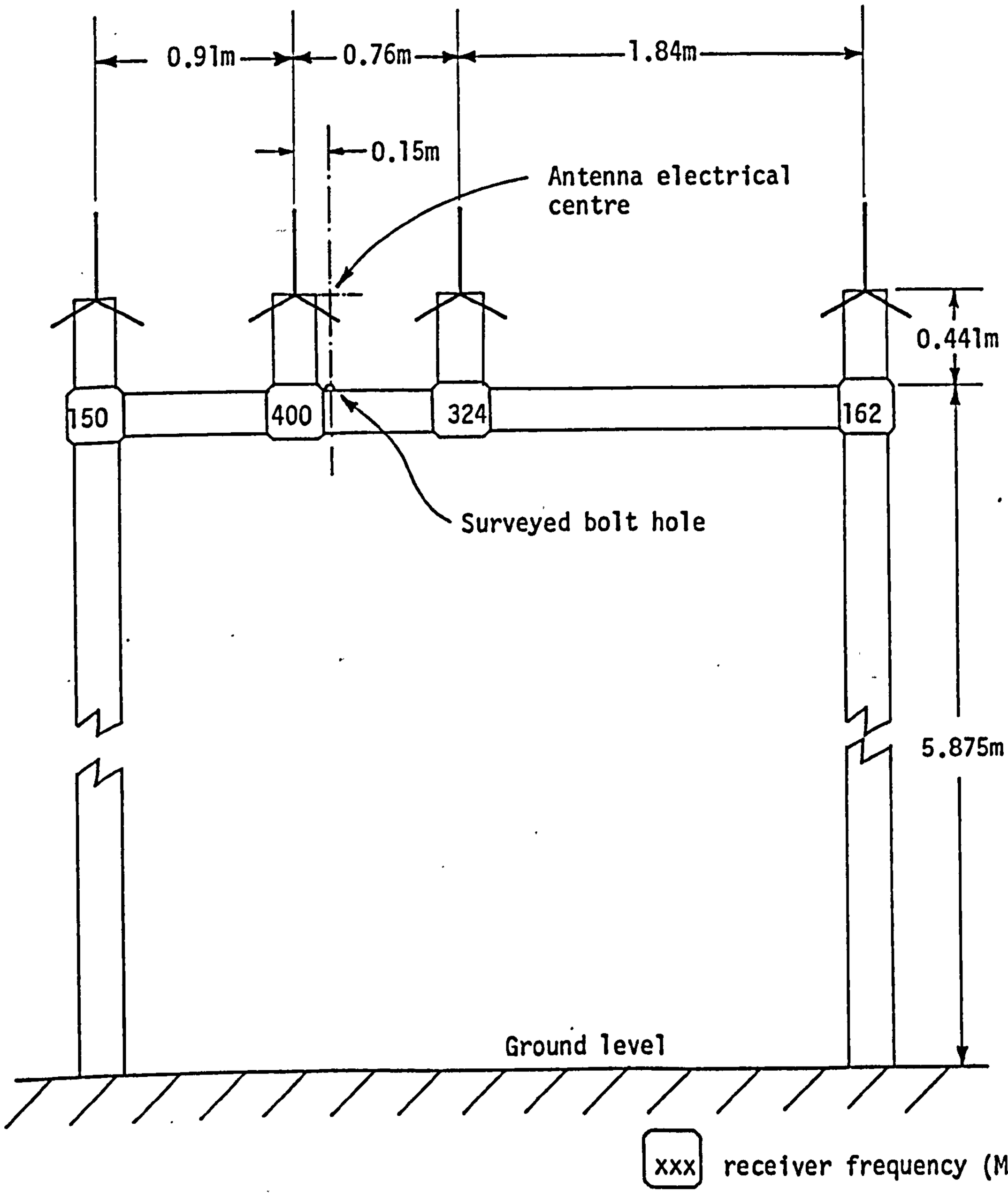

Fig. 6.IV Barton Stacey TRANET aerial

Antenna Location	Doppler Station	ϕ	λ	height (m)	Datum
Algonquin	683100A	45°57'21.260"N	78°04'18.061"W	235.34 above m.s.l.	NAD 27, Clarke's 1866 ellipsoid
	TELE N	45°57'20.731"N	78°04'15.793"W	231.85 above m.s.l.	
	TELE S	45°57'20.598"N	78°04'15.819"W	231.88 above m.s.l.	
Owens Valley	52105 BP ARIES I	37°13'50.640"N	118°16'55.544"W	1208.59 above m.s.l.	
Chilbolton	Chilbolton North Pillar	51°08'41.302"N	1°26'15.662"W	85.42 above spheroid (Cartesians: X = 4007900.17, Y = -100588.61, Z = 4943371.59)	OSGB 70 (SN), Airy's ellipsoid
	Barton Stacey 116 TRANET bolt hole	51°11'02-600"N	1°22'47.209"W	78.82 above spheroid (Cartesians: X = 4004595.66, Y = -96456.15, Z = 4946104.39)	

Table 6.X Co-ordinates of Doppler stations as determined from ground surveys

Antenna Location	Doppler Station	Δx(m)	Δy(m)	Δz(m)	Survey Organisation
Algonquin	683100A Tel.Ref. A	92.67	70.22	13.67	Geodetic Survey of Canada
	TELE N	142.39	71.21	-0.83	
	TELE S	142.45	68.19	-3.65	
Chilbolton	Chilbolton North Pillar	-40.514	-48.767	12.449	Ordnance Survey of Great Britain
	Barton Stacey 116 TRANET	-3345.026	4083.687	2745.242	
Owens Valley	52105 BP ARIES 1	-43.286	-19.206	-79.151	U.S. National Geodetic Survey
Haystack	51118	5.18	-23.83	-62.53	
Goldstone	51065	224.68	-167.33	-126.59	

(ARO, CH, and OVRO are taken from (Langley, 1979), Haystack and Goldstone are taken from (Strange et al, 1978))

Table 6.XI Components of the offset vector between the Doppler and antennae reference points (Doppler position - offset vector = antenna reference point position)

recorded at a point adjacent to the pillar upon which the Doppler antenna was mounted. At this time there were five observable satellites but, as the precise ephemeris was to be used for the data analysis, priority was given to observations of the two satellites for which this ephemeris was available, namely satellites 30190 and 30200. The general procedure and techniques for setting up and operating a Doppler receiver are well documented and therefore will not be dealt with here (see Ashkenazi et al, 1978b and Gough, 1978).

The data processing was performed by Jan Kouba of the Earth Physics Branch of the Department of Energy, Mines and Resources, Canada, using the GEODOP computer program (Kouba and Boal, 1976) and also by the University of Nottingham.

6.4.3 Barton Stacey, Algonquin and Owens Valley Doppler Observations

During both the May 1977 and January 1978 VLBI experiments (see §6.1) the TRANET station at Barton Stacey, Hampshire, was continually observing the transits of Doppler satellites as part of its role in the worldwide TRANET network. As described in §6.4.1, the position of the aerial had previously been positioned with respect to the radio telescope reference point at the Chilbolton Observatory. Table 6.X gives the co-ordinates of this point as determined by that survey relative to Ordnance Survey datum, as well as the co-ordinates of the other three stations at Algonquin, Owens Valley, and Chilbolton. Similarly, Table 6.XI gives the offsets of all the relevant Doppler reference points with respect to the reference points (see §2.2.1) of the three radio telescopes.

At the Radio Observatory, Algonquin Park, Canada, a survey by the Geodetic Survey of Canada during 1977 established the positions of six

triangulation stations in the vicinity of the dish, including the telescope reference point itself. Three of these stations were used during the two observing campaigns. The May 1977 observations were made from station 683100A (telescope reference A) using a CMA 722B receiver. The observations of January 1978 were made from two stations, TELE N and TELE S, equipped again with CMA 722B receivers.

The Doppler station at Owens Valley Observatory in California, 52105 BP ARIES 1, was manned for both experiments. The first campaign involved a Magnavox Geoceiver instrument while a CMA 722B receiver was used for the second experiment. This point had been connected to the radio telescope by survey observations performed by the National Geodetic Survey of the United States.

6.5 HAYSTACK AND GOLDSTONE SATELLITE-DOPPLER EXPERIMENTS

6.5.1 Local Surveys

A network of survey stations has been observed at both the Haystack and Goldstone radio telescope sites in order to determine the components of the vectors connecting the stations used in space system validation studies to the reference point of the radio telescope used for VLBI observations, and to determine the positions of these stations relative to the North American Datum. This work, performed by the National Geodetic Survey (NGS) of the National Ocean Survey (NOS) of the United States, was designed to determine these components to an accuracy of ±.1 cm. The results of the surveys (Hothem et al, 1978) are tabulated in Table 6.XI. The observations from both surveys were adjusted using the computer program HAVAGO (Horizontal and Vertical Adjustment of Geodetic Observations) developed by T. Vincenty (1979) of the NGS. This program combines horizontal and vertical angle, astronomic, and distance observations in a three-dimensional adjustment.

At the Goldstone site a network of eight stations was observed (Carter and Pettey, 1978) including the reference point of the MARS Deep Space Station (DSS14) antenna used for the VLBI observations, using a variety of terrestrial surveying instruments for each observation in order to minimise systematic errors caused by any one instrument make. The site was positioned by astronomical observations at three of the eight stations. The components of the offset vectors showed a maximum standard error of 0.002 m and therefore (Carter and Pettey, 1978) "even allowing for reasonable unknown systematic errors, the components should be accurate to ± 0.005 m".

The survey at the Haystack site (Carter, Fronczek, and Petty, 1979) consisted of 11 stations incorporating not only the Haystack antenna but also the Millstone and Westford antennae nearby. As for the Goldstone survey, several different instrument makes were used and astronomical observations were taken at three of the stations. The results obtained for the approximate vector between the Haystack to Westford antenna reference point were compared to VLBI results obtained over this baseline. The results of the two methods agreed to 4 mm in length and 0, 16, and -11 mm in the x, y and z components (Rogers et al, 1978).

6.5.2 Satellite-Doppler Observations

Several projects have been undertaken by the United States National Geodetic Survey (NGS) over the last few years involving satellite-Doppler measurements at both the Haystack and Goldstone Observatories. For use in this study, prior to 1978, observations were made at Haystack in January, May and November 1977, and at Goldstone during November 1976. No measurements were made simultaneously at both stations. In early 1978, a project was instigated with the purpose

of obtaining data from various space systems in order to compare and validate these systems, namely satellite-Doppler, VLBI, lunar laser ranging, and the Deep Space Network. Part of this project involved taking Doppler measurements at the Haystack and Goldstone sites. Results are presented for all the Doppler measurements detailed above in §7.4.1 (Strange et al, 1975, Hothem et al, 1978, and Strange and Hothem, 1978).

6.6 BURSA'S TRANSFORMATION

If the axes of two cartesian co-ordinate systems are not coincident, for example, as described in §6.3.3.3, the axes of the precise ephemeris system and a classically defined geodetic datum, a method is needed to compute the relationship between the two systems. Bursa's transformation relates them in terms of 7 parameters, namely 3 rotations, 3 translations, and a scale factor.

Consider a point P with co-ordinates in the first system of (x_1, y_1, z_1) and in the second system of (x_2, y_2, z_2), the equation of the transformation relating them is:

$$X_2 = (1 + \mu).R.X_1 + X$$

where $X_1 = [x_1, y_1, z_1]^T$,

$X_2 = [x_2, y_2, z_2]^T$,

$(1+\mu)$ = the scale factor between the two systems,

ΔX = the translation between the origins of the two systems expressed in terms of the second system such that $\Delta X = [\Delta x, \Delta y, \Delta z]^T$,

and $R = R_3(\theta_z).R_2(\theta_y).R_1(\theta_x)$, the product of three orthogonal rotations about the axes of the first system.

The general rotation matrix $R_i(\theta)$ is given in Appendix B and denotes an anticlockwise rotation of angle θ about the i^{th} axis when looking from the positive end of that axis towards the origin. The overall transformation is illustrated in Fig. 6.V.

For small rotation angles θ_z, θ_y, and θ_x encountered in a case such as the one being investigated here, the rotation matrix R becomes:

$$R = \begin{bmatrix} 1 & \theta_z & -\theta_y \\ -\theta_z & 1 & \theta_x \\ \theta_y & -\theta_x & 1 \end{bmatrix}$$

if all second and higher order terms are ignored. Disregarding all terms in $\mu\theta$, (6.) can be expressed as:

$$X_2 = X_1 + T.P \ ,$$

where

$$T = \begin{bmatrix} 1 & 0 & 0 & x_1 & 0 & -z_1 & x_1 \\ 0 & 1 & 0 & y_1 & z_1 & 0 & -x_1 \\ 0 & 0 & 1 & z_1 & -y_1 & x_1 & 0 \end{bmatrix} ,$$

and $P = [\Delta x, \Delta y, \Delta z, \mu, \theta_x, \theta_y, \theta_z]^T$.

From observations of station co-ordinates in both co-ordinate systems, a least squares adjustment (see §3.2.2) can be performed to compute the elements of the vector P. For small values of these elements, the initial approximate values of these co-ordinates can be regarded as zero in which case the observation equations are of the form:

$$T.P = X_2 - X_1 + v$$

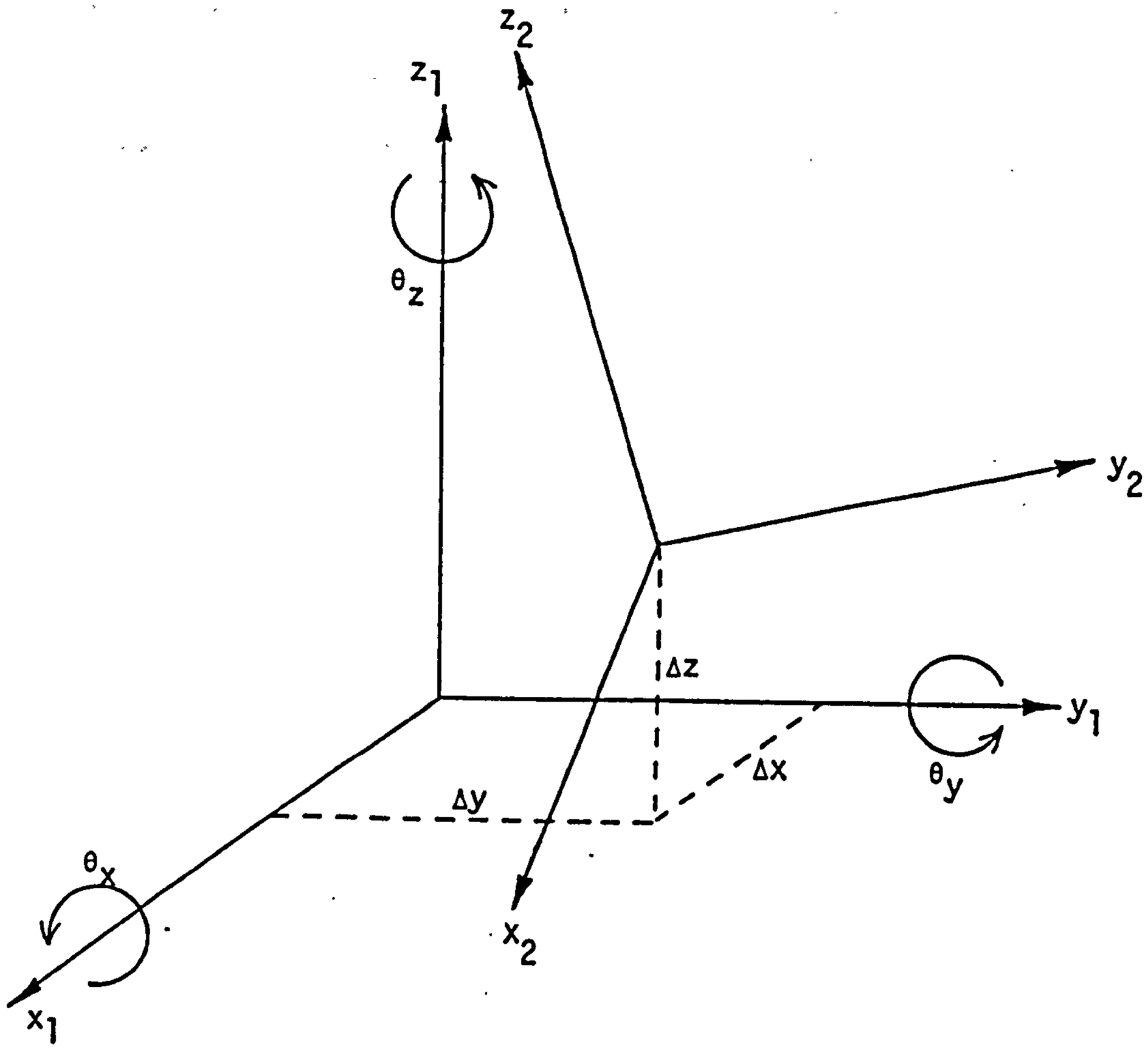

Fig. 6.V The Bursa Transformation Model

where v is the residual vector. If insufficient data is available to compute the full 7 parameter model, certain elements of the vector P may be held fixed in the adjustment. A 4 parameter adjustment would most likely involve the 3 translations and the scale factor, and a 5 parameter model would most probably involve the 3 translations, the scale factor, and one rotation. For the purposes of this test on the precise ephemeris system, the rotation used would be in longitude, i.e. θ_z.

CHAPTER 7:

RESULTS OF THE VLBI AND SATELLITE-DOPPLER OBSERVATIONS

7. RESULTS OF THE VLBI AND DOPPLER OBSERVATIONS

7.1 ALGONQUIN-CHILBOLTON-OWENS VALLEY VLBI RESULTS

7.1.1 Introduction

The data described in §6.1.1 has been adjusted for each separate observing period using the single baseline adjustment program, CCOM1, for each individual baseline, and the triple baseline program, TRIG4, for the entire array (see Chapter 5). In all the adjustments, the baseline components, relative clock error polynomial coefficients, and source co-ordinates have been solved for while taking allowance of the restrictions and limitations caused by observable types and the network definition (§3.4). All the adjustments have been performed using the fringe frequency data only. It was expected that the fringe frequency observations would dominate the delay observations due to the wide recorded bandwidth of the Canadian VLBI system. However, the latter shouldhave yielded information concerning the polar (z-) component of the baseline and the initial relative clock offset, expressed as the constant term c_0 of the relative clock error polynomial. Unfortunately, the adjustment of the delay data with the fringe frequency data did not prove satisfactory in yielding this information, even though the equatorial component of the baseline, as expected, was not greatly affected by the inclusion of the delay observations. Richard Langley, then at York University, Ontario, has adjusted similar delay data from these observing periods employing an adjustment based on the maximum likelihood method using the modified Gauss-Newton algorithm (Langley, 1979). It may be that this method is more suitable for the adjustment of this combination of data types derived from this particular interferometer system, than is the variation-of-co-ordinates solution using the method of weighted linear least squares employed here.

NOT TRUE.
MAXIMUM LIKELIHOOD is identically equal to least squares if uncorrelated obs are used, but is far less efficient computationally!

The origins of right ascension and declination in all the adjustments were defined by the adopted co-ordinates of the source 3C273B as given by (Clark et al, 1976). These co-ordinates have an estimated uncertainty of $\pm 0.01^{s}$ (0.15") in right ascension and ±0.13" in declination. The velocity of propagation of microwaves in vacuo was taken to be 299792.5 kms^{-1} as defined in the astronomical constants introduced in 1968 by the International Astronomical Union (IAU). This value differs from the currently accepted 'best' value of 299792.458 kms^{-1} (IAU, 1977) but it is used in order to maintain consistency with other VLBI results. This difference and its importance in comparing these results to satellite-Doppler or other data is discussed in §7.3 and §7.4. The values used for the rate of rotation of the Earth, Ω, in the adjustment were measured values for the observing periods and were taken from (Langley, 1979). These values are $7.292114897 \times 10^{-5}$ rad s^{-1} for May 1977 and $7.292114887 \times 10^{-5}$ rad s^{-1} for January, 1978. In practice, the use of the average value given by (2.52) makes little difference to the final solution.

The baseline results are presented in terms of both the baseline components relative to the Average Terrestrial system defined in §2.1.2.1, and also in terms of the length, hour angle (longitude), and declination of the baseline as defined in §3.4.1. Errors in UT1, UTC, the pole position, and source co-ordinates will exhibit themselves as changes in the components and direction of the observed baseline but not in its length. Consequently, it would be expected that the baseline length would remain constant from one observing period to the next. The baseline components are of limited use since the errors in their values are primarily due to errors in defining the orientation of the system, these component errors hence having a magnitude which

is a function of the baseline length. A comparison of the baseline hour angle and declination is of greater use as it allows model and observational errors to be more easily identified.

This particular three station interferometer array is, within the limitations of the general technique and this particular VLBI system, an efficient network. For a general three station network, the strongest shape is an equilateral triangle. However, for a VLBI antenna array it is advantageous and more efficient for all three antennae to be able to observe sources simultaneously. Consequently, although it is possible to observe over a longer baseline than here, the maximum longitude difference of 117^{o} for this case provides an efficient solution due to a reasonably shaped triangular network and sufficient sources being available for observation from all three stations simultaneously. This network is also suitable as the polar components of the baselines are small and hence the lack of delay data does not detract critically from the interpretation of the derived baseline parameters. As the network is an acute angled triangle, an error in the data from one station, which will directly affect the results for two baselines, may prove difficult to detect.

In the presented results, the value given for the z-component of the baseline is the a priori value used for it in the adjustment. Due to both this parameter having to be held fixed and the large relative equatorial baseline component, the standard deviation of the declination of the baseline is very small in all cases and should not be regarded as indicative of the quality of the results.

The clock readjustment at the Algonquin Radio Observatory during the May 1977 observations has caused two separate clock error models to be applied in all adjustments incorporating this antenna during this

campaign. For reasons explained in §2.4.7, a first-order (linear) clock error polynomial is used for both models and for all other clocks in all the adjustments. A comparison was performed between this method and one using a second-order polynomial model for the clock behaviour before the readjustment, and a first-order polynomial for the clock after the readjustment. There was little difference in the adjusted parameters and only a slight reduction in the root-mean-square observation residual value derived from this test when compared with the results using two first-order models.

The observational standard errors used in the adjustments were those provided with the data and are hence based on the signal-to-noise ratio of the received signals (i.e. high SNR, low standard error, see §4.3.2). Although a good signal-to-noise ratio is an indication of the quality of the recordings, it does not necessarily imply a good delay or delay rate observation. However, adjustments were performed using a mean standard error for all the observations which gave insignificantly different results from those presented here, apart from the rejection of a few extra observations which had initially been given low weights. The relative weighting of the observations is nevertheless a factor which requires further investigation.

7.1.2 Baseline Results

The results obtained by solving for each observed baseline individually are presented in Tables J.1 and J.2 for the May 1977 and January 1978 observations respectively. The results of the simultaneous adjustment of the data from the entire three-station array are given in Tables 7.I and 7.II for May 1977 and January 1978 respectively. Table 7.III presents the mean baseline parameters

Baseline Property	Baseline		
	Algonquin-Chilbolton	Algonquin-Owens Valley	Owens Valley-Chilbolton
x-component (m)	3090276.84	-3327635.71	6417912.55
y-component (m)	4245482.07	-132216.44	4377698.51
z-component* (m)	381825.41	-723368.48	1105193.89
length (m)	5264952.00 ±0.30	3407917.63 ±0.26	7846993.01 ±0.32
declination	$4^{o}09'31.902"$ ±0.001 " (0.02 m)	$-12^{o}15'17.618"$ ±0.003 " (0.06 m)	$8^{o}05'47.864"$ ±0.001 " (0.05 m)
hour angle	$53^{o}56'57.160"$ ±0.010 " (0.27 m)	$-2^{o}16'31.179"$ ±0.012 " (0.21 m)	$34^{o}17'53.319"$ ±0.011 " (0.43 m)
r.m.s. fringe frequency residual (mHz)	2.9	2.1	3.3
Observations accepted	99	91	92

* the z-component is held fixed in the adjustment.

Table 7.I May 1977 VLBI results for the Algonquin-Owens Valley-Chilbolton array using the 3 station-3 baseline adjustment method

Baseline Property	Baseline		
	Algonquin-Chilbolton	Algonquin-Owens Valley	Owens Valley-Chilbolton
x-component (m)	3090274.99	-3327634.95	6417909.93
y-component (m)	4245480.90	-132218.15	4377699.05
z-component* (m)	381825.41	-723368.48	1105193.89
length (m)	5264949.97 ±0.42	3407916.95 ±0.32	7846991.17 ±0.45
declination	$4^{o}09'31.908"$ ±0.001 " (0.03 m)	$-12^{o}15'17.627"$ ±0.004 " (0.07 m)	$8^{o}05'47.871"$ ±0.002 " (0.06 m)
hour angle	$53^{o}56'57.192"$ ±0.017 " (0.43 m)	$-2^{o}16"31.287"$ ±0.013 " (0.21 m)	$34^{o}17'53.370"$ ±0.017" (0.65 m)
r.m.s. fringe frequency residual (mHz)	2.1	1.8	2.9
Observations accepted	93	93	97

* the z-component is held fixed in the adjustment

Table 7.II January 1978 VLBI results for the Algonquin-Owens Valley-Chilbolton array using the 3 station-3 baseline adjustment method

Baseline Property	Baseline		
	Algonquin-Chilbolton	Algonquin-Owens Valley	Owens Valley-Chilbolton
x-component (m)	3090275.92	-3327635.33	6417911.24
y-component (m)	4245481.49	-132217.30	4377698.78
z-component* (m)	381825.41	-723368.48	1105193.89
length (m)	5264950.98	3407917.29	7846992.09
declination	$4^{o}09'31.905"$	$-12^{o}15'17.622"$	$8^{o}05'47.867"$
hour angle	$53^{o}56'57.176"$	$-2^{o}16'31.233"$	$34^{o}17'53.345"$

* the z-component is held fixed in the adjustment.

Fig. 7.III Mean values of thebaseline parameters derived from the three station solutions of May 1977 and January 1978

derived from these three station solutions.

The discrepancy between the two data sets is larger than the standard deviations of the individual parameters. However, the repeatability of these results, together with their comparison with satellite-Doppler results described in §7.3, would indicate an accuracy of the baseline determination of about ±1 metre in length. The baseline direction is well defined in declination, as described in §7.1.1. However, in hour angle, the discrepancy between observing periods is also greater than would be expected from the derived standard deviations. The computed baseline direction has an accuracy of about ±0.05".

The derived standard deviations of the parameters are smaller than theoverall accuracy primarily due to the lack of consideration for the geodetic applications of this data when planning the observing programs (see §5.5 and §6.1). Other systematic error sources affecting the attainable accuracy are atmospheric effects, clock instabilities, errors in the equipment at the receiving, recording, and processing stages, and source structure effects. Although the accuracy of the method could be improved, the values of ±1 m and 0.05" in length and hour angle respectively over baseline lengths of up to 8000 km are probably close to the overall capability of the system under realistic operating conditions, e.g. limited observing time.

The results indicate that the accuracy of the determination of the baseline parameters is independent of the distance between the antennae for these observations. This feature is one of the major advantages of the technique.

7.1.3 Source Co-ordinate and Clock Results

The results for the co-ordinates of the observed sources for the

three station solutions from May 1977 and January 1978, are presented in Table J.III. The a priori co-ordinates used are presented in Table 6.IV. These are quite recently determined values and can be assumed to be a reliable reference by which to assess these results. Most of the co-ordinates of the sources were in good agreement with the a priori values except for the declinations of two sources, 3C446 and 0235+16.

The results for the relative clock error polynomials for the three station solutions are presented in Tables J.IV and J.V for the May 1977 and January 1978 observations respectively. The results of all the single station solutions have been omitted for brevity. The magnitude of these results confirms the requirement to use such a model. The first of the two models for the Algonquin clock in the May 1977 adjustment doesnot show an appreciably greater relative clock error than that shown by the second model.

7.2 VLBI RESULTS FROM THE HAYSTACK-GOLDSTONE BASELINE

7.2.1 Introduction

The observations on the baseline connecting the Haystack and Goldstone Observatories have been described in §6.2. The adjustment of this data was performed using the COM7 program of the NULBIP suite, designed for NRAO Mk I data observed over a single baseline. In all results described here the unknowns of the adjustment (noting the requirements for the fixing of certain parameters described in §3.4 according to the observation type and the network definition) are the three baseline components, the source co-ordinates, the parameters of a first-order (linear) clock error polynomial, and a parameter at each station representing the mean zenith delay due to the atmosphere, Chao's Model (Appendix D.4) being the atmospheric model used.

The data was adjusted for the three cases of delay observations only, delay rate observations only, and both delay and delay rate observations. The latter is of greatest interest as it incorporates all the available data. For this particular VLBI system, the delay observations dominate the delay rate observations due to the observing method and system, in particular due to the use of the 'bandwidth synthesis' technique (§4.3.3) to accurately measure the group delay.

The origin of right ascension was defined as the adopted co-ordinates of the source 3C273B. The fixed declination in the delay rate data only adjustment was also taken to be that of 3C273B. These co-ordinates, obtained from (Clark et al, 1976), are quoted as being accurate to $\pm 0.01^{s}$ (0.15") in right ascension and ±0.13" in declination. The velocity of propagation of microwaves in vacuo was taken to be the IAU (1968) adopted value of 299792.5 kms^{-1}. The rate of rotation of the Earth was taken to be the mean value defined in (2.52).

The observational standards errors used in the adjustments were those given with the data and are based on the signal-to-noise ratio for each observation (see §7.1).

The application of Chao's Model without any indication of meteorological conditions or relative magnitudes of the dry and wet atmospheric effects, necessitates that an assumption is made for this latter factor. In the results presented, it has been assumed that the wet component accounts for 10% of the total effect. Tests performed with this proportion varying between 0 and 20% showed little effect on the baseline results.

7.2.2 Baseline Results

The baseline parameters derived from these three different

adjustments are presented in Table 7.IV. The dominance of the delay data is shown by the smaller standard deviations for this solution than those obtained from the delay rate data. Furthermore, the delay only and the combined delay and delay rate solutions are in close agreement both in absolute parameter values and in parameter standard deviations. The standard error in the baseline length is less than those in the y and z baseline components due to the dominance of the x-component in the solution. As the data was supplied in an edited and condensed form, no observations were rejected in the adjustment. Fig. 7.I shows a plot of the post-fit residuals against the epoch of observation, no systematic trend appears to exist.

The standard deviations quoted here are an assessment of the internal precision of the interferometer. Systematic errors exist due to clock and instrumental variations, atmospheric causes, source structure effects, errors in the Earth orientation parameters of UT1 and the pole position, and the 'fixed' source in the adjustment. The latter pair have no effect on the baseline length or the internal consistency of the adjustment but only on the baseline components.

Although the standard deviations of the baseline length, hour angle, and declination are 7 cm, 0.007" and 0.015" respectively, an indication of the overall accuracy of the system is very difficult with just this one observed baseline for the single observing period. However, other researchers (Robertson, 1975 and Shapiro et al, 1974) have analysed larger data sets obtained from the same VLBI system over this and other baselines. These have shown, in the case of 16 such observing periods on the Haystack-Goldstone baseline between 1972 and 1975, including this one, a scatter in the baseline lengths of 1.77 m and a root-mean-square deviation about the mean of 26.3 cm. The

Baseline Property	Adjustment Mode		
	Both delay and delay rate observations	Delay observations only	Delay rate observations only
x-component (m)	-3846026.55 ± 0.05	-3846026.54 ± 0.05	-3846026.47 ± 0.21
y-component (m)	-184075.55 ± 0.17	-184075.26 ± 0.18	-184076.44 ± 0.10
z-component (m)	-619828.27 ± 0.37	-619828.44 ± 0.37	-619828.28
length (m)	3899998.86 ± 0.07	3899998.86 ± 0.07	3899998.82 ± 0.39
declination	$-9^{o}08'41.340"$ ±0.015" (0.29 m)	$-9^{o}08'41.349"$ ±0.016" (0.30 m)	$-9^{o}08'41.341"$ ±0.062" (0.06 m)
hour angle	$177^{o}15'35.441"$ ±0.007" (0.13 m)	$177^{o}15'35.455"$ ±0.008" (0.15 m)	$177^{o}15'35.392"$ ±0.010" (0.19 m)
r.m.s. delay residual (ns)	0.30 (9 cm)	0.30 (9 cm)	-
r.m.s. delay rate residual (ps/s)	0.30 (0.009 cms^{-1})	-	0.16 (0.005 cms^{-1})
Observations accepted	~~192~~ 384	192	~~384~~ 192

Fig. 7.IV VLBI results from the Haystack-Goldstone baseline observed on August 29-30th, 1972

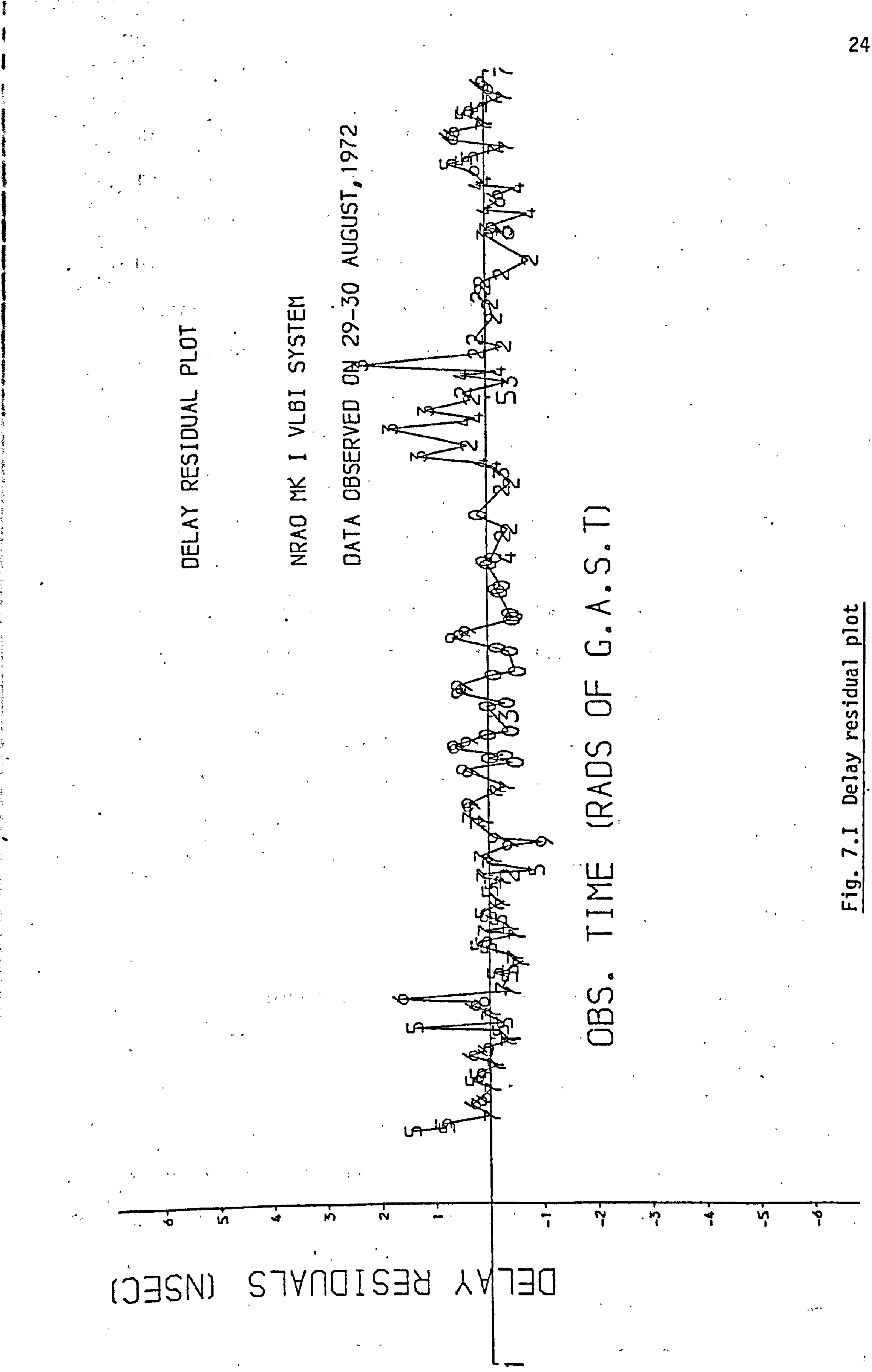

Fig. 7.1 Delay residual plot

error in direction is dominated by the errors in the earth orientation parameters. It should be noted that since these observations were made the VLBI systems have also been under constant improvement. The baseline length, declination, and hour angle obtained from this analysis differ from those obtained by D.S. Robertson (1975) by 3 cm, 0.004" (7 cm), and 0.04" (70 cm) respectively.

7.2.3 Clock, Source Co-ordinate, and Atmospheric Parameter Results

The solution for the clock error polynomial for the three adjustment modes is presented in Table J.VII. No solution for the clock offset is of course made for the delay rate observations. These results show good agreement between the different adjustments indicating that they are consistent. As described in §2.4.1 and §2.4.8 respectively, the clock error polynomials contain contributions due to antenna and instrumental delays, and relativity effects.

Adjusted co-ordinates of the observed sources are presented in Table J.VI for the adjustment of the combined data set only. The results of the individual data type adjustments have been omitted for brevity. The right ascension determinations are in good agreement with accepted values, as are the majority of the declinations. The relatively large discrepancies of the three near-equatorial sources 2134+00, 3C279, and 3C273B, is unexplained but it would appear to be a function of their declination.

The results for the mean zenith atmospheric delay at the two antennae are presented in Table J.VII. These show a maximum difference between adjustment modes amounting to only 0.2 nsec (6 cm). These differences are probably due to the tropospheric parameters absorbing unmodelled effects in the observations. As no measurements are available, nor allowance made in the model for ionospheric refraction,

this tropospheric model will incorporate the ionospheric correction to a limited extent.

7.3 VLBI/DOPPLER COMPARISON: ALGONQUIN-CHILBOLTON-OWENS VALLEY ARRAY

7.3.1 Doppler Results

The Doppler observations taken at the radio telescope sites at Algonquin, Owens Valley, and Chilbolton, together with those taken at the TRANET station at Barton Stacey, have been described in §6.4. The station positions obtained from the Doppler data are presented in Table 7.V for both the May 1977 and January 1978 observing periods. These results are taken from the thesis of Richard Langley (1979) and are derived using the GEODOP computer program (Kouba and Boal, 1976) by Jan Kouba of the Earth Physics Branch of the Department of Energy, Mines and Resources, Canada. The results are computed using the precise ephemeris supplied by the United States Defense Mapping Agency Hydrographic/Topographic Center (DMA) and are relative to the NWL-9D and the NSWC-9Z-2 co-ordinate reference systems, described in §6.3.3.2 and §6.3.3.3, for the May 1977 and January 1978 data respectively. The standard deviation in each component is estimated to be ±0.7 m (Kouba, 1978).

The only major problem encountered during both periods of observations was an intermittent timing error in the data acquisition by the CMA 722B receiver at Chilbolton during the May 1977 experiment. This problem has not proved critical, however, as there were still sufficient acceptable passes to obtain a good solution. All other receivers functioned satisfactorily throughout both the campaigns. The position quoted for the Algonquin Doppler site for the January 1978 experiments is the mean position obtained from the two receivers on

Observation Date	Doppler Station	Station position			No. of passes
		x-co-ordinate (m)	y-co-ordinate (m)	z-co-ordinate (m)	
May 1977	Algonquin 683100A Tel. Ref. A	918110.54	-4346068.94	4561982.08	48
	Owens Valley 52105 Aries 1	-2409663.10	-4478361.78	3838520.69	48
	Chilbolton North Pillar	4008271.06	-100717.23	4943806.36	31
	Barton Stacey 116 TRANET	4004967.0	-96583.94	4946538.28	25
January 1978	Algonquin TELE N TELE S	918160.68	-4346070.98	4561964.74	27
	Owens Valley BP Aries 1	-2409662.43	-4478361.83	3838520.54	37
	Barton Stacey 116 TRANET	4004966.66	-96583.21	4946537.68	32

Fig. 7.V Satellite-Doppler results for the May 1977 and January 1978 joint VLBI/Doppler campaigns

stations TELE N and TELE S. It is also noteworthy that the precise ephemeris is computed from data incorporating that obtained by the TRANET station at Barton Stacey. It would, therefore, be expected that the adjustment of the Barton Stacey data would exhibit a high internal consistency, though not necessarily a high accuracy.

The Doppler stations at all the sites are offset from the radio telescope reference points. These offsets are tabulated in Table 6.XI and are applied to the Doppler station results in order to give the interferometer baselines determined by the Doppler measurements as presented in Tables 7.VI and 7.VII for the May 1977 and January 1978 observations respectively. The accuracy estimates for these baselines, derived from the estimate for the standard deviation of the Doppler position components of 0.7 m, are 1 m in length for all the baselines, and 0.06", 0.04", and 0.03" in orientation for the Algonquin-Owens Valley, Algonquin-Chilbolton, and Owens Valley-Chilbolton baselines respectively. Whereas the orientation accuracy in VLBI is almost independent of the baseline length, this is not the case for satellite-Doppler measurements. The contribution to these values due to the errors in the observed offset vector between each Doppler station and the appropriate radio antenna is negligible in this case due to the care taken over the local surveys.

There is good agreement, to the order of less than 1 m in length and 0.05" in orientation, between the two separate data sets and between the baselines determined separately using the Doppler data from Chilbolton North Pillar and from Barton Stacey for May 1977. This agreement supports the values quoted for the standard deviations of the components of the Doppler positions.

Observing Sessions	Baseline Property	Baseline				
		Algonquin-Chilbolton (from Chilbolton N.P.)	Algonquin-Chilbolton (from Barton Stacey)	Algonquin-Owens Valley	Owens Valley-Chilbolton (from Chilbolton N.P.)	Owens Valley-Chilbolton (from Barton Stacey)
May 1977	x-component (m)	3090293.70	3090294.16	-3327637.68	6417931.38	6417931.84
	y-component (m)	4245470.70	4245471.53	-132203.41	4377674.11	4377674.94
	z-component (m)	381825.50	381824.63	-723368.57	1105194.07	1105193.20
	length (m)	5264952.74	5264953.61	3407919.07	7846994.82	7846995.54
	declination	$4^{o}09'31.903"$	$4^{o}09'31.867"$	$-12^{o}15'17.604"$	$8^{o}05'47.862"$	$8^{o}05'47.836"$
	hour angle	$53^{o}56'56.362"$	$53^{o}56'56.352"$	$-2^{o}16'30.368"$	$34^{o}17'52.502"$	$34^{o}17'52.514"$

Fig. 7.VI Interferometer baseline components derived from combination of May 1977 satellite Doppler data and ground survey ties

Jan 1978	x-component (m)		3090293.43	-3327637.40		6417930.83
	y-component (m)		4245473.78	-132201.94		4377675.72
	z-component (m)		381825.46	-723367.29		1105192.75
	length (m)		5264955.06	3407918.46		7846995.08
	declination		$4^{o}09'31.895"$	$-12^{o}15'17.533"$		$8^{o}05'47.826"$
	hour angle		$53^{o}56'56.442"$	$-2^{o}16'30.278"$		$34^{o}17'52.546"$

Fig. 7.VII Interferometer baseline components derived from combination of January 1978 satellite-Doppler data and ground survey ties

7.3.2 VLBI/Doppler Comparison

The Doppler results described in the previous section have been compared to the VLBI results described in §7.1, using the Bursa Transformation technique outlined in §6.6. In order to apply this transformation, the VLBI results must be transferred to co-ordinated positions for comparison with the Doppler derived positions. This is achieved by assuming a set of cartesian co-ordinates for one VLBI antenna and computing the co-ordinates of the other antenna relative to this one using the computed baselines from the VLBI adjustment. The initial assumed antenna position should be approximately correct but any error in it will be treated by the adjustment as a translation transformation between the VLBI and Doppler results. As the VLBI method measures baseline parameters and not absolute positions, the values of these three translation parameters obtained from the Bursa Transformation are irrelevant. The results of a 7 parameter transformation are presented in Table 7.VIII for the two observing periods, both separately and combined. The three translation parameters are not included in the table.

The results of the May 1977 data are internally consistent and also agree with the results obtained on the Haystack-Goldstone baseline as described in §7.4. Those of the January 1978 data are not as consistent and also differ from the May 1977 results significantly in the scale correction. This is primarily due to one of the VLBI baseline results but all exhibit this scale discrepancy when compared with the May 1977 results. For both the data sets, the longitude rotation (θ_z) results are in agreement and the results for the rotations about the two equatorial axes (θ_x and θ_y) are not significant. These differences between the two observing periods do not indicate a

Observing session	Doppler Stations	μ (ppm)	θ_x (secs)	θ_y (secs)	θ_z (secs)
May 1977	AR, CH OV, BS	-0.27 ± 0.06	-0.01 ± 0.05	0.01 ± 0.04	-0.81 ± 0.01
Jan 1978	AR, OV BS	-0.62 ± 0.28	0.08 ± 0.19	0.11 ± 0.15	-0.81 ± 0.07
May 1977 + Jan 1978 combined	AR, CH OV, BS from 1977. AR, OV, BS from 1978.	-0.37 ± 0.13	0.04 ± 0.1	0.06 ± 0.08	-0.81 ± 0.03

(Note: AR = Algonquin, OV = Owens Valley, CH = Chilbolton, BS = Barton Stacey, μ = scale correction, θ_i = rotation about the i^{th} axis)

Fig. 7.VIII Results of a 7 parameter Bursa transformation model comparing the satellite-Doppler derived antenna positions to those obtained by VLBI.

difference between the NWL-9D and NSWC-9Z-2 Doppler reference systems as such a significant difference does not exist.

The combined results indicate a scale discrepancy of -0.37 ppm and a longitude rotation of 0.81" eastward in order to relate co-ordinates in the Doppler system to co-ordinates in the system in which the VLBI positions have been computed. The VLBI co-ordinate system can be termed "classical" apart from the scale being too large due to the use of 299792.5 km s^{-1} as the velocity of light (IAU, 1968) rather than the currently accepted best value (IAU, 1977) of 299792.458 km s^{-1}. This discrepancy requires that all measurements based on the larger value be reduced by 0.14 ppm in order to refer them to a classical geodetic system.

Therefore, in conclusion, this comparison of Doppler and VLBI data over a three baseline array and two observing periods has shown that, in order to transform co-ordinates determined in the NWL-9D or NSWC-9Z-2 precise ephemeris Doppler system into a classical geodetic system, as detailed in §2.1.2.1, a scale correction of -0.51 ppm and a longitude rotation of 0.81" to the east are required. The direction of the polar axes of the Doppler and VLBI systems agree to 0.06". This is not significant, bearing in mind the standard deviations of the computed rotation angles. Furthermore, there is likely to be inconsistency in the Earth orientation parameters used for the two observing periods although this error is below the level of sensitivity of this observing system.

The value derived for the scale correction is larger than that obtained by other researchers (Hothem, 1979 and Hothem and Strange, 1978) of -0.4 ±0.1 ppm as derived from comparisons of Doppler with VLBI, Lunar Laser Ranging, and Deep Space Network. However, this disagreement

is within the quoted accuracy limits of the computations. Furthermore, the results reported here have been obtained using fewer observations and a much less precise VLBI system. As will be described in §7.4, the value of -0.4 ppm has been verified on the Haystack-Goldstone baseline for the one observing period studied in this thesis. The longitude rotation correction of 0.80" ± 0.05" eastward obtained in these other comparisons is in good agreement with that obtained here of 0.81" ± 0.03".

7.4 VLBI/DOPPER COMPARISON; HAYSTACK-GOLDSTONE BASELINE

7.4.1 Doppler Results

The results of the satellite-Doppler observing campaigns at Haystack and Goldstone are presented in Table 7.IX. The results obtained prior to 1978 (Hothem and Strange, 1978) and those obtained in the Space Systems Validation Project in January-February 1978 (Hothem, 1979), are given separately, the latter being observed using either a hydrogen-maser, rubidium or cesium standard to supply the receiver reference frequency. All these results were computed using the DMA's DOPPLR computer program using the precise ephemeris (Smith et al, 1976). Table 7.X presents the resulting components between the VLBI antennae reference points as derived from a combination of these Doppler positions and the ground survey ties presented in Table 6.XI.

The difference between these sets of results is well within the expected repeatability of the Doppler system. Furthermore, the difference in orientation of the baseline is within the accuracy limits of the Earth orientation parameters used to define the precise ephemeris system.

	Doppler Station			
	51118 Haystack		51065 Goldstone	
	Pre-1978	Jan-Feb 1978	Pre-1978	Jan-Feb 1978
x-co-ordinate	1492393.80	1492393.31	-2353414.67	-2353414.95
y-co-ordinate	-4457298.60	-4457299.29	-4641502.57	-4641502.84
z-co-ordinate	4296815.57	4296816.45	3676921.81	3676922.23
No. of passes	91	431	101	371

Fig. 7.IX Satellite-Doppler results at the Haystack and Goldstone Observations (pre-1978 from Hothem et al, 1978; Jan-Feb 1978 from Hothem , 1979)

	From Doppler results prior to 1978	From Doppler results in Jan-Feb. 1978
x-component	-3846027.97	-3846027.76
y-component	-184060.47	-184060.05
z-component	-619829.70	-619830.16
length	3899999.77	3899999.62
declination	-9°08'41.409"	-9°08'41.435"
hour angle	177°15'36.250"	177°15'36.273"

Table 7.X Results for the baseline defined by the VLBI antenna reference points at Haystack and Goldstone as derived from a combination of Doppler positions and ground surveys

7.4.2 VLBI/Doppler Comparison

For the Doppler results prior to 1978, and hence relative to the NWL-9D system, comparison with the VLBI results described in §7.2 shows that Doppler positions computed using the precise ephemeris require a scale correction of -0.23 ppm and a longitude rotation of 0.81" eastward in order to refer them to the co-ordinate system on which these VLBI results are based. Similarly, the 1978 Doppler results computed relative to the NSWC-9Z-2 co-ordinate system require a scale correction of -0.20 ppm and an eastward longitude rotation of 0.83". As described in §7.3.2, in order to refer positions on this co-ordinate system to a classical geodetic system, a further scale correction of -0.14 ppm is required to account for the presently accepted value of the speed of propagation ofmicrowaves in vacuo.

In conclusion, in order to transform Doppler derived co-ordinates

into co-ordinates relative to a classical geodetic datum, it has been shown that, using the pre-1978 Doppler data, a scale correction of -0.37 ppm and an eastward longitude rotation of 0.81" is required and, for the Doppler data of 1978, a scale correction of -0.34" ppm and an eastward longitude rotation of 0.83" is needed. These results are not presented in this way to imply any difference between the NWL-9D and NSWC-9Z-2 systems, nor do they indicate such a difference.

These results agree well with those of other researchers (Hothem, 1979, and Hothem and Strange, 1978) of 0.4 ± 0.1 ppm and 0.80" ± 0.05" as derived from comparisons with VLBI, Lunar Laser Ranging, and Deep Space Network. They also agree, within the quoted accuracies, with the results derived from the Algonquin-Chilbolton-Owens Valley interferometer array as described in §7.3.2.

CHAPTER 8:

GEODETIC AND GEOPHYSICAL APPLICATIONS

8.1 INTRODUCTION

The technique of VLBI has several characteristics which make it well suited for use in both geodesy and the study of certain geophysical effects. Primarily, this usefulness stems from the ability to measure very long intercontinental baselines to sub-metre accuracy in each of the three baseline components. This degree of accuracy results from the baseline measurements made by VLBI being relatively free of systematic errors, primarily due to its independence of the Earth's gravity field which is the major problem encountered with a satellite-based system. Furthermore, the reference system is defined in orientation by the catalogued positions of what are essentially "fixed" radio sources while the scale is defined by the speed of propagation of microwaves in vacuo, any error caused by the uncertainty in this value being less than those caused by other effects. As the method uses standard radio telescope structures, of which there are several around the world, and commercially available equipment which has been used and developed for work in the field of astronomy over a number of years, the technique is already at quite an advanced stage even though "geodetic VLBI" is a relatively recent (late 1960's) concept.

This chapter deals with the application of the technique to geodesy and geophysics and in doing so outlines the methods by which the different geodetic and geophysical phenomena can be detected. It also gives a brief outline of their origins, magnitudes, and effects, together with the current and near future capability of the VLBI systems to measure them. Among these are the application to conventional geodetic networks (§8.2), the assessment and calibration of "lower order" surveying systems (§8.3), the study of the Earth orientation parameters (§8.4), the detection and measurement of Earth tidal movement

(§8.5), and the monitoring of both tectonic plate motion and local crustal motion (§8.6). Finally, §8.7 gives a brief outline of three major developments which will further improve the capability of the VLBI technique, namely the use of small transportable telescopes, satellite VLBI, and the use of the phase observable described in §2.1.4.

This is by no means an exhaustive summary of the uses of VLBI but is merely a brief resume of its current status. As observing techniques improve and accuracies increase then more geodetic and geophysical phenemena will come within the range of the technique and those outlined here will be better measured and understood.

8.2 GEODETIC NETWORKS

8.2.1 Application of VLBI to Global Geodetic Networks

With the development of satellite-based geodetic observing systems, the establishing of a high accuracy global geodetic reference system is becoming increasingly feasible. VLBI can play an important role in this objective, primarily due to its capability of making precise measurements in a purely geometrical manner based on a celestial (absolute) reference system.

There have been several different satellite-based methods used in recent years which have now been largely superseded; for example, the satellite triangulation networks established by photogrammetric measurements of satellites against a stellar background (e.g. the Smithsonian Baker-Nunn Network (Whipple and Hynek, 1958) and the BC-4 Network (Schmid, 1973)), and the method of radar ranging to satellites (e.g. SECOR (Rohde, 1977 and Warden et al, 1977)). Currently, there are three main systems suitable for providing global control, namely laser ranging to satellites and to the Moon (IAG, 1978), satellite-Doppler (§6.3), and VLBI. The latter appears the most promising of the

three. A detailed examination of these and other satellite-based geodetic systems can be found in (Kelsey and Ashkenazi, 1979) and (Committee on Geodesy, 1978).

VLBI, a technique which is still under rapid development, is already capable of measuring intercontinental baselines to an accuracy of 0.01 ppm in scale and 0.05" in orientation (Clark, 1978, and Schilizzi and Campbell, 1978). However, with a system like VLBI which exhibits a higher accuracy than all other systems in use, these values are largely a measure of precision and repeatibility. Nevertheless, its accuracy is virtually independent of the baseline distance due to its geometrical nature and the independence of the hardware and software at the separate antennae sites. Observations made over a baseline between two radio telescopes yield the three components of that baseline relative to a classical geodetic system based on the CIO pole and BIH zero longitude. Irrespective of the number of telescopes in an interferometer array, the technique will not give any information as to the radio telescope positions relative to the geocentre, the origin of the co-ordinate system, unless one telescope position is assumed to be known. In this case, all positions determined by the observations and adjustment will possess the same error that is inherent in this 'fixed' position. Consequently, VLBI is suitable for providing distance and azimuth measurements for use in network adjustments but not absolute positions.

The critical factor in the use of VLBI measurements in geodetic networks is the reference surface upon which the adjustment is performed. It is conventional (§2.1.2.1) to adjust national networks on a suitably defined ellipsoid of revolution(spheroid) and to express a station position in terms of its latitude, longitude, and height above spheroid level. Consequently, all measurements taken on the Earth's surface

must be reduced to corresponding values on the spheroid surface prior to the adjustment process. It is at this stage that the major problem occurs. In order to reduce a distance to the spheroid surface, a knowledge of the geoid-spheroid separation is required. A 6 m error in this value incurs a 1 ppm error in the reduced distance and therefore typical current accuracies of around 1 m for the separation are too large to maintain the high accuracy achieved by the observations themselves. Having accepted this problem, the actual reduction to the spheroid can be performed without loss of accuracy using standard formulae. A position can be assumed for one of the antennae (as determined by satellite-Doppler observations or conventional terrestrial triangulation for example) and the other antenna position can be computed from the observed baseline components using the inverse of the formulae described in §2.1.2.2 making certain assumptions from the approximate antenna position of the second already determined by other methods (for example, its height above the spheroid surface). The application of a rigorous 'reverse' formula, for example, Rudoe's formula (Bomford, 1975), to compute the spheroidal distance and azimuth between these two positions will yield the required data. The error introduced by initially assuming a position for one of the antennae will be insignificant providing that the radio antenna reference point is connected to a local station which is itself connected to the local triangulation network.

Due to the difficulty in fitting a spheroidal reference system to a global network and also because of the measuring techniques that would be used to establish it, a cartesian co-ordinate system would be preferable as a global datum. For reference and comparison purposes, this system could be defined in terms of the CIO and BIH zero longitude

in the same manner as a spheroidal reference system. With regard to the use of VLBI observations this co-ordinate system has several advantages in that it enables the distance and three-dimensional direction measuring capability of VLBI to be utilised fully. The directions are related to star positions and hence provide a geometric reference which is independent of the gravity field. The distances do not require reduction and hence maintain their observational accuracy in the global adjustment. One of the major advantages of VLBI, that the accuracy is virtually independent of the baseline distance, is also maintained in this method although it is less useful over short distances (less than 1000 km) where other systems can also achieve the same order of accuracy with greater ease and less expense.

The realisation of a global reference system would currently involve probably VLBI and laser observations at a group of 'super control points' and an infill of this network by satellite-Doppler observations. Further stages would include terrestrial survey and inertial survey with the localised networks still being computed on a spheroidal reference system, this being the most suitable reference surface for small areas. A major factor in any such adjustment would be to ensurethe compatibility of the different measuring systems (for example, the definition of the scale of orientation of each system must be compatible with the other systems). Furthermore, a correct assessment of the relative weighting of the observations from different systems is vital, as is the correct modelling of the observations in the adjustment (Ashkenazi, 1979).

This section has dealt solely with the application of VLBI to global networks. Its application to national and international networks is discussed in the next section with the results of a simulation

experiment incorporating VLBI measurements in the Ordnance Survey Triangulation of Great Britain.

8.2.2 Ordnance Survey Triangulation/VLBI Experiments

The Ordnance Survey Primary Triangulation of Great Britain, OSGB 70(SN), is a dense network consisting of 292 primary stations connected by 1900 observed directions, 180 measured distances, and 15 Laplace azimuths (Ashkenazi et al, 1972). A series of network simulation tests (the principle of which is outlined for a different purpose in §3.6) has been carried out using the observations of the network and their appropriate standard errors as determined from the network adjustment (Cross, 1970). In the first series of experiments, VLBI measurements between primary triangulation stations close to the three existing fixed radio telescopes suitable for this purpose, at Jodrell Bank in Cheshire, Chilbolton, and Cambridge, were included in the simulation tests. The three resulting baselines were given standard errors in length ranging between 1 ppm and 0.01 ppm and in orientation between 0.5 secs and 0.1 secs. The precise details of the different combinations used in each model, together with a summary of the stations and data used, is given in Appendix H. The second set of tests involved the same three fixed radio telescopes but also an 'imaginary' mobile telescope in the very north of Scotland. This location was suitable for two reasons; firstly, it provides a high accuracy distance/direction tie to the other three stations which are much closer together and also nearer to the origin of the network and therefore whose positions relative to the origin are more accurately known, and secondly, it provides the network with a good coverage of VLBI measurements, both the east-west strength being supplied by the three fixed telescopes and

the north-south strength by the mobile telescope with any or all of the three fixed ones.

8.2.3 Ordnance Survey Triangulation/VLBI Results and Discussion

The results of the series of tests, described in the previous section, combining the Ordnance Survey Primary Triangulation of Great Britain and certain chosen VLBI measurements are presented in Appendix H. The mean azimuth and distance standard errors for four separate groups of test lines (short, medium, long, and very long) have been computed for each model applied. These results were derived using a computer program developed by S.A. Crane of the University of Nottingham.

The results of the first series of tests using just the three radio telescopes at Jodrell Bank, Chilbolton, and Cambridge are summarised in Table H.II. These show that VLBI observations over 'medium' length lines will not contribute significantly to the strength of the network in either azimuth or distance. The already existing strong and dense terrestrial triangulation dominates the simulation adjustment. Slight improvements in relative station standard errors will inevitably occur, especially between pairs of stations close to each end of the baselines, but these are minimal compared with the effort involved in obtaining such measurements. The results of the second series of tests simulating a transportable antenna located in the northern most area of Scotland are summarised in Table H.III. As envisaged, the application of these measurements yield strong distance and azimuth control over long lines along the length of the triangulation and has therefore caused a significant improvement in the network strength. The shorter the line between two stations, the less effect the VLBI observations have on its strength as the terrestrial

observations will still control the strength on a 'local' scale whereas the VLBI measurements contribute to the strength over the full network.

Clearly, over a network such as the Ordnance Survey's Primary Triangulation of Great Britain there is little need for such measurements. The network is one of the best surveyed in the world and due to its relatively small size is not grossly affected by cumulative systematic errors (but see Ashkenazi et al, 1978c). However, these tests are of interest in that they show the effect of high accuracy distance and azimuth observations on long baselines in a simulated adjustment of a dense conventional network. These experiments are really a scaled down version of the use of VLBI measurements in a much larger network, for example in the United States triangulation where 5000 km baselines could be observed using large fixed radio telescopes. This application is the basis behind the VLBI observation standard errors used in the tests described here. A VLBI observation with a standard error of 0.01 ppm on these baselines implies a measurement with an accuracy of a few millimetres. Clearly, systematic errors make this impractical but 0.01 ppm length accuracy has already been shown to be feasible on intercontinental baselines (Clark et al, 1978). One should note that the standard error in azimuth is larger than the corresponding value for the distance due to the determination of the baseline direction being affected by the continually changing Earth's orientation and the imperfections in the stellar reference frame to which the observations are referred. There are also several other factors which at the current time would render it impractical to incorporate a VLBI measurement of such high accuracy into a conventional geodetic network. Firstly, it is standard practice to adjust geodetic networks on a particular reference ellipsoid and hence all measurements must be reduced

to this surface. This process requires a knowledge of the geoid-spheroid separation in the area concerned and incurs an error of 1 ppm in the baseline length for an error of 6 m in the geoid-spheroid separation (see §8.2.1). Secondly, a connection of the telescopes to the triangulation by geodetic observations would be necessary (see §8.1.1), as described for the Chilbolton Observatory for example in §6.4.1. This again would result in errors which may lose the advantage gained in the precise VLBI measurement. Finally, the tests here simulate a 'mobile' or 'transportable' antenna. Such antennae do exist (see §8.7.1) but as yet do not approach the accuracy of fixed large antennae which would be capable of the required accuracy.

Having explained the problems associated with applying VLBI measurements to conventional geodetic networks and having simulated this procedure using the Ordnance Survey network, there is one valuable feature of the method not yet considered. If a network were to possess a small systematic error associated with, for example, all its measured distances, the cumulative effect of these errors would quite possibly be significant at the extremities of the network. A VLBI distance measurement across the network may be sufficiently accurate, depending on the VLBI system and the size of the error which is present, to detect the scale discrepancy. Similarly, the technique could detect azimuth control errors although this would be less effective due to the difficulties in determining baseline orientations described previously. The Ordnance Survey network OSGB 70(SN) is an example of such a network in that a 3-4 ppm scale error has been detected (Ashkenazi el al, 1978c) which is partly due to a 2.6 ppm scale difference between Tellurometer and Geodimeter distance measuring instruments. This causes a total displacement in the north of Scotland

of around 1 m, an effect within current VLBI capabilities using a mobile telescope together with a large fixed antenna as a base station (Neill et al, 1979).

A further method of detecting and correcting systematic scale, orientation, and position errors within a network is to solve for parameters describing these errors in the adjustment process (Ashkenazi and Crane, 1980). This method would benefit by the inclusion of VLBI (or satellite-Doppler) measurements in the network, allowing such measurements to make their full contribution to the strength of a network by avoiding the 'swamping' effect of the conventionally surveyed lines over the long VLBI line.

8.3 SURVEY SYSTEM CALIBRATION

The requirement for any surveying system to be used as a standard against which other systems can be compared and calibrated is not that the higher order system be more accurate than the lower order system, but that it is free from systematic biases affecting the lower order system (Ashkenazi, 1979). VLBI has certain inherent features which make it ideally suited to this task. The major asset and the prime advantage of the VLBI technique over most other systems is that it is purely geometrical and is independent of the Earth's gravity field, the limiting factor in most Earth-based systems, e.g. Doppler and laser ranging to satellites. It is therefore of great use in the control of gravity-dependent methods.

The scale is defined by the velocity of propagation of microwaves in vacuo, currently quoted as being accurate to ±0.001 km/s, and its orientation is referenced to a celestial (absolute) system. In defining the orientation, the origin of right ascension is defined by

holding the right ascension of one star fixed, hence all directions are referred to these particular star co-ordinates. The most common observed stars have an R.A. quoted with a standard deviation of $\pm 0.002^s$, the orientation is also defined by the relationship of the instantaneous pole position to the CIO using the published values. These values are accurate to ±0.01" . The accuracy of these three controlling factors means that the VLBI system is relatively free from systematic biases in both scale and orientation.

There are several points, however, which are noteworthy. Primarily, although the system is theoretically relatively free of systematic errors, an error in the mathematical model (see Chapter 2) may introduce a systematic bias into the solution. This would clearly have a damaging effect on the computed results and even if the error did not introduce a systematic bias, its contribution as a random error could degrade the solution. As the accuracy of VLBI is almost independent of the measured baseline distance it is of less use over short distances than it is over very long distances. Moreover, the method of application of the system to a calibration of another system is critical if the maximum benefit is to be attained from the tests (see §8.2).

As already explained, the one most important factor in the usefulness of VLBI as a means of calibrating other systems is the fact that it need not be more accurate than the other system but it must be free of systematic bias. This enables lower accuracy VLBI systems, such as the Canadian VLBI system used and described here, to be applied to this task as well as the higher order systems such as the NRAO Mk III which is expected to give accuracies of around 10 cm. A further feature of the technique is the determination from the adjustment process of the relative synchronisation of the clocks at each station. This

information is of benefit for several other purposes.

8.4 EARTH ORIENTATION PARAMETERS

8.4.1 UT1 and the Rate of Rotation of the Earth

The rate of rotation of the Earth, and hence UT1 (see Appendix A.4), is continually changing. These variations can be divided into three categories, namely secular, periodic, and irregular fluctuations (E.S.A., 1978). Seasonal changes in the distribution of atmospheric masses cause annual periodic variations exhibiting an amplitude of approximately 20 msec, while the zonal lunar waves of the Earth tides (see §2.4.3) cause monthly and fortnightly periodic changes of around 1 msec. Furthermore, irregular changes occur due to the interaction of the Earth's fluid core and the mantle, and also due to the forces exerted by seismic activity (see §8.6.2).

The precision of the VLBI technique allows studies of short term variations with periods of less than a day, of which little is at present known, as well as research into the longer period fluctuations. The latter are detected by the changing components of the baselines providing that the relative clock drifts (§2.4.7) can be isolated from UT1 changes. The baseline length is unaffected by all changes in Earth orientation. The short period fluctuations are detected by continually monitoring the changing phase measured by the interferometer, and hence measuring the rotation rate. However, this similarly suffers from problems caused by the relative clock drifts.

It is noteworthy that observations over a single baseline cannot detect all three orientation parameters (UT1 and spin axis direction) but only two independent combinations of the three. The baseline components, but not the baseline lengths, are affected by orientation

changes and these can be defined for a single baseline by two independent parameters (Shapiro, 1979). As a consequence of this, it is desirable that at least a three antenna array is used for these Earth orientation measurements. Clearly, all such measurements will provide information concerning the geophysical effects causing these changes (Macdonald, 1967) as well as being applicable to other geodetic observing techniques which depend on these data.

The traditional method of measuring UT1 is by optical methods using both photographic zenith tubes and polar telescopes. These methods yield an accuracy of at best 2-3 msec (Langley et al, 1979). The use of satellite-Doppler observations is less important for the determination of UT1 than it is for the determination of polar motion (see §2.2.2 and §8.4.2) due to the relative insensitivity of the system to changes in UT1. However, it can be measured efficiently by laser ranging techniques to reflectors on the Moon and on satellites. Results already achieved using the VLBI technique have shown it to yield valuable contributions to rotation rate measurements. Uncertainties in the observation of UT1 of the order of 0.6 msec from only 6 hours of data have already been reported (Fanselow et al, 1978), and the NRAO Mk III VLBI system is expected to determine variations in UT1 with an accuracy of 0.15 msec (Ryan et al, 1977). Several projects to study these effects are currently either in progress or in the planning stage (Carter et al, 1978, Robertson et al, 1978, and Langley et al, 1979).

UT1 changes will affect the equatorial components of the baseline and not the polar components. Therefore, an east-west baseline is the most efficient configuration for UT1 determinations as it has the maximum possible equatorial component for a given baseline

length. A baseline parallel to the rotation axis has no equatorial component and is hence totally insensitive to UT1 variations. Similarly, near equatorial sources are the best type of source for detecting UT1 changes, whereas polar sources, like polar baselines, are completely insensitive to the effect. Table 8.I summarises the effects of extreme baseline and source configurations on the determination of UT1.

8.4.2 Polar Motion

The causes, effects, and magnitudes of the motion of the axis of rotation of the Earth have already been described in §2.2.2 and will therefore not be dealt with again here. However, as a brief resumé, polar motion in this context is defined as the motion of the instantaneous axis of rotation of the Earth about an axis (in this case defined as the Conventional International Origin, or CIO) which is fixed in relation to the body of the Earth. This fixed axis also contributes towards the definition of the co-ordinate system upon which the baseline components and antennae co-ordinates are based (see §2.1.2.1). Monitoring of this motion will yield a variety of information on the wide range of geophysical effects causing it and will also be applicable to other geodetic measurement techniques and measurements affected by it.

As explained for changes in the rate of rotation of the Earth in §8.4.1, changes in the Earth's orientation affect the components of the baseline but not the overall baseline length. This feature enables the parameters of polar motion to be evaluated. This can be achieved to virtually the precision with which the baseline components themselves can be determined but the changes in pole position are determined with respect to a previously defined starting point rather than with respect

	East-West Baseline (parallel to equator)		North-South Baseline (perpendicular to equator)	
	Equatorial source ($\delta = 0^o$)	Polar source ($\delta = 90^o$)	Equatorial source ($\delta = 0^o$)	Polar source ($\delta = 90^o$)
pole position	no	yes	yes	no
UT1 and rate of rotation of the Earth, source right ascension	yes	no	no	no
source declination	no	yes	yes	no

Table 8.I Sensitivity of extreme baseline and radio source configurations with regard to the Earth orientation parameters and the source positions

to the CIO. The explanation given in §8.4.1 concerning the impracticality of determining all three Earth orientation parameters from observations over a single baseline should also be noted.

The VLBI method currently yields pole positions with an estimated precision of 0.6 m (E.S.A., 1978) but the NRAO Mk III system is expected to determine the polar motion to around 10 cm (Ryan et al, 1977). Furthermore, the overall technique of VLBI is currently in a rapid state of improvement both in accuracy and economy.

Although the determination of the polar motion favours observations of sources perpendicular to the baseline direction, the fact that the majority of suitable sources are nearer to the equator than to the pole, and that these sources are also more suited to applications other than the study of polar motion, means that a north-south baseline is most suited for this application. The effect of extreme baseline and source configurations on the determination of both the Earth orientation parameters and the source co-ordinates is shown in Table 8.I.

8.5 EARTH TIDES

The correction applied in the VLBI data adjustment process, together with a brief description of the phenomenon of Earth tidal movement has already been given in §2.4.3. The maximum tidal effect on the measured delay of an interferometer is of the order of one nanosecond. Clearly, with an a posteriori standard deviation for delay observations of 0.3 ns (equivalent to 10 cm), as was found in the Haystack-Goldstone observations described in §7 and §4.2, this effect is well within the measuring capability of the VLBI technique. Furthermore, the principle tidal wave is semi-diurnal in period

(Melchior, 1978) and hence is a distinctive feature which can be modelled with little ambiguity caused by other effects exhibiting the same period.

The disturbing force exerted on the Earth's crust by the Sun and Moon can be accurately computed and therefore the Love Number defining the vertical tidal component can be estimated from VLBI observations of sufficient accuracy.

A VLBI experiment results in the computation of the baseline components or, in other words, the baseline length and orientation. Consequently, tidal effects on the baseline can be separated from UT1 and polar motion effects (see §8.2) as the latter causes changes only in the orientation and not the length of the baseline, whereas the tides affect both the orientation and the length. Furthermore, VLBI is a direct measure of tidal movement and does not require the application of hypotheses to the observed gravity vector in order to deduce the tidal amplitude (Bonatz and Campbell, 1977) as is the case for present observing techniques. Measurements of this effect will be of great value in the study of the internal constitution of the Earth.

The Love Number was not estimated in this analysis for the data described in Chapters 6 and 7 as insufficient data of a high enough quality was available. However, Robertson (1975) obtained values within ±0.06 of the expected value with a larger data set than used here but which included the August 1972 Haystack-Goldstone data. Although a value for the Love Number was not obtained in this work, the tidal effect is clearly visible in the post-fit residuals obtained when the Earth tide correction was omitted from the mathematical model. This plot, illustrated in Fig. 8.I, was obtained by fixing the source

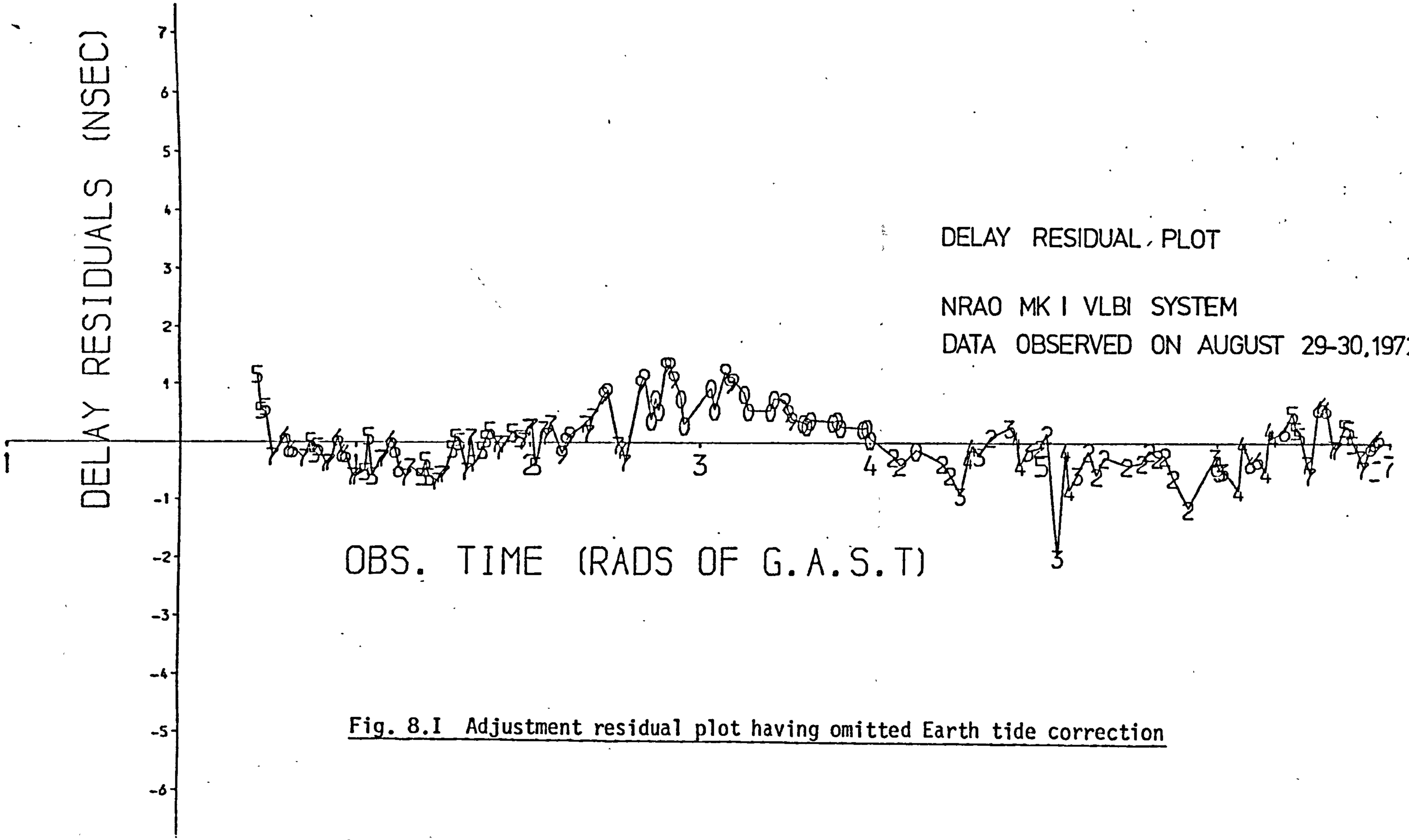

DELAY RESIDUAL PLOT

NRAO MK I VLBI SYSTEM
DATA OBSERVED ON AUGUST 29-30, 1972

Fig. 8.I Adjustment residual plot having omitted Earth tide correction

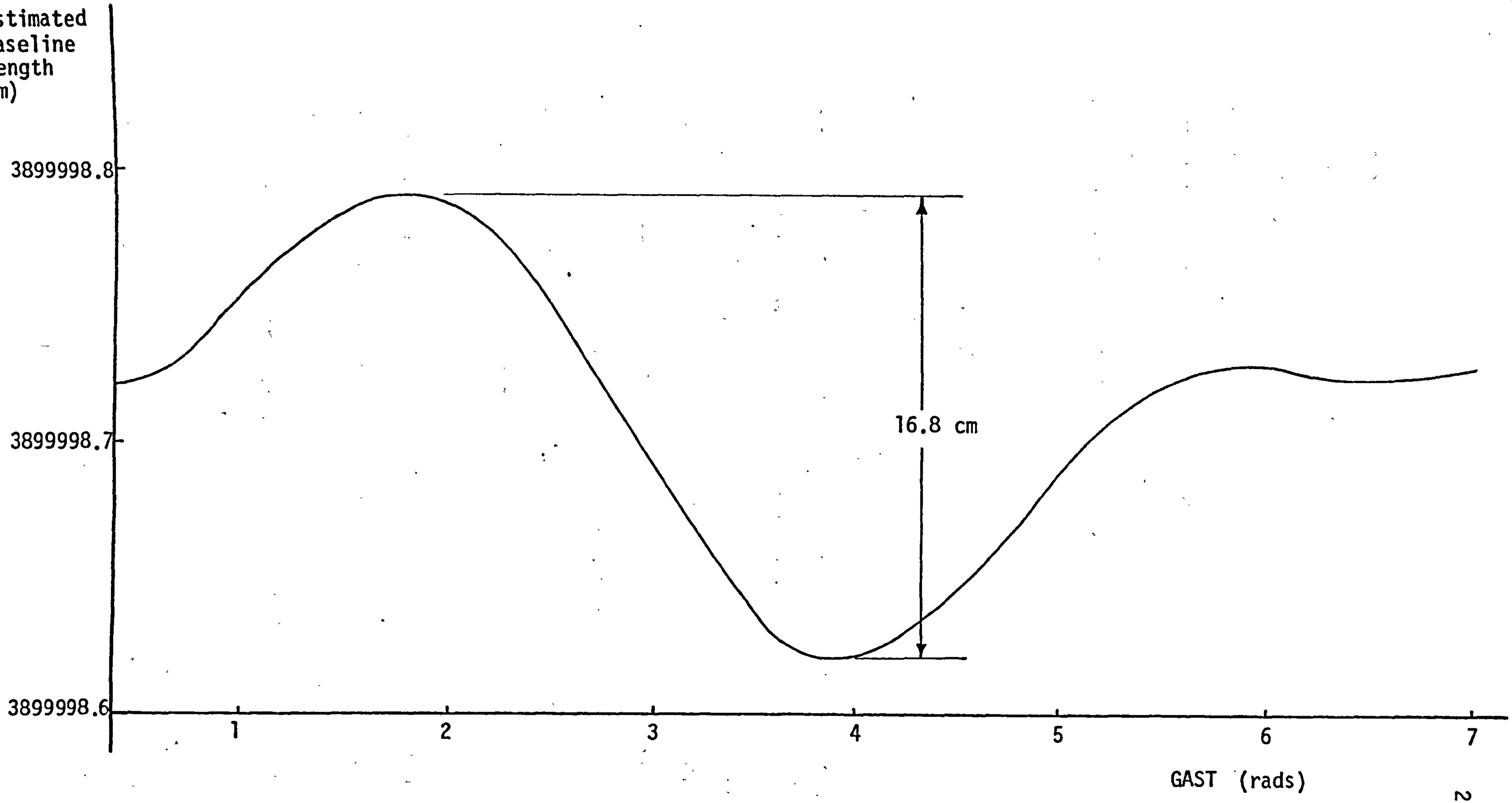

Fig. 8.II The computed time varying length, due to Earth tides, of the Haystack-Goldstone baseline during the experiment of August 29-30th, 1972

co-ordinates and performing a solution for the clock and baseline parameters only. This fixing of the source co-ordinates was necessary because in this experiment the different sources were observed in groups and their co-ordinates would have adjusted to fit the tidal effect within the span of observations on each source. Fig. 8.II is a plot of the computed Earth tides from the model described in §2.4.3. This clearly shows the relationship between the two graphs.

8.6 CRUSTAL MOVEMENTS

8.6.1 Tectonic Plate Movements

It has long been hypothesised that the Earth's crust consists of a number of rigid plates which float on the mantle and which are in relative motion due to convection processes within the interior of the Earth. These plates are known as 'tectonic' plates and are illustrated in Fig. 8.III. Their average movement is of the order of 1-5 cm/year but motions of as much as 15 cm/year have been detected on the 'Noyce' plate in the S.E. Pacific. This tectonic motion results in great strains being exerted at the edges of the plates which contribute greatly to earthquakes and other crustal deformations. The measurement of this movement is of great interest in the study of the Earth's structural properties.

With the advent of the NRAO Mk III VLBI system the measurement of the plate motion is within the capability of the VLBI technique. Even with the previous systems such as the NRAO Mk II interferometer system, long term observations over several years are capable of detecting the relative movement which will exhibit itself as a systematic change in both the length and orientation of a single baseline. Furthermore, with other suitable antennae comprising an interferometer array, the result will be a distortion of the total network. It must be remembered

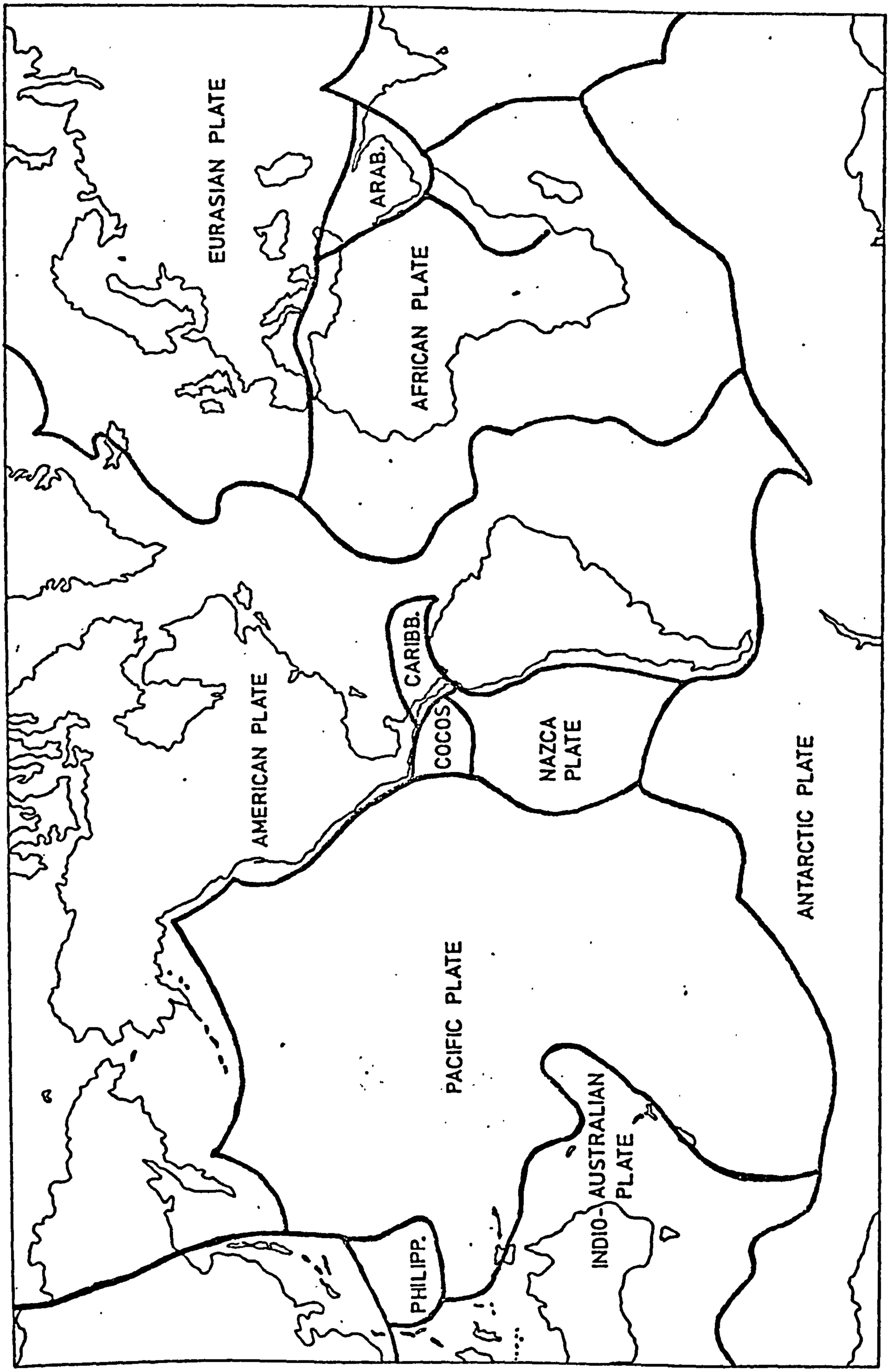

Fig. 8.III Tectonic plate boundaries

however that in performing a plate motion experiment, any local crustal motion(see §8.6.2) or telescope deformation must be established so as to be able to isolate the required information. The establishment of a global reference system has already been discussed in §8.2.1 and such a network would prove useful in the monitoring of tectonic plate motions.

8.6.2 Local Crustal Movements

Local or regional crustal movements occur both at tectonic plate boundaries and also within the plates themselves. The measurement of this motion is of interest for many reasons including its contribution to the understanding and monitoring of the Earth's behaviour and its effect on geodetic networks and engineering structures generally. As stated in §8.6.1, such information is also required for the interpretation of much larger scale deformation measurements.

The effect of local crustal motions on VLBI observations is, as for tectonic plate motion described previously, to change the length and orientation of the baseline.

The nature of the task of monitoring a small regional network as opposed to the worldwide network needed to monitor tectonic plate motion is such that different instrumentation is required. The primary difference is the need for transportable antennae in order to establish several stations in a small area. This topic is discussed further in §8.7.1.

8.7 FURTHER OBSERVING TECHNIQUES

8.7.1 Mobile VLBI

One of the major drawbacks of conventional VLBI is the requirement for large fixed radio telescopes with which to make the observations.

As the signal-to-noise ratio of an interferometer is directly proportional to the antennae surface areas, the sensitivity of an interferometer incorporating a small transportable dish is much less than that obtained using large fixed telescopes. However, the development of small transportable antennae which can be easily moved to different locations has greatly increased the flexibility of the VLBI method, especially in monitoring local crustal motions and small scale regional networks where these systems are most effective.

The major development of this method has been undertaken by the Jet Propulsion Laboratory (JPL) as part of the ARIES (Astronómical Radio Interferometric Earth Surveying) project. Since 1973, observations have been made with a 9 m transportable antenna in order to verify the system and in doing so obtain baseline data in the seismologically active area of California and measurements of the sea slope off the Californian coast. Using a large fixed dish as a base station, accuracies of the technique over baselines of 400 km are around 10 cm (Niell et al, 1979) as derived from comparison with conventional geodetic measurements. This 9 m dish requires about one month to perform the whole observing task and is hence of limited use. A 4 m dish has been developed which it is planned will be able to attain at least the same quality of results but also be able to perform all the operational procedures at a station within a few days. This type of system is of great benefit as it is able to observe a relatively large scale network in a relatively short time as compared with conventional geodetic methods. Furthermore, it exhibits a similar order of accuracy but greater opportunity to continually monitor the network by further observations due to the short time required to make the observations. Other transportable antennae have been used with much lower accuracy results (Nes et al, 1978) but the

concept has nevertheless been proven to be effective for geodetic purposes by the ARIES project.

8.7.2 Satellite VLBI

There are two distinct fundamental concepts in the use of a satellite in a long baseline interferometer. Firstly, there is the application of the satellite as a data link or processor. This would involve its use as a means of transmitting a common local oscillator signal to the antennae of the array and also using it either to transmit received data from the antennae to a processing centre or process the received data itself. The second method would be to use the satellite as a radio source instead of the usual extragalactic sources.

There are several potential modes in which a satellite link system could be used. These range from the use of the satellite simply to transfer a common clock and and local oscillator signal to all the stations, through to its use as a real time data processor to which the data from all observing stations could be transmitted. At the present time, the most practical case is the use of the satellite as a data link to transfer data from one station to another station at which the correlation process is performed. It is not necessary that the processing centre is at one of the antennae and therefore data from both antennae may be transmitted to a common processing centre. This technique has already been successfully tested by a joint United States-Canadian research team (Yen et al, 1977). The three primary advantages of this method are:

i) the facility to use the total received bandwidth of 100-200 MHz (the limit of the receiver system rather than the recording system as in conventional tape recorder interferometry);

ii) the provision of a phase stable connection by the transmission of a common local oscillator signal to all the antennae of the interferometer;

and iii) the capability to perform real-time data processing and correlation, thus saving time and providing a real-time check on the efficient functioning of all parts of the system.

The second of these would also lessen the problem caused by the relative drift of the station clocks disguising effects of geophysical interest. However, there are drawbacks to the method, mainly:

i) the requirement for additional ground stations to receive and transmit the signal from and to the satellite;

and ii) the high cost of satellite communications channels.

There is currently an Astronomy Working Group of the European Space Agency (ESA) examining the feasibility and implementation of a satellite-linked VLBI system in Europe (ESA, 1978, and ESA, 1980). This project has many objectives in the diverse fields in which VLBI is a useful research tool, geodesy and geophysics being included. The development of the system initially comprises of two stages, namely:

i) a clock synchronisation scheme using small ground stations equipped with the NRAO Mk II or Mk III recording systems,

and ii) wide bandwidth signal transmission with real-time data processing. Observations are planned to start in the early 1980's.

There are two proposed systems which use signals emitted from an orbiting satellite instead of the signals received from extragalactic sources, namely MITES (Miniature Interferometer Terminals for Earth Surveying) (Counselman and Shapiro, 1979) and SERIES (Satellite Emission

Radio Interferometric Earth Surveying) (Macdoran, 1979). These systems are designed for use with the NAVSTAR-GPS navigation satellites which have an orbital altitude of 20,000 kms, a period of approximately 12 hours, and are planned to total 24 in number when the system is fully operational (Parkinson, 1979 and Anderle, 1978).

The objective of the two systems is the same; to measure between small portable receivers, baselines of a few hundred kilometres in length to an accuracy of a few centimetres. This is achieved by observing, in an interferometric mode, the signals emitted from at least four satellites simultaneously. Whereas in the present satellite-Doppler system the accuracy is limited by the precision of the satellite ephemeris, this would not be a problem with these systems. The effect of satellite position errors is lessened since it is dependent on the ratio of the baseline length to the satellite altitude. With the high altitudes of the GPS satellites, satellite position errors at the metre level only cause baseline errors at the centimetre level. As ever, the atmosphere would be one of the major sources of error but, with stable conditions and accurate atmospheric modelling, instrumental effects could be a dominant factor.

The major difference between the two systems is in the satellite signal required. The MITES system is designed to use a signal transmitter specially fitted in the satellite for this purpose. On the other hand, the SERIES system uses the random noise signals from the satellites in the same way that noise from extragalactic sources is used in conventional VLBI. Both systems are designed to enable real-time data processing.

8.7.3 Phase Observable

The phase observable has been previously described in §2.1.4.

As explained there and in §4.1.2, the major problem in its use is the unknown number of whole cycles travelled by the signal between its arrival at each of the antennae of the interferometer. This difficulty is primarily caused by phase effects in the atmosphere and in the receiving and recording equipment at the antennae, and these can consequently, with great care and effort, be evaluated and eliminated. If this can be achieved, then the increased resolution of the technique over that obtainable using the group delay observable will prove extremely useful for geodynamical purposes.

The removal of integer cycle ambiguities is easier on short baselines where the atmospheric correction is similar for both antennae and where the delay times are small. However, it is on the long baselines that these high resolution observations are of most significance. In order to achieve these aims it may be necessary or convenient to use techniques such as satellite linked local oscillators, instrumental delay calibrations to reduce instrumental phase errors, dual frequency receiving systems to correct for ionospheric refraction, water vapour radiometers to measure the atmospheric water vapour content, and also lower frequency (i.e. longer wavelength) observations than are currently common for delay measurements for geodetic purposes. All these techniques are currently under development and are being used and tested in varying forms. There are several methods used for observing phase but these will not be discussed here (see Campbell, 1979).

The group delay observing technique is capable of achieving delay resolutions of $\leq$ 0.1 ns providing that large bandwidths of the order of 100 MHz are used. The realisation of this goal is both very costly and complex and it is consequently beyond the scope of many observatories.

However, if the conditions of removing the integer-cycle ambiguities can be met, currently used small bandwidth systems, for example the NRAO Mk II system, will be capable of achieving this order of resolution using the phase observable. Although the analysis of phase observations does not determine the z-component of the observed baseline, observations on east-west baselines will enable studies of all the geophysical effects outlined in this chapter.

CHAPTER 9:

CONCLUSIONS AND SUGGESTIONS FOR FURTHER WORK

9.1 CONCLUSIONS

1. The technique of Very Long Baseline Interferometry determines the distance and direction of the baseline connecting separate radio telescopes, but does not compute the absolute positions of the radio telescopes on the Earth's surface.

2. The Canadian analogue VLBI system used on the Algonquin-Owens Valley-Chilbolton interferometer array, has shown an accuracy of about ±1 m in length and ±0.05" in orientation, from observations of fringe frequency.

3. It proved not possible to adjust delay observations from the Canadian system. This omission resulted in no solution being made for the polar (z-) component of the observed baselines although it had little effect on the accuracy of the determination of the equatorial baseline components due to the dominance of the fringe frequency observations caused by the wide recorded bandwidth of the system.

4. The standard deviations of the baseline parameters are not a true indication of their accuracy. This is primarily due to the observing programme design, unmodelled atmospheric effects, clock instabilities, and equipment errors.

5. The accuracy of the determination of the baseline distance and direction is independent of the baseline length.

6. The accuracy of the NRAO Mk I digital VLBI system has been estimated as about 40 cm in baseline length while the accuracy of the baseline orientation is dominated by the Earth orientation parameters.

7. In the NRAO Mk I system, the delay observations are dominant over the delay rate observations due to the "bandwidth synthesis" technique providing a wide effective (sampled) bandwidth. However, the delay rate data provides a good solution for the equatorial

baseline components (≃ ±1 m).

8. Comparison of results derived using the NULBIP programs have shown good agreement with independently derived results.

9. The VLBI adjustment method computes the co-ordinates of the observed sources, the relative clock synchronisation, and several other parameters (e.g. atmospheric and Earth tidal) within the standard adjustment model.

10. Satellite-Doppler observations computed using the precise ephemeris on the Algonquin-Owens Valley-Chilbolton network have shown an estimated standard error in each component of around 0.7 m. This is consistent with the expectation of the system.

11. A comparison of Doppler and VLBI results over the Algonquin-Chilbolton-Owens Valley array have shown the Doppler precise ephemeris system to require a scale correction of -0.51 ± 0.13 ppm and an eastward longitude rotation of 0.81" ± 0.03" to relate it to a classical geodetic reference system.

12. A comparison of Doppler and VLBI results on the Haystack-Goldstone baseline has shown the Doppler precise ephemeris system to require a scale correction of -0.36 ppm and an eastward longitude rotation of 0.82" to relate it to a classical geodetic reference system.

13. The demonstrated accuracy of the VLBI technique has illustrated its ability to measure UT1, polar motion, local crustal motion, tectonic plate motion, and Earth tides.

14. VLBI has been shown to contribute to the strength of geodetic networks (here the Ordnance Survey Primary Triangulation) although when the measurements are input as distances and directions with their relevant weights they tend to be dominated by the dense terrestrial network and do not contribute efficiently to the adjustment.

9.2 SUGGESTIONS FOR FURTHER WORK

1. Very Long Baseline Interferometry, and specifically its use in geodesy and geophysics, is a rapidly developing field. With the radio astronomy facilities currently available and active, the work which has been started here with the writing and use of the NULBIP suite of computer programs should be continued in order to develop both the method itself and geodetic participation further.

2. Currently, the VLBI data is received in a highly condensed and edited form. Efforts should be made to develop a procedure by which the observations are derived from the raw data in order to establish a greater control and understanding of the observed quantities. YOU MUST BE KIDDING !.

3. The NULBIP suite of programs could be split into two sections, the first being dependent on the particular VLBI observing system and the second being a general adjustment program suitable for any kind of data. This would increase the program efficiency and also enable the use of data from different systems in the same adjustment. GOOD THINKING

4. The application of VLBI measurements to a large geodetic control network should be tested by series of adjustments incorporating a full model of systematic scale and orientation errors.

SEE CRANE, 1980

APPENDIX A

SYSTEMS OF TIME MEASUREMENT

APPENDIX A

SYSTEMS OF TIME MEASUREMENT

A.1 INTRODUCTION

This appendix gives a basic outline of the time systems used in VLBI data reduction. It also explains the specific methods required in this application and, where necessary, gives example calculations. A fuller description of these and other time systems can be found in Explanatory Supplement to the Astronomical Ephemeris* (1961), Smart (1977), and Robbins (1967). All systems of time measurement must be related to a physical phenomenon which can be observed and measured. These phenomena vary for the different time systems and will be indicated in the following explanations.

A.2 EPHEMERIS TIME

Of the three primary time systems, namely Ephemeris, Universal, and Sidereal Times, Ephemeris Time (ET) is the only one which is uniform. It is defined by the gravitational dynamics of the solar system and is independent of the rate of rotation of the Earth, the factor causing non-uniformity in the other two systems.

The fundamental epoch of Ephemeris Time is defined as follows (Trans I.A.U., 10, 72, 1960):

"Ephemeris time is reckoned from the instant, near the beginning of the calendar year A.D. 1900, when the geometric mean longitude of the Sun was 279^{o} 41' 48".04, at which instant the measure of ephemeris time was 1900 January 0^{d} 12^{h} precisely."

---

* Explanatory Supplement to the Astronomical Ephemeris is usually abbreviated to E.S.A.E.

This fundamental epoch is also termed '1900 January 0 at 12^h ephemeris time' or '1900 January 0.5 E.T'. January 0 is the conventional alternative description of December 31st of the previous year. The term January 0.5 implies the epoch half-way through the day January 0 and, as a further example, July 21.4 ET is the epoch $9^h\ 36^m$ Ephemeris Time on July 21 0.4.

The primary unit of Ephemeris Time is the tropical year at the fundamental epoch of 1900 January 0, 12 hr ET and is defined as (E.S.A.E, 1961) "the interval during which the Sun's mean longitude, referred to the mean equinox of date, increases by 360^o". In this definition, the Sun's mean longitude is the longitude of a fictitious Sun apparently moving around the Earth with a constant angular velocity equal to the mean angular velocity of the true Sun. The mean equinox of date is the equinox corrected for the effect of precession only (see §2.3.3) and not for the effect of nutation (see §2.3.4).

To illustrate this definition, referring to Fig. A.I, AγB is the celestial equator when the mean Sun is at γ (the vernal equinox) and the Sun is moving around the ecliptic in the direction of the arrow. At the same time, the vernal equinox moves in the opposite direction, due to the precessional motion of the pole of the equator around the pole of the ecliptic, until the mean Sun and the vernal equinox are again coincident at γ', at which point the celestial equator is defined as A'γ'B'. The tropical year is the time taken to describe 360^o less γγ'.

By observation:

1 tropical year = 365.2422 ephemeris days.

The definition of the ephemeris second is $1/31556925.9747^{th}$ of the tropical year beginning at 1900 January 0.5 ET.

For certain applications the Besselian year is used rather than the

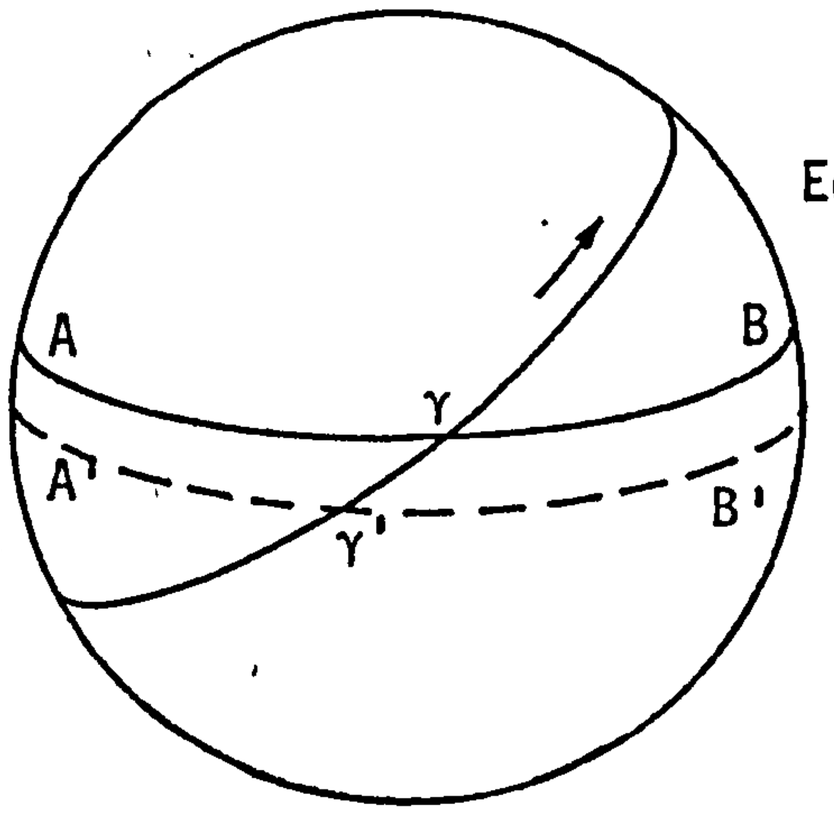

Fig. A.I Ephemeris Time Geometry

tropical year. Its fundamental epoch is defined as being the beginning of the Besselian (fictitious) solar year 1900.0, or 1900 January $0^d.813$ ET. There is aslight difference between the length of the Besselian solar year and the length of the tropical year but this is quite small and may be ignored in these applications. The beginning of the Besselian year is defined as the instant at which the mean longitude of the Sun is $18^h\ 40^m$ or 280^o. The beginning of any Besselian year can therefore be easily calculated. For example, the beginning of the Besselian year 1975, termed 1975.0, is derived from:

1900 January 0.813 ET + (365.2422 x 75) = 1975 January 0.978 ET

Ephemeris Time is computed from observations of Universal Time (UT) and ΔT (the difference ET - UT, equal to 45.6 seconds in 1975 and changing very slowly) and is, in practice, accessible about three years in arrears. Ephemeris Time is of little interest for geodetic applications.

A.3 SIDEREAL TIME

Sidereal Time is the hour angle of the vernal equinox and is a measure of the diurnal rotation of the Earth. Each meridian on the

Earth has its own Local Sidereal Time which is related to Greenwich Sidereal Time (GST) by the relation:

$$LST = GST + \lambda,$$

where λ = the longitude of the local meridian reckoned from Greenwich and measured positive eastwards in units of time.

The vernal equinox is continually in motion due to the effects of precession (§2.3.3) and nutation (§2.3.4). This gives rise to two separate and slightly different sidereal time scales, namely Apparent Sidereal Time (AST) and Mean Sidereal Time (MST). Apparent Sidereal Time is defined as the hour angle of the true equinox. The true equinox is the intersection of the true equator of date and the ecliptic of date which are established by correcting for the effects of both precession and nutation. Apparent Sidereal Time is therefore subject to periodic inequalities. Mean Sidereal Time is the hour angle of the mean equinox defined by the intersection of the mean equator of date and the mean ecliptic. 'Mean' in this context implying corrected for the effect of precession only and not for the effect of nutation. The mean sidereal day is $0^s.0084$ shorter than the actual period of rotation of the Earth due to precession. The difference (AST - MST) is termed the 'equation of the equinoxes' and is a maximum of $1^s.2$ (Robbins, 1967). Both Greenwich Apparent Sidereal Time (GAST) and Greenwich Mean Sidereal Time (GMST) are tabulated for 0 hr UT of each day of the year in the Astronomical Ephemeris. The relationship between Sidereal and Universal Time is given in (2.38). Greenwich Apparent Sidereal Time is the 'true' time and hence is used in the VLBI data reduction process.

A.4 UNIVERSAL TIME

Universal Time (UT) is a very close approximation to the mean diurnal motion of the Sun and is defined as (E.S.A.E., 1961), *"12 hours plus the Greenwich hour angle of a point on the equator whose right ascension, measured from the mean equinox of date is:*

$$R_u = 18^h\ 38^m\ 45^s.836 + 8640184^s.542T_u + 0^s.0929T_u^2$$

where T_u is the number of Julian centuries (see §X.5) of 36525 days of universal time elapsed since the epoch of Greenwich mean noon (regarded as 12^h UT) on 1900 January 0."

There are four slightly different types of UT, namely UT0, UT1, UT2, and UTC. Universal Time is determined (Bomford, 1975) from observations of star transits over the local meridians of several observatories (54 in 1967) in order to determine their own versions of UT. Each observatory therefore determines from these observations its own particular UT0. As the observations on which each UT0 is based contain many errors, the value of UT0 for each observatory is reduced to the mean axis of rotation of the Earth (CIO) in order to give the individual observatory value of UT1 by the equation:

$$UT1 = UT0 - \frac{1}{15}(x_p \sin\lambda + y_p \cos\lambda)\tan\phi\ ,$$

where x_p and y_p = the co-ordinates of the instantaneous pole relative to the CIO pole in seconds of arc, x_p being positive southwards along the Greenwich meridian and y_p being positive along the meridian 90^oW,

and ϕ and λ = adopted values for the latitude and longitude of the observatory.

The final value of UT1 is determined by taking the weighted mean of the

participating observatories. UT2 is UT1 plus a correction to account for the annual fluctuation in the rate of rotation of the Earth. The procedures used to determine all these values are described in Robbins, (1967). UTC (Co-ordinated UT) is the measure of UT defined by atomic time. Since 1972 January 1 0 hr UT, UTC has been a system based on seconds of atomic time (AT) such that the duration of 1^s UTC is 1^s AT, and is a constant. At this epoch, UTC was defined to be International Atomic Time (IAT) minus 10^s exactly. A fuller description of atomic time and the adjustments used to maintain UTC after this epoch will not be dealt with here (see Robbins, 1976*). Previous to this change, the procedure was as described in (Bomford, 1971) and (Robbins, 1967). The relationships between UT1, UT2 and UTC are published monthly in the BIH Circular D and annually in the BIH Rapport Annuel.

UT1 is the type of Universal Time of most interest to the geodesist as it is the 'true' UT representing the actual orientation of the Earth at any instant. The station clocks at the VLBI receiving stations provide either UTC or a form of atomic time which can easily be related to UTC. Consequently, observation epochs derived from VLBI experiments using atomic frequency standards can be easily related to the desired UT1 epochs.

A.5 JULIAN DATE

The Julian day number is defined to be the number of astronomical days, measured from Greenwich noon of the day in question, since Greenwich

---

* Robbins, A.R., 1976, *Military Engineering, Vol. XIII – Part IX, Field Geodetic Astronomy*, Ministry of Defence.

mean noon on BC 4713 January 1. The Julian day number of the first day in each month during this century is tabulated in the Astronomical Ephemeris and the E.S.A.E. The Julian date can be expressed, in the same manner as for Ephemeris Time (see §A.2), as the Julian day number plus the fraction of the day elapsed since the preceding noon.

This principle may be extended to define the Julian Ephemeris Date (J.E.D.) which relates the beginning of the Julian ephemeris day to 12 hr ET. This distinction is of no significance in the application to VLBI but may be for other purposes. The fundamental epoch 1900 January 0.5 ET is defined as J.E.D. 2415020.0.

A.6 COMPUTATION OF TIME INTERVAL

A.6.1 Tropical Year Interval

If, given an epoch of observation, the time interval between a fundamental epoch and that epoch in terms of tropical years is required, then the following procedure should be adopted:

i) determine the Julian Day Number at 0 hrs UT on the day of observation (see §A.5);

ii) compute the fraction of the day from 0 hr UT to the epoch of observation;

iii) add the above two quantities to give the Julian Date of observation;

iv) subtract the Julian Date of the fundamental epoch;

v) divide by the number of days in a tropical year (see §A.2), i.e. 365.2422.

A.6.2 Julian Centuries Interval

This computation proceeds in the following manner:

i) determine the Julian Day Number at 0 hrs UT on the day of observation;

ii) compute the fraction of the day from 0 hr UT to the epoch of observation and incorporating the difference between UT and ET;

iii) add the above two quantities to give the Julian Ephemeris Date of the observation;

iv) subtract the Julian Ephemeris Date of the fundamental epoch;

v) divide by 36525, the number of Ephemeris Days per Julian Ephemeris Century.

The difference between an interval in tropical centuries and an interval in Julian centuries is small enough to be insignificant in these VLBI applications.

A.7 LORAN C

Commissioned in 1957, Loran C is primarily a navigation system using a low frequency pulsed signal in a hyperbolic position fixing mode (Powell, 1978). A large part of the northern hemisphere is covered by Loran C "chains" which feature a master station and up to four slave stations continuously transmitting recognisable pulse patterns. Each master station emits nine pulses and each slave station emits eight pulses at a set interval after the master station emission. Therefore, the signals from each chain and from each individual station within each chain are easily recognisable. The emission times of the signals are precisely related to the US Naval Observatory's (USNO) Master Clock and hence synchronisation between a VLBI station clock and Loran C pulse emissions relates the VLBI station clock to the USNO Master Clock providing that the propagation delay can be computed. The 100 kHz

pulsed transmission means that it is a ground wave system having little interference from the resulting sky waves. This also results in the system being affected very little by ionospheric changes.

The Loran C system and its use and accuracy as a navigation aid is described in Senus (1976).

APPENDIX B

ROTATION MATRICES

APPENDIX B

ROTATION MATRICES

If a rotation about the k^{th} axis of a right-handed co-ordinate system through an anticlockwise angle θ, when looking from the positive end of the axis towards the origin, is denoted by $R_k(\theta)$, then the three rotation matrices are:

$$R_1(\theta) = \begin{bmatrix} 1 & 0 & 0 \\ 0 & \cos\theta & \sin\theta \\ 0 & -\sin\theta & \cos\theta \end{bmatrix} ,$$

$$R_2(\theta) = \begin{bmatrix} \cos\theta & 0 & -\sin\theta \\ 0 & 1 & 0 \\ \sin\theta & 0 & \cos\theta \end{bmatrix} ,$$

$$R_3(\theta) = \begin{bmatrix} \cos\theta & \sin\theta & 0 \\ -\sin\theta & \cos\theta & 0 \\ 0 & 0 & 1 \end{bmatrix} .$$

The product of, say, three rotations of firstly an angle γ about the 1-axis, followed by an angle α about the 3-axis of the transformed system, and lastly through an angle β about the 2-axis of the doubly-transformed system, is represented by:

$$R_2(\beta)\ R_3(\alpha)\ R_1(\gamma)_Z \ .$$

The multiplication of these rotation matrices is not commutative.

If a reflection about the k^{th} axis is denoted by P_k then the reflection matrices are:

$$P_1 = \begin{bmatrix} -1 & 0 & 0 \\ 0 & 1 & 0 \\ 0 & 0 & 1 \end{bmatrix} ,$$

$$P_2 = \begin{bmatrix} 1 & 0 & 0 \\ 0 & -1 & 0 \\ 0 & 0 & 1 \end{bmatrix} ,$$

$$P_3 = \begin{bmatrix} 1 & 0 & 0 \\ 0 & 1 & 0 \\ 0 & 0 & -1 \end{bmatrix} .$$

Reflection matrices are commutative and an odd number of reflections changes the handedness of the co-ordinate system.

APPENDIX C

THE NUTATION ANGLES

APPENDIX C

THE NUTATION ANGLES

C.1 COMPUTATION OF THE NUTATION ANGLES

The nutation in obliquity and the nutation in longitude are computed from tables published in the Explanatory Supplement to the Astronomical Ephemeris (E.S.A.E.). These tables are reproduced here together with the expressions for the required arguments, ℓ, ℓ', F, D, and Ω. These parameters are derived from:

$$\begin{aligned} \ell &= \lambda_m - \Omega - \omega_m \\ \ell' &= \lambda_s - \omega_s \\ F &= \lambda_m - \Omega \\ D &= \lambda_m - \lambda_s \\ \Omega &= \Omega \end{aligned} \qquad \text{(C.1)}$$

where Ω = the longitude of the mean ascending node of the lunar orbit on the ecliptic as measured from the mean equinox of date,

ω_m = the 'argument' of the point when the Moon is nearest to the Earth (i.e. the lunar perigee),

ω_s = the mean longitude of the solar perigee measured from the mean equinox of date,

and λ_s = the geometric mean longitude of the Sun as measured from the mean equinox of date.

These terms are illustrated in Fig. C.I.

The expressions for these parameters are:

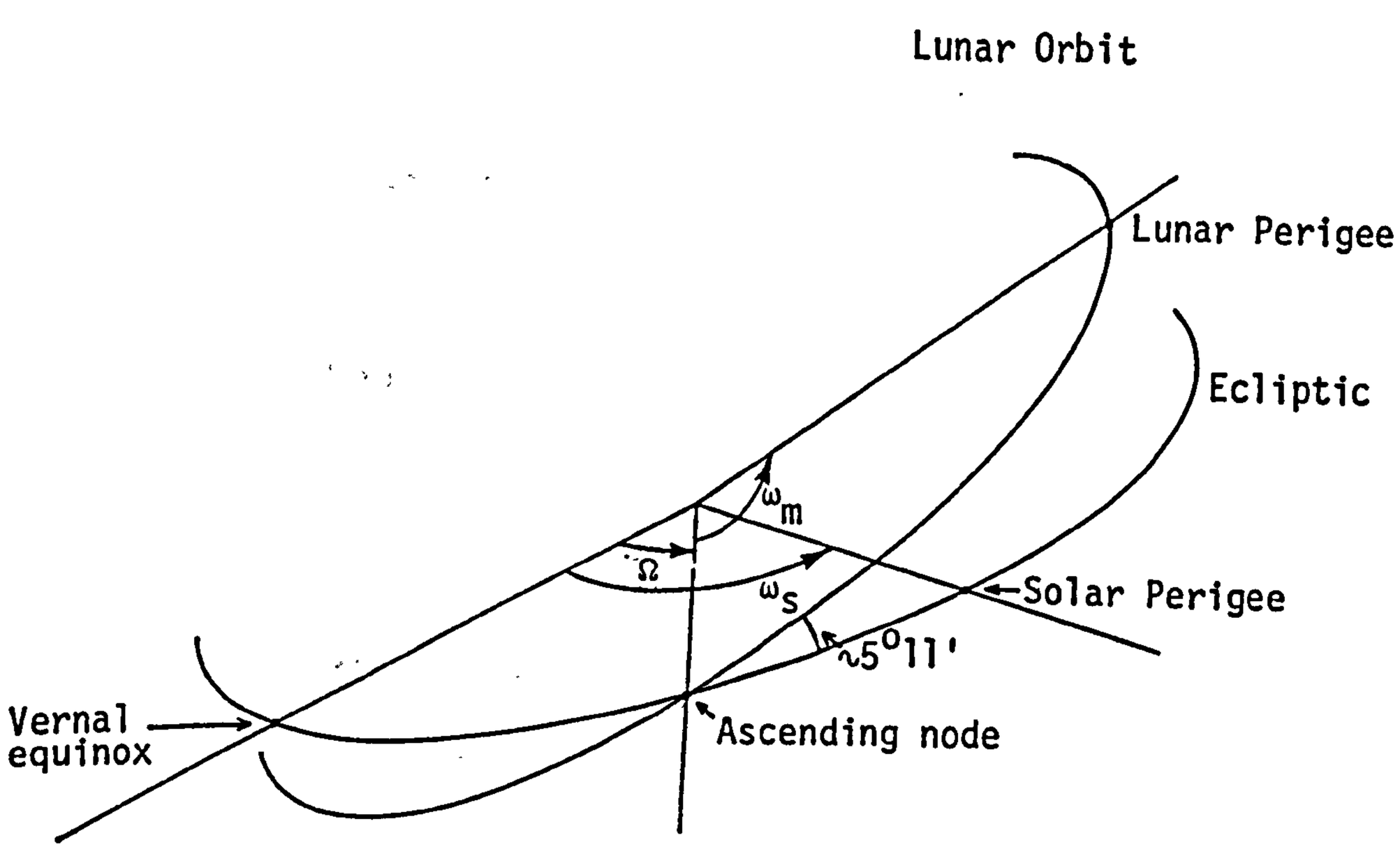
Lunar Orbit
Lunar Perigee
Ecliptic
ω_m
Ω
ω_s
Solar Perigee
$\sim 5^o 11'$
Vernal equinox
Ascending node

Fig. C.I

$$\ell = 296^{o}.10460\ 8 + 13^{o}.06499\ 24465d + 0^{o}.00068\ 90D^{2} + \\ + 0^{o}.00000\ 0295D^{3}$$

$$\ell' = 358^{o}.47583\ 3 + 0^{o}.98560\ 02669d - 0^{o}.00001\ 12D^{2} - \\ - 0.00000\ 0068D^{3}$$

$$F = 11^{o}.25088\ 9 + 13^{o}.22935\ 04490d - 0^{o}.00024\ 07D^{2} - \\ - 0^{o}.00000\ 0007D^{3} \qquad (C.2)$$

$$D = 350^{o}.73748\ 6 + 12^{o}.19074\ 91914d - 0^{o}.00010\ 76D^{2} + \\ + 0^{o}.00000\ 0039D^{3}$$

$$\Omega = 259^{o}.18327\ 5 - 0^{o}.05295\ 39222 + 0^{o}.00015\ 57D^{2} + \\ + 0^{o}.00000\ 0046D^{3}$$

where the fundamental epoch is 1900 January $0^{d}.5$ ET (J.E.D. 241 5020.0), d is measured in days, and D is measured in units of 10000 days. With T being the time measured in Julian centuries of 36525 days since the fundamental epoch, the series for the nutation angles comprising 69 terms in $\Delta\psi$ and 40 terms in $\Delta\varepsilon$ are tabulated as:

Period (days)	ARGUMENT Multiple of					LONGITUDE Coefficient of sine argument		OBLIQUITY Coefficient of cosine argument	
	ℓ	ℓ'	F	D	Ω	Unit = 0".0001			
6798					+1	-172327	-173.7T	+92100	+9.1T
3399					+2	+2088	+0.2T	-904	+0.4T
1305	-2		+2		+1	+45		-24	
1095	+2		-2			+10			
6786		-2	+2	-2	+1	-4		-2	
1616	-2		+2		+2	-3		+2	
3233	+1	-1		-1		-2			
183			+2	-2	+2	-12729	-1.3T	+5522	-2.9T
365		+1				+1261	-3.1T		

/contd

Period (days)	ARGUMENT Multiple of					LONGITUDE Coefficient of sine argument		OBLIQUITY Coefficient of cosine argument	
	ℓ	ℓ'	F	D	Ω	Unit = 0".0001			
122		+1	+2	-2	+2	-497	+1.2T	+216	-0.6T
365		-1	+2	-2	+2	+214	-0.5T	-93	+0.3T
178			+2	-2	+1	+124	+0.1T	-66	
206	+2			-2		+45			
173			+2	-2		-21			
183		+2				+16	-0.1T		
386		+1			+1	-15		+8	
91		+2	+2	-2	+2	-15	+0.1T	+7	
347		-1			+1	-10		+5	
200	-2			+2	+1	-5		+3	
347		-1	+2	-2	+1	-5		+3	
212	+2			-2	+1	+4		-2	
120		+1	+2	-2	+1	+3		-2	
412	+1			-1		-3			
13.7			+2		+2	-2037	-0.2T	+884	-0.5T
27.6	+1					+675	+0.1T		
13.6			+2		+1	-342	-0.4T	+183	
9.1	+1		+2		+2	-261		+113	-0.1T
31.8	+1			-2		-149			
27.1	-1		+2		+2	+114		-50	
14.8				+2		+60			
27.7	+1				+1	+58		-31	
27.4	-1				+1	-57		+30	
9.6	-1		+2	+2	+2	-52		+22	
9.1	+1		+2		+1	-44		+23	
7.1			+2	+2	+2	-32		+14	
13.8	+2					+28			
23.9	+1		+2	-2	+2	+26		-11	
6.9	+2		+2		+2	-26		+11	
13.6			+2			+25			
27.0	-1		+2		+1	+19		-10	
32.0	-1			+2	+1	+14		-7	

/contd

Period (days)	ARGUMENT Multiple of					LONGITUDE Coefficient of sine argument	OBLIQUITY Coefficient of cosine argument
	ℓ	ℓ'	F	D	Ω	Unit = 0".0001	
31.7	+1			-2	+1	-13	+7
9.5	-1		+2	+2	+1	-9	+5
34.8	+1	+1		-2		-7	
13.2		+1	+2		+2	+7	-3
9.6	+1			+2		+6	
14.8				+2	+1	-6	+3
14.2		-1	+2		+2	-6	+3
5.6	+1		+2	+2	+2	-6	+3
12.8	+2		+2	-2	+2	+6	-2
14.7				-2	+1	-5	+3
7.1			+2	+2	+1	-5	+3
23.9	+1		+2	-2	+1	+5	-3
29.5				+1		-4	
15.4		+1		-2		-4	
29.8	+1	-1				+4	
26.9	+1		-2			+4	
6.9	+2		+2		+1	-4	+2
9.1	+1		+2			+3	
25.6	+1	+1				-3	
9.4	+1	-1	+2		+2	-3	
13.7	-2				+1	-2	
32.6	-1		+2	-2	+1	-2	
13.8	+2				+1	+2	
9.8	-1	-1	+2	+2	+2	-2	
7.2		-1	+2	+2	+2	-2	
27.8	+1				+2	-2	
8.9	+1	+1	+2		+2	+2	
5.5	+3		+2		+2	-2	

These are combined in a form such that for the nutation in longitude:

$$\Delta\psi = (-17.2327" - 0.01737"T)\sin\Omega + (0.2088" + 0.00002"T)\sin 2\Omega$$

$$+ 0.0045"\sin(\Omega + 2F - 2\ell) + \ldots. \text{ etc.}$$

or, more generally:

$$\Delta\psi = \sum_{i=1}^{69} (a_i+b_iT)\sin(c_i\ell+d_i\ell'+e_iF+f_iD+g_i\Omega). \qquad (C.3)$$

A similar process applies to the formulation of the nutation in obliquity using the appropriate coefficients and arguments such that:

$$\Delta\varepsilon = \sum_{i=1}^{40} (y_i+x_iT)\cos(c_i\ell+d_i\ell'+e_iF+f_iD+g_i\Omega). \qquad (C.4)$$

C.2 RATE OF CHANGE OF NUTATION

For use in the computation of the rate of change of nutation (§2.5.2), the rate of change of $\Delta\psi$ and $\Delta\varepsilon$ must be computed. From (C.3):

$$\dot{\Delta\psi} = \sum_{1}^{69} \Big[b_i\sin(c_i\ell+d_i\ell'+e_iF+f_iD+g_i\Omega)\frac{dT}{dt}$$

$$+ \left(c_i \frac{d\ell}{dt} + d_i \frac{d\ell'}{dt} + e_i \frac{dF}{dt} + f_i \frac{dD}{dt} + g_i \frac{d\Omega}{dt}\right) (a_i+b_iT) \qquad (C.5)$$

$$\cos(c_i\ell+d_i\ell'+e_iF+f_iD+g_i\Omega)\Big] \text{ arcsec/sec}$$

and from (C.4):

$$\dot{\Delta\varepsilon} = \sum_{i=1}^{40} \Big[y_i\cos(c_i\ell+d_i\ell'+e_iF+f_iD+g_i\Omega)\frac{dT}{dt}$$

$$- (x_i+y_iT)\sin(c_i\ell+d_i\ell'+e_iF+f_iD+g_i\Omega). \qquad (C.6)$$

$$\left(c_i \frac{d\ell}{dt} + d_i \frac{d\ell'}{dt} + e_i \frac{dF}{dt} + f_i \frac{dD}{dt} + g_i \frac{d\Omega}{dt}\right)\Big] \text{ arcsec/sec}$$

The differentials of (C.2) with respect to time for incorporation into (C.5) and (C.6) are expressed in deg/sec and are given by:

$$\frac{d\ell}{dt} = 13.0649924465^{o}\,\frac{dd}{dt} + 0.001378^{o}\,D\,\frac{dD}{dt} + 0.000000885^{o}D^{2}\,\frac{dD}{dt}\,,$$

$$\frac{d\ell'}{dt} = 0.9856002669^{o}\,\frac{dd}{dt} - 0.0000224^{o}D\,\frac{dD}{dt} - 0.000000204^{o}D^{2}\,\frac{dD}{dt}\,,$$

$$\frac{dF}{dt} = 13.229350449^{o}\,\frac{dd}{dt} - 0.0004814^{o}D\,\frac{dD}{dt} - 0.000000021^{o}D^{2}\,\frac{dD}{dt}\,, \quad (C.7)$$

$$\frac{dD}{dt} = 12.1907491914^{o}\,\frac{dd}{dt} - 0.0002152^{o}D\,\frac{dD}{dt} + 0.000000117^{o}D^{2}\,\frac{dD}{dt}\,,$$

$$\frac{d\Omega}{dt} = -0.0529539222^{o}\,\frac{dd}{dt} + 0.0003114^{o}D\,\frac{dD}{dt} + 0.000000138^{o}D^{2}\,\frac{dD}{dt}\,,$$

where $\frac{dd}{dt} = \frac{1}{86400}$,

and $\frac{dD}{dt} = \frac{1}{86400 \times 10000}$

Furthermore, for use in the computation of the nutation matrix N and its derivative $\dot{N}$, the rate of change of the obliquity of the ecliptic is given by:

$$\dot{\varepsilon} = -0.0130125\,\frac{dT}{dt} - 0.00000328T\,\frac{dT}{dt} + 0.000001509T^{2}\,\frac{dT}{dt} \quad \text{deg/sec} \quad (C.8)$$

where T = the time measured in tropical centuries since epoch 1900 January 0.5 ET (see Appendix A.6),

and $\frac{dT}{dt} = \frac{1}{26524.22 \times 86400}$

---

* The table of the nutation angles $\Delta\psi$ and $\Delta\varepsilon$ is taken from (E.S.A.E., 1977) and is reproduced by kind permission of Her Majesty's Stationery Office.

APPENDIX D

MATHEMATICAL MODELLING OF THE TROPOSPHERE

APPENDIX D

MATHEMATICAL MODELLING OF THE TROPOSPHERE

D.1 INTRODUCTION

A knowledge of the meteorological conditions prevailing at the time of a VLBI observation enables a correction to be computed and applied to that observation in order to account for the effect of the refraction, in the Earth's atmosphere, of the incoming radio wave. This appendix outlines two mathematical models, namely Chao's Model and the simplified Hopfield Model, which compute the required tropospheric correction to an observation. It also relates the different units in which meteorological data are observed to those units which are required in the derived formulae for each model.

D.2 METEOROLOGICAL DATA UNITS AND CONVERSION FACTORS

Meteorological data is observed in several different units depending on the type, age, and country of manufacture of the equipment and also the country of observation. The simplified Hopfield Model derived inthis appendix employs atmospheric and partial water vapour pressures in millibars, and temperature in degrees Kelvin. Chao's model uses the relative humidity (RH, $0 \leqslant RH \leqslant 1$) in preference to the partial water vapour pressure. This section covers the conversion factors between other commonly used units and those required.

D.2.1 Atmospheric Pressure

Atmospheric pressure can be measured by means of either a barometer or an altimeter. The conversion factors from several commonly used units of pressure to millibars are tabulated in Table D.I. These values are

Pressure unit	Conversion factor to millibars (mb)
Standard Atmosphere	1013.25
Torr	1.3332
1 inch of Mercury	33.864
1 cm of Mercury	13.332
1 foot of water	29.892

Table D.I Conversion factors for pressure units

taken from the Smithsonian Meteorological Tables and are sufficiently accurate for use in tropospheric models, even though they assume standard conditions. The Smithsonian Tables contain all the necessary formulae if a higher degree of accuracy is required. The Smithsonian Tables also contain standard tables of conversion factors between observed altimeter readings and the equivalent pressure in millibars.

The application of the atmospheric pressure to the mathematical model requires that the observed pressure be at the station location. This is not generally possible but a simple correction can be applied to the observed pressure in order to account for the height difference between the station and the place of observation. Similarly, observed pressure supplied in terms of mean sea level by many weather stations can be easily converted. The formula for the variation of pressure with height can be simplified, without significant loss of accuracy, to (Bomford, 1975):

$$\frac{dP}{dh} = -\frac{0.0342P}{T} \text{ mb/m} ,$$

where P = observed atmospheric pressure (mb),

T = air temperature (K),

and h = height above mean sea level (m).

Integrating this formula gives:

$$P_2 = P_1 \exp\left[\frac{-0.0342\Delta h}{T}\right] \text{ mb} , \qquad (D.1)$$

where P_1 and P_2 = observed and adjusted pressures respectively,

and Δh = height difference between the two positions.

D.2.2 Temperature

Air temperatures are commonly measured in either degrees Centrigrade (^{o}C

or degrees Fahrenheit (^{o}F). The conversion to degrees Kelvin (K) is:

$$K = {}^{o}C + 273.16 = ({}^{o}F - 32) \times {}^{5}/_{9} + 273.16 \qquad (D.2)$$

Temperatures should preferably be taken using an aspirated thermometer with radiation screening which should be away from any heat sources and sufficiently elevated to avoid the effects of ground radiation.

D.2.3 Partial Water Vapour Pressure

The partial water vapour pressure can be computed from observations of either relative humidity or 'wet bulb' temperature. Both these observations can prove troublesome and great care should be taken to ensure reliable readings (Deeth, 1978). From observations of dry and wet bulb temperatures (T and T_w respectively) the partial water vapour pressure is given by:

$$e = e_w - 4.527 \times 10^{-4}(1 + 1.677 \times 10^{-3}T_w)(T-T_w).P \ , \qquad (D.3)$$

where e = partial water vapour pressure (mb),

e_w = saturation water vapour pressure (mb),

P = atmospheric pressure (mb),

and T and T_w are expressed in degrees Kelvin.

The saturation water vapour pressure is given by (Goff and Gratch, 1946):

$$e_w = e_{ws}\left[\frac{T_s}{T_w}\right]^{5.02808} \exp[-g(T_w)] \qquad (D.4)$$

where T_s = steam point temperature (373.16K),

e_{ws} = saturation water vapour pressure at T_s (1013.246 mb),

and $g(T_w)$ is a series of terms such that:

$$g(T_w) = g_1(T_w) + g_2(T_w) + g_3(T_w), \qquad (D.5)$$

where $g_1(T_W) = 18.19728\left[\frac{T_s}{T_W}\right] - 1$,

$$g_2(T_W) = 0.01872651 - \exp\left\{-8.03945\left[\frac{T_s}{T_W} - 1\right]\right\} ,$$

and $$g_3(T_W) = 3.1813 \times 10^{-7}\left\{\exp\left[26.1205\left[1 - \frac{T_W}{T_s}\right]\right] - 1\right\} .$$

If measurements of relative humidity are available, the formula for relative humidity of:

$$R_H = \frac{e/(P - e)}{e_W^*/(P - e_W^*)} , \qquad (D.6)$$

where e_W^* = saturation water vapour pressure at the temperature computed using (D.4) with T_W replaced by T,

may be rearranged to give:

$$e = \frac{e_W . R_H P}{P + e_W^*(R_H - 1)} . \qquad (D.7)$$

D.3 HOPFIELD'S SIMPLIFIED MODEL

Retardation and bending of a signal path passing through the atmosphere is a function of the refractive index, n, of the atmosphere. The refractive index will usually be non-uniform along the signal path and is a function of temperature, pressure, and partial water vapour pressure, such that the refractivity can be expressed as an empirical relationship between these terms. One such relationship is (Smith and Weintraub, 1953):

$$N = (n-1)10^6 = \frac{77.6}{T}\left[P + \frac{4810e}{T}\right], \qquad (D.8)$$

where N = refractivity,

T = air temperature (K),

P = atmospheric pressure (mb),

and e = partial water vapour pressure (mb).

It is clear from (D.8) that the refractivity can be split into separate wet and dry components such that:

$$N = N_d + N_w \,.$$

A model given by Hopfield (1969) assumes the horizontal gradient of the refractive profile to be negligible and gives the dry refractivity N_d as:

$$N_d = \frac{N_{ds}}{(h_d - h_s)^{\mu}} \cdot (h_d - h)^{\mu} \qquad (D.9)$$

where h_d = model height above the geoid at which the dry refractivity becomes negligible,

h_s = station height above the geoid,

N_{ds} = surface dry refractivity depending on surface measurements of temperature and pressure,

h = height of a general point above the geoid,

and $\mu = \frac{g}{R\alpha} - 1$

where α = temperature lapse rate,

g = acceleration due to gravity,

and R = gas constant for a unit mass of air.

Similarly, the wet refractivity is given by:

$$N_w = \frac{N_{ws}}{(h_w - h_s)^{\mu}} \cdot (h_w - h)^{\mu} \qquad (D.10)$$

The adoption of a quartic profile (i.e. $\mu = 4$) closely approximates to observed data (Hopfield, 1977). The model height for the dry component

has been determined as (Hopfield, 1976):

$$h_{ds} = h_d - h_s = 40110.0 + 148.81(T - 273.16) \text{ m},$$

and can be assumed constant both temporally and on a global basis.

The model height of the wet refractivity profile is much more difficult to establish as it is subject to diurnal and seasonal changes (larger at night and in summer) and varies with the sunspot cycle (Hopfield, 1976). The distribution of water vapour within the atmosphere is also unpredictable and causes inaccuracy in the modelling process. An average value for the model height of the wet profile is (Hopfield, 1972):

$$h_{ws} = h_w - h_s = 11000 \text{ m}.$$

The effect of the inaccuracy in modelling the wet component on the total atmospheric correction is lessened by the fact that the wet component forms only 10% of the total refractivity.

The contribution to the signal path length due to atmospheric refraction, neglecting the effect of bending of the signal path (see §2.4.5) is given by:

$$\Delta s = \int (n-1) ds,$$

$$= \int_{r_o}^{r_t} (N \times 10^{-6}) \frac{ds}{dr} \cdot dr , \qquad (D.11)$$

where r_o = geocentric radius to the station,

and r_t = geocentric radius at which N becomes negligible.

The relationship between the distance of any point along the signal path from a source and its geocentric radius is illustrated in Fig. D.I and is given by:

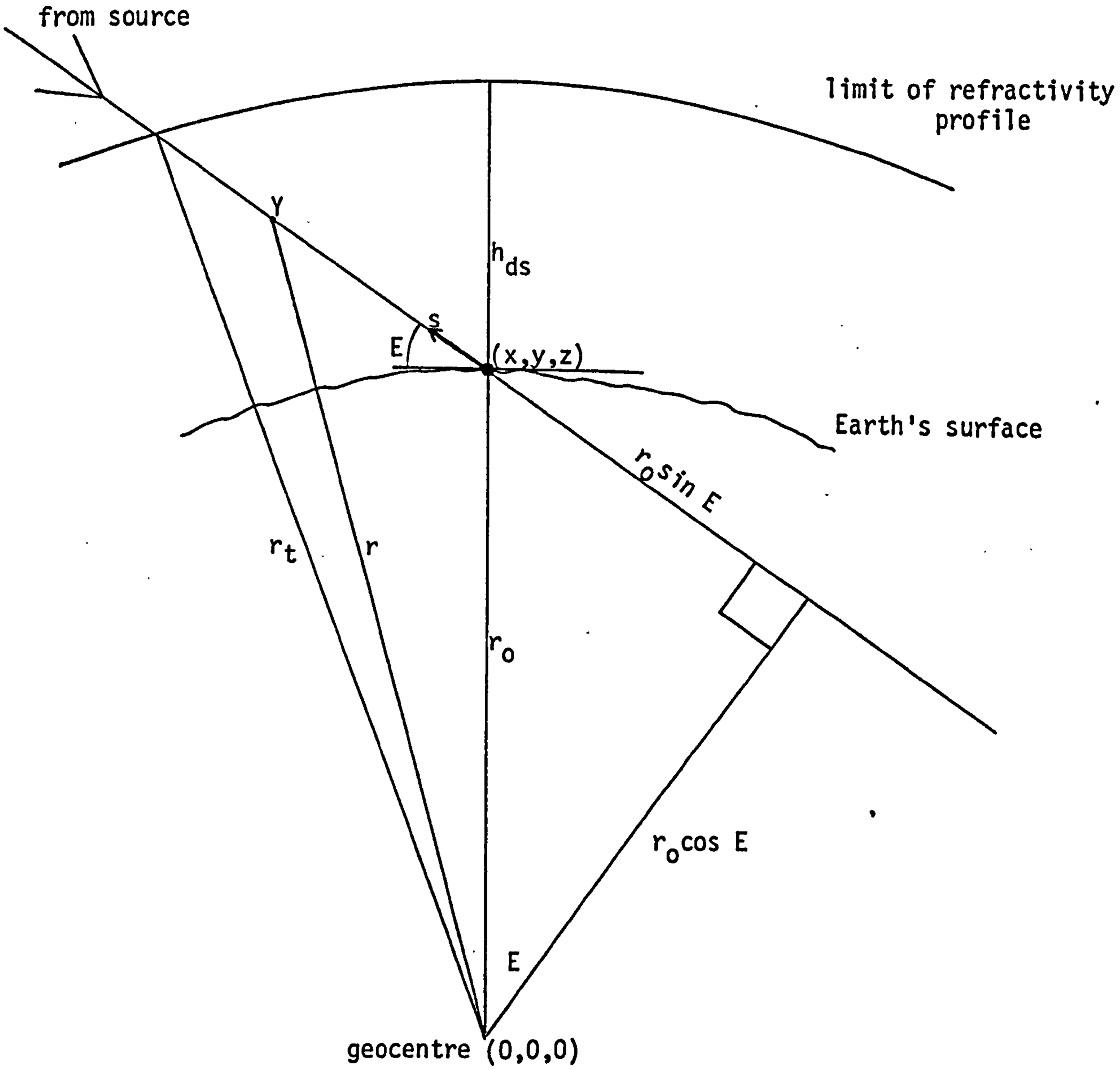

Fig. D.I Tropospheric Refraction Geometry

$$(r_o \sin E + s)^2 + (r_o \cos E)^2 = r^2$$

where E = elevation of the line of sight to the horizon and is given in (D.17).

Rearranging and differentiating gives:

$$\frac{ds}{dr} = \frac{r}{(r^2 - r_o^2 \cos^2 E)^{\frac{1}{2}}} \qquad (D.12)$$

Considering the dry component, substituting (D.10) and (D.11) in (D.12) and using:

$$h_d - h = r_{td} - r = -z \ ,$$

and $$h_{ds} = r_{td} - r_o \ ,$$

where r_{td} = geocentric radius of the limit of the refractivity profile, gives (Hopfield, 1963 and Wells, 1974):

$$\Delta s_d = \frac{N_{ds} \times 10^{-6}}{h_{ds}^4} \int_{-h_{ds}}^{o} \frac{(r_{td} + z) z^4 \, dz}{[(r_{td} + z)^2 - r_o^2 \cos^2 E]^{\frac{1}{2}}} \qquad (D.13)$$

The wet component of refractivity yields a similar expression for Δs_w with the subscript 'd' in (D.13) being replaced by the subscript 'w'.

The total correction is given by:

$$\Delta s = \Delta s_d + \Delta s_w \ . \qquad (D.14)$$

This is the standard Hopfield Model correction to a range. In order to derive the simplified Hopfield Model, the zenith dry correction is evaluated from:

$$\Delta s_d\ (E = 90^o) = \frac{N_{ds} \times 10^{-6}}{h_{ds}^{\ 4}} \int_{-h_{ds}}^{o} z^4\ dz\ ,$$

$$= \frac{N_{ds} \times 10^{-6}\ h_{ds}}{5} \qquad (D.15)$$

A similar expression is derived for the zenith wet component. The application of a cosecant law (Moffett, 1971) to (D.15) and the use of (D.8) gives the equations for the simplified Hopfield model as:

$$\Delta s_d = \frac{77.6 \times 10^{-6}.P.h_{ds}}{5T.\sin(E^2+2.5^2)^{\frac{1}{2}}}$$

$$\Delta s_w = \frac{77.6 \times 4810 \times 10^{-6}.e.h_{ws}}{5T^2.\sin(E^2+1.5^2)^{\frac{1}{2}}} \qquad (D.16)$$

The elevation of the line of sight to the source above the horizon is computed by taking the scalar product of the vector from the geocentre to the station and the unit vector in the direction of the source to give (see Fig. D.I):

$$90^o - E = \cos^{-1} \frac{\vec{r}_o.\hat{s}}{|\vec{r}|}\ , \qquad (D.17)$$

where $\vec{r}_o = [x,y,z]^T$,

and $\hat{s}$ = unit vector in the direction of the source.

The maximum error introduced by making this geometric approximation is 0.2^o (Gough, 1978).

The tropospheric correction to the propagation time of a signal is given by:

$$\Delta\tau = \frac{\Delta s}{c},$$

where c = velocity of propagation of microwaves.

The rate of change of the propagation time of a signal with respect to time is:

$$\dot{\Delta\tau}_{atm} = \frac{\dot{\Delta s}_d + \dot{\Delta s}_w}{c} \qquad (D.18)$$

where $\Delta s_d = \dfrac{77.6 \times 10^{-6}.P.h_{ds}.E.\cos(E^2+2.5^2)^{\frac{1}{2}}.\dot{E}}{5T(\sin(E^2+2.5^2)^{\frac{1}{2}})^2(E^2+2.5^2)^{\frac{1}{2}}}$

$$\dot{\Delta s}_w = \frac{77.6 \times 4810 \times 10^{-6}.e.h_{ws}.E.\cos(E^2+1.5^2)^{\frac{1}{2}}.\dot{E}}{5T^2[\sin(E^2+1.5^2)^{\frac{1}{2}}]^2(E^2+1.5^2)^{\frac{1}{2}}}$$

and $$\dot{E} = \Omega \frac{r.\dot{\hat{s}}}{\sqrt{r.r - (r.\hat{s})^2}}$$

where Ω = rate of rotation of the Earth in radians/second.

D.4 CHAO'S MODEL

The model developed by C.C. Chao for the 1971 Mariner Mars Space Mission (Chao, 1974) expresses the tropospheric range correction at any elevation angle as a function of the zenith range correction such that:

$$\Delta s_E = \Delta s_{z_{dry}} R_{E_{dry}} + \Delta s_{z_{wet}} R_{E_{wet}} \qquad (D.19)$$

where Δs_E = range correction, for an elevation above the horizon of angle E,

R_E = ratio for mapping zenith ranges down to an elevation angle, E,

and the subscripts z, dry, and wet represent the zenith direction, and the dry and wet refractive components respectively. The values of R_E can be obtained from standard tables (Chao, 1974) which account for seasonal variations in the atmospheric refractivity. However, the approximation:

$$R_E = \frac{1}{\sin E + \frac{A}{\tan E + B}} \tag{D.20}$$

can be used where, for the dry component:

$$A = 0.00143,$$

$$B = 0.0445,$$

and for the wet component:

$$A = 0.00035,$$

$$B = 0.017.$$

This approximation has been shown to agree with results of ray-tracing to ±1% for elevation angles over 1^o (Chao, 1971).

The atmospheric delay in the zenith correction can be computed in several ways. Chao suggests using the method developed by Berman (Berman, 1970) which gives:

$$\Delta s_{z_{dry}} = 2.276P \tag{D.21}$$

$$\Delta s_{z_{wet}} = 0.566 \times 10^3 \frac{R_H}{\gamma} \left(1 - \frac{C}{T}\right)^2 \exp\left(\frac{FT - G}{T - H}\right) \tag{D.22}$$

where P = surface atmospheric pressure (in bars),

γ = temperature lapse rate (K/km),

T = linearly extrapolated surface temperature (K),

R_H = surface relative humidity ($0 \leq R_H \leq 1$),

F = 17.1488,

G = 4684.1331,

H = 38.45.

If the assumptions of static equilibrium, perfect gas in the troposphere, and constant acceleration due to gravity, are true, then

(D.21) has the capability of computing the dry zenith range correction with an uncertainty of ±2 mm for an observed pressure with a precision of ±1 mbar (Hopfield, 1971). The wet component correction is claimed (Berman, 1968) to have a standard error of 2.8 cm although experiments have shown errors as large as 5 cm to occur (Chao, 1974) due to the variability of the atmospheric water vapour content.

The time delay of a signal due to atmospheric refraction is given by:

$$\Delta\tau_{atm} = \frac{\Delta s_E}{c} \qquad (D.23)$$

where c = velocity of propagation of microwaves.

The rate of change of the signal delay due to the atmosphere with respect to time is given by differentiating (D.19), (D.20), and (D.23) to give:

$$\dot{\Delta\tau}_{atm} = \Delta s_{z_{dry}} \dot{R}_{E_{dry}} + \Delta s_{z_{wet}} \dot{R}_{E_{wet}} ,$$

$$\text{where } \dot{R}_E = \dot{E} \frac{\frac{A}{(\cos^2 E(B+\tan E)^2} - \cos E}{\left(\frac{A}{B+\tan E} + \sin E\right)^2}$$

$\dot{E}$ is given in (D.18), and A and B are given in (D.20) for the dry and wet components respectively.

APPENDIX E

SPHERICAL TRIANGLE FORMULAE

APPENDIX E

SPHERICAL TRIANGLE FORMULAE

Considering the spherical triangle illustrated in Fig. E.I, the angles A, B and C are the internal angles of the triangle, measured on the surface of the sphere and the angles a, b and c are the angles subtended at the centre of the sphere by the arcs XY, ZY and ZX respectively. The spherical triangle formulae used to compute unknown angles from known angles are;

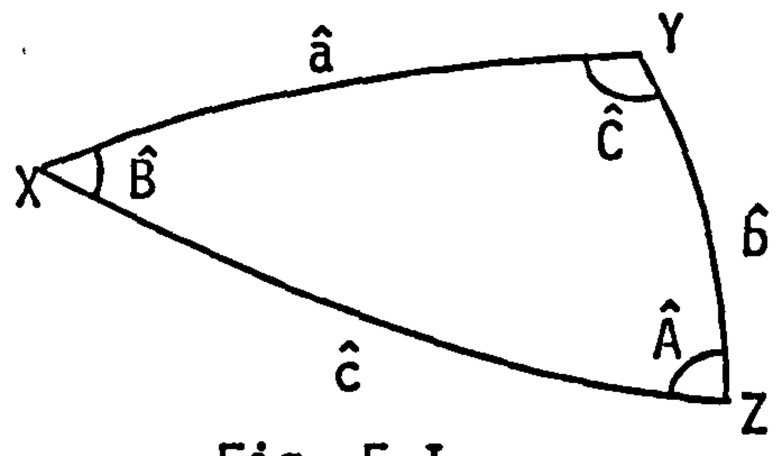

Fig. E.I

i) the Sine Rule

$$\frac{\sin A}{\sin a} = \frac{\sin B}{\sin b} = \frac{\sin C}{\sin c}$$

ii) the Cosine Rule

$$\cos a = \cos b \cos c + \sin b \sin c \cos A$$

$$\cos A = \cos B \cos C + \sin B \sin C \cos a$$

(These can, of course, be reorganised to compute b, c, B and C if the known angles are suitable.)

iii) the Four-Part Formula (uses any four sequential elements)

cos (middles) = cot (outerside) sin (innerside)
- cot (outer angle) sin (inner angle)

e.g. for BcAb, cos c cos A = cot b sin c - cot B sin A.

iv) the Five-Part Formulae

$$\sin a \cos B = \cos b \sin c - \sin b \cos c \cos A$$

$$\sin A \cos b = \cos B \sin C + \sin B \cos C \cos a.$$

(These again may be reorganised depending on the known information.)

APPENDIX F

SOLUTION OF A SURVEYING NETWORK BY VARIATION OF CO-ORDINATES USING THE WEIGHTED LEAST SQUARES TECHNIQUE

APPENDIX F

SOLUTION OF A SURVEYING NETWORK BY VARIATION OF CO-ORDINATES USING THE WEIGHTED LEAST SQUARES TECHNIQUE

This appendix is not an exhaustive description of the method of adjustment of a set of VLBI observations but is designed to clarify and detail the description given in §3.2.

F.1 Weighted least squares formulae

The principle of weighted least squares states that the most probable values of the unknowns of an adjustment of a set of overdetermined linear equations is that which minimises the sum of the squares of the weighted residuals. For a formal proof of this, see (Rainsford, 1957, Thompson, 1962, and Cross, 1970).

From (3.5), the residual vector can be expressed in terms of the observation equations as:

$$v = Ax - b.$$

Introducing the weight matrix for the observations, $W(= \sigma_{bb}^{-1}$, see §F.2), gives the sum of the squares of the weighted residuals as:

$$v^T W v = (Ax-b)^T W (Ax-b), \qquad (F.1)$$

and in order to satisfy the minimum condition on which the principle is based:

$$\frac{\partial (v^T W v)}{\partial x} = 0. \qquad (F.2)$$

Expanding and differentiating (F.1) gives:

$$\frac{\partial(v^T W v)}{\partial x} = 2A^T WAx - 2A^T Wb.$$

and satisfying (F.2) gives the expression, known as the normal equations:

$$A^T WAx = A^T Wb. \qquad (F.3)$$

The vector of unknowns is given by:

$$x = (A^T WA)^{-1}(A^T Wb) \qquad (F.4)$$

F.2 Covariance Formulae

The covariance matrix has been described in §3.2.3. This section presents proofs, taken from (Ashkenazi, 1970), of the covariance formulae.

1) The two basic Gaussian 'propagation of error' theorems state that given:

$$m = f_1(x,y,z,....)$$
$$n = f_2(x,y,z,....)$$

$$\text{then } \sigma_m^2 = \left(\frac{\partial m}{\partial x}\right)^2 \sigma_x^2 + \left(\frac{\partial m}{\partial y}\right)^2 \sigma_y^2 + \left(\frac{\partial m}{\partial z}\right)^2 \sigma_z^2 + ... \qquad (F.5)$$
$$.... + 2\left(\frac{\partial m}{\partial x}\cdot\frac{\partial m}{\partial y}\right)\sigma_{xy} + ...$$

$$\text{and } \sigma_{mn}^2 = \left(\frac{\partial m}{\partial x}\cdot\frac{\partial n}{\partial x}\right)\sigma_x^2 + \left(\frac{\partial m}{\partial y}\cdot\frac{\partial n}{\partial y}\right)\sigma_y^2 + ... \qquad (F.6)$$
$$.... + \left(\frac{\partial m}{\partial x}\cdot\frac{\partial n}{\partial x}\cdot\frac{\partial m}{\partial y}\cdot\frac{\partial n}{\partial y}\right)\sigma_{xy} + ...$$

2) From (F.5), if:

$$y = f^T x,$$

where $f^T = [f_1, f_2, ...]$,

$$x = [x_1, x_2, \ldots] \ ,$$

$$\text{and} \quad \sigma_{xx} = \begin{bmatrix} \sigma^2_{x1} & \sigma_{x1x2} \cdots \\ \sigma_{x2x1} & \sigma^2_{x2} \cdots \\ \vdots & \vdots \end{bmatrix}$$

$$\text{then} \quad \sigma^2_y = f^T \sigma_{xx} f. \qquad \text{(F.7)}$$

3) Similarly, it follows from (F.5) and (F.6) that if:

$$y = R.x,$$

where $x^T = [x_1, x_2, \ldots, x_m]$,

$y^T = [y_1, y_2, \ldots, y_m]$,

and R is a conformable (nxm) matrix, then,

$$\sigma_{yy} = R\sigma_{xx}R^T. \qquad \text{(F.8)}$$

4) The application of the above formulae to a solution by variation of co-ordinates, as detailed in §3.2 and §F.1, and applying (F.8) to (F.4), gives:

$$\sigma_{xx} = [(A^T W A)^{-1} A^T W] \sigma_{bb} [(A^T W A)^{-1} A^T W]^T \ , \qquad \text{(F.9)}$$

where σ_{bb} is the unbiased covariance matrix of the observations given by $\sigma_{bb} = \sigma_o{}^2 W^{-1}$. (F.9) can be simplified to:

$$\sigma_{xx} = \sigma_o{}^2 (A^T W A)^{-1} \qquad \text{(F.10)}$$

F.3 Proof of Unit Variance Formula

The following proof has been taken from (Ashkenazi, 1970).

Given $A.x = b + v$ (F.11)

and $A(x + \delta x) = b + \delta b$ (F.12)

where x = most probable set of unknowns,

b = observed values,

A = a rectangular matrix of order n x k,

v = least squares residuals,

δx = true errors in x,

δb = true observational errors,

pre-multiply both sides of (F.12) by $v^T W$ to obtain

$$v^T WA(x + \delta x) = v^T Wb + v^T W\delta b \qquad (F.13)$$

or $$v^T W(Ax - b) + (v^T WA)\delta x = v^T W\delta b \qquad (F.14)$$

But, $(v^T WA)\delta x = 0$

because

$$A^T Wv = (v^T WA)^T = A^T W(Ax - b)$$

$$= A^T WAx - A^T Wb = 0 \text{ (least squares normal equations)}$$

Therefore,

$$v^T Wv = v^T W\delta b = \delta b^T Wv \qquad (F.15)$$

Similarly pre-multiplying (F.12) by $\delta b^T W$ gives

$$\delta b^T WA(x + \delta x) = \delta b^T Wb + \delta b^T W\delta b \qquad (F.16)$$

or $$\delta b^T W(Ax - b) + (\delta b^T WA)\delta x = \delta b^T W\delta b$$

However, considering (F.15), $\delta b^T Wv = v^T Wv$

thus $$v^T Wv + (\delta b^T WA)\delta x = \delta b^T W\delta b \qquad (F.17)$$

By definition,

$$\delta b^T W \delta b = n\sigma_o^2 \qquad \text{(F.18)}$$

and it will be shown that

$$(\delta b^T W A)\delta x = k\sigma_o^2 \qquad \text{(F.19)}$$

Substituting (F.18) and (F.19) in (F.17),

$$n\sigma_o^2 = v^T W v + k\sigma_o^2$$

$$\underline{\sigma_o^2 = \frac{v^T W v}{(n-k)}} \qquad \text{(F.20)}$$

To prove (F.19)

Pre-multiply (F.12) by $A^T W$

$$A^T W A(x + \delta x) = A^T W b + A^T W \delta b$$

But, $A^T W A x = A^T W b$

Hence,

$$A^T W A \delta x = A^T W \delta b$$

$$\delta x = [(A^T W A)^{-1} A^T W]\delta \qquad \text{(F.21)}$$

The left hand side of (F.19) thus equals:

$$(\delta b^T W A)\delta x = (\delta b^T W A)(A^T W A)^{-1} A^T W \delta b$$

$$= \text{trace } [(A^T W \delta b)(\delta b^T W A)(A^T W A)^{-1}] \qquad \text{(F.22)}$$

But for a large number of observations we can <u>expect</u>

$$W \delta b \delta b^T = \sigma_o^2 [I]$$

Hence:

$$(\delta b^T WA)\delta x = \text{trace}\left[(A^T(\sigma_o{}^2 I)WA)(A^T WA)^{-1}\right]$$

$$= \sigma_o{}^2 \text{ trace}(I)$$

$$(\delta b^T WA)\delta x = k\sigma_o{}^2 \qquad \text{(F.23)}$$

F.4 Solution of a Set of Normal Equations

F.4.1 Choleski's Decomposition Method

The normal equations coefficient matrix, $A^T WA$, in (F.3) is a symmetrical positive definite square matrix. Any square matrix, N, may be decomposed such that:

$$N = L'D\,U',$$

where U' and L' are upper and lower triangular matrices respectively, and D is a diagonal matrix. It follows that if the diagonal matrix has only positive elements then,

$$N = L.U = L'D^{\frac{1}{2}}D^{\frac{1}{2}}U',$$

where L and U are also lower and upper triangular matrices respectively. Extending this further to the normal equations coefficient matrix, its particular properties result in the decomposition,

$$A^T WA = L.L^T . \qquad \text{(F.24)}$$

The computational algorithm to derive the elements of this triangular matrix are attributed to Choleski and are given by:

$$\ell_{ii} = \left[n_{ii} - \sum_{k=1}^{i-1} \ell_{ik}^2 \right]^{\frac{1}{2}}$$

$$\ell_{ij} = \frac{\left[n_{ij} - \sum_{k=1}^{j-1} \ell_{ik} . \ell_{jk} \right]}{\ell_{jj}} \qquad \text{for } i > j \qquad \text{(F.25)}$$

where ℓ_{ij} is a general element of L in the i^{th} row and j^{th} column, and n_{ij} is a general element of A^TWA in the i^{th} row and j^{th} column.

F.4.2 Forward and Back Substitution

Having decomposed the normal equations coefficient matrix, (F.3) can be solved for the vector of unknowns x by a process of forward and back substitution. The normal equations, having decomposed A^TWA, are of the form:

$$LL^Tx = A^TWb$$

As L is a triangular matrix, this set of equations can be solved for a vector f, equal to L^Tx, by forward substitution such that,

$$Lf = A^TWb, \qquad \text{(F.26)}$$

and then by back substitution into

$$L^Tx = f \qquad \text{(F.27)}$$

to give the solution vector, x.

The solution of the forward substitution stage in (F.26) for the vector f is achieved by using the algorithm:

$$f_1 = d_1/\ell_{11}$$

$$f_i = \left[(A^T Wb)_i - \sum_{j=1}^{i-1} f_j \ell_{ij}\right]/\ell_{ii} \quad \text{for } i > 1 \qquad \text{(F.28)}$$

and the solution for the back substitution expressed in (F.27) is achieved by using the algorithm:

$$x_n = f_n/u_{nn}$$

$$x_{n-i} = \left[f_{n-i} - \sum_{j=0}^{i-1} u_{n-1,n-j} \cdot x_{n-j}\right]/u_{n-i,n-i} \qquad \text{(F.29)}$$

where $U = L^T$ and n is the number of unknowns.

F.4.3 Computation of the inverse normal equations matrix

This can be achieved quite simply using the decomposed normal equations matrix derived for the solution of the vector of unknowns.

The inverse may be assembled column by column from the expression

$$(A^T WA).S_i = r_i$$

$$\Rightarrow L.L^T S_i = r_i$$

where S_i is the i^{th} column of the inverse matrix,

r_i is the i^{th} column of the unit matrix.

The forward and back substitution method can then be used to solve for each column of the inverse matrix in turn.

APPENDIX G

STAGES OF INPUT DATA PREPARATION

APPENDIX G

STAGES OF INPUT DATA PREPARATION

The format and content of the input data to NULBIP has been described in §5.2. This appendix presents an example of the NRAO Mk I system data in §G.1, and examples of the data files produced in the preprocessing phase of the data from the Canadian system in §G.2. For the Canadian data, only an example of the formation of a fringe frequency data file is presented although a delay data file is formed in the same manner.

source no.	source code no.	source name	source right ascension h m s	source declination d m s
	1143C120		4 30 31,589	-5 14 59,253
	2270J287		8 51 57,231	20 17 58,44
	3284C39		9 23 55,297	39 15 23,73
	4333C273B		12 26 33,246	2 19 43,31
	5360Q208		14 04 45,626	28 41 29,417
	6433C345		16 41 17,635	39 54 10,954
	7592134'00		21 34 05,226	0 28 25,146
	863VRO		22 00 39,387	42 02 08,41
	9673C454,3		22 51 29,534	15 52 54,24
	10353C279		12 53 35,834	-5 31 7,99

coded observing baseline	observed source code no.	epoch of observation (month, day, year, hour, min)	observed delay (μs)	standard error of delay (ns)	observed delay rate (ps/s)	standard error in delay rate (ps/s)
HG 59	82972 310	5666.361562	.208		-840635.582	.148
HG 59	82972 315	5412.837162	.198		-849463.767	.148
HG 59	82972 320	5156.724473	.196		-857885.447	.148
HG 67	82972 330	8569.568214	.144		-684760.848	.148
HG 63	82972 345	5240.114180	.175		-634513.223	.148
HG 63	82972 350	5048.850209	.236		-640531.120	.443
HG 63	82972 355	4855.826593	.179		-646242.398	.148
HG 67	82972 410	6812.094460	.139		-776061.063	.148
HG 59	82972 420	1927.215480	.175		-925970.927	.148
HG 59	82972 425	1648.986818	.177		-928814.232	.148
HG 59	82972 430	1369.971467	.179		-931213.168	.148
HG 67	82972 440	5365.369347	.139		-829103.100	.148
HG 67	82972 445	5115.507261	.149		-836577.795	.148

Fig. G.I Part of the condensed NRAO Mk I system data provided on punched cards

observation epoch minus one minute y	d	h	m	observed source name	observing baseline	'residual' delay (μs)	standard error of delay (μs)	'residual' fringe frequency (Hz)	standard error of fringe frequency (Hz)	'expected' delay (μs)	'expected' fringe frequency (Hz)
77133	0	38		4C39.25	ARCH	1.325	0.034	-0.2516	0.0021	-0.1126943360 05	-0.4851214840 04
77133	0	41		4C39.25	ARCH	1.339	0.033	-0.1421	0.0021	-0.1135015230 05	-0.4727484380 04
77133	0	43		4C39.25	ARCH	1.308	0.034	-0.1514	0.0021	-0.1140280470 05	-0.4644476560 04
77133	0	44		4C39.25	ARCH	1.353	0.039	-0.1694	0.0025	-0.1142878130 05	-0.4602835940 04
77133	0	46		4C39.25	ARCH	0.882	0.040	-0.1318	0.0025	-0.1148003130 05	-0.4519296880 04
77133	0	47		4C39.25	ARCH	1.105	0.035	-0.0062	0.0021	-0.1150530080 05	-0.4477398440 04
77133	0	49		4C39.25	ARCH	1.839	0.039	-0.1754	0.0025	-0.1155513670 05	-0.4393343750 04
77133	0	52		4C39.25	ARCH	1.404	0.039	-0.0042	0.0025	-0.1162811720 05	-0.4266628910 04
77133	0	53		4C39.25	ARCH	0.940	0.039	0.0000	0.0000	-0.1165196880 05	-0.4224226560 04
77133	0	55		4C39.25	ARCH	0.000	0.000	-0.0028	0.0004	-0.1169895310 05	-0.4139183590 04
77133	1	16		4C39.25	ARCH	0.072	0.023	-0.0552	0.0015	-0.1213386330 05	-0.3228273680 04
77133	1	17		4C39.25	ARCH	-0.043	0.039	0.1433	0.0025	-0.1215187500 05	-0.3184158450 04
77133	1	19		4C39.25	ARCH	0.558	0.033	-0.1618	0.0021	-0.1218715630 05	-0.3095798830 04
77133	1	21		4C39.25	ARCH	0.933	0.039	-0.1789	0.0025	-0.1222144140 05	-0.3007148930 04
77133	1	22		4C39.25	ARCH	-0.144	0.034	0.1746	0.0021	-0.1223821090 05	-0.2962737300 04
77133	1	26		4C39.25	ARCH	0.322	0.039	0.1802	0.0025	-0.1230278910 05	-0.2784532230 04
77133	1	29		4C39.25	ARCH	0.571	0.039	0.0028	0.0025	-0.1234858980 05	-0.2650315430 04
77133	1	31		4C39.25	ARCH	0.686	0.039	-0.1564	0.0025	-0.1237786330 05	-0.2560582760 04
77133	1	32		4C39.25	ARCH	3.415	0.038	0.1958	0.0025	-0.1239212500 05	-0.2515642330 04
77133	1	33		4C39.25	ARCH	0.000	0.000	-0.0032	0.0025	-0.1240612890 05	-0.2470653810 04
77133	1	34		4C39.25	ARCH	0.000	0.000	-0.1556	0.0025	-0.1241988280 05	-0.2425617920 04
77133	1	35		4C39.25	ARCH	3.318	0.039	-0.1354	0.0025	-0.1243338280 05	-0.2380535640 04
77133	1	36		4C39.25	ARCH	-2.570	0.039	0.1012	0.0025	-0.1244663280 05	-0.2335467960 04
77133	1	39		4C39.25	ARCH	-2.194	0.033	-0.1626	0.0021	-0.1248485160 05	-0.2199759770 04

Fig. G.II DATA FILE 1 - Canadian system data as provided by the Herzberg Institute of Astrophysics on magnetic tape

obs. no. within source observing period	Observation epoch minus one minute second				GAST (hrs)	observed source name	coded observing baseline	sample rate of data processing		observing frequency (MHz)	UT1-UTC (secs)	delay tap separation (μs)	'offset' delay (μs)	'offset' fringe frequency (Hz)
	y	d	h	m										
0	77133	0	38		16.011	4C39.25	ARCH	1	60	-10680.0	0.270	0.120	0.000	0.100
1	77133	0	39		16.028	4C39.25	ARCH	1	60	-10680.0	0.270	0.120	0.000	0.100
2	77133	0	40		16.044	4C39.25	ARCH	1	60	-10680.0	0.270	0.120	0.000	0.100
3	77133	0	41		16.061	4C39.25	ARCH	1	60	-10680.0	0.270	0.120	0.000	0.000
4	77133	0	42		16.078	4C39.25	ARCH	1	60	-10680.0	0.270	0.120	0.000	0.000
5	77133	0	43		16.094	4C39.25	ARCH	1	60	-10680.0	0.270	0.120	0.000	0.000
6	77133	0	44		16.111	4C39.25	ARCH	1	60	-10680.0	0.270	0.120	0.000	0.000
7	77133	0	45		16.128	4C39.25	ARCH	1	60	-10680.0	0.270	0.120	-0.600	0.000
8	77133	0	46		16.145	4C39.25	ARCH	1	60	-10680.0	0.270	0.120	-0.600	0.000
9	77133	0	47		16.161	4C39.25	ARCH	1	60	-10680.0	0.270	0.120	-0.600	0.000
10	77133	0	48		16.178	4C39.25	ARCH	1	60	-10680.0	0.270	0.120	-0.600	0.000
11	77133	0	49		16.195	4C39.25	ARCH	1	60	-10680.0	0.270	0.120	-0.600	0.000
12	77133	0	50		16.211	4C39.25	ARCH	1	60	-10680.0	0.270	0.120	-0.600	0.000
13	77133	0	51		16.228	4C39.25	ARCH	1	60	-10680.0	0.270	0.120	-0.600	0.000
14	77133	0	52		16.245	4C39.25	ARCH	1	60	-10680.0	0.270	0.120	-0.600	0.000
15	77133	0	53		16.262	4C39.25	ARCH	1	60	-10680.0	0.270	0.120	-0.600	0.000
16	77133	0	54		16.278	4C39.25	ARCH	1	60	-10680.0	0.270	0.120	-0.600	0.000
17	77133	0	55		16.295	4C39.25	ARCH	1	59	-10680.0	0.270	0.120	-0.600	0.000
18	77133	1	16		16.646	4C39.25	ARCH	1	60	-10680.0	0.270	0.120	0.360	0.053
19	77133	1	17		16.663	4C39.25	ARCH	1	60	-10680.0	0.270	0.120	0.360	0.053
20	77133	1	18		16.679	4C39.25	ARCH	1	60	-10680.0	0.270	0.120	0.000	0.000
21	77133	1	19		16.696	4C39.25	ARCH	1	60	-10680.0	0.270	0.120	0.000	0.000
22	77133	1	20		16.713	4C39.25	ARCH	1	60	-10680.0	0.270	0.120	0.500	0.000

Fig. G.III DATA FILE 2 - Canadian system data as provided by the Herzberg Institute of Astrophysics on magnetic tape

source no.	source code	source name	source right ascension h m s	source declination d m s
1	14C39.25		9 23 55.320	39 15 23.570
2	2BLLAC		22 0 39.365	42 2 8.55
3	3NRAO150		3 55 45.262	50 49 20.27
4	43C273		12 26 33.248	2 19 43.273
5	53C345		16 41 17.610	39 54 10.824
6	60J287		8 51 57.252	20 17 58.35

observed source code no.	y	h	m	s	observed source name	coded observing baseline	'residual' delay (μs)	standard error in delay (μs)	'residual' fringe frequency (Hz)	standard error of fringe frequency (Hz)	'expected' fringe frequency (Hz)
1	77133	0	38	40	39.25	ARCH	1.325	0.034	-0.2516	0.0025	-0.485121484D 04
1	77133	0	41	40	39.25	ARCH	1.339	0.033	-0.1421	0.0025	-0.4727484 38D 04
1	77133	0	43	40	39.25	ARCH	1.308	0.034	-0.1514	0.0025	-0.4644476 56D 04
1	77133	0	44	40	39.25	ARCH	1.353	0.039	-0.1694	0.0025	-0.4602835 94D 04
1	77133	0	46	40	39.25	ARCH	0.882	0.040	-0.1518	0.0025	-0.4519296 88D 04
1	77133	0	47	40	39.25	ARCH	1.105	0.035	-0.0062	0.0025	-0.447739844D 04
1	77133	0	49	40	39.25	ARCH	1.839	0.039	-0.1754	0.0025	-0.439334375D 04
1	77133	0	52	40	39.25	ARCH	1.404	0.039	0.0042	0.0025	-0.426662891D 04
1	77133	0	53	40	39.25	ARCH	0.940	0.039	0.0000	0.0005	-0.422422656D 04
1	77133	0	55	40	39.25	ARCH	0.000	0.000	-0.0028	0.0005	-0.413918359D 04
.....											
2	77136	9	58		BLLAC	ARCH	0.850	0.011	0.0674	0.0004	-0.966874609D 04
2	77136	9	59		BLLAC	ARCH	0.839	0.010	0.0696	0.0004	-0.965571484D 04
			99				0.0	0.0	0.0	0.0	0.0 E 00

Fig. G.IV FREQUENCY DATA FILE 1 - Formed on-line using the UNILINE system by appending the source data and terminator and shortening the file width

```
 1 14C39.25          9 23 55.320 39 15 23.5700.0000 0.0000
 2 2BLLAC           22  0 30.365 42  2  8.5500.0000 0.0000
 3 3NRAO150          3 55 45.262 50 49 20.2700.0000 0.0000
 4 430273           12 26 33.248  2 19 43.2730.0000 0.0000
 5 530345           16 41 17.610 39 54 10.8240.0000 0.0000
 6 600287            8 51 57.252 20 17 58.3500.0000 0.0000
 1 77133  0 46 4C39.25   ARCH -0.1318 0.0025  0.000 -0.451229688E 04
 1 77133  0 55 4C39.25   ARCH -0.0028 0.0005  0.000 -0.413918359E 04
 1 77133  1 22 4C39.25   ARCH  0.1746 0.0025  0.000 -0.296273730E 04
 1 77133  1 33 4C39.25   ARCH -0.0032 0.0025  0.000 -0.247065381E 04
 1 77133  1 41 4C39.25   ARCH -0.1659 0.0025  0.000 -0.210911548E 04
 2 77133 10 14 BLLAC     ARCH  0.0000 0.0004  0.000 -0.961272266E 04
 2 77133 10 22 BLLAC     ARCH -0.1696 0.0024  0.000 -0.940712500E 04
 2 77133 10 28 BLLAC     ARCH  0.0016 0.0014  0.000 -0.940278125E 04
 2 77133 10 35 BLLAC     ARCH -0.1391 0.0014  0.000 -0.928453125E 04
 2 77133 10 43 BLLAC     ARCH -0.0027 0.0014  0.000 -0.913873438E 04
 2 77133 10 51 BLLAC     ARCH -0.1465 0.0024  0.000 -0.898173828E 04
 2 77133 12 43 BLLAC     ARCH  0.0631 0.0014  0.053 -0.573926953E 04
 2 77133 12 48 BLLAC     ARCH  0.0625 0.0014  0.053 -0.555580469E 04
 2 77133 12 54 BLLAC     ARCH  0.0619 0.0015  0.053 -0.533214844E 04
 2 77133 12 59 BLLAC     ARCH  0.0628 0.0015  0.053 -0.514295313E 04
```

approximately 300 observations plus the data terminator

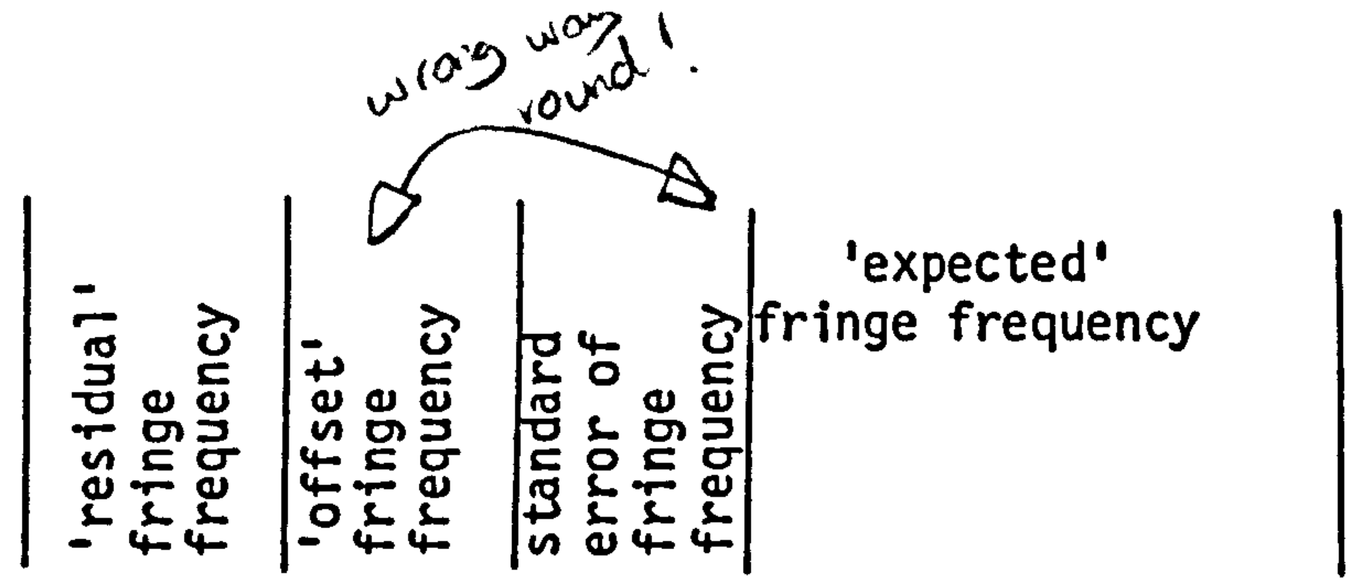

Fig. G.V CONDENSED FREQUENCY DATA FILE - produced from the preprocessing program by the combination of 'frequency data file 1' and 'data file 2'

```
 1 14C39.25        9 23 55.320 39 15 23.5700.0 0.0
 2 2BLLAC         22  0 39.365 42  2  8.55 0.0 0.0
 4 43C273         12 26 33.248  2 19 43.2730.0 0.0
 5 53C345         16 41 17.610 39 54 10.8240.0 0.0
 6 60J287          8 51 57.252 20 17 58.35 0.0 0.0
1 77133  0 46 4C39.25  ARCH -0.1318 0.0025  0.000 -0.451929688E 04
1 77133  1 39 4C39.25  ARCH -0.1626 0.0021  0.000 -0.219975977E 04
2 77133 10 44 BLLAC    ARCH  0.0018 0.0006  0.000 -0.911971875E 04
2 77133 12 53 BLLAC    ARCH  0.0705 0.0017  0.053 -0.536968359E 04
2 77133 13 19 BLLAC    ARCH  0.0635 0.0011  0.053 -0.436248828E 04
      :
      :
2 77133 19 23 BLLAC    AROV -0.1301 0.0017  0.129 -0.155278638E 04
4 77134  1  9 3C273    AROV -0.0569 0.0003  0.143  0.778384766E 04
4 77134  1 23 3C273    AROV -0.0537 0.0004  0.143  0.799952344E 04
4 77134  1 36 3C273    AROV -0.0537 0.0004  0.143  0.817294531E 04
      :
      :
2 77136  8 52 BLLAC    CVCH  0.0705 0.0014  0.037 -0.141277734E 05
2 77136  9  8 BLLAC    CVCH  0.0739 0.0012  0.037 -0.144370586E 05
2 77136  9 15 BLLAC    CVCH  0.0713 0.0009  0.037 -0.145502109E 05
2 77136  9 24 BLLAC    CVCH  0.0727 0.0012  0.037 -0.146756289E 05
      :
      :
```

plus data terminator

Fig. G.VI COMBINED CONDENSED FREQUENCY DATA FILE - produced by manual editing on the UNILINE system of the three separate condensed data files from the individual baselines

APPENDIX H

VLBI/OSGB TEST RESULTS

APPENDIX H

VLBI/OSGB TEST RESULTS

This appendix presents the results of a series of simulated tests, described in §8.2, involving the inclusion of VLBI measurements in the Ordnance Survey Triangulation of Great Britain.

The first series of tests simulated the incorporation of interferometric measurements of distance and azimuth between the three existing radio telescopes at Jodrell Bank, Cheshire, Chilbolton, Hampshire, and Cambridge (Fig. H.I.). The nearest primary triangulation pillar was used as the end point of the baseline measurement at each station. The different models used are summarised in Table H.I and the results of these tests are presented in Tables H.II(i) and (ii).

The results are presented in terms of the mean standard errors in distance and azimuth for a number of test lines. These have been categorised for the presentation of the results into short, medium, long, and very long lines and are illustrated in Figs H.II and H.III.

The second series of tests simulated a four station interferometric array comprising the three stations used in the previous test plus one station in the north of Scotland, a simulated transportable antenna location (Fig. H.I). The measurements are again input as distances and azimuths and the same models are applied as in Table H.I, there being six of each measurement instead of three. The results of these tests are presented in Tables H.III(i) and (ii), and are given in the same format as the first series of tests.

The Shetlands are not shown but are in the Primary Network

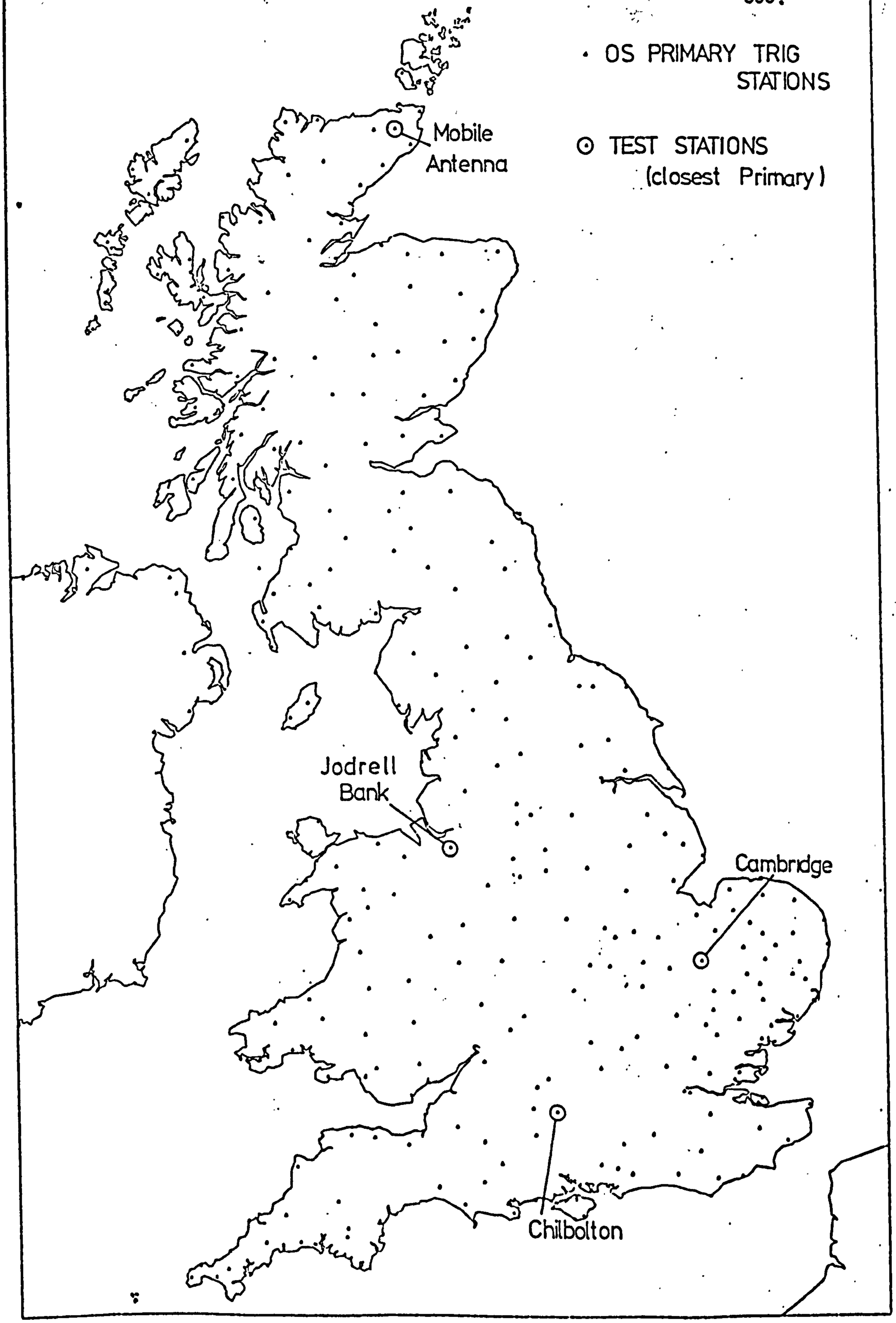

Fig. H.I Primary triangulation stations nearest to the VLBI antennae for the simulation experiments

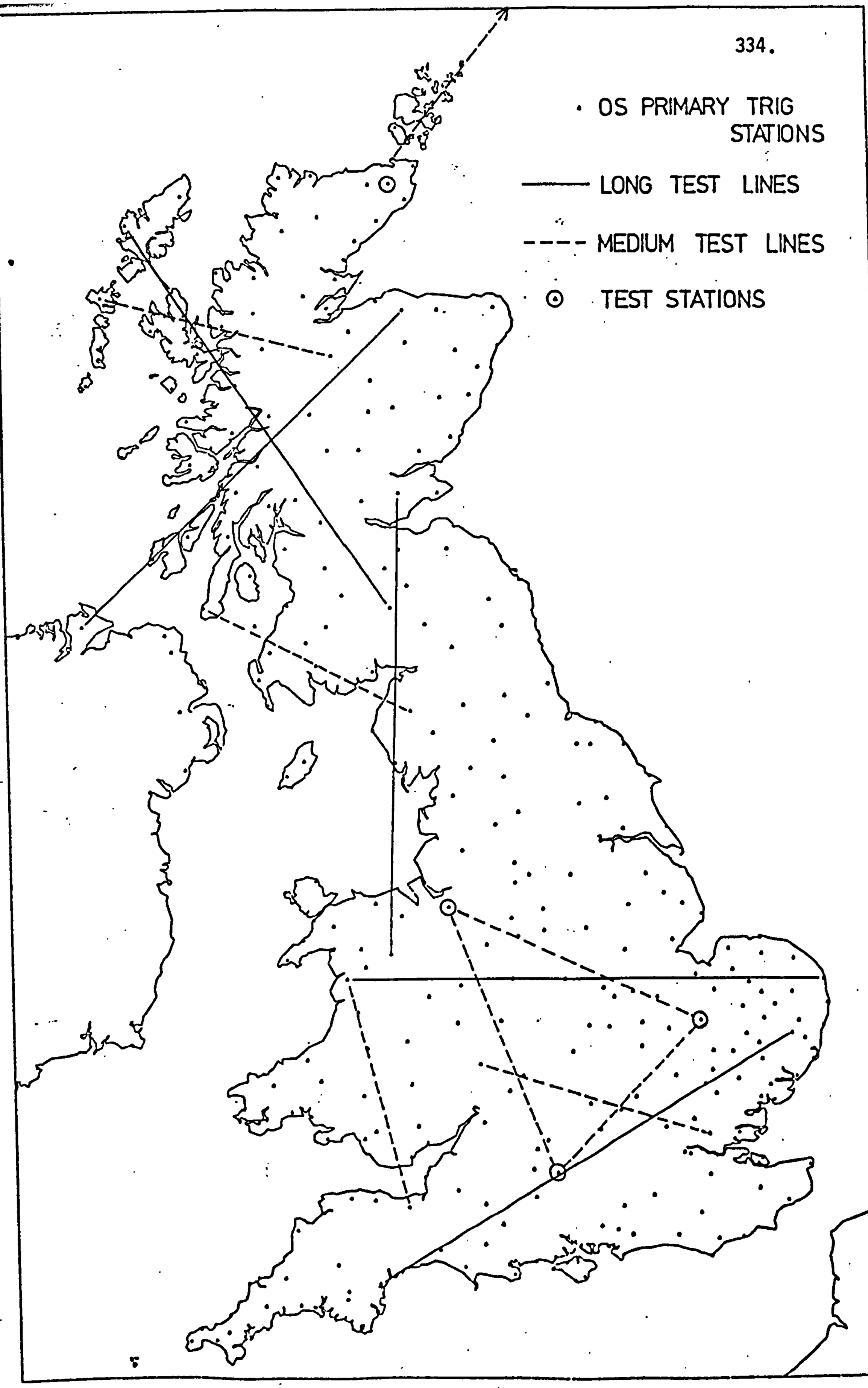

Fig. H.II Long and medium test lines

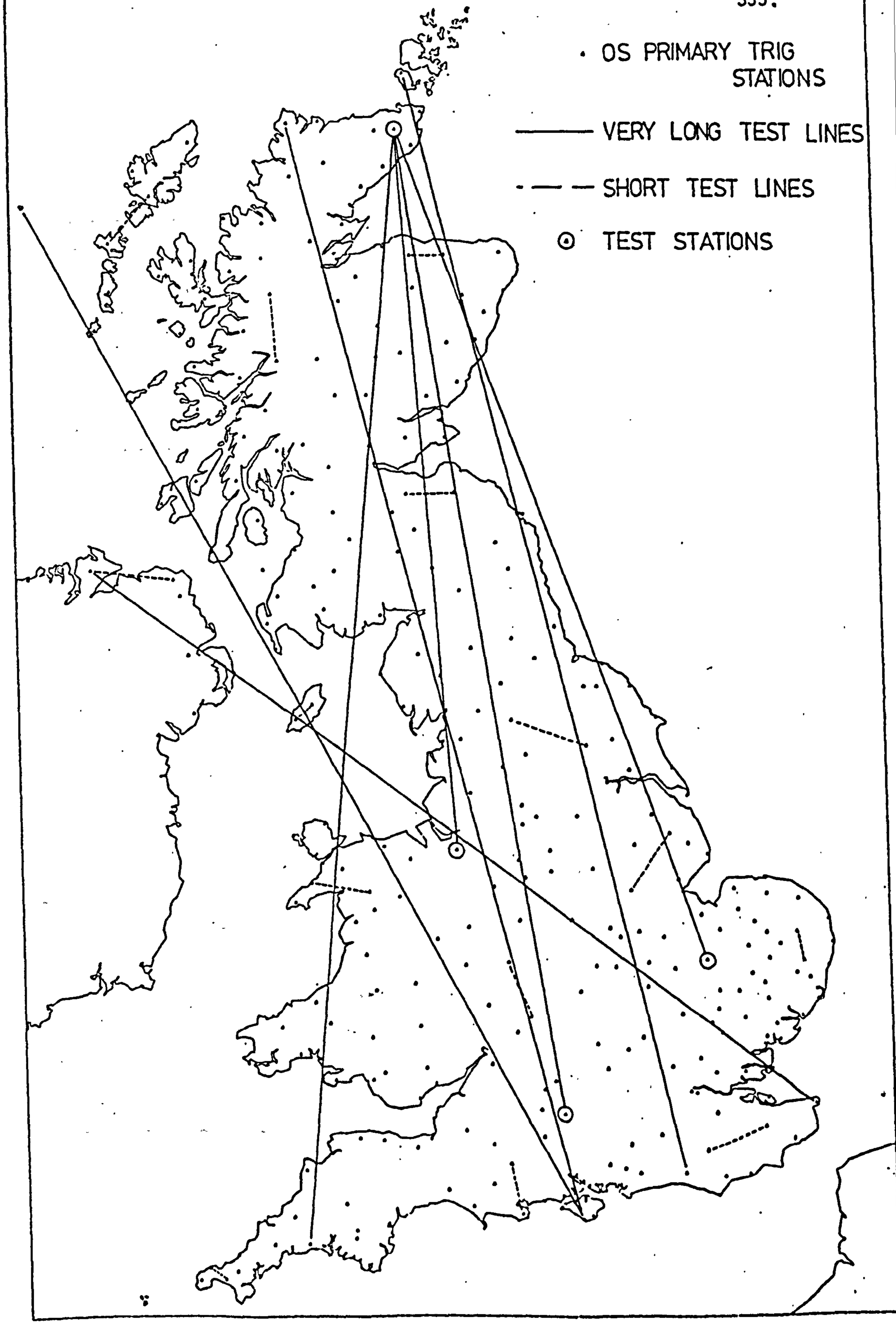

Fig. H.III Short and Very Long test lines

Model No.	Data summary		
	Standard OSGB network data	Standard errors of input VLBI distances (ppm)	Standard errors of input VLBI azimuths (secs)
0	Yes	Not input	Not input
1	Yes	1	0.5
2	Yes	0.1	0.5
3	Yes	0.01	0.5
4	Yes	1	0.3
5	Yes	0.1	0.3
6	Yes	0.01	0.3
7	Yes	1	0.1
8	Yes	0.1	0.1
9	Yes	0.01	0.1

Table H.I Summary of themodels used in the simulation tests incorporating VLBI measurements in the OSGB primary triangulation network

Model	Test Line Lengths			
	Short	Medium	Long	V. Long
0	0.494	0.275	0.240	0.188
1	0.489	0.260	0.228	0.178
2	0.488	0.251	0.228	0.178
3	0.487	0.251	0.228	0.178
4	0.485	0.244	0.218	0.168
5	0.485	0.234	0.218	0.168
6	0.485	0.234	0.218	0.168
7	0.479	0.205	0.196	0.156
8	0.477	0.196	0.196	0.156
9	0.477	0.196	0.196	0.156

Table H.II(i) Mean azimuth standard errors for tests described in Table H.I

Model	Test Line Lengths			
	Short	Medium	Long	V. Long
0	2.719	0.764	0.662	0.421
1	2.718	0.727	0.650	0.417
2	2.714	0.578	0.626	0.409
3	2.713	0.544	0.625	0.408
4	2.717	0.725	0.649	0.416
5	2.713	0.578	0.626	0.408
6	2.713	0.544	0.625	0.408
7	2.716	0.706	0.644	0.414
8	2.713	0.577	0.626	0.407
9	2.713	0.544	0.625	0.406

Table H.II(ii) Mean distance standard errors for tests described in Table H.I

Model	Test Line Lengths			
	Short	Medium	Long	V. Long
0	0.494	0.273	0.240	0.201
1	0.481	0.244	0.210	0.169
2	0.473	0.221	0.192	0.155
3	0.469	0.215	0.182	0.149
4	0.471	0.224	0.190	0.136
5	0.464	0.201	0.172	0.126
6	0.461	0.196	0.164	0.123
7	0.456	0.178	0.142	0.078
8	0.453	0.165	0.138	0.075
9	0.452	0.159	0.134	0.071

Table H.III(i) Mean azimuth standard errors for tests described in Table H.I

Model	Test Line Lengths			
	Short	Medium	Long	V. Long
0	2.719	0.764	0.662	0.420
1	2.715	0.725	0.643	0.374
2	2.706	0.571	0.599	0.222
3	2.704	0.537	0.596	0.191
4	2.715	0.721	0.641	0.370
5	2.706	0.570	0.599	0.221
6	2.704	0.537	0.596	0.191
7	2.711	0.701	0.634	0.359
8	2.705	0.569	0.598	0.217
9	2.704	0.537	0.596	0.191

Table H.III(ii) Mean distance standard errors for tests described in Table H.I

APPENDIX J

BASELINE, SOURCE, CLOCK AND ATMOSPHERIC PARAMETER RESULTS FROM THE VLBI ADJUSTMENTS

APPENDIX J

BASELINE, SOURCE, CLOCK, AND ATMOSPHERIC PARAMETER RESULTS FROM THE VLBI ADJUSTMENTS

Firstly, this appendix contains the baseline parameter results of the individual baseline adjustments of the May 1977 and January 1978 observations using the Canadian VLBI system on the Algonquin-Owens Valley-Chilbolton array. These results are described in §7.1.

The remainder of this chapter comprises the results for the source co-ordinates and the relative clock error polynomial coefficients from the three station adjustments of the Algonquin-Owens Valley-Chilbolton array, followed by the results for the source co-ordinates, relative clock error polynomial coefficients, and the mean zenith atmospheric delays at the separate antennae for the Haystack-Goldstone baseline.

Baseline Property	Baseline		
	Algonquin-Chilbolton	Algonquin-Owens Valley	Owens Valley-Chilbonton
x-component (m)	3090277.39 ± 0.47	-3327635.63 ± 0.41	6417909.70 ± 0.79
y-component (m)	4245482.60 ± 0.60	-132217.07 ± 0.17	4377706.66 ± 1.67
z-component* (m)	381819.90	-723368.67	1105188.57
length (m)	5264952.35 ± 0.70	3407917.61 ± 0.40	7846994.48 ± 0.66
declination	4^{o} 09' 31.685" ±0.002" (0.05 m)	-12^{o} 15' 17.630" ±0.005" (0.09 m)	8^{o} 05' 47.717" ±0.002" (0.09 m)
hour angle	53^{o} 56' 57.155" ±0.021" (0.54 m)	182^{o} 16' 31.219" ±0.014" (0.23 m)	34^{o} 17' 53.541" ±0.045" (1.73 m)
r.m.s. fringe frequency residual (mHz)	2.7	2.0	3.6
observations accepted	281	298	299

* The z-component was not adjusted in the solution.

Fig. J.I May 1977 VLBI results for the Algonquin-Owens Valley-Chilbolton array using the single baseline adjustment method

Baseline Property	Baseline		
	Algonquin-Chilbolton	Algonquin-Owens Valley	Owens Valley-Chilbolton
x-component (m)	3090272.66 ± 0.51	-3327633.97 ± 0.26	6417906.29 ± 1.23
y-component (m)	4245484.53 ± 0.87	-132217.42 ± 0.12	4377703.21 ± 2.08
z-component* (m)	381819.90	-723368.67	1105188.57
length (m)	5264951.13 ± 0.47	3407916.01 ± 0.25	7846989.76 ± 0.56
declination	4^{o} 09' 31.688" ±0.001" (0.03 m)	12^{o} 15' 17.651" ±0.003" (0.05 m)	8^{o} 05' 47.735" ±0.002" (0.08 m)
hour angle	53^{o} 56' 57.350" ±0.035 (0.89 m)	182^{o} 16' 31.244" ±0.009" (0.15 m)	34^{o} 17' 53.516" ±0.058" (2.21 m)
r.m.s. fringe frequency residual	2.3	6.1	2.7
observations accepted	295	294	256

* The z-component was not adjusted in the solution.

Fig. J.II January 1978 VLBI results for the Algonquin-Owens Valley-Chilbolton array using the single baseline adjustment method

Source	Source Co-ordinates			
	May 1977		January 1978	
	Right Ascension (h-m-s)	Declination (d-m-s)	Right Ascension (h-m-s)	Declination (d-m-s)
4C39.25	9-23-55.319 ± 0.001 s	39-15-23.518 ± 0.020"	-	-
BLLAC	22-00-39.368 ± 0.001 s	42-02-08.609 ± 0.0011"	22-00-39.372 ± 0.001 s	42-02-08.495 ± 0.012"
3C273B*	12-26-33.248	2-19-43.273	12-26-33.248	2-19-43.273
3C345	16-41-17.609 ± 0.001 s	39-54-10.859 ± 0.010"	16-41-17.615 ± 0.002 s	39-54-10.870 ± 0.012"
0J287	8-51-57.255 ± 0.001 s	20-17-58.303 ± 0.025"	8-51-57.257 ± 0.001 s	20-17-58.297 ± 0.019"
NRA0 150	-	-	3-55-45.269 ± 0.002 s	50-49-20.204 ± 0.009"
3C446	-	-	22-23-11.084 ± 0.004 s	-5-12-16.722 ± 0.279"
0235 + 16	-	-	2-35-52.632 ± 0.008 s	16-24-03.683 ± 0.181"

* 3C273B was used as the fixed origin of right ascension and declination in the adjustment.

Fig. J.III Source co-ordinate results from the three station adjustments of the Algonquin-Owens Valley-Chilbolton data

(these co-ordinates include the E-terms of elliptic aberration)

Antenna	Relative clock drift rate, c_1 (sec/sec)
Algonquin - Model 1	$0.18304 \times 10^{-11} \pm 0.579 \times 10^{-13}$
- Model 2	$0.15536 \times 10^{-11} \pm 0.332 \times 10^{-13}$
Owens Valley	0
Chilbolton	$0.3352 \times 10^{-12} \pm 0.705 \times 10^{-13}$

Fig. J.IV Relative clock drift rate solutions (c_1 in $\Delta\tau = c_0 + c_1 t$), relative to the Owens Valley clock, for the May 1977 data (two models were required at Algonquin due to the resetting of the clock during the observations)

Antenna	Relative clock drift rate, c_1 (sec/sec)
Algonquin	$-0.4506 \times 10^{-12} \pm 0.630 \times 10^{-12}$
Owens Valley	0
Chilbolton	$0.18748 \times 10^{-9} \pm 0.104 \times 10^{-12}$

Fig. J.V Relative clock drift rate solutions, relative to the Owens Valley clock, for the January 1978 data

Source	Source Co-ordinates	
	Right ascension (h-m-s)	Declination (d-m-s)
0J287	8-51-57.226 ± 0.0004 s	20-17-58.433 ± 0.012"
4C39	9-23-55.292 ± 0.0007 s	39-15-23.716 ± 0.006"
3C273B*	12-26-33.248	2-19-43.129 ± 0.036"
0Q2Ø8	14-04-45.623 ± 0.0008 s	28-41-29.422 ± 0.029"
3C345	16-41-17.631 ± 0.0009 s	39-54-10.955 ± 0.009"
2134+00	21-34-05.222 ± 0.0005 s	0-28-25.236 ± 0.052"
VR0	22-00-39.385 ± 0.0007 s	42-02-08.422 ± 0.006"
3C454.3	22-51-29.532 ± 0.0003 s	15-52-54.267 ± 0.007"
3C279	12-53-35.835 ± 0.0010 s	-5-31-07.698 ± 0.060"
3C120	4-30-31.587 ± 0.0004 s	5-14-59.265 ± 0.027"

Fig. J.VI Source co-ordinate results derived from the Haystack-Goldstone baseline adjustment using both delay and delay rate data

(these co-ordinates include the E-terms of elliptic aberration)

* RA Held Fixed

	Adjustment Mode		
	Both delay and delay rate observations	Delay observations only	Delay rate observations only
Relative clock offset, c_0 (sec)	$-0.151571 \times 10^{-4} \pm 0.5705 \times 10^{-9}$	$-0.151582 \times 10^{-4} \pm 0.6577 \times 10^{-9}$	-
Relative clock drift rate, c_1 (sec/sec)	$0.141447 \times 10^{-10} \pm 0.107 \times 10^{-14}$	$0.141448 \times 10^{-10} \pm 0.105 \times 10^{-14}$	$0.140912 \times 10^{-10} \pm 0.879 \times 10^{-13}$
Mean zenith atmospheric delay at Haystack (ns)	8.231 ± 0.036	8.159 ± 0.048	8.293 ± 0.089
Mean zenith atmospheric delay at Goldstone (ns)	6.908 ± 0.046	7.055 ± 0.060	6.668 ± 0.122

Fig. J.VII Clock error polynomial ($\Delta\tau = c_0 + c_1 t$) coefficients and mean zenith atmospheric delays as derived from the Haystack-Goldstone baseline using various adjustment modes

REFERENCES AND BIBLIOGRAPHY

REFERENCES AND BIBLIOGRAPHY

Abramowitz, M. and Stegun, I.A., 1965. *Handbook of Mathematical Functions.* Dover Publ. Inc., New York.

Anderle, R.J., 1974. Transformation of Terrestrial Survey Data to Doppler Satellite Datum. *Journal of Geophysical Research, Vol. 79, No. 35.*

Anderle, R.J., 1976. Error Model for Geodetic Positions Derived from Doppler Satellite Observations. *Bull. Geod., 50.*

Anderle, R.J., 1976. Point Positioning Concept Using Precise Ephemeris. Int. Geod. Symp. on Satellite Doppler Positioning, Las Cruces.

Anderle, R.J., 1978. The Global Positioning System. Satellite Doppler Tracking and Its Geodetic Applications, Royal Society, London.

Arur, M.G., 1977. Experiments for Improved Positioning by means of Integrated Doppler Satellite Observations and the NNSS Broadcast Ephemeris. *Rep. No. 258 of the Dept. of Geod. Sci., Ohio State Univ.*

Ashkenazi, V., 1968. An Introduction to Matrix Algebra. Seminar, Univ. of Nottingham.

Ashkenazi, V., 1968. Solutions and Error Analysis of Large Geodetic Networks. Part 1. Direct Methods. *Survey Review, Nos 146 and 147, Vol XIX.*

Ashkenazi, V., 1970. Adjustment of Control Networks for Precise Engineering Surveys. *Chart. Surv., No. 102.*

Ashkenazi, V., 1972. Criteria for Strength Analysis and Optimisation of Terrestrial Triangulation Networks. I.A.G. Symp. on Satellite and Terrestrial Triangulation, Graz.

Ashkenazi, V., 1973. Criteria for Optimisation: a Practical Assessment of Free Network Adjustment. I.A.G. Symp., Oxford, U.K.

Ashkenazi, V., 1979. Models for Establishing National and Continental Networks. XVII General Assembly of the IUGG, Canberra.

Ashkenazi, V. and Crane, S.A., 1980. Systematic Scale & Orientation Errors in Geodetic Control Networks, Preprint.

Ashkenazi, V., Cross, P.A., Davies, M.J.K. and Proctor, D.W., 1972. The Readjustment of the Retriangulation of Great Britain and its Relationship to the European Terrestrial and Satellite Networks. *Ordnance Survey Paper, No. 24.*

Ashkenazi, V., Gough, R.J. and Sykes, R.M., 1977. Satellite Doppler Positioning. Int. Sem. on Satellite Doppler Positioning and its Application to Surveying, Nottingham.

Ashkenazi, V. and Grafarend, E., 1975. Network Analysis: Singularity, Rank and Invariant Criteria. 1st Con. Venez. Geod., Maracaibo, Venezuela.

Ashkenazi, V., McLintock, D.N. and Sykes, R.M., 1978. Doppler Integration Intervals and Correlation. Satellite Doppler Tracking and its Geodetic Applications, Royal Soc., London.

Ashkenazi, V. and Sykes, R.M., 1978. Doppler Translocation and Orbit Relaxation Techniques. Satellite Doppler Tracking and its Geodetic Applications, Royal Soc., London.

Ashkenazi, V., Sykes, R.M., Gough, R.J. and Williams, J.W., 1978a. First United Kingdom Doppler Campaign: Results and Interpretation. Satellite Doppler Tracking and its Geodetic Applications, Royal Soc., London.

Ashkenazi, V., Dodson, A.H., Sykes, R.M., Dean, J.D.A. and Blanchard, W.F., 1978b. United Kingdom Doppler Campaigns: Field Operations and Instrumentation. Satellite Doppler Tracking and its Geodetic Applications, Royal Soc., London.

Ashkenazi, V., Crane, S.A., Williams, J.W. and Dean, J.D.A., 1978c. Terrestrial-Doppler Adjustment and Analysis of the Primary Triangulation of Great Britain: Preliminary Report. Satellite Doppler Tracking and its Geodetic Applications, Royal Soc., London.

Barber, P.C., 1973. The Extraction of Interference Fringes from Long Baseline Interferometer Recordings. *SRC Appleton Labs, Internal Report.*

Barber, P.C., 1977. Correspondence.

Bare, C., Clark, B.G., Kellerman, K.I., Cohen, H. and Jauncy, D.L., 1967. An Interferometer Experiment Using Independent Local Oscillators. *Sci. 157.*

Berman, A.L., 1970. A New Tropospheric Range Refraction Model. *In: The Deep Space Network Space Programs Summary 37-65, Vol. 11, Jet Propulsion Lab., Pasadena, California.*

Bomford, G., 1975. *Geodesy.* 3rd Edition Reprint, Oxford University Press, London.

Bonatz, M. and Campbell, J., 1977. Paper presented at the 8th Int. Symp. on Earth Tides, Bonn.

Broten, N.W., 1970. *The Role of Long Baseline Interferometry in the Measurements of Earth's Rotation.* Earthquake Displacement Fields and the Rotation of the Earth (edited by L. Mansinha et al), D. Reidel Publ. Co., Dordrecht, Holland.

Broten, N.W., Legg, T.H., Locke, J.L., McLeish, C.W. and Richards, R.S., 1967. Long Base Line Interferometry: A New Technique. *Science, Vol. 156.*

Bureau International de l'Heure, 1973. *Rapport Annuel pour 1972.* Paris.

Bureau International de l'Heure, 1978. *Rapport Annuel pour 1977.* Paris.

Bureau International de l'Heure, 1978. *Circular D136*. Paris.

Campbell, J., 1978. Monitoring Crustal Dynamics in Seismotectonic Zones by Very Long Baseline Interferometry. ESC Workshop on Crustal Dynamics, Strasbourg.

Campbell, J., 1978. Recent Advances of VLBI as a Tool for Geodynamical Research. J.L.G. Meeting (Sept 25-27), Luxembourg.

Campbell, J., 1979. Phase Versus Delay in Geodetic VLBI. *Proc. Radio Interferometry Techniques for Geodesy, Cambridge, Massachusetts.*

Cannon, W.H., 1978. The Classical Analysis of the Response of a Long Baseline Radio Interferometry. *Geophys. Journ. Roy. Astr. Soc., Vol. 53.*

Cannon, W.H., Langley, R.B., Petrachenko, W.T., Broten, N.W., Legg, T.H., Fort, D.N., Yen, J.L., Barber, P.C. and Quigley, M.J.S., 1975. Geodetic and Astrometric Analysis of Fringe Rate Residuals from the Algonquin-Chilbolton 2.8 cm Long Baseline Interferometer. Int. Symp. New Methods of Space Geodesy, Leningrad.

Cannon, W.H., Langley, R.B. and Petrachencko, W.T., 1979. Geodesy and Astrometry by Transatlantic Long Base Line Interferometry. *Journal of Geophysical Research, Vol. 84, No. B1.*

Carter, W.E., Fronczek, C.J. and Pettey, J.E., 1979. Haystack-Westford Survey. *NOAA Technical Memorandum NOS NGS 21.*

Carter, W.E. and Pettey, J.E., 1978. Goldstone Validation Survey - Phase 1. *NOAA Technical Memorandum NOS NGS-15.*

Carter, W.E., Robertson, D.S. and Abell, M.D., 1978. An Improved Polar Motion and Earth Rotation Monitoring Service using Radio Interferometry. *IAU Symp. No. 82, "Time and the Earth's Rotation", San Fernando, Spain (Publ. D. Reidel, Doordrecht, Holland).*

Chao, C.C., 1971. Improved Estimation of the Parameters and Mapping, Tables of Tropospheric Calibration for MM71. *IOM 391-3-352 (JPL Internal Document)*.

Chao, C.C., 1974. The Tropospheric Calibration Model for Mariner Mars 1971. *JPL Technical Report 32-1587*.

Chatfield, C., 1970. *Statistics for Technology*. Penguin Books Ltd, Harmondsworth.

Clark, B.G., 1973. The NRAO Tape Recorder Interferometer System. *Proc. of the IEEE, Vol. 61, No. 9.*

Clark, T.A., 1978. Survey of Geodesy and Astrometry. Symp. on Very Long Baseline Interferometry, Heidelburg.

Clark, T.A., Hutton, L.K., Marandino, G.E., Counselman, C.C., Robertson, D.S., Shapiro, I.I., Wittels, J.J., Hinteregger, H.F., Knight, C.A., Rogers, A.E.E., Whitney, A.R., Niell, A.E., Ronnang, B.O. and Rydbeck, O.E.H., 1976. Radio Source Positions from Very Long Baseline Interferometry Observations. *The Astronomical Journal, Vol. 81, No. 8.*

Cohen, M.H. and Schaffer, D.B., 1971. Positions of Radio Sources from Long Baseline Interferometry. *The Astronomical Journal, Vol. 76, No. 2.*

Committee on Geodesy, 1978. Geodesy: Trends and Prospects. National Academy of Sciences, Washington, D.C.

Counselman, C.C. and Shapiro, I.I., 1979. Miniature Interferometer Terminals for Earth Surveying. *Bull. Geod., Vol. 53.*

Counselman, C.C., Shapiro, I.I., Rogers, A.E.E., Hinteregger, H.F., Knight, C.A., Whitney, A.R. and Clark, T.A., 1977. VLBI Clock Synchronisation. *Proc. of the IEEE, Vol. 65, No. 11.*

Crane, R.K., 1976. *Refraction Effects in the Neutral Atmosphere.*

In: Methods of Experimental Physics, Vol. 12, Part B, Radio Telescopes, Academic Press, New York.

Cross, P., 1970. Strength analysis of large geodetic triangulation networks. Ph.D. Thesis, Dept. of Civil Eng., Univ. of Nottingham.

Deeth, C.P., 1978. Report on the Construction and Calibration of the 3-Channel Met. Recorder and its Baseline Derivatives. Internal Rep., Univ. of Nottingham.

Dermanis, A., 1977. Design of Experiment for Earth Rotation and Baseline Parameter Determination from Very Long Baseline Interferometry. *Report No. 245, Dept. of Geod. Sci., Ohio State Univ.*

Dodson, A.H., 1977. The Measurement of Spatial Displacements by Geodetic Methods. Ph.D. Thesis, Dept. of Civil Eng., Univ. of Nottingham.

Eady, Major J., RE, 1979. Correspondence.

European Space Agency, 1978. Very Long Baseline Radio Interferometry Using a Geostationary Satellite. A Mission Definition Study.

European Space Agency, 1980. Very Long Baseline Radio Interferometry Using a Geostationary Satellite. Phase A Study.

Explanatory Supplement to the Astronomical Ephemeris and the American Ephemeris and Nautical Almanac, 1961, Fourth Impression 1977. H.M.S.O., London.

Fanselow, J.L., Thomas, J.B., Cohen, E.J., MacDoran, P.F., Melbourne, W.G., Mulhall, B.D., Purcell, G.H., Rogstad, D.H., Skjerve, L.J., Spitzmesser, D.J., Urech, J. and Nicholson, G., 1978. Determination of UT1 and Polar Motion by the Deep Space Network using Very Long Baseline Interferometry. IAU Symp. No. 82, San Fernando, Spain.

Fliegel, H.F. and Wimberly, R.N., 1974. Time and Polar Motion. *JPL Technical Report 32-1587.*

Fricke, W. and Kopff, A., 1963. Fourth Fundamental Catalog (FK4). Braun, Karlsruhe.

Goff, J.A. and Gratch, S., 1946. Low Pressure Properties of Water from -160 to 212°F. *Trans. Am. Soc. of Heating, Refrigerating and Air-Conditioning Engineers, Vol. 52.*

Gough, R.J., 1978. Satellite Doppler: Geocentric Positioning of the Triangulation of Great Britain. Ph.D. Thesis, Dept. of Civil Eng., Univ. of Nottingham.

Grafarend, E. and Schaffrin, B., 1974. Unbiased Free Net Adjustment. *Survey Review, Vol. XXII, No. 200.*

Hagfors, T., 1976. *The Ionosphere.* In: Methods of Experimental Physics, Vol. 12, Part B, Radio Telescopes, Academic Press, New York.

Henriksen, S.R., 1977. Systems for the Determination of Polar Motion. *NOAA Technical Report NOS 72 NGS 7.*

Hopfield, H.S., 1963. The Effect of Tropospheric Refraction on the Doppler Shift of a Satellite Signal. *Journal of Geophysical Research, Vol. 68, No. 18.*

Hopfield, H.S., 1969. Two Quartic Refractivity Profile for Connecting Satellite Data. *Journal of Geophysical Research, Vol. 74, No. 18.*

Hopfield, H.S., 1971. Tropospheric Effect on Electromagnetically Measured Range: Prediction from Surface Weather Data. *Radio Sci., Vol. 6, No. 3.*

Hopfield, H.S., 1972. Tropospheric Range Error Parameters: Further Studies. *Goddard Space Flight Centre Rep. X-551-72-285.*

Hopfield, H.S., 1976. Tropospheric Effects on Low Elevation Angle Signals: Further Studies (Final Report). *JHU/APL Rep. SDO-4588.*

Hopfield, H.S., 1977. Tropospheric Connection of Electromagnetic Ranging Signals to a Satellite: Study of Parameters. IAG Symposium on EDM and the Influence of Asmospheric Refraction, Wageningen.

Hothem, L.D., 1979. Determination of Accuracy, Orientation, and Scale of Satellite Doppler Point-Positioning Coordinates. 2nd Int. Geod. Symp. on Satellite Doppler Positioning, Austin.

Hothem, L.D., Robertson, D.S. and Strange, W.E., 1978. Orientation and Scale of Satellite Doppler Results Based on Combination and Comparison with other Space Systems. Second Int. Symp. on Problems Relating to the Redefinition of North American Geodetic Networks, Washington, D.C.

Hotter, F.D., 1967. Preprocessing Optical Satellite Observations. *Report No. 82, Dept. of Geod. Sci., Ohio State Univ.*

International Association of Geodesy, 1978. 3rd International Workshop on Laser Ranging Instrumentation. Lagonissi.

International Astronomical Union, 1977. *Proc. of the Sixteenth General Assembly. ed. Edith A. Müller and Arnost Jappel, D. Reidel Publishing Co., Dordrecht, Holland.*

Jones, H.E., 1969. Geodetic Ties Between Continents by means of Radio Telescopes. *Canadian Surveyor, Vol. 23.*

Kelsey, J. and Ashkenazi, V., 1979. Contribution of space techniques to National and Continental Geodetic Networks. *Publ. of the Finnish Geodetic Institute, No. 89.*

Knowles, S.H., Waltman, W.B., Broten, N.W., Fort, D.N., Kellerman, K.I., Rayhrer, B., Swenson, G.W. and Yen, J.L., 1978. Real Time Accurate Time Transfer and Frequency Standards Evaluation via Satellite Link Long Baseline Interferometry. *Proc. of the 9th Ann. Precise Time and Time Interval Applications and Planning Meeting, NASA Technical Memorandum 78104.*

Kouba, J., 1978. Correspondence.

Kouba, J. andBoal, J.D., 1976. Program GEODOP. Dept. of Energy, Mines and Resources, Ottawa.

Kraus, J.D., 1966. *Radio Astronomy*. McGraw-Hill.

Langley, R.B., 1979. Precision Geodesy and Astronomy with a Three Station Long Baseline Interferometer. Ph.D. Thesis, York University, Toronto, Ontario.

Langley, R.B., Cannon, W.H., Petrachenko, W.T. and Kouba, J., 1978. LBI and Satellite Doppler: Baseline Comparisons. Second Int. Geod. Symp. on Satellite Doppler Positioning, Austin.

Langley, R.B., Petrachenko, W.T. and Cannon, W.H., 1979. Geodetic Long Baseline Interferometry Research in Canada.

Lennox, S. and Chadwick, M., 1972. *Mathematics for Engineers and Applied Scientists*. Heinemann Educational Books, London.

Lloyd, I., 1973. Geodetic Applications of VLBI. *Unisurv G-19, Reports of School of Surveying, Univ. of New South Wales.*

MacDoran, P.F., 1979. Satellite Emission Radio Interferometric Earth Surveying: SERIES-GPS Geodetic System. *Bull. Geod., Vol. 53.*

Mark III VLBI System User's Manual. NASA(GSFC), Haystack Observatory and NRAO.

Mathur, N.C., Grossi, M.D. and Pearlman, M.R., 1970. Atmospheric Effects in Very Long Baseline Interferometry. *Radio Science, Vol. 5, No. 10.*

McLintock, D.N., 1976. Computer Simulation of Surveying Networks, B.Sc. Thesis, Univ. of Nottingham.

Meeks, M.L., 1976. *Essentials of Radiometric Measurements*. In: Methods of Experimental Physics, Vol. 12, Part B, Radio Telescopes, Academic Press, New York.

Melbourne, W.G., Mulholland, J.D., Sjogren, W.L. and Sturms, F.M., 1968. Constants and Related Information for Astrodynamic Calculations. *JPL Technical Report, 32-1306.*

Melchior, P., 1966. *The Earth Tides*. Pergamon Press.

Melchior, P., 1978. *The Tides of the Planet Earth*. Pergamon Press, Oxford.

Mittermayer, A., 1972. A generalisation of the least squares method for the adjustment of free networks. *Bull. Geod., No. 104*.

Moffett, J.B., 1971. Program Requirements for Two Minute Integrated Doppler Satellite Navigation Solution. *JHU/APL TG-819-1*.

Moran, J.M., 1976. *Very Long Baseline Interferometric Observations and Data Reduction*. In: Methods of Experimental Physics, Vol. 12, Part C, Radio Observations, Academic Press, New York.

Mueller, I.I., 1969. *Spherical and Practical Astronomy as applied to Geodesy*. Ungar.

Nes, H., Hagfors, T., Stette, G. and Blankenburgh, J.C., 1978. A Scandinavian VLBI - Experiment using a Small Telescope.

Niell, A.E., Ong, K.M., MacDoran, P.F., Resch, G.M., Fite, D.W., Skjerve, L.J., Spitzmesser, D.J., Morabito, D.D., Tanida, L.L. and Claflin, E.S., 1979. Comparison of a Radio Interferometric Differential Baseline Measurement with Conventional Geodesy. *Tectonophysics, Vol. 52*.

Ong, K.M., MacDoran, P.F., Thomas, J.B., Fliegel, J.F., Skjerve, L.J., Spitzmesser, D.J., Batelaan, P.D., Paire, S.R. and Newsted, M.G., 1976. A Demonstration of a Transportable Radio Interferometric Surveying System with 3 cm Accuracy on a 307 m Base Line. *Journal of Geophysical Research, Vol. 81, No. 20*.

Ordnance Survey, 1977. Report No. CR21366.

Pacholczyk, A.G., 1970. *Radio Astrophysics*. W.H. Freeman and Co.

Parkinson, B.W., 1979. The Global Positioning System (NAVSTAR). *Bull. Geod., Vol. 53*.

Pooley, G., 1976. *Connected Element Interferometry.* In: Methods of Experimental Physics, Vol. 12, Part C, Radio Observations, Academic Press, New York.

Powell, J.M., 1978. Position Fixing at Sea - A review for Inclusion in an Engineers guide to Submersible Work. Plymouth Polytechnic.

Quigley, M., 1978. SRC Appleton Labs. Internal Report.

Rainsford, H.F., 1957. Survey Adjustments and Least Squares. Constable and Co., U.K.

Rinner, K., 1979. Control Survey, a Fundamental Task of Geodesy. *Publ. of the Finnish Geodetic Institute, No. 89.*

Robbins, A.R., 1967. Time in Geodetic Astronomy. *Survey Review, No. 143.*

Robertson, D.S., 1975. Geodetic and Astronometric Measurements with Very Long Baseline Interferometry. Ph.D. Thesis, M.I.T.

Robertson, D.S., 1975. Special Relativity and Very Long Baseline Interferometers. *Nature, Vol. 257.*

Robertson, D.S., Carter, W.E., Corey, B.E., Cotton, W.D., Counselman, C.C., Shapiro, I.I., Wittels, J.J., Hinteregger, H.F., Knight, C.A., Rogers, A.E.E., Whitney, A.R., Ryan, J.W., Clark, I.A., Coates, R.J., Ma, C. and Moran, J.M., 1978. Recent Results of Radio Interferometric Determinations of Polar Motion and Earth Rotation. IAU Symp. No. 82, "Time and the Earth's Rotation", San Fernando, Spain. (Publ. D. Reidel, Doordrecht, Holland.)

Robinson, J.H., 1972. *Astronomy Data Book.* David & Charles, Newton Abbot.

Rogers, A.E.E., 1970. Very-Long-Baseline Interferometry with large effective bandwidth for phase-delay measurements. *Radio Science, 5.*

Rogers, A.E.E., 1976. *Theory of Two-Element Interferometers.* In: Methods of Experimental Physics, Vol. 12, Part C, Radio Observations, Academic Press, New York.

Rogers, A.E.E., Knight, C.A., Hinteregger, H.F., Whitney, A.R., Counselman, C.C., Shapiro, I.I., Gourevitch, S.A. and Clark, T.A., 1978. Geodesy by Radio Interferometry: Determination of a 1.24 Km Base Line Vector with ~5 mm Repeatability. *Journal of Geophysical Research, Vol. 83, No. B1.*

Rohde, F.W., 1977. Geodetic SECOR system. National Geodetic Satellite Program, Part I, NASA, Washington D.C.

Ryan, J.W., Clark, T.A., Coates, R., Ma, C., Robertson, D.S., Corey, B.E., Counselman, C.C., Shapiro, I.I., Wittels, J.J., Hinteregger, H.F., Knight, C.A., Rogers, A.E.E., Whitney, A.R. and Moran, J.M., 1977. Precision Surveying using Very Long Baseline Interferometry. *Goddard Space Flight Center Report No. X-922-77-242.*

Schilizzi, R.T. and Campbell, J., 1978. Very Long Baseline Interferometry in Geophysics, Geodesy and Astrometry.

Schmid, H.H., 1973. Results and Analysis of Worldwide Geometrical Satellite Triangulation - Preliminary Version. Int. Symp. on the use of Artificial Satellites for Geodesy and Geophysics, Athens.

Scott, F.P. and Hughes, J.A., 1964. Computation of Apparent Places for the Southern Reference Star Program. *Astronomical Journal, Vol. 69, No. 5.*

Sears, F.W. and Brehme, R.W., 1968. *Introduction to the Theory of Relativity.* Addison-Wesley Publ. Co., U.S.A.

Senus, W.J., 1976. In: Electronic Surveying and Navigation, by S.H. Laurilla, Publ. by J. Wiley & Sons.

Seppelin, T.O., 1974. The Department of Defense World Geodetic System, 1972. Int. Symp. on Problems Related to the Redefinition of North American Geodetic Networks, Fredericton.

Shapiro, I.I., 1976. *Estimation of Astrometric and Geodetic Parameters.*

In: Methods of Experimental Physics, Vol. 12, Part C, Radio Observations, Academic Press, New York.

Shapiro, I.I., 1978. Principles of Very Long Baseline Interferometry. *Proc. of the 9th GEOP Conference, Report No. 280, Dept. of Geod. Sci., Ohio State Univ.*

Shapiro, I.I. and Knight, C.A., 1970. *Geophysical Applications of Long Baseline Radio Interferometry.* Earthquake Displacement Fields and the Rotation of the Earth (edited by L. Mansinha et al), D. Reidel Publ. Co., Dordrecht, Holland.

Shapiro, I.I., Robertson, D.S., Knight, C.A., Counselmann, C.C., Rogers, A.E.E., Hinteregger, H.F., Lippincott, S., Whitney, A.R., Clark, T.A., Niell, A.E. and Spitzmesser, D.J., 1974. Transcontinental Baselines and the Rotation of the Earth Measured by Radio Interferometry. *Science, Vol. 186.*

Smart, W.M., Sixth edition 1977. *Textbook on Spherical Astronomy.* Cambridge University Press.

Smith, E.K. and Weintraub, S., 1953. The Constants in the Equation for Atmospheric Refractive Index at Radio Frequencies. *Proc. Inst. of Radio Eng., Vol. 41.*

Smith, R.W., Schwarz, C.R. and Googe, W.D., 1976. DOPPLR: a point positioning program using integrated Doppler satellite observations. Int. Geod. Symp., Las Cruces.

Strange, W.E., Hothem, L.D. and White, M.B., 1975. Results of Doppler Station Positioning in the United States. 56th Annual Meeting of the A.G.U.

Strange, W.E. and Hothem, L.D., 1978. Establishment of Scale and Orientation for Satellite Doppler Positions. Satellite Doppler Tracking and its Geodetic Applications, Royal Soc., London.

Sykes, R.M., 1979. Translocation and Orbit Relaxation Techniques in Satellite Doppler Tracking. Ph.D. Thesis, Dept. of Civil Eng., Univ. of Nottingham.

Thomas, J.B., 1975. Reformulation of the Relativistic Conversion between Coordinate Time and Atomic Time. *The Astronomical Journal, Vol. 80, No. 5.*

Thomas, J.B., Fanselow, J.L., MacDoran, P.F., Skjerve, L.J., Spitzmesser, D.J. and Fliegel, H.F., 1976. A Demonstration of an Independent-Station Radio Interferometry System with 4 cm Precision on a 16 km Base Line. *Journal of Geophysical Research, Vol. 81, No. 5.*

Thompson, E.H., 1962. The Theory of the Method of Least Squares. Photogrammetric Rec., Vol. 4, No. 19.

Vessot, R.F.C., 1976. *Frequency and Time Standards.* In: Methods of Experimental Physics, Vol. 12, Part C, Radio Observations, Academic Press, New York.

Vincenty, T., 1979. The Navago Three-Dimensional Adjustment Program. *NOAA Technical Memorandum NOS NGS-17.*

Warden, M.A., et al, 1977. Stations on the SECOR Equatorial Network. National Geodetic Satellite Program, Part I, NASA, Washington D.C.

Welch, W.J., 1976. *Types of Astronomical Antennas.* In: Methods of Experimental Physics, Vol. 12, Part B, Radio Telescopes, Academic Press, New York.

Wells, D.E., 1974. Electromagnetic Metrology, Hilbert space optimization, and their application to Doppler satellite control. Ph.D. Thesis, Univ. of New Brunswick.

Wells, D.E. and Krakiwsky, E.J., 1971. The Method of Least Squares. *Lecture Notes 18, Dept. of Surv. Eng., Univ. of New Brunswick.*

Whipple, F.L. and Hynek, J.A., 1958. Optical and Visual Tracking of Artificial Satellites. *Proc. of 8th Int. Astron. Congress, Springer-Verlag, Vienna.*

Whitney, A.R., Rogers, A.E.E., Hinteregger, H.F., Knight, C.A., Levine, J.I., Lippincott, S., Clark, T.A., Shapiro, I.I. and Robertson, D.S., 1976. A Very Long Baseline Interferometer System for Geodetic Applications. *Radio Science, Vol. 11, No. 5.*

Williams, D.R.W., 1976. *Fundamentals of Spectral Line Measurements.* In: Methods of Experimental Physics, Vol. 12, Part C, Radio Observations, Academic Press, New York.

Wood, L.E. and Thompson, M.C., 1970. Oscillator Synchronization via Satellite. *Radio Science, Vol. 5, No. 10.*

Woolard, E.W., 1953. Theory of the Rotation of the Earth around its Centre of Mass. *The Astronomical Journal, Vol. 58, No. 2.*

Woolard, E.W. and Clemence, G.M., 1966. *Spherical Astronomy.* Academic Press.

Yen, J.L., Kellerman, K.I., Rayhrer, B., Broten, N.W., Fort, D.N., Knowles, S.H., Waltman, W.B. and Swenson, G.W., 1977. Real Time, Very Long Baseline Interferometry based on the use of a Communications Satellite. *Science, Vol. 198.*

Yumi, S., 1972. Non-Polar Variation of Latitude. Int. Astr. Union Colloquium 1, La Plata, Argentina, Vol. 93.